2001

Structural behavior of composite steel beams strengthened/repaired with carbon fiber reinforced polymer plates

Abdullah Hilal Al-Saidy
Iowa State University

INFORMATION TO USERS

This manuscript has been reproduced from the microfilm master. UMI films the text directly from the original or copy submitted. Thus, some thesis and dissertation copies are in typewriter face, while others may be from any type of computer printer.

The quality of this reproduction is dependent upon the quality of the copy submitted. Broken or indistinct print, colored or poor quality illustrations and photographs, print bleedthrough, substandard margins, and improper alignment can adversely affect reproduction.

In the unlikely event that the author did not send UMI a complete manuscript and there are missing pages, these will be noted. Also, if unauthorized copyright material had to be removed, a note will indicate the deletion.

Oversize materials (e.g., maps, drawings, charts) are reproduced by sectioning the original, beginning at the upper left-hand corner and continuing from left to right in equal sections with small overlaps.

Photographs included in the original manuscript have been reproduced xerographically in this copy. Higher quality 6" x 9" black and white photographic prints are available for any photographs or illustrations appearing in this copy for an additional charge. Contact UMI directly to order.

ProQuest Information and Learning
300 North Zeeb Road, Ann Arbor, MI 48106-1346 USA
800-521-0600

Structural behavior of composite steel beams strengthened/repaired with carbon fiber reinforced polymer plates

by

Abdullah Hilal Al-Saidy

A dissertation submitted to the graduate faculty

in partial fulfillment of the requirements for the degree of

DOCTOR OF PHILOSOPHY

Major: Civil Engineering (Structural Engineering)

Major professors: Terry J. Wipf and F. Wayne Klaiber

Iowa State University

Ames, Iowa

2001

UMI Number: 3016688

UMI Microform 3016688

Bell & Howell Information and Learning Company
300 North Zeeb Road
P.O. Box 1346
Ann Arbor, MI 48106-1346

Graduate College
Iowa State University

This is to certify that the Doctoral dissertation of

Abdullah Hilal Al-Saidy

has met the dissertation requirement of Iowa State University

Signature was redacted for privacy.

Co-major Professor

Signature was redacted for privacy.

Co-major Professor

Signature was redacted for privacy.

For the Major Program

Signature was redacted for privacy.

For the Graduate College

TABLE OF CONTENTS

LIST OF FIGURES

LIST OF TABLES

ACKNOWLEDGEMENTS

First of all, the author of this dissertation would like to thank and acknowledge The Almighty ALLAH (GOD) for His countless bounties. Without His guidance and help this work would not have been possible.

The author was supported by a scholarship from the Government of the Sultanate of Oman throughout the Ph.D. program, which is greatly acknowledged.

The CFRP plates and the epoxy system were donated by Structural Composites. The shear connectors and the welding equipment were provided by TRW-Nelson. These contributions are highly acknowledged.

The author would like to express his gratitude to fellow students, staff, and faculty of the Civil and Construction Engineering Department of the Iowa Sate University for their help and assistance. Douglas Wood, the Structural Lab Manager, was a great help in the laboratory experiments. Special thanks go to Dr. F. Wayne Klaiber and Dr. Terry J. Wipf for all the guidance, generous time, and constructive criticism they provided throughout this study. I would also like to thank Dr. Lowell Greimann, Dr. Vinay Dayal, Dr. Loren Zachary, and Dr. Sri Sritharan for serving in my committee.

Last, but not least, I would like to thank those special ones to whom I am greatly indebted. I owe more than I can ever express to my parents; my wife, Amna; my sons, Mohammed and Yaser; and my daughter, Arwa, for their never-ending patience, love, and support. My wife made a lot of sacrifices in order for me to accomplish this work; her encouragement provided a source of strength that enabled me to achieve one of my goals.

ABSTRACT

Of the approximately 600,000 bridges in the United States, more than 110,000 are either structurally deficient or functionally obsolete. Causes of deterioration are attributed to the age of the structure, steady increase in legal load limits, increase in traffic density, deterioration due to environmental attack, and the lack of proper maintenance. A large number of these bridges are constructed out of structural steel. One significant cause of deterioration in these structures is corrosion due to extensive use of de-icing salts in severe winter weather. These bridges either have to be replaced or strengthened to extend their service life. In most cases, strengthening of these structures is more cost effective than replacement. Among the popular strengthening methods used in the past on steel bridges are post-tensioning and the bonding of steel plates to the tension flange of the girders. However, these methods are labor intensive and disturbance to the traffic flow is inevitable. This investigation focused on the behavior of steel composite beams strengthened with carbon fiber reinforced polymer (CFRP) plates attached to their tension side. In the experimental part of this study, a total of ten beams were tested under a four-point bending; six of the beams were in the undamaged state (two control beams and four strengthened), while the remaining four beams were damaged and repaired (one control beam and three repaired). Since this technique depends on the shear strength of the adhesive, extensive instrumentation was utilized to measure shear stresses along the CFRP plate in all load ranges (i.e. elastic and inelastic); this is something that was not emphasized in the previous research available. Another contribution of this work was the study of the effect of damage on the stiffness and strength of the section as well as the effect of repair schemes in restoring both the lost

stiffness and strength of the section. The test results showed a significant increase in the strength and the stiffness of the strengthened/repaired beams. To help implement this strengthening technique, a nonlinear analytical procedure was developed to predict the behavior of the section/member in the elastic, inelastic, and ultimate states. A parametric study was also conducted to investigate the effect of some of the important variables on the behavior of the composite section. In addition, damage analyses of a bridge system were completed using grillage analysis to investigate the influence of the damage in the girders on load distribution. Based on the damage analyses results, an analysis/design methodology to determine the required repair or strengthening system was developed.

1. INTRODUCTION

1.1 Background

Many of the nation's bridges are considered either structurally or functionally deficient. The majority of these bridges were built before the 1940s and in many cases they do not conform to current standard requirements due to deterioration caused by age or environmental factors, increasing highway traffic volumes, and the use of heavier vehicles. This deterioration of infrastructure elements has lead to a multi-billion dollar problem that requires collective efforts and appropriate measures to solve it. Of the approximately 600,000 bridges in the United States [1], more than 110,000 are either structurally deficient or functionally obsolete due to various reasons. Causes of the deterioration are attributed to the age of the structure, steady increase in the weight of highway vehicles (as high as 40% over the original design loads [2]), increase in traffic density, deterioration due to environmental attack; and the lack of proper maintenance. A large number of these bridges are constructed out of steel. One significant cause of deterioration in steel structures is the corrosion of flexural elements due to extensive use of de-icing salts in severe winter weather. In addition to deterioration, some of these bridges must be upgraded to meet the present and future traffic needs. These bridges, either have to be replaced or strengthened to extend their service life.

In most cases, strengthening these structures is more cost effective than replacement. Replacing existing bridges in most instances is more expensive and will have a greater impact in terms of delays and inconvenience over considerably long periods of time. Thus,

there is a need for developing rapid and cost-effective strengthening technique. Various methods have been used in the past to strengthen steel bridges as reported by Klaiber et al. [1] and Dorton and Reel [3]. Some of the popular methods used in the past on steel bridges are post-tensioning and bonding of steel plates to the tension flange of the girder. However, these methods are labor intensive and disturbance to the traffic flow is inevitable.

The addition of steel cover plates is the most common method to increase a given bridge's load carrying capacity. The standard procedure for attaching steel cover plates to steel beams is welding, but this procedure has several problems. This includes fatigue cracking at cover plate ends, some clearance reduction, or stress concentration along the weld line. These problems have been addressed by bonding the cover plate with special adhesives. This will normally reduce the stress concentration at the plate ends and the stresses are distributed evenly along the plate [4]. However, steel plate bonding has some disadvantages. One is the difficulty of installing the heavy steel plates at the bridge site. Another is the limited plate length that can be delivered to the site. This requires the introduction of lap (splice) joints to get the desired length, which creates a weak link (or discontinuity) along the plate. Another problem is the risk of corrosion in the joints between the steel and the adhesive.

Due to the problems associated with bonding steel plates, researchers have explored the potential of using fiber composite materials in strengthening of structures. Composite materials have been used in recent years to strengthen concrete bridges and buildings in Japan, Europe as well as the United States. Fiber composites are made of fibers such as glass, carbon, or kevlar embedded in a resin matrix. The main characteristics of fiber composite materials are high strength, lightweight, corrosion resistance and high fatigue

properties. This makes fiber composites very attractive in strengthening and repairing steel beams. Their high strength to weight ratio means that only thin plates are needed. This in turn means that repair work can be carried from a mobile platform and erection of temporary scaffolding is either unnecessary or less extensive when compared to conventional methods of rehabilitating steel girders. Conventionally, the addition of heavy steel cover plates will require temporary scaffolding to hold the cover plate in place while the adhesive cures. Because composite materials can be installed more easily and quickly than steel, the construction traffic delays are reduced.

While adhesively bonded carbon fiber reinforced polymers (CFRP) have been used to strengthen concrete beams, very little research has been completed to investigate the feasibility of using CFRP in the rehabilitation of steel composite sections. If this technique (using CFRP plates) can be used instead of the more labor-intensive conventional methods such as post tensioning or the use of steel cover plates, the procedure of strengthening steel bridges would be greatly simplified.

1.2 Objective/Scope

The main objective of the project described herein is to evaluate the feasibility of using CFRP plates in strengthening and repair of steel-concrete composite bridges.

The scope of the work can be defined by the following tasks:

a. to develop an analytical model to predict the behavior of the strengthened sections. The model needs to predict the moments (stresses) and curvatures (deformations) in the elastic, inelastic and ultimate state.

b. to perform a parametric study on the effect of the major variables on the behavior of the section. This will include the effect of using different strengthening schemes, concrete compressive strengths, structural steel yield strengths, CFRP plate thicknesses, CFRP plate stiffnesses, and the remaining area of the tension flange of the steel section which is reduced to simulate corrosion of the flange.

c. to develop a simplified nonlinear model to predict the response of the strengthened member at service, inelastic and ultimate states.

d. to test steel-concrete composite beams specimens and to determine the influence of the various strengthening schemes and important variables on the behavior.

e. to perform damage analyses on a typical slab-girder bridge system and to develop a methodology for determining the required repair or strengthening system. Damage analyses will be completed using the grillage analysis method to investigate the behavior of the bridge system with/without damaged members.

To accomplish the proposed research objectives, the tasks that were performed in this study are briefly described below:

1.2.1 Analytical study

1.2.1.1 Moment- Curvature analysis

To evaluate the behavior of the strengthened section, an analytical model was developed. The model related moments (stresses) and curvatures (deformations). Since closed form solutions, (where a continuous expression can be written for the moment-curvature relation), are only valid in the elastic range, a numerical technique was utilized to predict the behavior over the entire range of elastic and inelastic deformations.

1.2.1.2 Parametric study

A computer program was developed to perform the required calculations and to complete the parametric study. The computer program was used to investigate the effect of different variables on the behavior of the section; variables investigated included:

- the slab concrete compressive strength.
- the yield strength of the steel section being strengthened.
- the area of the tension flange (reduced to simulate corrosion).
- the CFRP plate area (thickness)
- the CFRP plate stiffness.
- different strengthening schemes.

1.2.1.3 Load – deflection analyses

The theoretical moment-curvature relation developed in the previous task was used to develop the theoretical load deflection relations. Response at the critical section of the member was predicted using an energy method and a numerical integration technique. The goal was to evaluate and compare the response of the strengthened member with that of unstrengthened member to determine the effectiveness of strengthening system in the elastic (service) and inelastic ranges and at ultimate load.

1.2.1.4 Damage analyses

To evaluate the effect of damaged members in a bridge system on the overall bridge behavior, the grillage method was used to perform a damage analyses on a slab-girder bridge.

Small as well as severe damage in the girders and their effect on the load distribution in the bridge were investigated. In the analyses of the bridge, several load cases were investigated on both the undamaged and damaged states. Based on the damage analyses results, an analysis/design methodology to determine the required repair or strengthening system was also presented.

1.2.2 Experimental study

Based on the analytical study, 10 composite specimens (steel beams + reinforced concrete slab) were tested in the laboratory; this testing is briefly described in the following sections. CFRP plates were attached to the tension face of the steel beam with epoxy adhesive (for specimen details refer to Chapter 3). Since a large percentage of bridges in Iowa that are in need of repair and strengthening are located on the secondary roads system, it was decided to test beams that are representative of a typical prototype single span bridge. Due to the fact that this was an exploratory study, small-scale specimens were selected to save materials cost and thus makes it possible to test several specimens that covered the important aspects of the study. The specimen dimensions were selected based on Iowa Department of Transportation (Iowa DOT) standard design drawings. The composite section consisted of a W8x15 steel beam with a 3 in. thick by 32 in. wide reinforced concrete composite slab; the overall length of the beams was 11 ft with a span length (center to center of supports) of 10 ft.

The beams tested were divided into two groups: undamaged/strengthened beams; and damaged/repaired beams. In both groups, extensive instrumentation was used to collect the test data. Deflections were measured along the beams using deflection devices mounted to

the steel bottom flange and the bottom of the concrete slab. Slip between the concrete slab and the steel beam was also measured by devices installed at the beam ends. Strains in the concrete slabs, steel beams, and the CFRP plates were measured using strain gages; the data were collected using a computerized data acquisition system.

1.2.2.1 Undamaged beams

A total of six beams were tested to evaluate the effectiveness of the CFRP to upgrade the strength of existing beams to support additional load. Different strengthening schemes were used (see Chapter 3 for details); the test series evaluated the following parameters:

- the effect of using various stiffness of CFRP plates.
- the effect of different strengthening schemes.

1.2.2.2 Damaged beams

Since the tension flange in most cases is the part of the beam that is damaged due to corrosion in the field, it was important to simulate this condition in the laboratory by removing part of the flange. The beam was then tested to determine the amount of strength and stiffness loss; this beam was used as a control specimen and was tested to failure to observe the behavior in the service (elastic), inelastic, and ultimate state. Three more beams were also damaged and repaired by the CFRP plates; these beams were also tested to failure to observe the behavior in the elastic and inelastic ranges.

2. LITERATURE REVIEW

2.1 General

There is wide spread deterioration of the nation's infrastructure that needs immediate attention and cost-effective methods of rehabilitation. Numerous studies have been completed in the past to evaluate the extent of deterioration in the nation's bridges and identify available methods for strengthening such as the one reported by Klaiber et al. [1] and Dorton and Reel [3]. Strengthening of concrete members by steel plates and CFRP plates is becoming accepted practice due to the numerous laboratory experiments and field applications in the past two decades. A study by Mckenna et al. [2] compiled data from the previous studies on the application of CFRP in the strengthening of concrete bridges in North America, Europe, and Japan. However, there are very few studies in the application of CFRP to steel structures. In the investigation reported in this dissertation, the focus will be on strengthening steel beams by bonding CFRP laminates to their tension side. In the next sections, a literature review is presented on pertinent issues concerning the aspects of bonding CFRP plates to steel. In Section 2.2, issues related to the adhesive joints are reviewed. A review of the performance aspects of composites and adhesives under various states of stress is presented in Section 2.3. Previous studies dealing with the strengthening of steel structures with CFRP materials will be presented in Section 2.4.

2.2 Adhesive bonded joints

2.2.1 Background

Adhesives had been used since the earliest times. In the nature there are many materials with adhesive properties, for example clay, mud, starch, egg white, and many more. The Chinese, the Egyptians as well as the Greeks and the Romans made and used adhesives during their respective civilization periods. Natural adhesives such as starch, animal glues and plant resins have been used for centuries and are still in use widely today for packaging and for joining wood. Modern structural adhesives became available in the early twentieth century with the introduction of pheno-formaldehyde resins. The first synthetic adhesives were sold in the form of hard processing films. Due to the expansion of the aircraft industry during the Second World War, adhesives were developed to be more easily handled. The construction of wooden wartime aircraft was facilitated by the availability of phenol-, resorcinol- and urea-formaldehyde adhesives, and since then reactive formaldehyde-based adhesives have continued to be used in the manufacture of timber building elements such as plywood, and laminated timber beams [5].

Over the past five decades there have been numerous synthetic adhesives developed to meet many new technical applications. These synthetic polymers, which include thermoplastic and thermosetting types, have been developed with properties that enables them to adhere readily to other materials, to have an adequate cohesive strength, appropriate mechanical characteristics when cured, and to posses good durability.

Thermosetting adhesives may soften when heated but re-harden upon cooling. Thermosetting materials are so called because, when cured, the molecular chains are locked

permanently together in a large three-dimensional structure; they may, therefore, be regarded as structural adhesives. Unlike thermoplastic adhesives they do not melt or flow when heated, but become more rubbery and lose strength with increasing temperature [5]. Epoxies, which are in this group of thermosetting adhesives, find wide spread use in civil engineering applications.

2.2.2 General considerations

The adhesive, which is similar to a plastic material, represents a low modulus interlayer and is likely to be the weakest link in a structural joint. Design considerations generally involve the geometry of the bond, the selection of an adhesive and the necessary bonding process, a knowledge of the properties of the adhesive and the adherends (i.e. the materials being joined), and finally the stresses that the bonded assembly is likely to encounter in service. Petronio [6] states that for maximum success in designing joints, the following general principles need to be addressed:

- Stress the adhesive in the direction of maximum strength (i.e. in compression or in shear)
- Provide the maximum bond area .
- Make adhesive layer as uniform as possible
- Maintain a thin and continuous bondline
- Avoid stress concentrations

Most of the adhesives used in structural applications are relatively strong in shear, and weak in peel or cleavage. The lapped joint shown in Fig. 2.1 is one of the most common occurring joints in practice and is therefore the configuration most often used for testing

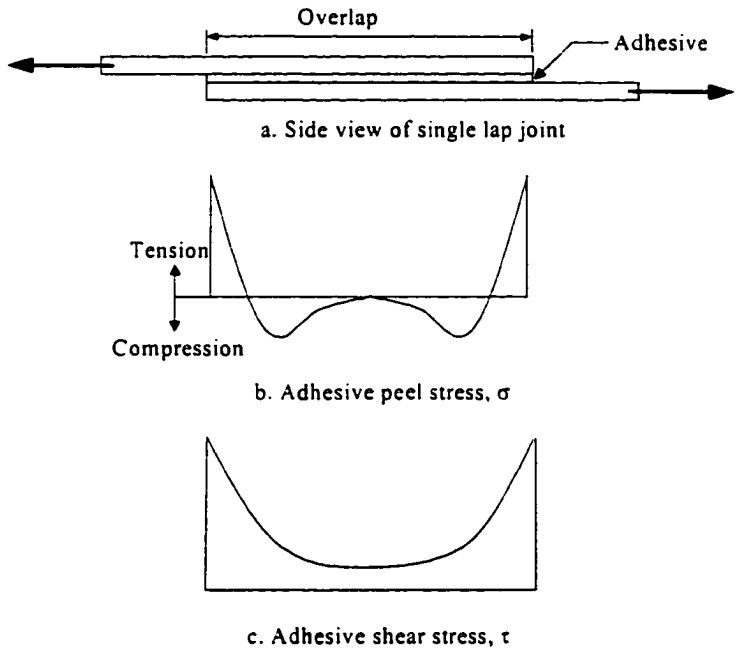

Figure 2.1. Adhesive shear and peel stress distributions for a single lap joint.

adhesives. As seen in this figure, the highest shear and peel stresses occur at the ends of the joints. Many researchers observed debonding of steel cover plates (adhesively bonded to either concrete or steel beams) due to peeling stresses. Studies reported by Johns et al. [7] and Albrecht and Sahli [8] show that peeling stresses are caused by high shear forces together with high interface bond stresses at the end of bonded plates which causes delamination of these plates. Some practical details can reduce the stress concentration at the joint ends. Hart-Smith [9] stated that the combination of an adequate overlap with sufficiently thin ends of the adherends (i.e by tapering the adherends ends) will minimize the effects of adhesive peel stresses on single-lap joints. However, Adams et al. [10] reported that tapering is of limited benefit since the adherends have to be tapered to a fine edge if significant benefit is to be achieved, and this is usually impracticable. In this study, several

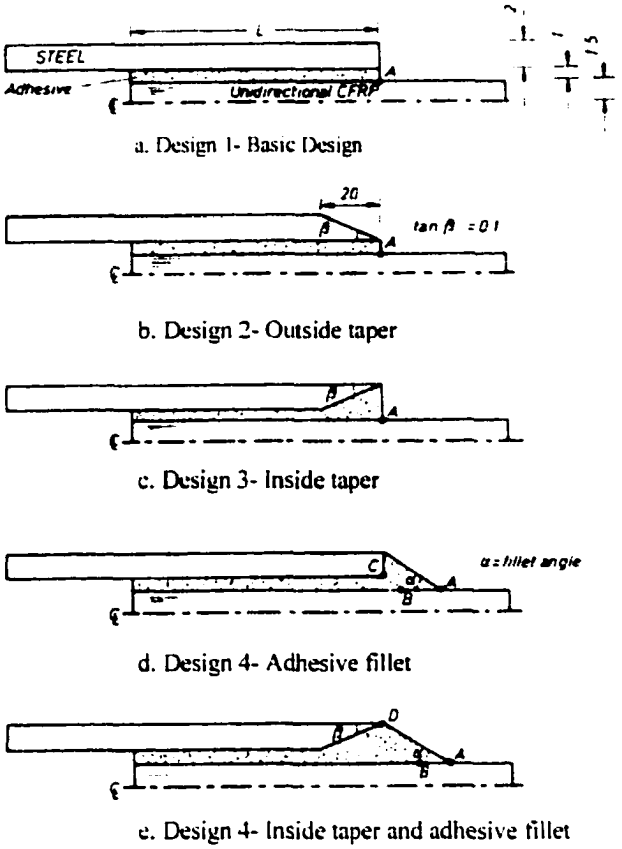

Figure 2.2. Designs of double lap joints [10].

joint configurations, as shown in Fig. 2.2, were tested and analyzed using a finite element method of analysis. As shown in Fig. 2.2, Designs 2 and 3 were a modification of the basic Design 1 by tapering the outer adherends. Design 4 shows the original joint modified to include an adhesive fillet at the end. In Design 5, both a taper and a fillet were incorporated. It was concluded from this study that in Designs 1-3 tapering the outer (steel) adherends had a negligible effect on reducing the peel stress. By introducing a fillet in Design 4 with an angle (α) just under 35°, the maximum peel stress in the CFRP was reduced to approximately a one-third of that in the basic design (Design 1).

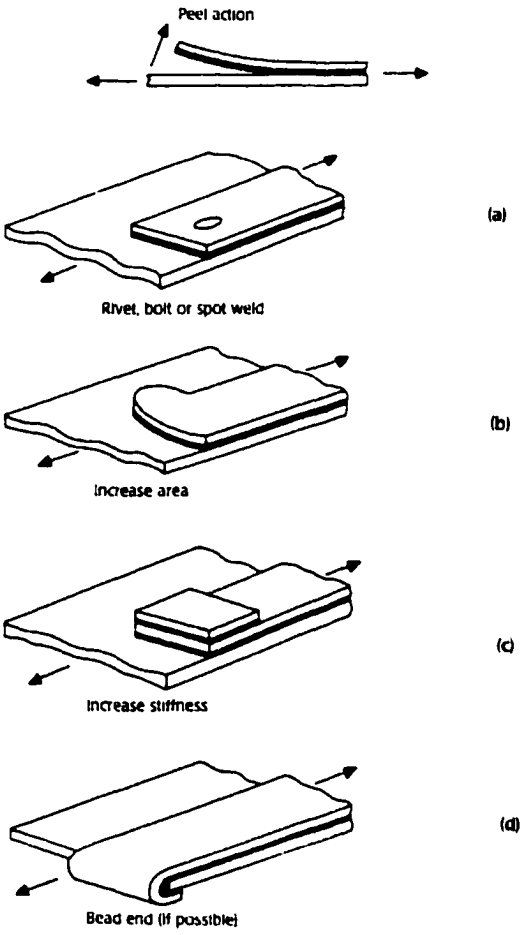

Figure 2.3. Techniques for combatting peel [11].

A combination of an "internally" tapered steel adherend with an adhesive fillet (Design 5) results in further reduction in the stress concentration. Adams et al. [11] suggested the use of the techniques illustrated in Fig. 2.3 to minimize the effect of peel stresses. The techniques are for lap joints in general; however, for bonding composites, Techniques a and b are more practical. In Technique a, the peeling stresses are resisted by the clamping force of the bolt(s). In the second technique (Technique b), the stresses are reduced by the distribution over a larger adhesive area.

The shear strength of adhesive joints is determined according to the ASTM standard test D1002. Hart-Smith [9] noted that the shear strength of adhesive joints based on the ASTM Test Method for Strength Properties of Adhesives in Shear by Tension Loading (Metal-to-Metal) (D 1002) test coupon (similar to that shown in Fig. 2.1) does not reflect the behavior of the joint in a real structure. Failure of such coupons is rarely if ever affected by the shear strength of most adhesives. Nevertheless, it should be acknowledged as an effective and inexpensive quality assurance coupon, when used in cure-monitoring records and with tests to verify the adequacy of the preparation of the surface for bonding. He found that the peek peel stresses in a structurally configured joint with an overlap of 5 in. is approximately 3.5% of that in the equivalent ASTM D 1002 test coupon (with an overlap of 1/2 in.). This clearly shows that the length of the overlap of the joint will significantly affect the distribution of the stresses. In practice, most joints will have adequate overlap length and the stresses will be less than that predicted by the ASTM D 1002 lap joint shear test.

2.2.3 Advantages and limitations

It has bean observed that the application of adhesives to metal fabrication, in common with many other technological innovations, was pioneered by the aircraft industry. It is ironic that this industry, in which safety and reliability command paramount attention, should lead the departure from traditional methods of joining. Today adhesives are used to bond critical parts in commercial and military aircraft and helicopters, spacecraft, rockets, missiles and US Space shuttles [5]. The motivation in the aerospace industry to replace mechanical fasteners with adhesives stems from the desire to prolong aircraft life and to reduce costly

maintenance. Rivets holes, for example, are points of weakness where fatigue cracks can form, and metal fasteners can corrode or loosen.

It has been reported by Albrecht and Sahli [8] that bonding cover plates to the tension flange of steel beams increased the fatigue life by a factor of 20 as compared to that of conventionally welded cover plates. Replacing the welds with adhesives and bolts virtually fatigue-proofs structural steel details subjected to highway bridge loading. Albrecht attributed the increase in the fatigue strength of structural details when adhesives are used to the more even stress distribution (distribution over a larger area) and the absence of stress concentration that normally occur in welded or fastened joints.

Besides the better stress distribution and increase in fatigue life of bonded parts, there are other advantages of using adhesive joints. Some other advantages include: bonding of dissimilar materials, e.g. metals and composites, reduction in weight due to the absence of the mass of mechanical fasteners, no destruction is induced in the adherends as would normally occur with mechanical fastening and welding, and reduced assembly time [5].

However, there are some limitations in using adhesively bonded joints such as the need for careful surface preparation of the bonded parts and the variation in properties of the adhesive with time, temperature, and humidity.

2.3 Performance of composite materials and adhesive bonded joints

Much literature is available on the durability and performance of adhesive joints, both in general textbooks on adhesives [5,12] and specific studies [13-22]. In particular, extensive work has been done for the aerospace and automotive industries. Most of the laboratory

studies found in the literature established that moisture is the most hostile environment structural adhesive joints commonly encountered.

Before reviewing the different studies on the performance of composite materials, it is necessary to define the basic fundamentals of a composite lamina. The basic building of a composite structure is the lamina (ply), which consists of a combination of fibers oriented in a specific direction and a matrix that binds the fibers together and protects the fibers at the same time from external effects. However, a single lamina is generally not very useful as a structural element due to its poor transverse properties. Most structural members require a certain thickness with multiple laminae, or plies, oriented in the desired directions and bonded together in a structural unit; these are called laminates. In fiber composites, two right-handed coordinate systems are considered in the analysis of any laminate. These are the 1-2-z and x-y-z systems as shown in Fig. 2.4. Both the 1-2 and x-y axes are in the plane of the laminate, and the z-axis is normal to this plane. In the 1-2-z system, 1 and 2 are associated with the fiber direction in the laminate and are usually defined as the principal material axes. In the x-y-z system, the x and y represent loading direction. The angle between the positive x-axis and the 1-axis is called the fiber orientation angle and is represented by θ.

2.3.1 Composite materials

Springer [13] conducted a literature survey on the effects of the environment on the performance of epoxy matrix composites (mostly graphite epoxy). The laminates that were studied were divided into three groups: 0 degree laminates (loads applied along the fiber orientation), $\pi/4$ laminates (plies were stacked in (90/±45/90)), and 90 degree laminates

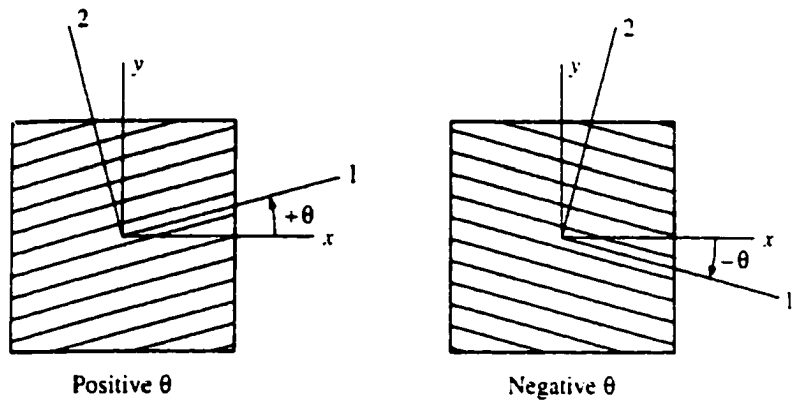

Figure 2.4. Coordinate systems and fiber orientation in a lamina.

(loads applied perpendicular to fiber orientation). For 0-deg and $\pi/4$ it was found that changes in temperature in the range of 200 to 380 K had negligible effects on the ultimate tensile strength, regardless of the moister content of the material. There was about 20% reduction in strength as the temperature increased from 380 to 450 K. For 90-deg laminates, the increase in temperature from 200 to 450 K causes a significant decrease in the ultimate tensile strength; the reduction in strength can be as high 60 to 90 percent [13].

Similarly, the moisture content of the composite material has only a small effect on the ultimate strength of 0-deg and $\pi/4$ laminates when the moisture content is less than 1 percent. At moisture content above 1 percent, the tensile strength decreased with the increase in moisture content. The maximum decrease in the ultimate strength observed was approximately 20 percent. For 90-deg laminates, the moisture content had a significant effect on the ultimate strength. The reduction in strength can be as high as 60 to 90 percent.

Based on durability studies conducted by Chajes et al. [14], reinforced concrete beams strengthened with externally bonded composite fabrics experienced varying amounts of degradation due to aggressive environments. In the presence of chlorides, both wetting and drying, and freezing and thawing led to reduced ultimate beam strengths. Of the two conditions, the wet/dry cycling led to greater degradation. Of the three fabrics tested, both aramid and E-glass lost roughly half of their strength advantage after environmental exposure. On the other hand, the graphite (carbon) reinforced beams lost approximately 9 percent of their strength after 100 freeze/thaw cycles and approximately 14 percent of their strength after 100 wet/dry cycles. The study concluded that the graphite fabric reinforcement was the least sensitive to environmental conditions and may be better to use in applications involving wet/dry and thaw/freeze cycling. Other studies [14,15] showed that the properties of glass fiber composites would degrade considerably when exposed to a severe hot and humid environment.

GangarRao [17] conducted a study on the hygrothermal effects on carbon composite coupons; the test specimens were conditioned under varying temperature and humidity. Temperature was varied from -20°F to 120°F and relative humidity (R.H.) varied from 0% R.H. to 100% R.H. Some specimens were also soaked in 3% sodium chloride solution. The study concluded that exposing the test specimens to these conditions resulted in a reduction of no more than 7% of the original strength and stiffness values. It was also found that there was no substantial decrease in the strength or stiffness of the carbon plate coupon specimens after exposure to environmental conditioning for 180 days and that the degradation leveled off beyond this period.

2.3.2 Adhesive bonded joints

For efficient use of composites in the repair of steel bridges, a strong and durable bond must exist. Damaged or corroded substrates could present dirt, oily surfaces containing weak oxides that must be removed before bonding. The surface treatment, by bead blasting and degreasing, was found to be important in the resulting performance of steel/composite joints. Silane coupling agents were seen to be effective in improving the hot-wet durability of steel/composite bonds. To repair damaged steel structures successfully, adhesives having good corrosion protection need to be used in combination with adhesion promoters like silane since their interaction can significantly affect joint performance [18].

Karbhari [19] studied bond durability in composite-steel system through the wedge test (ASTM D3762). Composites used in the study included both carbon and glass fiber reinforced epoxy systems. The resin system was an epoxy curable at room temperature, with a glass transition of 48°C and 62°C for the glass and carbon reinforced systems, respectively. Before application of the composite, the steel surface was degreased, beadblasted, and treated with a silane solution. The specimens were subjected to one of six different environments:

1. Ambient
2. Synthetic sea water (ASTM D1141) at 25°C
3. Hot water at 65°C
4. Room-temperature water (25°C)
5. Freezing (-18°C)
6. Freezing thaw (alternative 12 hr cycles between -18°and 25°C)

Each specimen was exposed to the selected environment for two weeks before testing. The study concluded that the S-glass-type system has the most durable bonding attribute with the environments tested. However, to satisfy durability and performance criteria, the best overall combination would be a hybrid of S-glass and carbon, with the glass being in contact with the steel. The inner layer of S-glass would not only help in overall durability, but also would significantly decrease the potential for long-term degradation due to galvanic corrosion triggered by the presence of carbon fibers in contact with steel. The hot-water environment was the most aggressive environment, causing severe breakdown of the bond due to rapid formation of oxides at the interface.

GangaRao [17] tested 9 ft long W8X24 steel beams reinforced with a 6 in. x 3/16 in. CFRP composite plates with span length of 8 ft. Two different CFRP plate lengths were used for reinforcement. Full reinforcement was considered to be 2/3 of the 8 ft while partial length reinforcement was taken to be 1/2 of the 8 ft span. The addition of the CFRP plates increased the moment of inertia of the reinforced beam, I_{hyb}, by 7.9% and 8.3% for the beam with partial length and full length cover plate, respectively. The beams were tested statically using four –point bending after six months of accelerated environmental aging. A reduction was noted in the increase in I_{hyb} from 7.9% to 4.3% for the hybrid beam with partial length cover plate and 8.3% to 4.02% for the full length cover plate.

2.3.3 Effect of cyclic loading on adhesive bonded joints

The proposed study is concerned with adhesively bonding CFRP plate to steel beams. In a highway bridge, the loads due to moving traffic will impose cyclic stresses on the

bonded elements. The effect of fatigue performance of adhesive bonded joints was reported by Cusens and Smith [20], by Mays and Tilly [21], and by Macdonald [22].

Cusens and Smith [20] tested steel-to-steel double lap joints using three types of adhesive and four types of surface treatment: (1.)standard clean rough surface; (2.) standard surface blasted with grade 50 sand; (3.) standard surface allowed to rust over 15% of area; and (4.) standard surface dipped in salt solution and rusted over 20% of area. Tests showed that the static strength were reduced by between 12 and 47% for the three adhesives and treatments (2.), (3.), and (4.).

Mays and Tilly [21] investigated the fatigue performance of steel-to-steel lap joints using two different resins. The tests involved the following conditions: (1.) specimens cured at different temperature and tested at room temperature; (2.) specimens cured at room temperature and tested at temperatures ranging from -25°C to 55°C; and (3.) specimens weathered prior to testing. The study concluded that the fatigue performance was temperature dependent. For the resins used in this study there was little change in performance over the temperature range -25°C to 45°C but it is considerably weaker at 55°C. A lower bound fatigue life for the range -25°C to 45°C was provided; it was also recommended that for optimum performance of bonded joints, curing temperature as low as 0°C should be avoided.

In a study conducted by Macdonald [22], the effect of cyclic loading during curing of the adhesive was investigated. Two different resin systems (A and B) were used in the fabrication of single lap shear specimens. Both resin systems were two component epoxy adhesives with inert mineral fillers having a paste like consistency when mixed. Although, no precise data were available in this study, it was indicated that epoxy type A was much stiffer

than epoxy type B. The tested specimens with adhesive A showed a reduction in shear strength of between 7 and 31 % due to cyclic loading. For adhesive B there was no reduction in strength. The difference in material modulus may account for the difference in performance of the two adhesive systems.

2.4 Strengthening of steel structures using CFRP composites

Unlike the use of CFRP composites in the strengthening of concrete structures, there has been minimal research in the area of strengthening steel structures with advanced composite materials. The previous research of strengthening steel structures is presented in the next section. A few cases of field application in the United Kingdom have been reported and are presented in Section 2.4.2.

2.4.1 Research

Sen et al. [23] tested six 20 ft long steel composite beam, each consisting of a W8 x 24 steel beam composite with 4 in. thick by 28 in. wide reinforced concrete slab. Three of the beams had a yield strength of 45 ksi and the remaining three beams had a yield strength of 54 ksi. The beams were initially loaded in four-point static bending past yield of the tension flange and subsequently strengthened using 12 ft. lengths of 2 mm or 5 mm thick unidirectional carbon fiber reinforced plastic (CFRP) plates. The average tensile strength of the CFRP plates was 268 ksi and the tensile modulus was 16,500 ksi. Three beams were strengthened by adhesively bonding 2 mm CFRP plates; two beams were strengthened by attaching 5 mm CFRP plates with a combination of adhesive and bolts; the last beam was strengthened by adhesively bonding a 5 mm CFRP plate. Estimated increase in the ultimate

strength ranged from 11% to 50% depending on the yield strength of the specimen and the mode of failure. Both beams that were strengthened with 5 mm CFRP plates attached to steel flange using fasteners failed when the bolts sheared through the CFRP plate.

In another study, Mertz and Gillespie [23] investigated the possibility of strengthening steel beams with CFRP plates. Small as well as large scale girders were strengthened using CFRP plates. Small scale specimens consisted of 5 ft long, W8 x 10 rolled-beams that were strengthened by adhesively bonding 6 mm thick CFRP plates to the tension flange. The beams were loaded in a four-point bending. There was approximately 20% increase in the elastic stiffness and more than 50% in strength before the test was stopped due to buckling of top cover plate. Full scale tests were carried out on two girders taken from a demolished bridge that had severely corroded bottom flanges (approximately 40% loss of the tension flange). The girders were 2 ft deep I-beams with a 21 ft. span. Corrosion of specimen 1 was significantly worse than specimen 2. The inside and outside of each tension flange was sand blasted to remove the oxide layer; then the 6 mm CFRP plates were adhesively bonded to both faces of the bottom flange. Both girders were loaded in a three-point bending. The elastic stiffness of each member was approximately improved by 25%. Significant increases in the ultimate strength beyond the original capacity were also achieved. Failure of the girders was due to local buckling of the top flange.

2.4.2 Field applications

Taylor et al. reported [25] that Slattocks Canal Bridge in the United Kingdom; a steel bridge built in 1936, was strengthened using CFRP plates. According to Taylor et al., this is the first steel highway bridge to be strengthened with laminated CFRP plates in Europe. Two

4 mm thick CFRP plates were factory bonded (i.e. 8 mm total thickness) were used to strengthen the beams. No heavy equipment was required to lift the plates, but temporary clamps were installed to support the plates while the adhesive cured. The strengthening operation was carried out while bridge was carrying traffic.

Another case, also in the United Kingdom, involved a demonstration project to strengthen a steel underbridge at Acton for the London Underground [26]. CFRP plates were applied to the underside of two steel cross girders of the bridge. Again, the strengthening operation was carried out while the bridge was operational. The objective of the project was to reduce the stresses in those beams by at least 20%. A third beam, at a location remote from the strengthened two beams was used as a control. The bridge was monitored for two weeks after the strengthening operation and found that stresses were reduced by 20%. The strengthening was completed in April, 2000.

Another potential area for the use of CFRP materials is the offshore industry. The first major use of composites in the reinforcement of existing structures in the offshore industry was the strengthening of grid 3 on the Mobile Beryl B Platform located in the United Kingdom sector of the Northern North Sea [27]. The scope of the project was to increase the blast capacity of two walls of size 8 m deep by 40 m long. A threefold increase in blast capacity was required. A total of 13 critical columns were strengthened to provide the necessary blast resistance of the wall. The CFRP laminates were approximately 7 m long by 16 cm wide; the maximum CFRP thickness used was 25 mm. Strengthening operations were carried out in temperatures from 7°C to 18°C. This operation was completed over three two-week sessions during September and October,1995.

3. SIMPLIFIED NONLINEAR ANALYSIS

3.1 General

The strengthening technique proposed in this study introduces CFRP laminates which behave differently than conventional materials such as concrete and steel which are frequently used in the field of civil engineering. In order to understand the behavior of the strengthened section with the combination of steel, concrete and CFRP, an analytical procedure must be developed which will predict the deformations of the strengthened section in the elastic and inelastic ranges. The analytical tool will not only help understand the behavior of the section, but it will also be useful in extending the analytical study of the behavior of the member by predicting its response and deformation at critical sections. It will also serve as a preliminary design tool for determining the best strengthening scheme and thus avoid resorting to a more complex finite element modeling (FEM) at the preliminary stage. This will be more obvious in the development of the analysis which is described in the following sections.

3.2 Moment – curvature relation

This section will describe the method used for evaluating the moment and curvature relationship for a general concrete-steel composite cross section with the option of including the CFRP material. For cross sections consisting of linearly elastic materials it is possible, and generally more convenient, to write a single continuous expression relating the moment and curvature. Unfortunately the response of concrete and steel to external effects is nonlinear at high stresses; therefore, it is difficult to write and evaluate an expression describing the moment and curvature relationship over the full range of their stresses.

Instead, it is easier and more convenient to define the relationship by a number of discrete points.

The analytical method developed herein for the determination of the relation between moment (M) and curvature (ϕ) evolves directly from the application of basic principles of mechanics of materials. This method however differs from routine methods of stress analysis in that the internal effects (strains or stresses) are assumed first, then the external effects (moments) are determined.

3.2.1 Assumptions

The analytical results obtained in this study are based on the following assumptions:

1. Small deformations
2. Plane sections before bending remain plane after bending (i.e. linear strain distribution through the full depth of the section).
3. Tensile strength of concrete is neglected.
4. Perfect bond between CFRP plate and the steel beam, and between the concrete slab and the steel beam.
5. The stress-strain relations of steel, concrete and CFRP are known.

3.2.2 Materials' constitutive relations

Composite beams are fabricated from various construction materials, each of which has its own unique constitutive relationship. Materials considered here are reinforced concrete, structural steel, and CFRP. The stress-strain curve of structural steel is approximated as elastic perfectly plastic and strain hardening is neglected as shown in Fig. 3.1a. Neglecting strain hardening will result in a more conservative response (less

strength) at the ultimate strength as a result of ignoring the little stiffness of the steel on the onset of strain hardening. CFRP has a stress-strain relationship that is linear elastic up to failure as illustrated in Fig. 3.1b. The relationship assumed for concrete is the well known Hognestad's parabola [28] as shown in Fig. 3.1c. As may be seen in this figure, the relation is defined by a second order equation for strains less than ε_o, strain at maximum stress, and as a linear relation for strains greater than ε_o and less than ultimate strain , ε_u, which is taken here as 0.003 as recommended by AASHTO specifications; $f_c^{'}$ is the concrete compressive strength at 28 days.

3.2.3 Numerical model

The curvatures associated with a range of bending moments will be determined using the above assumptions and from the requirements of strain compatibility and equilibrium of stresses. The most convenient method to determine the moment curvature relation, keeping in mind the complicated geometry of the section and stress distribution, is subdividing the cross section into a large number of thin horizontal elements (slices), as shown in Fig. 3.2, which permits the strain distribution to be idealized as a unique linear function. The procedure used to obtain the moment-curvature relationship for a given cross section can be summarized as follows:

1. Divide the section into N-number of horizontal elements, each having the width of the section at that level
2. The strain in the extreme fiber (concrete or CFRP) is incremented to find discrete points on M - ϕ curve. The extreme fiber strain is increased in specified

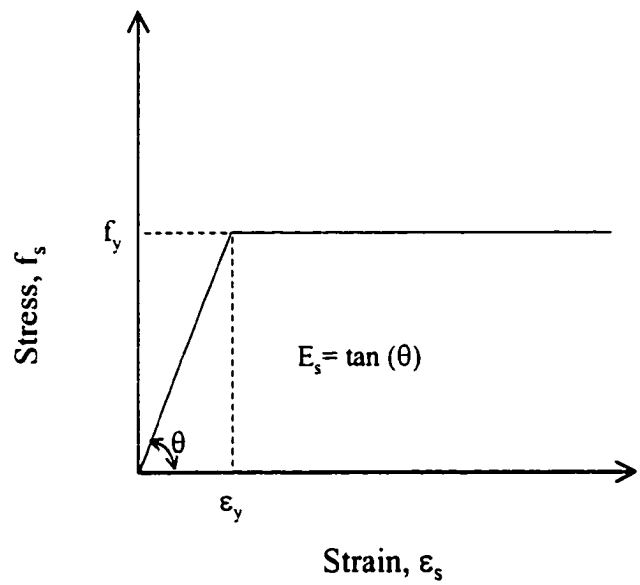

a. structural steel

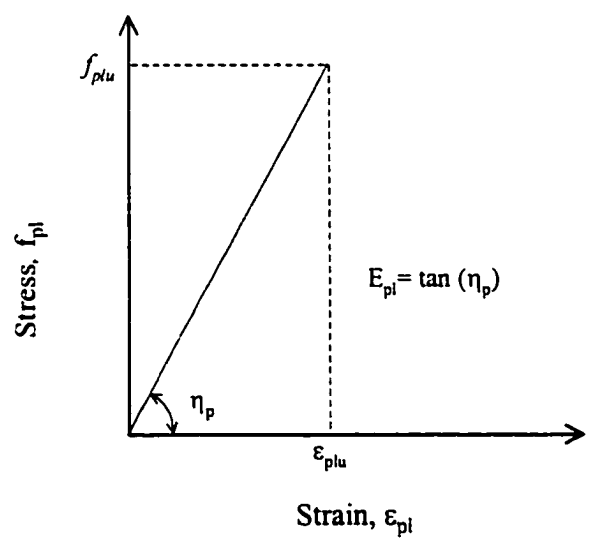

b. CFRP

Figure 3.1. Assumed stress-strain relations for steel, CFRP, and concrete.

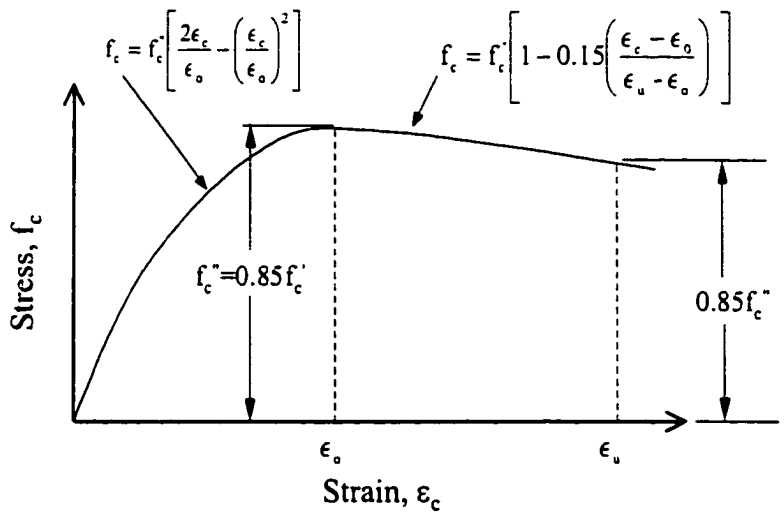

c. concrete

Figure 3.1. Continued.

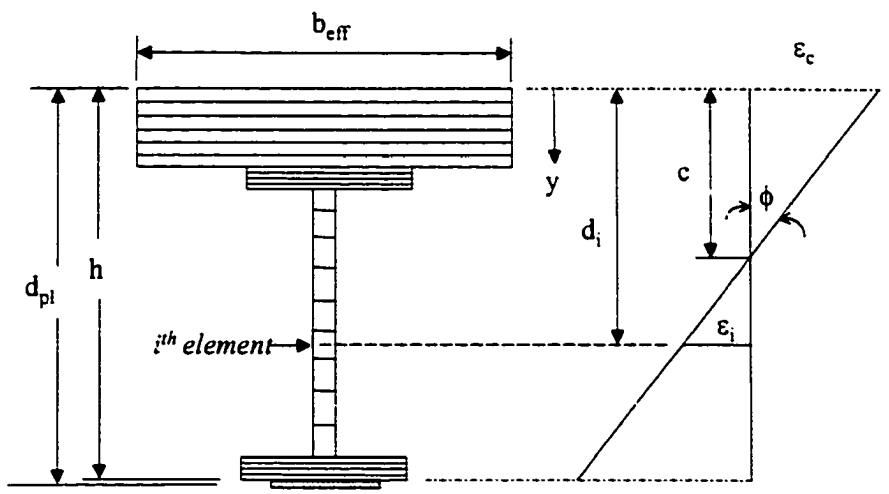

Figure 3.2. Subdivision of cross-section and strain profile.

increments until failure is reached which is when either the concrete reaches its ultimate crushing strain or the CFRP plate reaches its ultimate strain.

3. For a given strain as described in step 2, the neutral axis (N.A.) position, c, is assumed for the first trial calculation and then revised.
4. The strain in each element (see Fig. 3.2) is then calculated based on strain-compatibility relation

$$\varepsilon_i = \varepsilon_c \times (c - d_i)/c \tag{3.1}$$

5. The stress in each element, taken at its centroid, is then calculated using the constitutive relationships of each material described previously for the following cases:

   Steel

$$f_{si} = E_s \cdot \varepsilon_{si} \qquad if \quad \varepsilon_{si} \le \varepsilon_y \tag{3.2}$$

$$f_{si} = f_y \qquad if \quad \varepsilon_{si} > \varepsilon_y \tag{3.3}$$

where f_{si}, f_y, ε_{si}, ε_y, and E_s are stress in steel element, steel yield stress, strain in steel element, steel yield strain, and steel modulus of elasticity, respectively.

CFRP

$$f_{pl} = E_{pl} \cdot \varepsilon_{pl} \tag{3.3}$$

where f_{pl}, E_{pl}, and ε_{pl} are stress in CFRP plate, modulus of elasticity of CFRP plate, and strain in CFRP plate, respectively.

Concrete

$$f_c = f_c^{*}\left[\frac{2\varepsilon_c}{\varepsilon_o} - \left(\frac{\varepsilon_c}{\varepsilon_o}\right)^2\right] \qquad if \quad 0 \le \varepsilon_c < \varepsilon_o \tag{3.4}$$

$$f_c = f_c^{*}\left[1 - 0.15 * \left(\frac{\varepsilon_c - \varepsilon_o}{\varepsilon_u - \varepsilon_o}\right)\right] \qquad if \quad \varepsilon_o \le \varepsilon_c < \varepsilon_u \tag{3.5}$$

where $f_c^{*} = .85\, f_c^{'}$, $\varepsilon_o = (2f_c^{*} / E_c)$
$f_c^{'}$ is the compressive strength at 28 days
E_c is the modulus of elasticity of concrete

6. The location of the neutral axis, c, is determined from equilibrium of internal forces as expressed by the following integral.

$$P = \int_{y=0}^{y=h} \sigma \, dA \tag{3.6}$$

where P is the resultant force in the section, σ is the stress in the element, and dA is the area of the element. P must be equal to zero for equilibrium. The integral can be represented by the sum of forces in each element as

$$\sum c_i + \sum s_i + \sum f_{pl_i} \times A_{pl_i} = 0 \tag{3.7}$$

where c_i, s_i, f_{pli}, *and* A_{pli} are the forces in the i[th] concrete element; force in steel element; stress in CFRP layer; and area of CFRP plate at that layer, respectively.

If the above equilibrium equation is not satisfied, a new neutral axis is assumed and the process is repeated until the solution converges and equilibrium is reached. The summation of forces will actually yield a quadratic equation in c; a detailed derivation of the equilibrium equation is presented in the next section.

7. The internal moment is then determined by summing the moments of the internal forces about some convenient axis.

$$M = \int_{y=0}^{y=h} y' \sigma \, dA \tag{3.8}$$

where y′ is the moment arm of the force in a particuler element and the chosen reference axis. For programming convenience, the top surface of the concrete slab was selected for the reference axis. The above integral can be expressed in the following summation form:

$$M = \sum c_i \times d_{ic} + \sum s_i \times d_{is} + \sum (\ f_{pl_i} \times A_{pl_i} \ ) \times d_{pli} \tag{3.9}$$

where d_{ic}, d_{is}, and d_{pli} are the moment arms from the centroids of the concrete, steel, and CFRP elements, respectively.

8. The curvature, ϕ, is determined by computing the angle between the line representing the strain distribution and zero strain line (see Fig. 3.2).

$$\phi = \frac{\varepsilon_c}{c} \tag{3.10}$$

9. The above procedure will produce one point on the moment-curvature curve. The strain is incremented again and the procedure is repeated as in step 1 through 8 for additional points.

3.2.4 Neutral axis

As mentioned in step 6, the equilbrium of forces acting on the section (see Eq. 3.7) will result in a quadratic equation in c:

$$\sum c_i + \sum s_i + \sum f_{pl_i} \times A_{pl_i} = 0 \tag{3.7}$$

Or simply $$\sum F_i = 0 \tag{3.11}$$

where F_i is the force in the i^{th} element.

Before expanding the above equation, it should be mentioned that due to variation in strain distribution across the depth of the section, the following four cases are checked in order to calculate the coefficients of the quadratic equation as shown next.

Case(1) $0 < \varepsilon_s < \varepsilon_y$ and $0 < \varepsilon_c < \varepsilon_o$

Case(2) $0 < \varepsilon_s < \varepsilon_y$ and $\varepsilon_o < \varepsilon_c < \varepsilon_u$

Case(3) $\varepsilon_s \geq \varepsilon_y$ and $0 < \varepsilon_c < \varepsilon_o$

Case(4) $\varepsilon_s \geq \varepsilon_y$ and $\varepsilon_o < \varepsilon_c < \varepsilon_u$

Case (1)

$$\sum F_i = 0$$

$$F_i = \sigma_i \times A_i$$

$$\sum F_i = \sum f_{pli} \times A_{pli} + \sum f_{is} \times A_{is} + \sum f_{ic} \times A_{ic} = 0 \qquad (3.12)$$

where subscripts c, and s refer to concrete and steel, respectively.

Using Hooke's law for the steel and CFRP (see Eq. 3.2), the equilibrium equation becomes

$$\sum \varepsilon_{pli} E_{pli} A_{pli} + \sum \varepsilon_{is} E_{is} A_{is} + \sum f_{ic} A_{ic} = 0 \qquad (3.13)$$

The strain at any element is given by Eq. 3.1, which is repeated here.

$$\varepsilon_i = \varepsilon_c \times (c - d_i)/c \tag{3.1}$$

Substitute the above relation for strain in the steel and CFRP elements; and the stress in concrete by the relation given by Eq. 3.4; Eq. 3.12 is rewritten as:

$$\sum \varepsilon_c \left(\frac{c - d_{pli}}{c}\right) E_{pli} A_{pli} + \sum \varepsilon_c \left(\frac{c - d_{is}}{c}\right) E_{is} A_{is}$$
$$+ \sum f_c'' \left[2\frac{\varepsilon_{ci}}{\varepsilon_o} - \left(\frac{\varepsilon_{ci}}{\varepsilon_o}\right)^2\right] \times A_{ic} = 0 \tag{3.14}$$

Substitute the value of ε_{ci} in terms of ε_c in the above equation.

$$\sum \varepsilon_c \left(\frac{c - d_{pli}}{c}\right) E_{pli} A_{pli} + \sum \left(\frac{c - d_{is}}{c}\right) \varepsilon_c E_{is} A_{is}$$
$$+ \sum f_c'' \frac{\varepsilon_c}{\varepsilon_o} \left(\frac{c - d_{ic}}{c}\right) \left[2 - \frac{\varepsilon_c}{\varepsilon_o} \left(\frac{c - d_{ic}}{c}\right)\right] A_{ic} = 0 \tag{3.15}$$

Multiply the above equation by c^2

$$\sum \left(c^2 - c d_{pli}\right) \varepsilon_c E_{pli} A_{pli} + \sum \left(c^2 - c d_{is}\right) \varepsilon_c E_{is} A_{is}$$
$$+ \sum f_c'' \frac{\varepsilon_c}{\varepsilon_o} \left(c^2 - c d_{is}\right) \left[2 - \frac{\varepsilon_c}{\varepsilon_o} \left(\frac{c - d_{ic}}{c}\right)\right] A_{ic} = 0 \tag{3.16}$$

Expanding and rearranging the terms in the above equation , the equation can be written in the following form.

$$A_1 c^2 + B_1 c + D_1 = 0 \tag{3.17}$$

where

$$A_1 = \left[(\varepsilon_c E_{is} A_{is}) + (\varepsilon_c E_{pli} A_{pli}) + A_{ic} f_c^{"} \left\{ 2\left(\frac{\varepsilon_c}{\varepsilon_o}\right) - \left(\frac{\varepsilon_c}{\varepsilon_o}\right)^2 \right\} \right] \tag{3.17a}$$

$$B_1 = -\left[(\varepsilon_c E_{is} A_{is} d_{is}) + (\varepsilon_c E_{pli} A_{pli} d_{pli}) + 2A_{ic} f_c^{"} d_{ic} \left\{ \left(\frac{\varepsilon_c}{\varepsilon_o}\right) - \left(\frac{\varepsilon_c}{\varepsilon_o}\right)^2 \right\} \right] \tag{3.17b}$$

$$D_1 = -A_{ic} f_c^{"} \left(\frac{\varepsilon_c}{\varepsilon_o}\right)^2 d_{ic}^2 \tag{3.17c}$$

Similarly, the other three cases will result in quadratic equations as illustrated in Appendix A. The contribution from all four cases will result in the general quadratic equation:

$$A c^2 + B c + D = 0 \tag{3.18}$$

where

$$A = \sum_{i=1}^{4} A_i \quad , \quad B = \sum_{i=1}^{4} B_i \quad , \quad D = \sum_{i=1}^{4} D_i$$

where i is the case number.

The coefficients A, B, and D are found by summing up the contribution from each element of the section depending on the state of strain in the element or slice. As was shown previously, the various cases of strain will result in different terms that will make up the coefficients in the quadratic equation. This equation is solved once the strains and stresses in each element of the section are calculated and the values of A, B, and D are evaluated. The

new value of c is compared to the previous value of c and the procedure is repeated until the solution converges to the defined tolerance.

3.2.5 Computer program

Due to the iterative nature of the above procedure, a computer program using FORTRAN 77 code was developed to perform the above analysis. The program (which is included in Appendix B) was written in an interactive mode and requires very minimal input data. Running the program will require input of the section geometry, which include the thickness and width of concrete slab; the thickness and width of the steel beam flanges and web; the number of CFRP layers; and the area of the CFRP plates and their location. It will also require the input of the following material properties: the concrete compressive strength; the concrete ultimate crushing strain; the steel yield strength and modulus of elasticity; and the CFRP ultimate stress and modulus of elasticity. When the midspan deflections are required, as discussed in the next section, it is also required to input the span length of the beam and the positions of the loads. Output of the program will include strains; location of the neutral axis; moments and curvatures; and loads and midspan deflections.

3.2.5.1 Validation of the computer program

To validate the analytical procedure and the computer program, the moment-curvature relation of a W8x15 beam section (bare beam) and the same beam section acting compositely with a reinforced concrete slab was calculated using conventional strength of materials methods. Figure 3.3a compares the moment-curvature relation of the bare beam section obtained from the computer program and the relation calculated using strength of

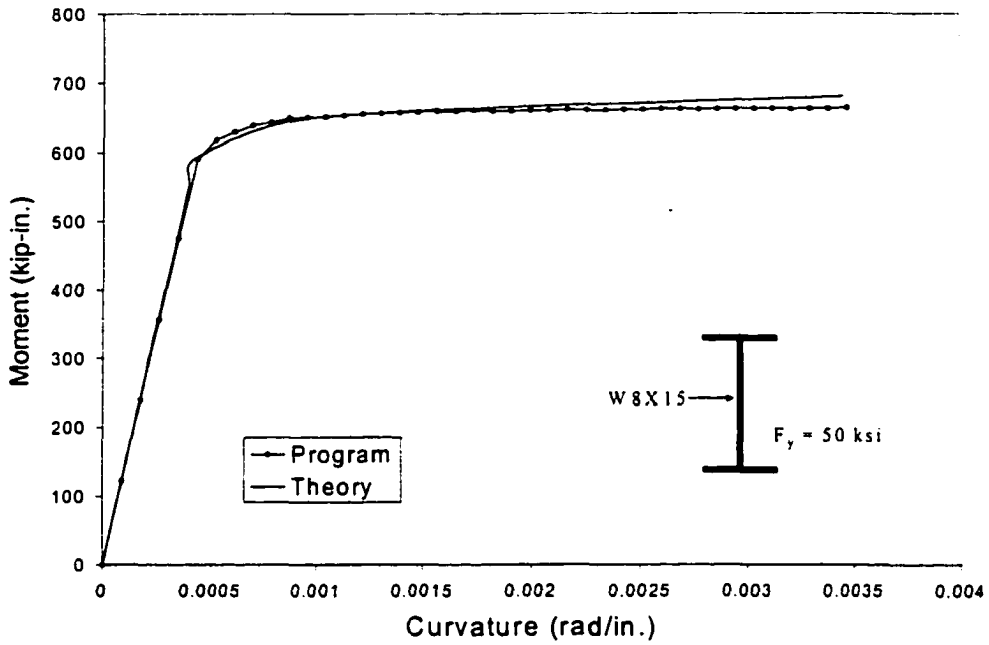

a. steel beam

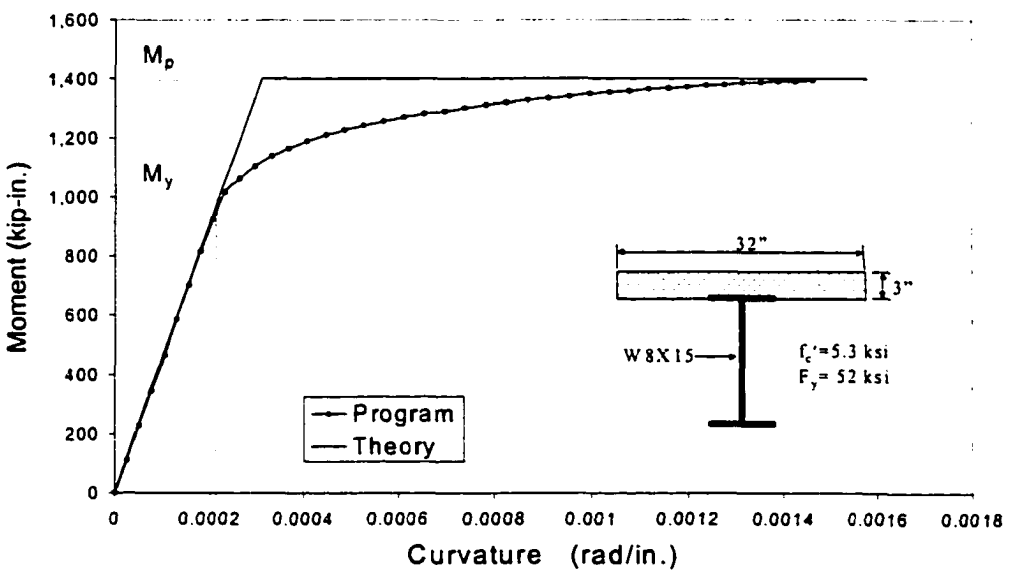

b. composite beam

Figure 3.3. Moment-Curvature relations of various beam sections used to validate the computer program.

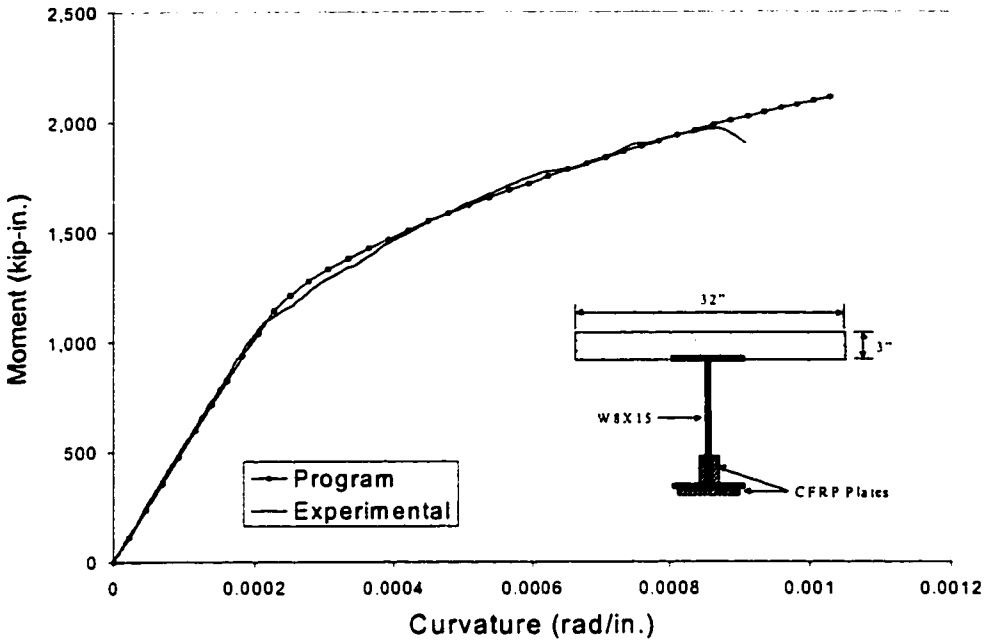

c. Composite beam strengthened with CFRP

Figure 3.3. Continued.

materials method. The calculated ultimate moment (plastic moment) of this beam was 675 in-kip (56.25 ft-kip), which was very close to the tabulated values of plastic moment of this section listed in the AISC LRFD manual of steel construction [29], which is 680 in.-kip (56.6 ft-kip). The ultimate curvature was based on ultimate steel strain of 0.02 (i.e. neglecting strain hardening), which is approximately ten times the yield strain. Comparison of the two curves in Fig. 3.3a shows a very good agreement between the computer generated and the calculated curves.

For the composite section, the moment-curvature relation generated by the computer program is compared with the idealized bi-linear relation calculated using conventional strength of materials method, which simplifies the relation as elastic-perfectly plastic; this is

illustrated in Fig. 3.3b. The cross-section of this beam is shown in the same figure: a W8 x 15 steel beam and a 32 in. wide by 3 in. thick composite concrete slab. The assumed yield stress of the steel beam and the concrete compressive strength are 52 ksi and 5.3 ksi, respectively. The idealized curve is normally used because of the difficulty of developing the curve manually due to the complexity of the geometry of the section and the stress distribution in the non-linear stages. Each point in the moment-curve, in the in elastic range, requires several iterations before finding the correct neutral axis that satisfies the equilibrium of forces acting on the section. This becomes even more difficult when considering the contribution of the CFRP plate force in the section. For example, the ultimate moment of a composite section is easily calculated by assuming that the entire steel beam section has yielded and the concrete stress in the deck slab is approximated by the well-known Whitney's stress block. However, if the section is strengthened with CFRP plate(s), the force in the CFRP plate can only be determined from equilibrium and strain compatibility requirements as in the elastic analysis. This is again a trial and error process that is best determined by a computer program such as the one proposed in this study.

Figure 3.3c compares the moment curvature of the same section shown in Fig. 3.3b that was strengthened with CFRP plates attached to the bottom flange and the bottom part of the web. The program results are compared to the experimental results (discussed in Chapters 5 and 6) since there is no theoretical procedure available in the literature for the analysis of this section. Again a very good agreement between the experimental moment-curvature relation and the predicted curve using the computer program is observed. It therefore can be concluded that the computer program can be used for the analysis of a general composite beam section strengthened with CFRP plate(s).

3.3 Midspan deflections

In the previous section, the moment –curvature response was developed which is needed for calculating the member deformations. The analytical model for calculating midspan beam deflections is presented in this section. The method presented herein is based on the well-known principle of the virtual work and a numerical integration technique.

In order to calculate the midspan deflections due to the applied loads shown in Fig. 3.4, a virtual load of unit magnitude is applied at the midspan. From conservation of energy principle, the external work should be equal to the internal work.

$$W_e = W_i \tag{3.19}$$

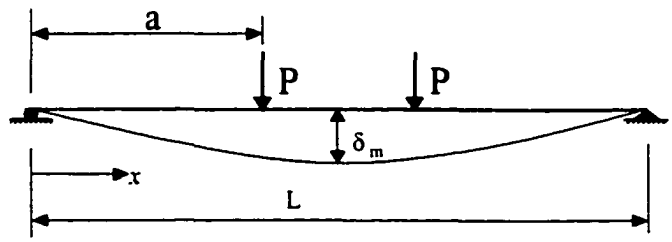

Figure 3.4 Applied loads used in calculating midspan deflections.

From Eq. 3.19, the midspan deflection is determined as

$$\delta_m = \int_0^L \phi(x)\ m(x)\ dx \tag{3.20}$$

where $\phi(x)$, $m(x)$ are the real curvature and virtual moment, respectively.

To evaluate the above integration, a numerical integration method must be used due to the non-linear relation of M-ϕ at large loads. For higher accuracy, Simpson's rule is used to carry out the numerical integration. According to Simpson's method, the integral of any function $F(x)$ may be written as in the following relation

$$\int_0^L F(x)dx = \frac{\Delta x}{3}(F_0 + F_n + 2\sum_{n=2}^{n-2} F_{even} + 4\sum_{n=1}^{n-1} F_{odd}) \tag{3.21}$$

where

Δx = interval length

F_0 = value of $F(x)$ at $x = 0$

F_n = value of $F(x)$ at $x = L$

F_{even} = value of $F(x)$ at even intervals

F_{odd} = value of $F(x)$ at odd intervals

Replacing $F(x)$ in Eq. 3.21 with $\phi(x)m(x)$, the procedure of evaluating the midspan deflections for the entire loading range can be summarized as follows:

1. Divide the beam into n number of uniform segments or intervals having a length of Δx as shown in Fig. 3.5.

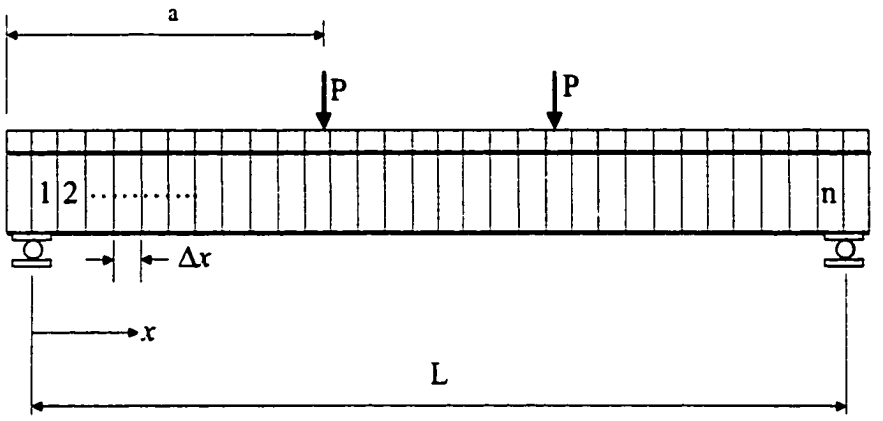

Figure 3.5. Subdivision of the beam used in the numerical integration.

2. Apply the load P, which is taken as a fraction of the ultimate load capacity of the beam P_{ult}
3. Calculate the moment, $M(x)$, at the boundary of each interval
4. Find the corresponding curvature, $\phi(x)$, based on the analysis of section 3.2. A linear interpolation is used when the value of $M(x)$ falls between two discrete points determined in the previous section(see section 3.2)
5. Perform the numerical integration using Eq. 3.21; this will produce one point on the load-deflection curve
6. Increment the value of P and repeat steps 1 through 5 until the failure load, P_{ult}, is reached.

The computer program discussed previously (see section 3.5.2) was modified to carry out the above analysis, which is presented in Appendix B. The analysis presented in the previous section was verified using the experimental results that will be presented and discussed in the next chapters (i.e. Chapters 4, 5,and 6). Figure 3.6a shows a comparison of the predicted midspan deflections with the experimental midspan deflections of one of the

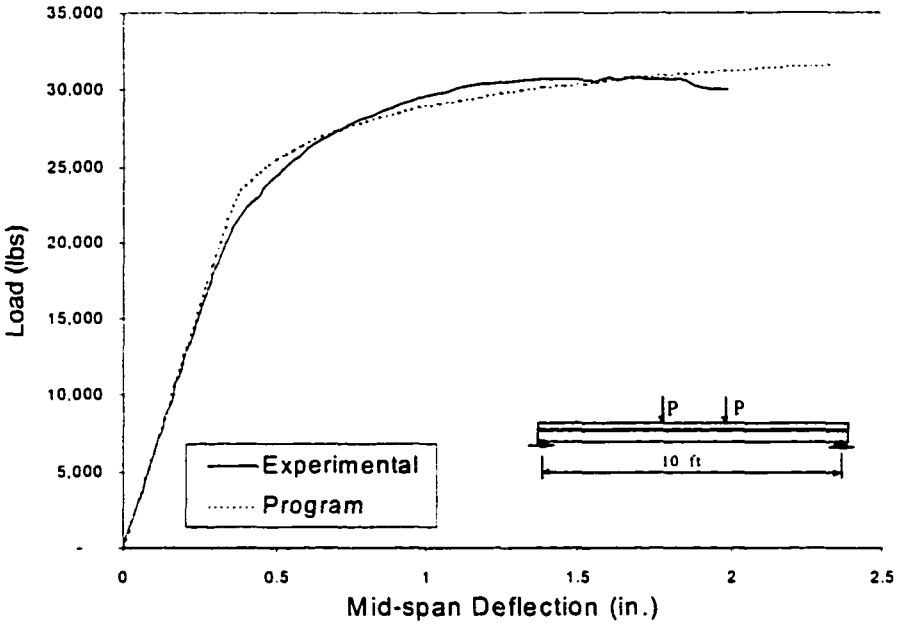

a. Midspan deflections of Beam U

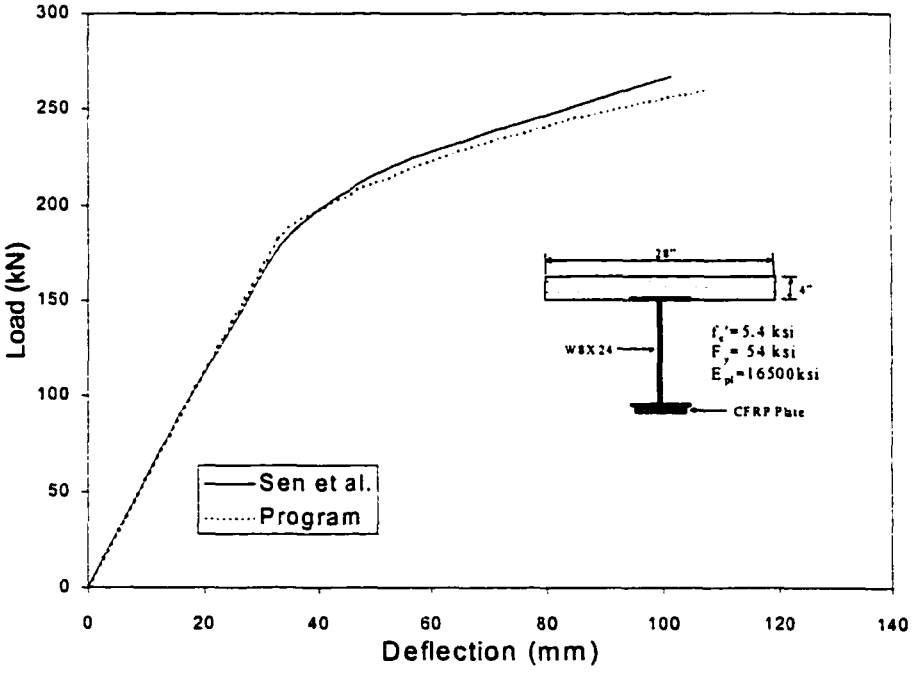

b. Midspan deflection of the beam tested by Sen et al. [30].

Figure 3.6. Validation of the analytical midspan deflections by comparison with experimental test results.

tested beams that has the same cross-section previously presented in Fig. 3.3b. Midspan deflection in the elastic range was also calculated using conventional beam theory for an applied load of 20,000 lbs, which was found to be 0.3 in. compared to 0.32 in. found from the experiment. However, in the inelastic range, the analytical results were compared with the experimental results as shown in Fig. 3.6a. This figure shows a very good correlation between the predicted and the experimental response.

The only work that was found in the literature dealing with the use of CFRP plates to strengthen steel composite beams was by Sen et al. [30]. In the reported article, the composite beam consisted of a W8x24 steel section and a 28 in. wide by 4 in. thick composite reinforced concrete slab. The beam was strengthened with 2 mm (0.079 in.) thick CFRP plate attached to the full width (6.5 in.) of the bottom flange of the steel beam. The ultimate strength and modulus of elasticity of the CFRP plate were 267 ksi and 16,500 ksi, respectively; the yield strength of the steel beam and the compressive strength of the slab concrete were 45 ksi and 6 ksi, respectively. A four point bending was used to test the beam with a span length of 20 ft and a shear span of 8 ft. Figure 3.6b shows the experimental load-midspan deflection reported by Sen et al. [30] and the analytical deflection determined by the computer program. As may be seen in this figure, the correlation between the experimental and the analytical responses is very good which further validates the proposed analytical procedure.

3.4 Parametric study

As seen in the previous section, the analytical results were verified with the experimental results, which will be shown in a more detail in the next chapters. In this

section, a parametric study is presented which investigated the influence of some of the important parameters on the behavior of the section. This includes the effect of the concrete concrete compressive strength; the yield strength of the steel beam; the stiffness of the CFRP plate; the thickness of the CFRP plate; the ultimate strain of the CFRP plate; and the area of the bottom flange of the steel beam. The effect of each of these parameters will be discussed in the following sections.

In order to select a realistic beam section, the Iowa DOT standard bridge plans were reviewed for the various bridge sections. For small span bridges (< 50 ft), the section shown in Fig. 3.7 was commonly used in bridges. A slab thickness, h_{slab}, of 7.5 in. was assumed based on an average of the slab thickness of the various bridge sections that ranged between 6.5 and 8.75 in. The effective slab width, b_{eff}, was calculated based on the following relations (according to AASHTO [31]):

$$b_{eff} \leq \begin{cases} \bullet \text{ stringers spacing} \\ \bullet \text{ span length / 4} \\ \bullet\ 12 * h_{slab} \end{cases}$$

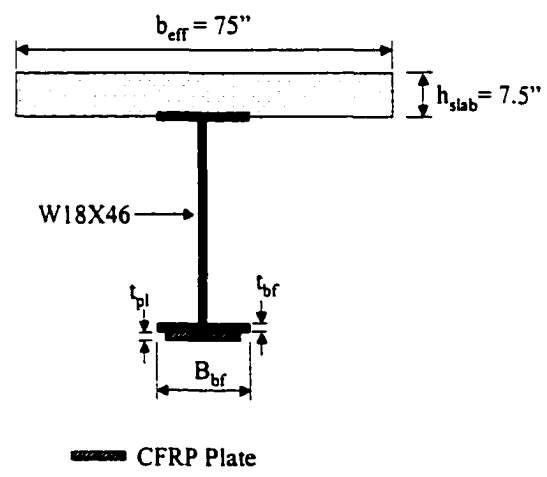

Figure 3.7. Beam cross-section used in the parametric study.

Based on the standard bridge plans, a 75 in. effective width of concrete slab was found to reasonably represent the effective width of short simple span bridges.

3.4.1 Effect of the bottom flange damage

Since corrosion mainly affects the bottom flange of the steel girders of bridges, the width of the bottom flange, B_{bf}, was varied between 6.0 (undamaged) and 1.5 in. to simulate damage caused by corrosion. Figure 3.8a shows the moment curvature plots for an undamaged section, which is labeled by B_{bf}, and damaged sections with the level of damage varied between 25 to 75 percent. For instance, the curve that is labeled with 0.75 B_{bf} basically means that the width of the bottom flange was reduced by 25 percent. As may be seen in this figure, that for small damage (25%), no significant reduction in the elastic stiffness is observed; however, the strength was reduced by approximately 10%. On the other hand, both the stiffness and the strength are considerably reduced for severe damage (i.e. 75 percent), but a more ductile behavior is observed in the damaged sections. The effect of damage on strength is also shown in Fig. 3.8b, which shows a linear relation between strength and damage. As may be seen in this figure, when the damage in the bottom flange is 75%, the ultimate moment of the section is reduced by approximately 32%. In other words, the ratio between the damage in the bottom flange and the reduction in the section ultimate moment is approximately 2.5:1.

3.4.2 Effect of CFRP ultimate strain

The ultimate strain of the CFRP plate depends on the type and the stiffness (modulus of elasticity) of the plate. It is defined as the strain at which the CFRP plate will rupture.

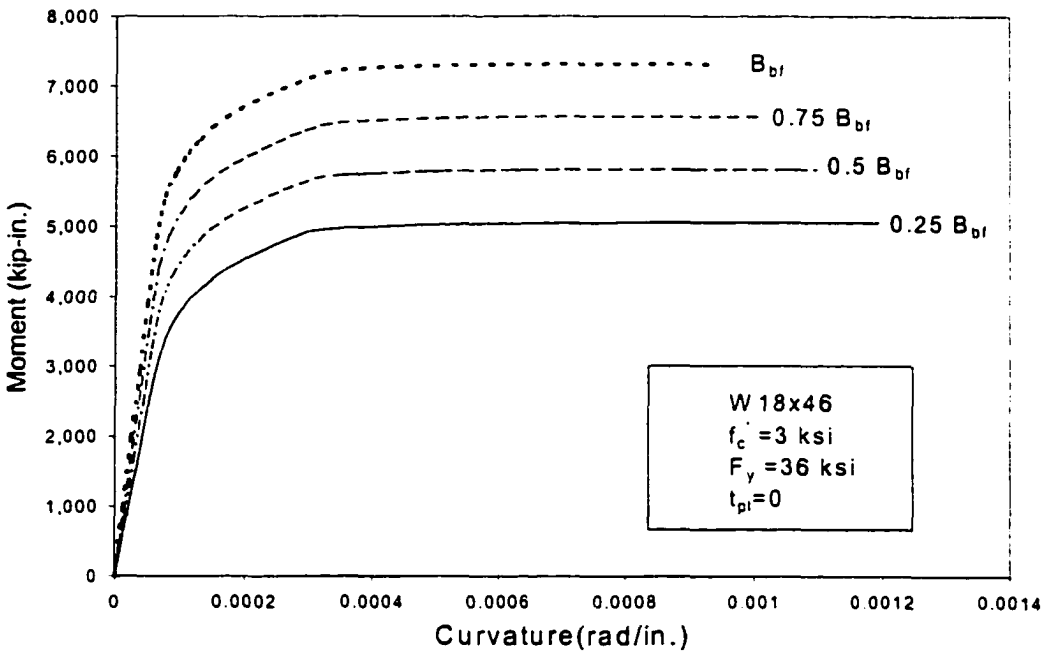

a. Moment vs. curvature

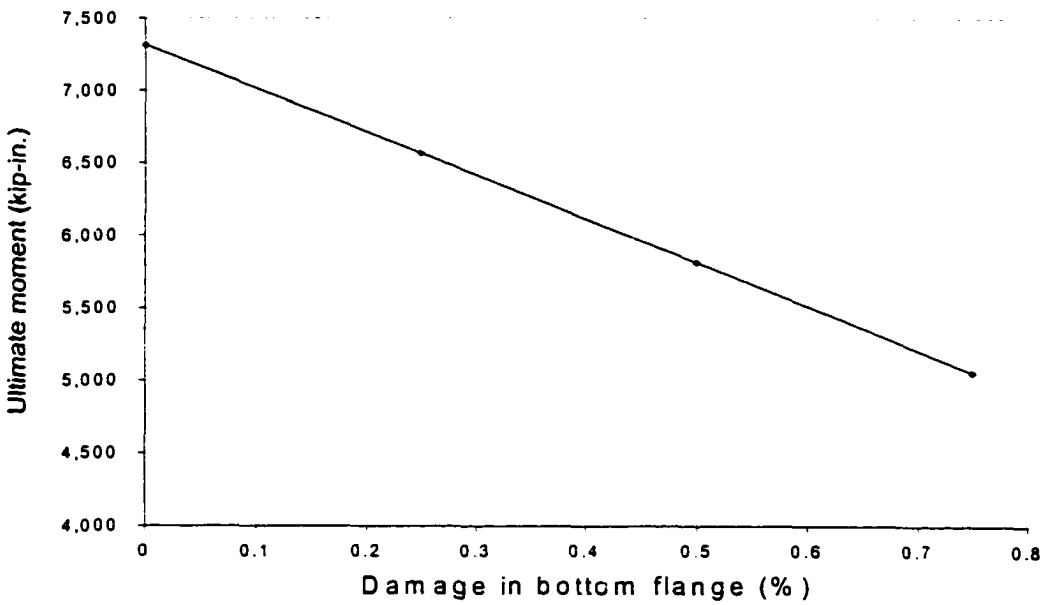

b. Moment vs. damage

Figure 3.8. Effect of damage in the bottom flange on the section behavior.

If the CFRP plate has a high ultimate strain, a more ductile failure is expected due to the large deformation the section (or the member) will experience provided the bond between the CFRP plate and the steel remains intact. It is desired in certain situations to impose a limit on the CFRP ultimate strain; one situation is when the shear stresses in the adhesive layer is to be limited to prevent shear failure. In this case, the maximum strain is the limiting strain rather than the strain causing rupture

In this study, the range of ultimate strain was varied between 0.5 percent and 1.5 percent as practical minimum and maximum limits. Moment and curvature relations for limiting CFRP strains of 1% and 1.5 % are shown in Figs. 3.9a and 3.9b. As may be seen in this figure, the strength of the section increases with the increase of the CFRP plate thickness; the section stiffness (in the inelastic range) also increases with the increase of the plate thickness. It is observed that the behavior is more ductile when the limiting strain is taken as 1.5 % instead of 1%. However, the strengthened sections for both strain limits displayed a less ductile behavior than the unstrengthened section (i.e when t_{pl}=0.0 mm).

The relation between the ultimate moment of the section and the ultimate strain in the CFRP is shown in Fig. 3.9c; the continuous line is for an unstrengthened section and the dashed lines are for strengthened section with CFRP plates having a thickness ranging between 1 mm and 6 mm. As may be observed in this figure, the ultimate moment of the section increases linearly for ultimate strains less than 1%; however, the relation becomes non-linear beyond this strain. For strain less 1%, the mode of failure is controlled by the CFRP ultimate strain; however, for strains higher than 1%, the mode of failure is controlled by the CFRP ultimate strain for plate thickness less than 4 mm and by crushing of concrete for the thicker plates. It should be noted that the relation becomes non-linear beyond

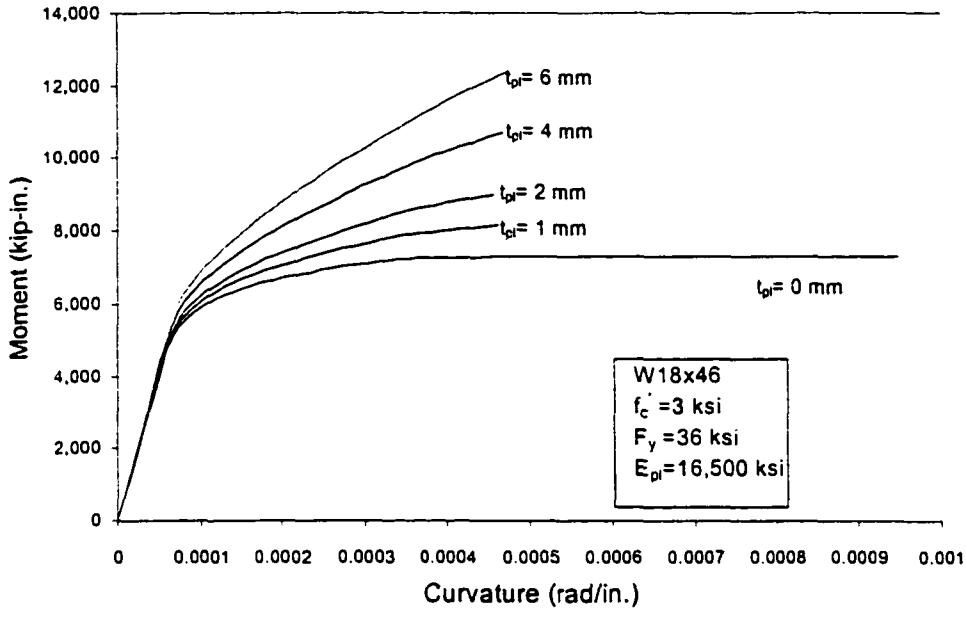

a. Moment vs. curvature (CFRP limiting strain = 1 %)

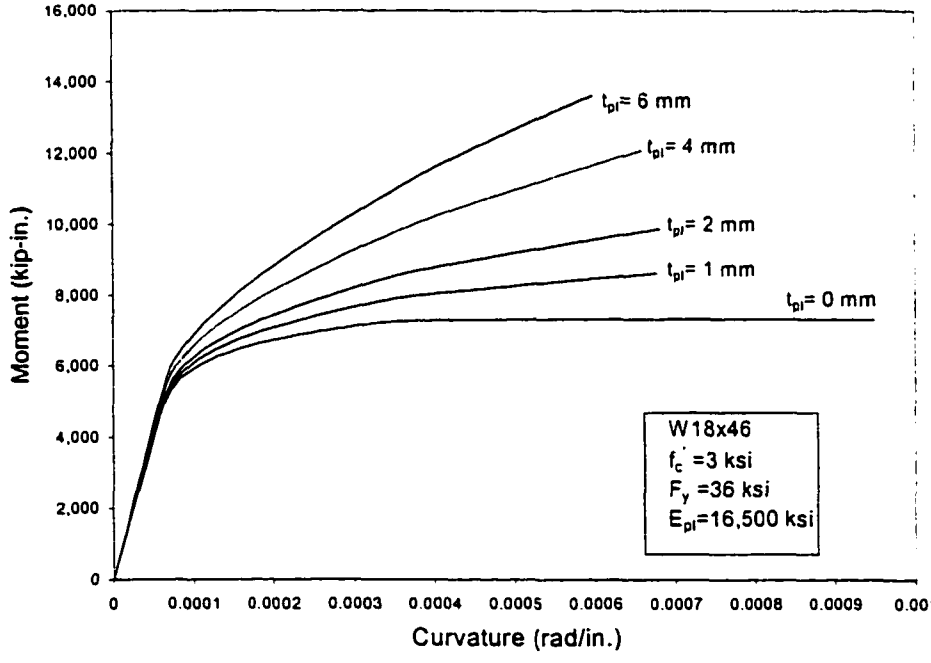

b. Moment vs. curvature (CFRP limiting strain = 1.5 %)

Figure 3.9. Effect of the CFRP ultimate strain on the section behavior

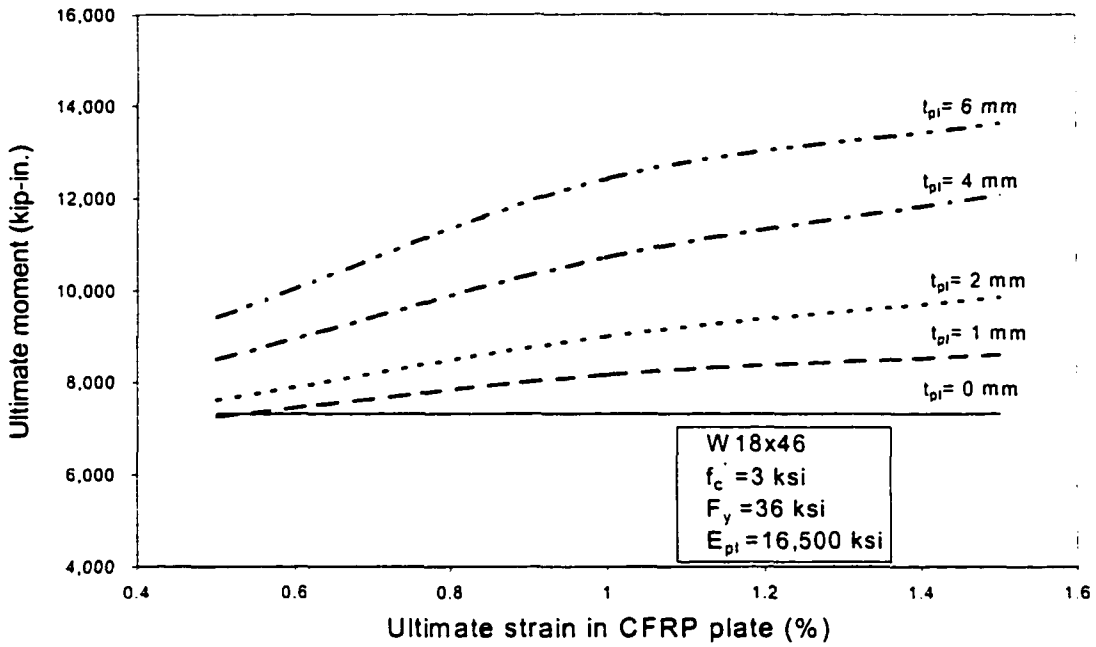

c. Moment vs. CFRP strain

Figure 3.9. Continued.

1 % strain because the section undergoes large plastic deformation (yielding); thus, the increase in the ultimate moment is not as significant as for strains less than 1%. It is worth mentioning, as will be shown in the next chapters, that the measured ultimate strains in the CFRP plates in the beams tested were found to be around 1%. Thus, in the next sections the ultimate strain in the CFRP is assumed to be 1%.

3.4.3 Effect of the modulus of elasticity of the CFRP plate

CFRP plates are made for different applications and with different fiber to matrix ratios. Therefore, the CFRP plates come with different modulus of elasticity (MOE) and plate thickness; the effect of this combination on the behavior of the section should be investigated

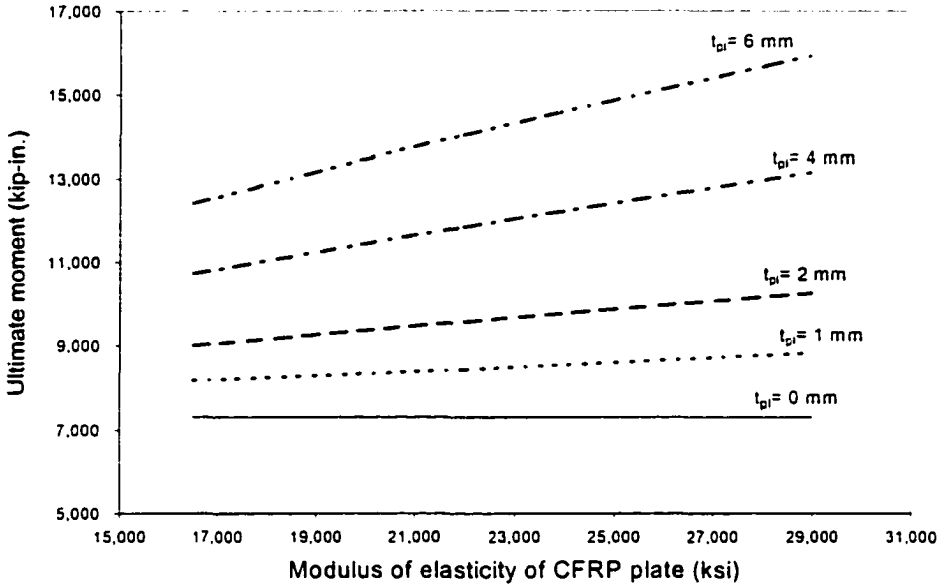

Figure 3.10. Effect of the modulus of elasticity of the CFRP plate.

so that one can select a suitable strengthening scheme. Figure 3.10 shows the effect of the CFRP MOE on the ultimate moment of the section; the MOE was varied between 16,500 ksi and 29,000 ksi. This figure shows that the ultimate moment increases linearly with the increase of the MOE of the plate, but the increase is higher (steeper slope) in the case of thicker plates. It should be noted, however, that it is more efficient to achieve the required strength by using a combination of a thin plate with high stiffness rather than using a thick plate with low stiffness. This is due to the fact that peeling stresses at the end of the bonded CFRP plate will increase with the increase in CFRP plate thickness.

3.4.4 Effect of the concrete compressive strength

The concrete compressive strength was varied between 3 and 6 ksi. Figure 3.11a shows the effect of the concrete compressive strength on the behavior of the section; in this

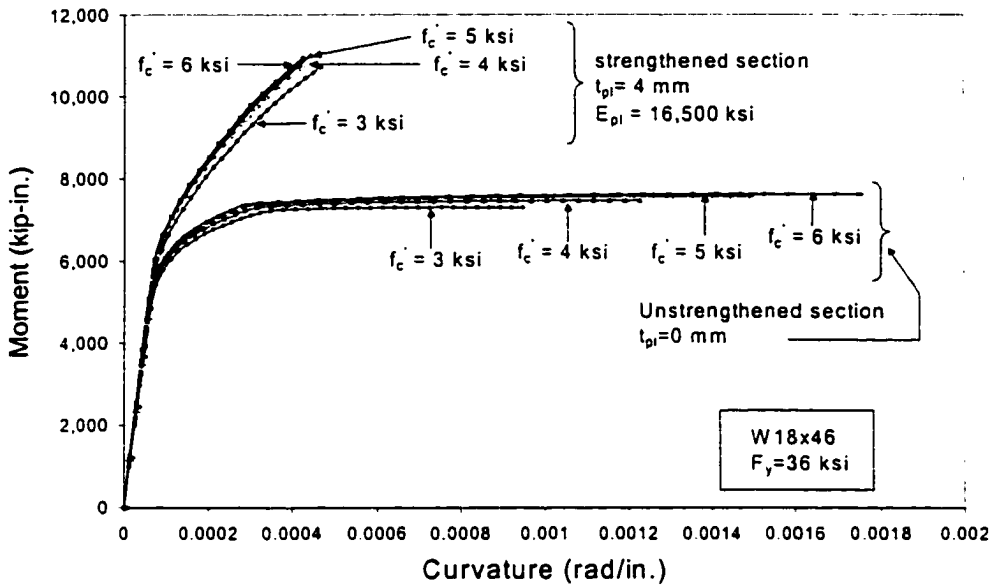

a. Moment vs. Curvature

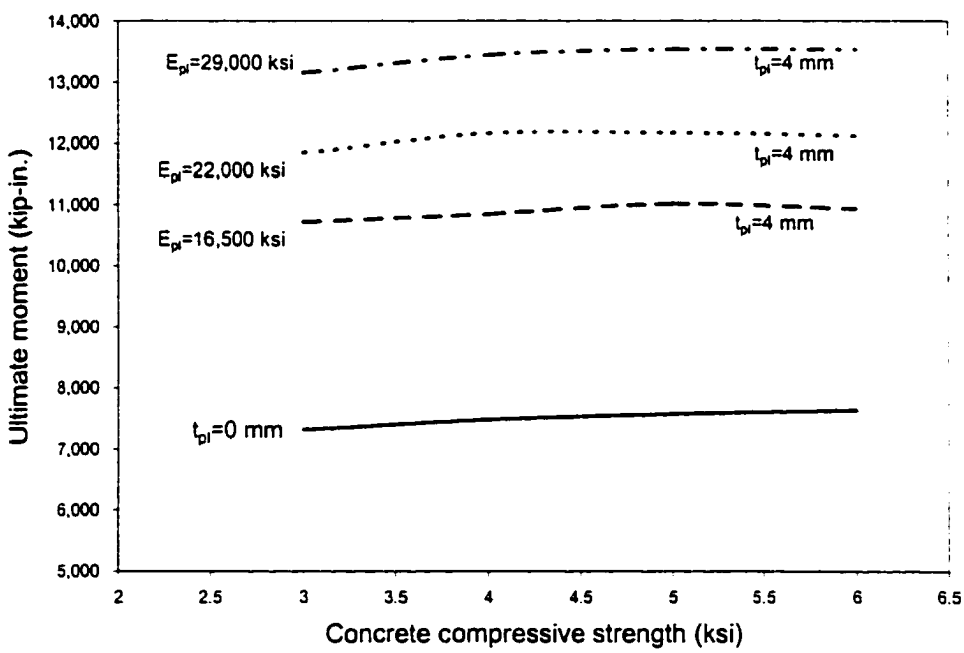

b. Moment vs. compressive strength

Figure 3.11. Effect of concrete compressive strength on the section behavior.

figure one sees that an increase in the concrete compressive strength in the unstrengthened sections (t_{pl} =0.0) will slightly increase the strength of the section. In addition, the ductility will increase with the increase in the compressive strength. In the strengthened sections, a 4 mm thick CFRP plate was used; the response of the strengthened section is also shown in Fig. 3.11a. As seen in this figure, no significant increase in strength is observed with the increase in the concrete compressive strength; it is also observed that the ductility of the strengthened sections is smaller than the unstrengthened sections. Figure 3.11b shows that the strength is significantly increased with an increase in the MOE of the CFRP plate, but is essentially independent of the concrete compressive strength.

3.4.5 Effect of the steel yield stress

Three different yield stresses were investigated: 36, 43, and 50 ksi. Moment and curvature relations for strengthened and unstrengthened sections are shown in Fig. 3.12a. As may be seen in this figure, for unstrengthened sections (t_{pl}=0.0 mm), the increase in the yield stress will increase both the stiffness and the strength; however, the ductility is reduced with the increase in the yield stress. Strengthened sections (t_{pl}=4.0 mm) on the other hand show an increase in the strength, but show a reduction in ductility in comparison with unstrengthened sections. The observed reduction in ductility was due to the limiting CFRP strains (i.e. failure of the section was due to the CFRP rupture). It is noted however, that the gain in strength is slightly higher for sections with a lower yield stress. This can be seen in Fig.3.12b, which compares the strengthening effect due to yield stress variation and the CFRP modulus of elasticity.

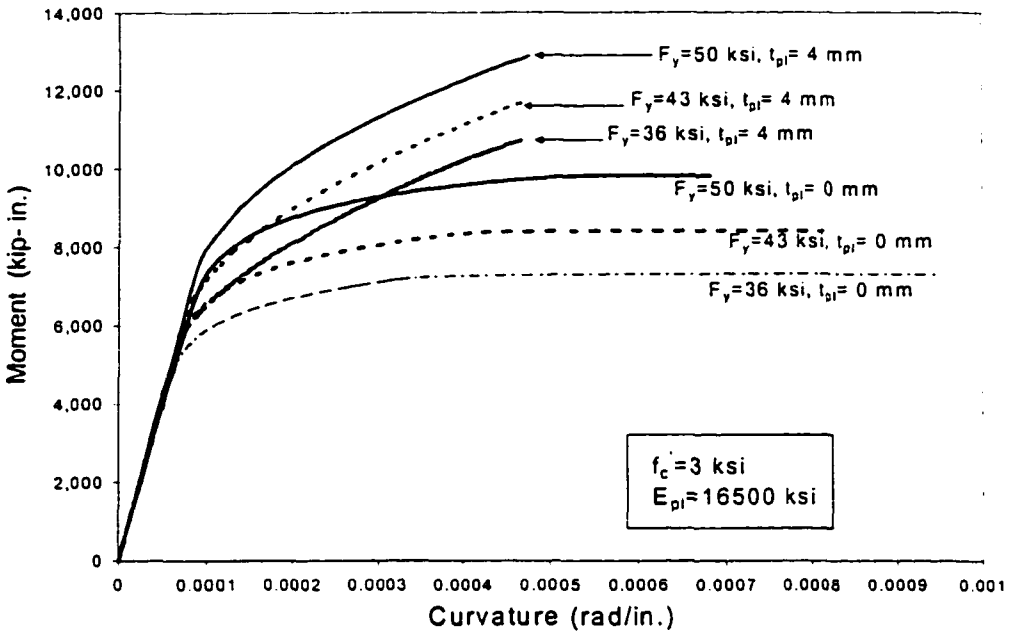

a. Moment vs. curvature

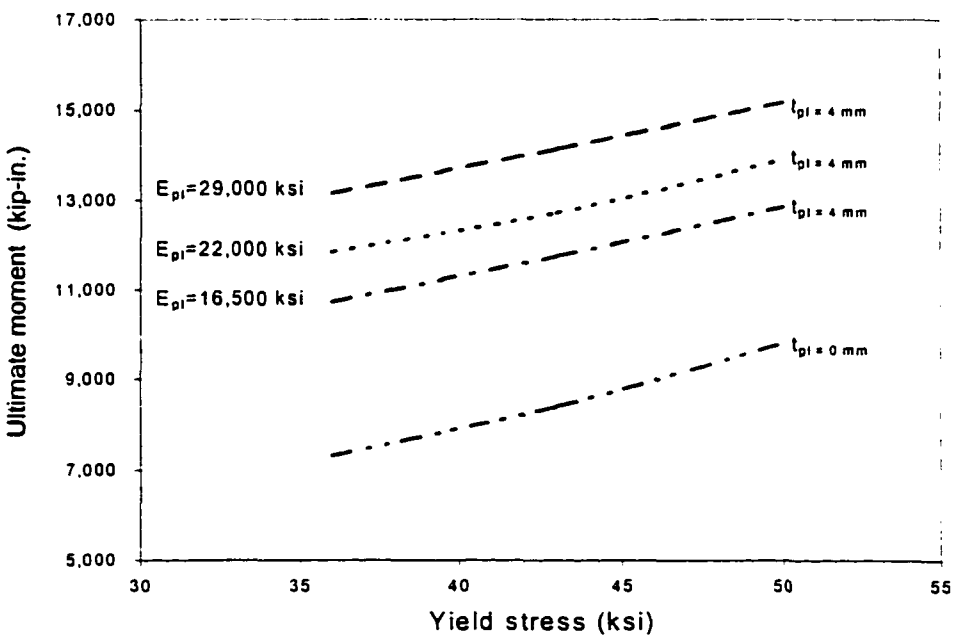

b. Moment vs. yield stress

Figure 3.12. Effect of yield stress on the section behavior.

3.5 *Damage analysis of a bridge system*

The foregoing analysis was focusing on the analysis of a single beam. However, before the decision is made on what type of strengthening or repair scheme to use, it is necessary to analyze the effect of damaged member(s) on the overall behavior of the bridge system. Although it is relatively simple to analyze a single beam in the inelastic range, it is a very complex and tedious task to run a nonlinear analysis on a bridge system. Even the current AASHTO (1994) LRFD design [32], which is based on ultimate design, uses simplified equations to determine the transverse load distribution that are based on elastic analysis. In this section, elastic analyses using the grillage method will be utilized to investigate the effect of damaged beam members on load distribution. In other words, how a damaged member(s) (due to corrosion for example) will affect the overall behavior of the bridge system? The intent here is to present a methodology for determining the required repair or strengthening system. This analyses can be applied to any slab-girder bridge; for demonstration of the methodology a bridge from Barker [33] was selected. This bridge is a single span with a span length of 35 ft and a cross section that is shown in Fig. 3.13.

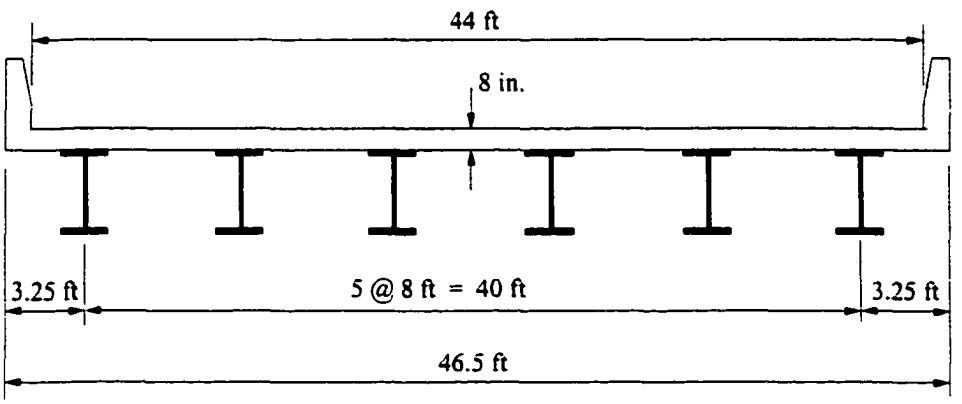

Figure 3.13. Cross-section of a slab-girder bridge.

3.5.1 Grillage Idealization of slab-girder bridge

The idealization of a bridge system, in this case a slab-girder bridge without diaphragms, by an assembly of interconnected beams is referred to as a 'grillage'. One reason for selecting the grillage method is its simplicity, which any practicing engineer will find conceptually easy to understand. It is true that finite element method is considered by far a more rigorous and accurate method. However, many practicing engineers do not have the expertise of using the method and it is quite expensive to develop accurate finite element models due to the time required to build the model as well as the requirements of sophisticated software and hardware. Furthermore, the output from the finite element analysis is normally in the form of element stresses which further requires post-processing to find the moments in the critical members, which in many cases has to be done manually. On the other hand, it is extremely easy for the engineer to visualize and prepare the data for a grillage provided that he or she has the basic background on the proper ways of idealizing the bridge structure and determining the appropriate section properties of the grillage members. In this section, a brief background of the grillage method is presented and a list of references that deal thoroughly with the subject of grillage modeling is also discussed.

One of the most comprehensive treatments of the grillage method subject is presented by Hambly [34]. This reference provides basic guidelines on the formulation of the grillage models for different bridge types. The basic idea behind this method is replacing the three dimensional nature of the bridge system by a two dimensional grid of intersecting members. In the longitudinal direction, the steel beam and part of the deck slab are replaced by an equivalent member which has section properties obtained from the contribution of the beam and the deck slab. In the transverse direction, a tributary width of the slab is replaced by an

equivalent member with the properties of that of the chosen tributary slab. A slab-girder type bridge can be idealized by one of two forms, the plane grillage or the downstand grillage as shown in Fig. 3.14. The plane grillage consists of coplanar longitudinal and transverse members; this idealization ignores the difference between the centroids of the intersecting members. On the other hand, the downstand grillage takes into account the difference in height between the intersecting members by using rigid links to connect these members as shown in Fig. 3.14b. In this study, the plane grillage idealization was used and the subsequent discussion will focus on this idealization only.

To determine the appropriate mesh size of the grillage, Hambly [34] recommends that the longitudinal grillage members should be placed coincident with the centerlines of the prototype's beams. However, due to the poor characteristics of the girder-slab bridges, the longitudinal grillage members should not be placed further apart than 1/10 of the span. In the case of widely spaced beams, notional longitudinal members should be placed between the members coinciding with the actual beams. Additionally, the exterior longitudinal grillage members shall have different section properties than the interior members to reflect the effect of the edge stiffening resulting from the barrier walls. In the transverse direction, the number of the transverse members is somewhat arbitrary, but he suggested a spacing of 1/4 to 1/8 of effective span.

West [35] conducted an extensive study on the use of grillage idealization of bridge structures. In this study, he compared the experimental results of 53 bridge decks of different types with the results obtained from the grillage analysis. The comparisons were made between deflections, longitudinal and transverse bending moments, and reactions. He concluded that the agreement between the results for all the grillage and the experiments

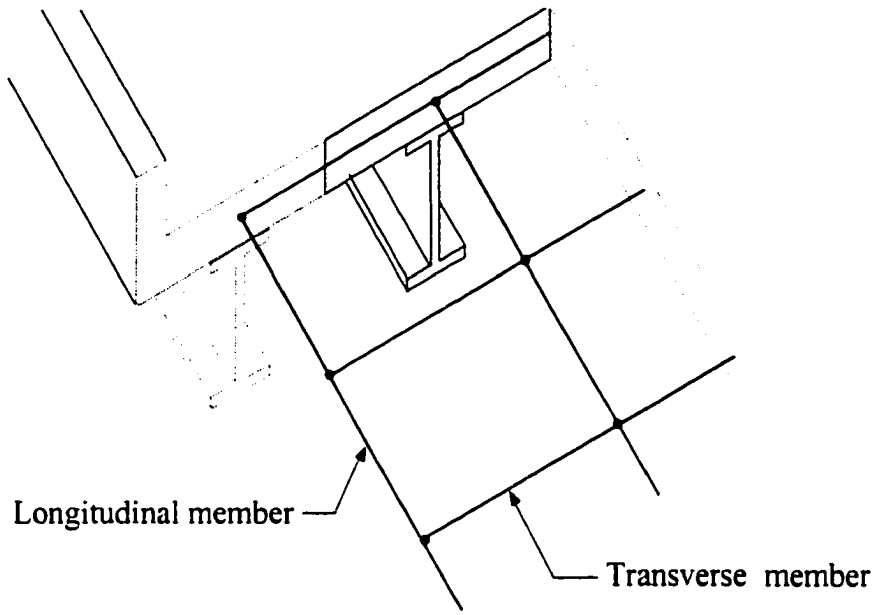

a. Plane Grillage

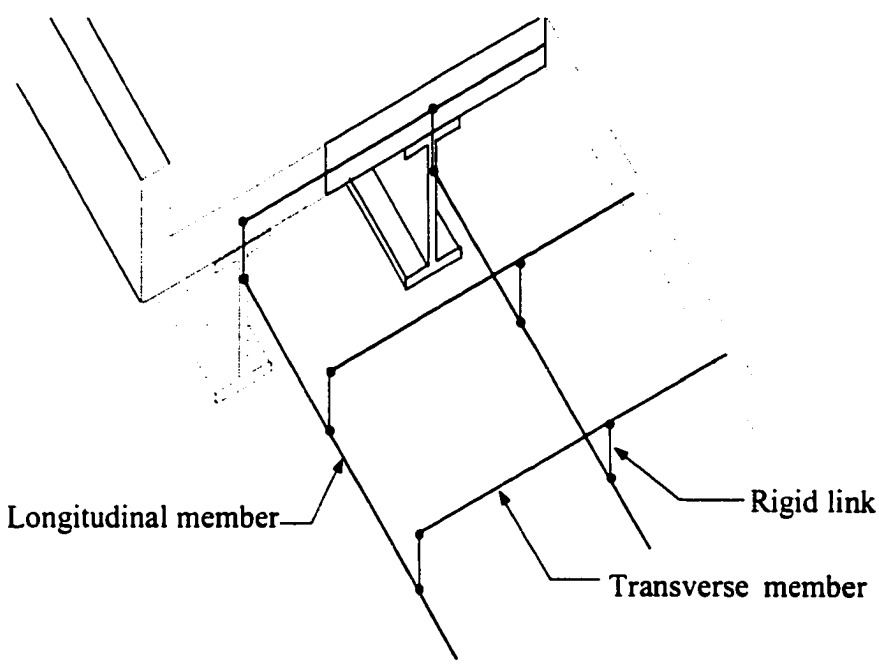

b. Downstand grillage

Figure 3.14. Grillage idealization of slab-girder bridge.

were remarkably good. The conclusions of this study were formulated in a set of design recommendations, which were published in Reference 36. The recommendations by West [36] were similar to those given by Hambly [34]. However, West [36] recommends that all longitudinal grillage members should have the same sectional properties, which is based on an interior member section properties; this ignores the narrower effective width of the exterior girders. The justification here is that the stiffening effect due to the barrier wall will compensate for the narrower effective width. The effect of the edge stiffening can be significant as the case for short span. A study by Smith and Mikelsteins [37] on the effect of edge stiffening on bridge behavior considered different types of edge stiffening such as small curb, sidewalk, curb and parapet wall, barrier wall, etc. Three types of bridges were studied: slab-on-prestressed concrete girder, slab-on-steel plate girder, and prestressed concrete voided slab. Plane grillage idealization was used in this study. It was found that all types of edge stiffening significantly affected the edge beam bending moment and deflection at midspan; the bending moment increased while the deflection decreased due to the increased stiffness. Nevertheless, the effect decreases with the increase of the span length.

Other studies also dealt extensively with the grillage analogy in bridge analysis such as the ones presented by Jaeger [38] and Bakht [39]. Jaeger [38] provided guidance on the mesh layout, load idealization, and members with varying moments of inertia. Since the study presented in this section deals with the effect of damage of bridge girders, the work presented by Jaeger [38] and Bakht [39] provided some insight on modeling girders with variable moment of inertia. In the later reference [39], the grillage method was compared to a more rigorous mathematical analysis to study the response of bridges with girders of varying moments of inertia. There was a reasonable agreement between the results of both

analyses. This study gives one more confidence in using the grillage method for the analysis of damaged bridge system.

Other studies were also presented by several researchers [40-43] that compared the results of grillage analysis with that of a more accurate three-dimensional finite element analysis. In all of these studies, it was concluded that the grillage analysis could provide very comparable results to that of finite element method. Considering the time saving in constructing the grillage models, it is assumed that the results from grillage analysis can provide reasonable results in the global sense; however, if local effects are required, then the finite element modeling is more appropriate.

To construct the grillage model of the bridge, two important properties are required for the grillage members: the flexural moment of inertia and the torsional constant. These properties are evaluated as follows [33]:

Longitudinal members:

$$I_l = I_{girder} + e_g^2 A_{girder} \tag{3.22}$$

$$I_L = I_l \times n + I_{slab} \tag{3.22a}$$

$$J_l = \sum J_{girder} + J_{slab} \tag{3.23}$$

where, I = moment of inertia, e_g is the eccentricity of the girder centroid from the slab centroid, A_{girder} is the area of the girder, n is the modular ratio, and J is the torsional constant.

Transverse members:

$$I = bh^3/12 \tag{3.24}$$

$$J = bh^3/6 \tag{3.25}$$

where b is a unit width of slab, and h is the thickness of slab.

For longitudinal members, the moment of inertia, I_L, is calculated about the centroid of the slab; the members cross-sectional properties are calculated on a per unit length basis. These properties then multiplied by the center-to-center spacing of the members (tributary width) to obtain the members properties. The torsional constant, J, is taken as the sum of the torsional constant of the girder and the slab. Transverse grillage members represent the slab and the section properties are obtained by multiplying the unit width slab properties by the transverse tributary width.

The grillage mesh of the bridge from Barker [33] was selected so that the longitudinal elements will coincide with the bridge girders; also an equal number of elements was used in the transverse direction. The mesh size was identical to that used by Barker [33]. The HS20 AASHTO design truck was used as live load. Several load cases (that will cause maximum bending moments in the exterior girders as well as the interior girders) were investigated; these load cases are shown in Fig. 3.15a. Figure 31.5b shows the grillage mesh and the applied live load of case 1. Odd numbered cases are one lane loaded and even numbered cases are two lane loaded. Case 1 and case 2 were used to produce maximum moments (stresses) in the exterior girder (i.e. girder 1), while case 3 and case 4 were used to produce maximum moments in a typical interior girder (girder 3).

This bridge was first analyzed in the undamaged state (i.e. as is) to verify the analysis results; then an exterior or interior girder was "damaged." The analysis was completed using STAAD III [44], commonly used structural analysis software available in most design offices. The distribution factor, DF_i was calculated based on the total axle load of the truck and given by the following relation [33]:

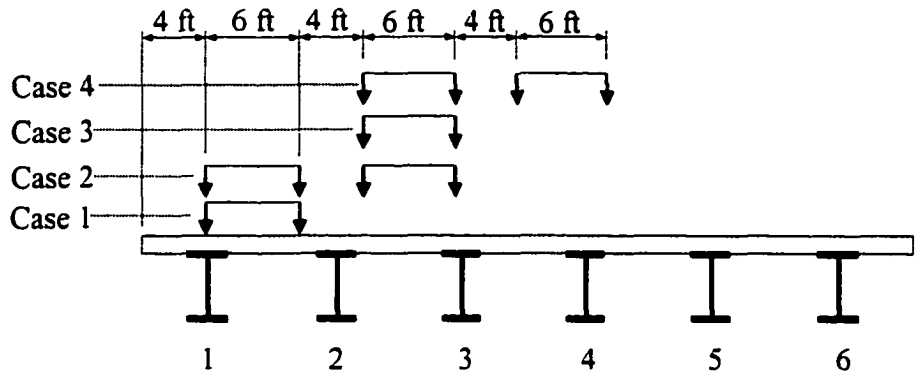

a. Load cases investigated

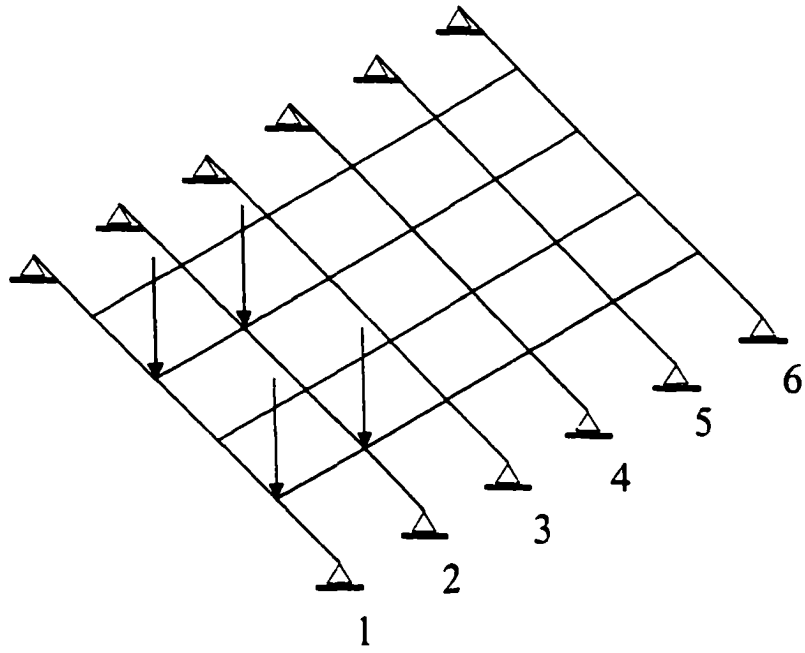

b. Grillage with loading case 1

Figure 3.15. Load cases investigated and the grillage idealization of the bridge.

$$DF_i = \frac{M_i}{\sum_{i=1}^{6} M_i} \tag{3.26}$$

where M_i is the maximum moment in the i^{th} girder.

Table 3.1 shows a comparison between the load distribution factors, as defined by Eq. 3.26 [33], obtained using STAAD III and the values published by Barker [33] for all load cases in the undamaged state of the bridge. As may be seen in this table, the results from STAAD III compare favorably with the data published by Barker [33]. Therefore, it can be concluded that the STAAD III can accurately predict the response of the bridge and can be used for the analysis of the damaged cases of the bridge.

The damage in the girder was simulated by reducing the area of the bottom flange; the reduction of the bottom flange area was varied between 24 and 83 percent, which corresponds to between 10 and 40 percent reduction in the moment of the inertia of the girder.

3.5.2 Distribution factors for the undamaged bridge

Figure 3.16 shows the load distribution for the undamaged bridge for all load cases. As may be seen in this figure, the maximum moments in the exterior girder (girder 1) are caused by cases 1 and 2; and the maximum moments in the interior girder (girder 3) are caused by cases 3 and 4.

Table 3.1. Distribution factors in the undamaged bridge.

Load case	Girder no.	Distribution Factor (STAAD III)	Distribution Factor (Barker [33])
1	1	0.58	0.57
1	2	0.35	0.34
1	3	0.08	0.10
1	4	-0.01	0.00
1	5	-0.01	-0.01
1	6	0.00	0.00
	Sum	1.00	1.00
	Total Moment (ft-Kips)	358.0	358.5
2	1	0.64	0.66
2	2	0.74	0.72
2	3	0.52	0.51
2	4	0.13	0.14
2	5	-0.01	-0.01
2	6	-0.02	-0.02
	Sum	2.00	2.00
	Total Moment (ft-Kips)	716.7	716.7
3	1	0.08	0.10
3	2	0.42	0.41
3	3	0.39	0.37
3	4	0.14	0.13
3	5	-0.01	0.00
3	6	-0.02	-0.01
	Sum	1.00	1.00
	Total Moment (ft-Kips)	358.6	358.5
4	1	0.06	0.07
4	2	0.45	0.47
4	3	0.73	0.72
4	4	0.58	0.57
4	5	0.21	0.19
4	6	-0.03	0.01
	Sum	2.00	2.03
	Total Moment (ft-Kips)	718.4	716.9

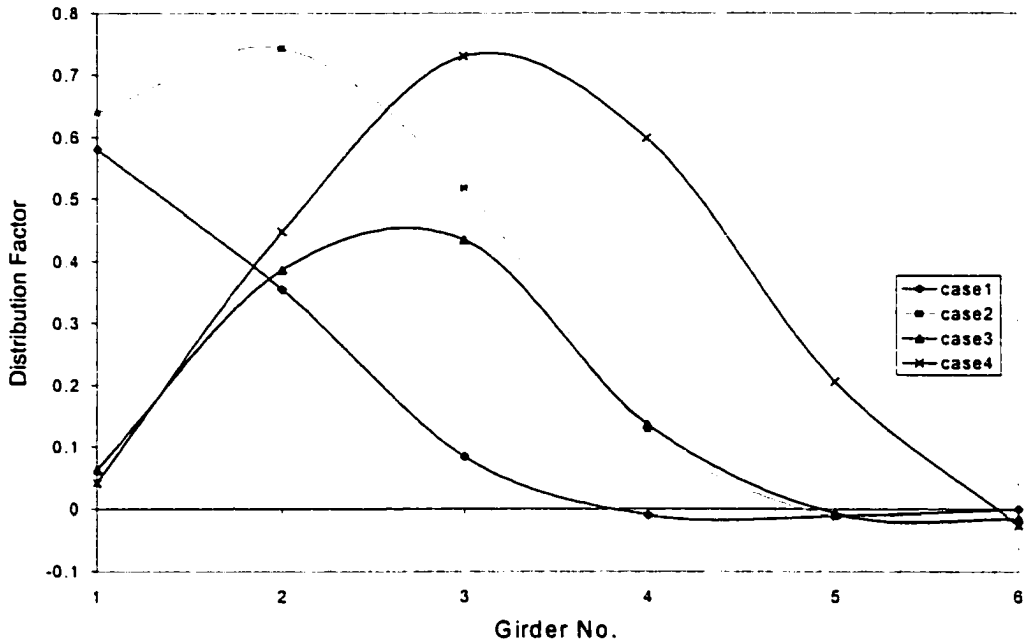

Figure 3.16. Distribution factors in the undamaged bridge

3.5.3 Distribution factors when an exterior girder (girder 1) is damaged

As mentioned earlier, the damage in the exterior girder is simulated by incrementally reducing the bottom flange area of the steel girder. Figure 3.17 shows the distribution factors for all the six girders due to cases 1 through 4. In this figure, the level of damage is indicated by the moment of the inertia of the exterior girder, I_g. The control case indicated by I_g (i.e. no damage) and the severe damage case is indicated by $0.6I_g$,which reflects a 40 percent reduction in the moment of inertia of the girder. It must be remembered that only girder 1 is damaged and the remaining girders are intact. As may be seen in Figs. 3.17a and 3.17b, for small damage (< 20 percent), no major redistribution of moments is observed. However, for 40 percent damage (i.e. $I = 0.6I_g$) a more noticeable redistribution is observed; the moment in the neighboring girder 2 will increase as a result of damage in girder 1. Load cases 3 and 4

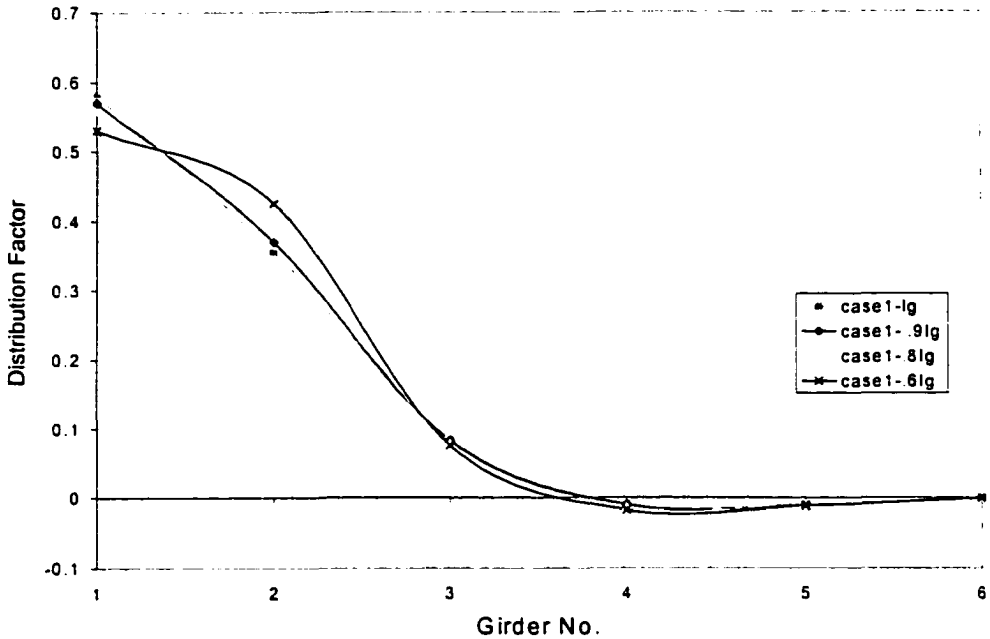

a. Loading case 1

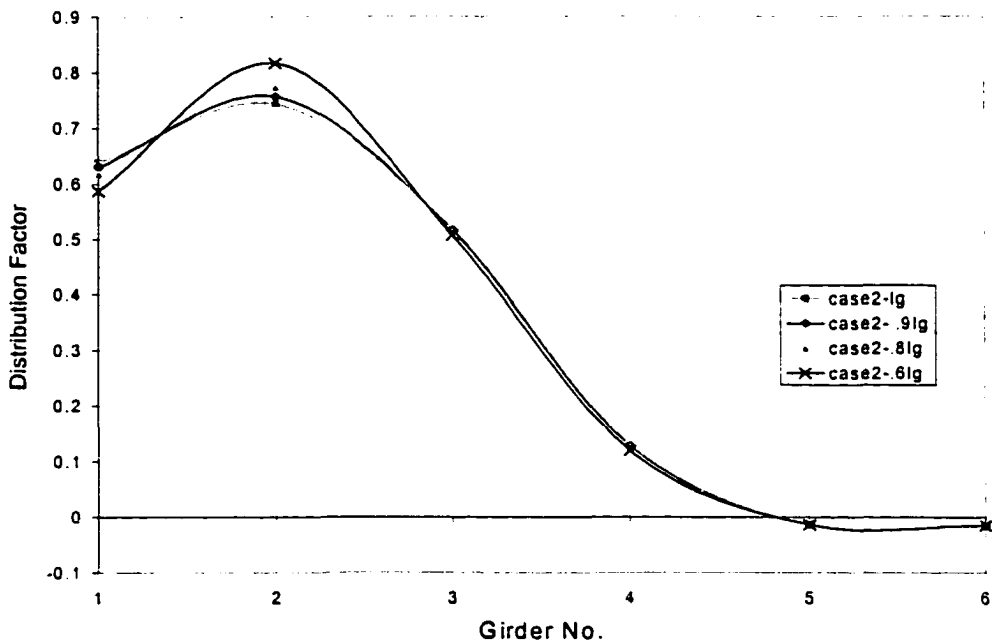

b. Loading case 2

Figure 3.17. Distribution factors in the bridge with a damaged exterior girder.

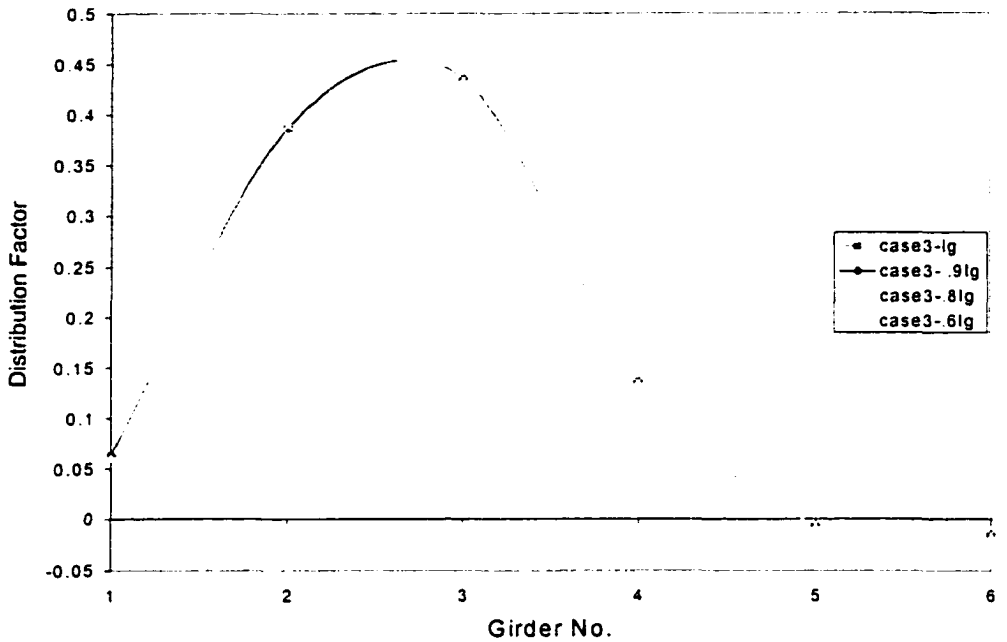

c. Loading case 3

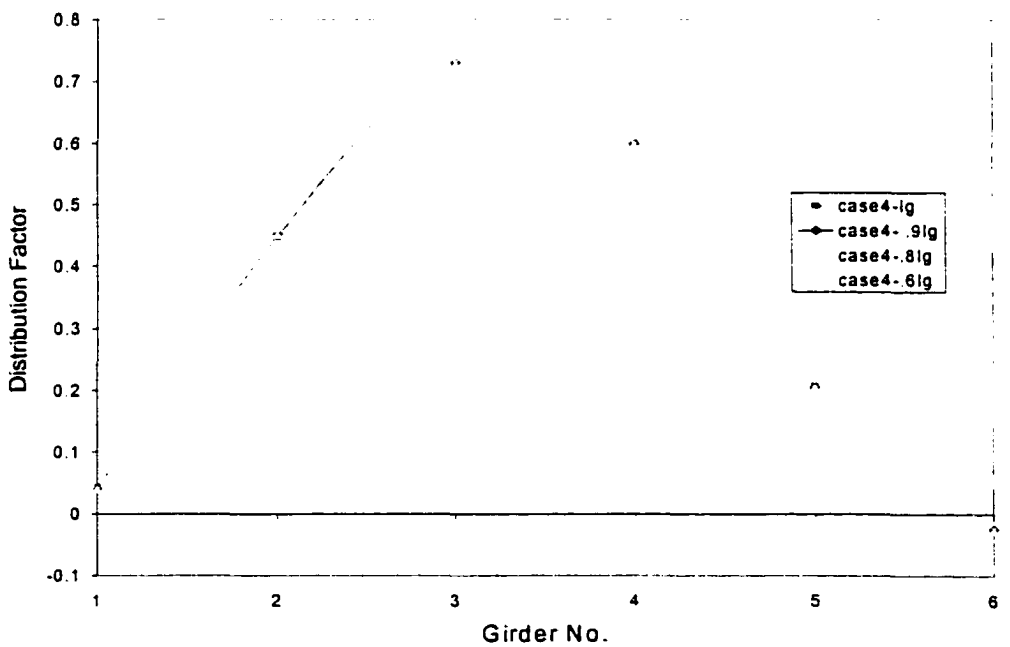

d. Loading case 4

Figure 3.17. Continued.

are shown in Figs. 3.17c and 3.17d; no significant change in the distribution factor is observed in these cases since the load positions are remote from the damaged girder.

3.5.4 Distribution factors when an interior girder (girder 3) is damaged

The effect of damage on a typical interior girder, in this case girder 3, on the moment distribution will be discussed in this section. A similar approach to that described in the previous section is used to induce damage to the selected girder. Analysis results are presented in Fig. 3.18. In this figure it may be observed that loading case 1 (see Fig. 3.18a) does not cause any load redistribution due to the position of the loads that are directly above girders 1 and 2. However, the remaining load cases (see Figs. 3.18b, 3.18c, and 3.18d) will cause considerable load redistribution when the girder 3 is severely damaged (i.e. $I = .6I_g$), but no significant load redistribution is observed for small damage.

As stated earlier, this analysis is meant only to illustrate a methodology of bridge damage analysis; therefore, it is not comprehensive. There are different possible scenarios of damage cases that are not covered in this analysis such as the case when there is more than one damaged member or a combination of exterior and interior members or two adjacent members are damaged, etc. Each case is unique and must be analyzed separately. However, the previous analysis shows clearly that for small damage, there is no major redistribution of load paths and the damaged beam can be repaired and analyzed as illustrated at the beginning of this chapter. On the other hand, when the damage is significant, the neighboring girders will attract higher loads than what they will normally experience in the undamaged state. In this case, these girders also need to be strengthened to accommodate this additional load

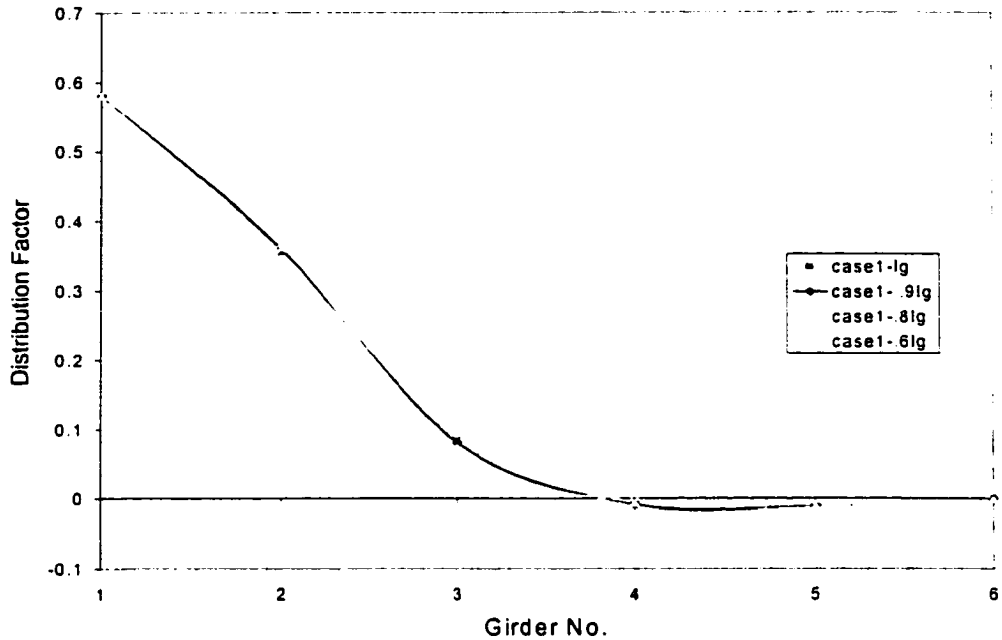

a. Loading case 1

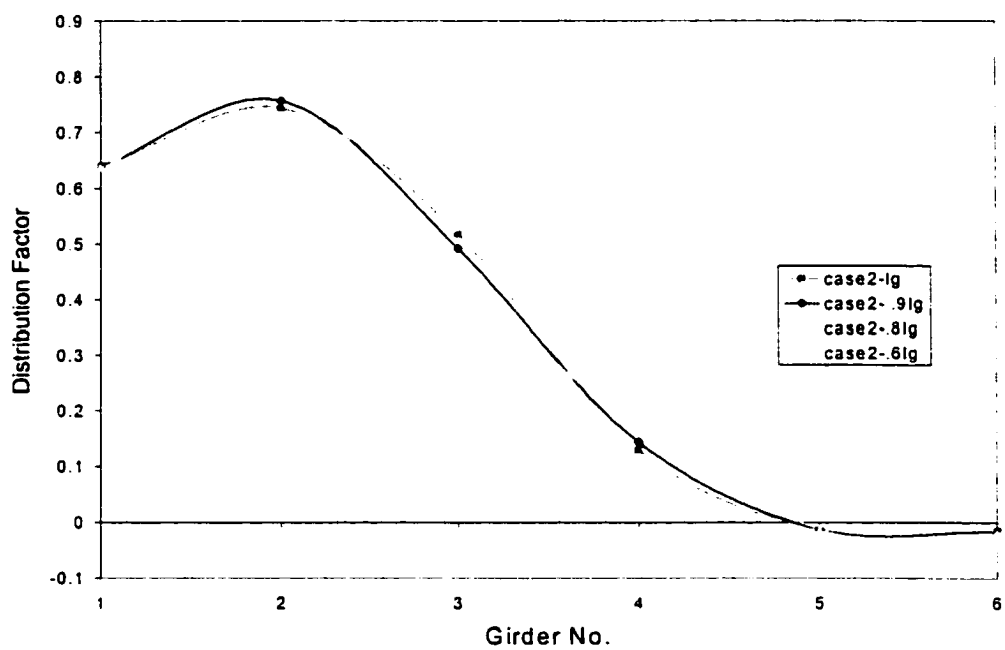

b. Loading case 2

Figure 3.18. Distribution factors for the bridge with a damaged interior girder.

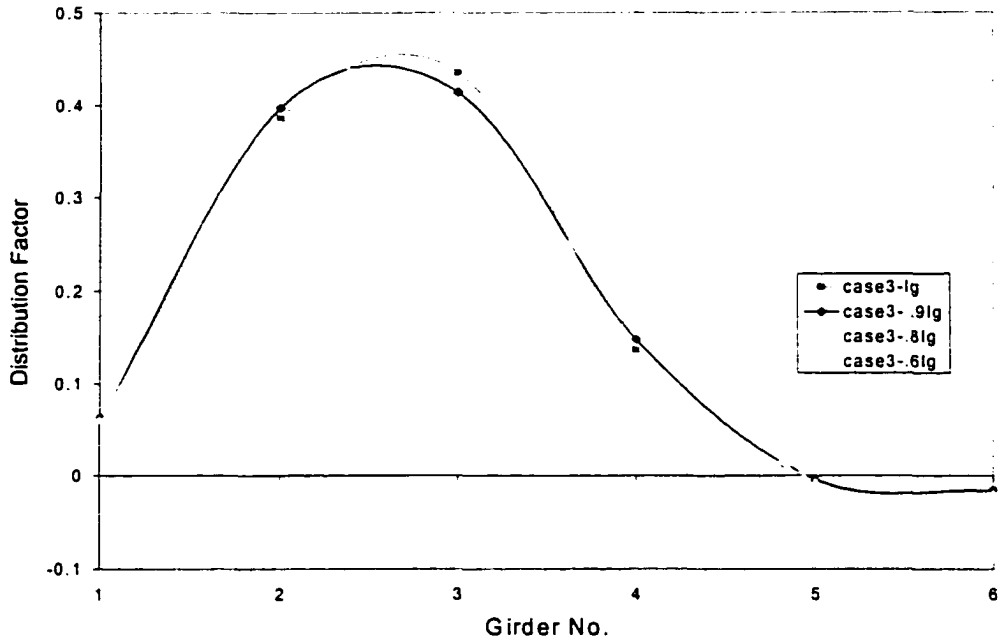

c. Loading case 3

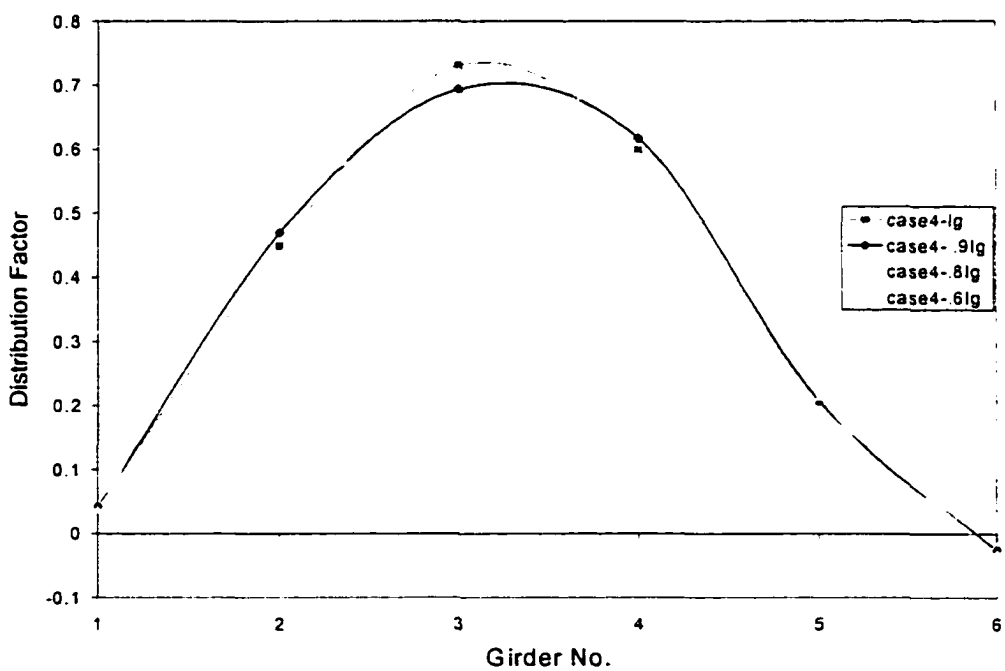

d. Loading case 4

Figure 3.18. Continued.

caused by the inadequacy of the damaged member in proportion to the change in the distribution factors.

3.6 Shear stresses

Since the strengthening method presented in this study depends highly on the shear strength of the applied adhesive, it is necessary to determine stresses along the CFRP plate. In the tested specimens, the longitudinal strains along the CFRP plates were recorded based on the instrumentation plans that are presented in the next chapter. Figure 3.19 shows a typical strain gages locations along the CFRP plate. These gages are used to measure the longitudinal strains along the plate; the shear stresses were then calculated based on basic principles of engineering mechanics, which will be briefly presented as follows:

The stresses acting on an infinitesimal length of the CFRP plate is shown in Fig. 3.20. From equilibrium of forces acting on the plate:

$$\sum F_x = 0 \tag{3.27a}$$

$$(\sigma + \Delta\sigma)(t_{pl} \cdot 1) - \sigma(t_{pl} \cdot 1) - \tau(\Delta x \cdot 1) = 0 \tag{3.27b}$$

Simplifying and rearranging the above equation, the shear stress is given by

$$\tau_x = \frac{\Delta\sigma}{\Delta x} t_{pl} \tag{3.28a}$$

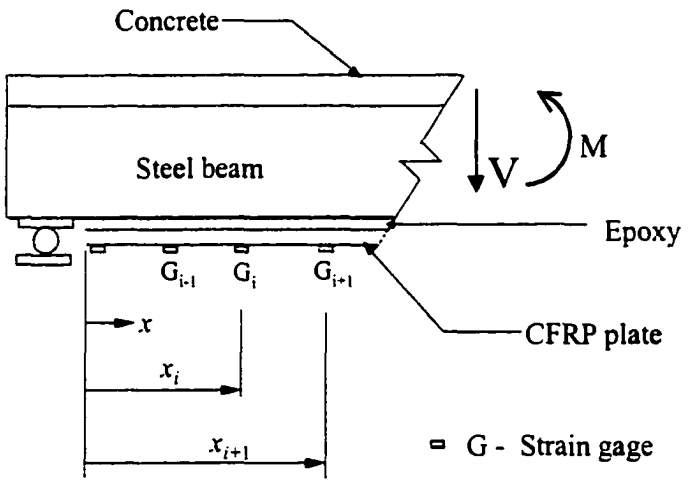

Figure 3.19. Locations of strain gages on the CFRP plate.

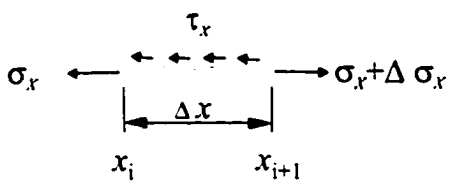

Figure 3.20. Stresses acting on the CFRP plate.

From Hooke's law, $\Delta\sigma = E(\Delta\varepsilon)$; this relation is assumed to be valid for all load ranges since the CFRP has a linear constitutive relation up to failure.

$$\tau_x = \frac{E_{pl}(\Delta\varepsilon)}{\Delta x} t_{pl} \tag{3.28b}$$

$$\tau_x = \frac{\varepsilon_{i+1} - \varepsilon_i}{x_{i+1} - x_i} (E_{pl} t_{pl}) \tag{3.28c}$$

where ε_i is the longitudinal strain in the CFRP plate at x_i (see Fig. 3.19); E_{pl} and t_{pl} are the modulus of elasticity of the CFRP plate and the thickness of the CFRP plate, respectively. Note that the shear stress is an average between any two adjacent strain gages.

4. EXPERIMENTAL INVESTIGATION

4.1 General

A total of 10 steel-concrete composite beams were tested in this study. The steel beams were W8x15grade A572 structural steel. A composite concrete slab 32 in. wide by 3 in. thick was used with all beams. Shear studs (1/2 in. in diameter by 2 in. long) provided the shear connection between the slab and the steel beams.

The dimensions of the beams investigated were dictated by economical reasons. It was decided to test scaled down specimens to reduce costs thus making it possible to test several beams to investigate the important variables. Also, since this was an exploratory study, the outcome of one test might impose certain modifications to the next; therefore, full scale specimens would be very expensive and unjustified.

Two groups of beams were investigated in this study. The first group consisted of six steel beams that were not damaged (i.e. in their original condition) and then strengthened with Carbon Fiber Polymers (CFRP) plates . The second group consisted of four steel beams that were damaged by removing part of their bottom flange (i.e. a percentage of the bottom flange area) to simulate corrosion in the field and then repaired by adding the CFRP plate to restore the beam to its original strength.

In order to distinguish between the two groups of the specimens, the following notation was adopted to describe each specimen. The first group of specimens start with a letter "U" to define them as Undamaged; the letter "U" is followed by a letter and a number such as "S1" to reflect the strengthening scheme, in this case, Strengthening Scheme1. This

in turn is followed by a letter and two numerals such as "E22" to indicate the MOE of the CFRP plate used in the strengthening.

For example, "U" means undamaged beam without strengthening (i.e. control beam). For a strengthened specimen, "US1E22" describes an undamaged beam that is strengthened using Strengthening Scheme1 and a CFRP plate that has a modulus of elasticity of 22 ksi. The various schemes of strengthening used in this group, are shown in Fig. 4.1. Strengthening Scheme1 is achieved by applying the CFRP plate to the bottom flange of the steel beam. On the other hand, Strengthening Scheme2 is achieved by applying the CFRP plate to the bottom flange as well as to part of the web of the steel beam.

The notation in the second group was adopted to reflect the extent of the damage to the bottom flange of the steel beam and starts with the letter "D" to indicate a damaged

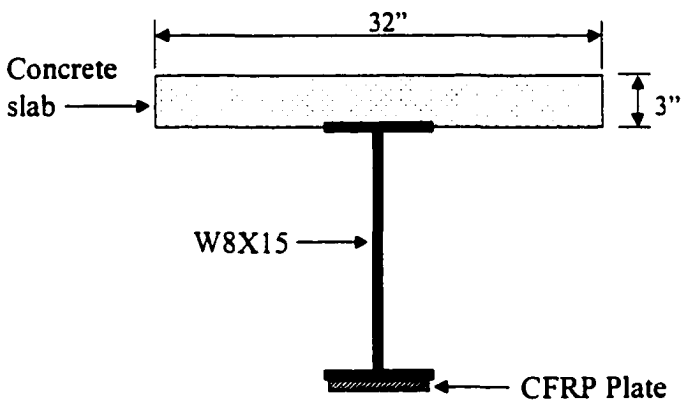

a. Scheme 1

Figure 4.1. Strengthening Schemes used on undamaged beams.

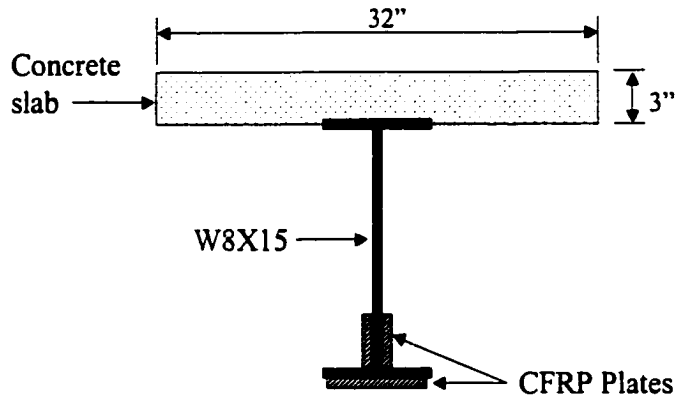

a. Scheme 2

Figure 4.1. Continued.

beam. In the case of the control beam, this letter was used alone to indicate that no repair was done. In the case of beams that were repaired, the letter "D" is followed by two numerals to show the percentage of damage to the bottom flange. For example, "50" means that the bottom flange was damaged by removing 50% of its original area. The two numerals then followed by a combination of a letter and a number such as "R1" to reflect the type of the repair scheme used. This then is followed by a letter and two numerals such as "E22" to reflect the MOE of the CFRP plate being used. For example, "D50R1E29"describes a beam with 50% damaged bottom flange repaired using scheme1 with a CFRP plate that has a MOE (E_{pl}) of 29 ksi. The two repair schemes used on the damaged beams are shown in Fig. 4.2. Details on the various test specimens are presented Table 4.1.

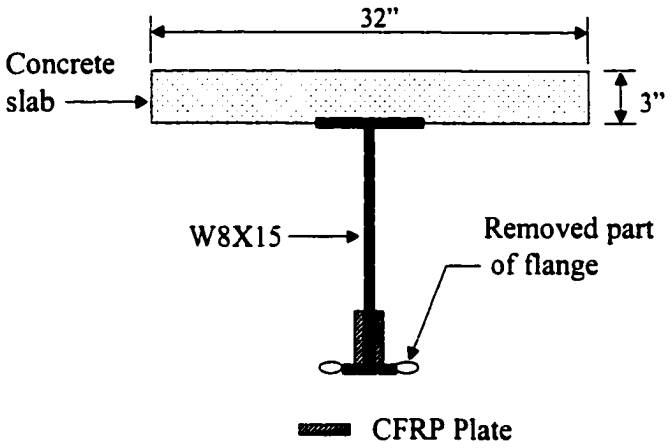

a. Repair scheme1

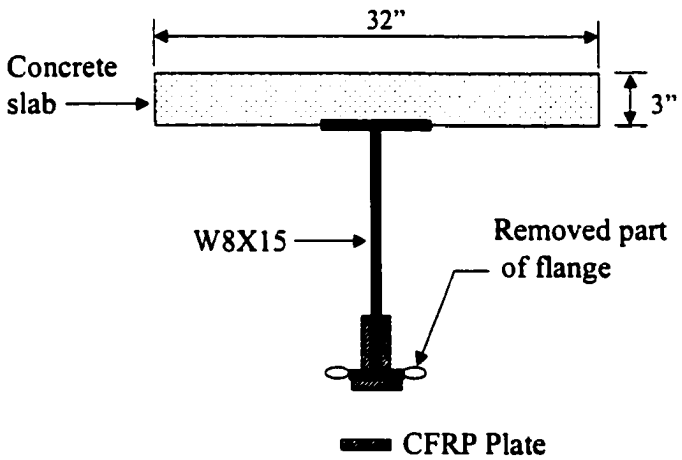

b. Repair scheme 2

Figure 4.2. Repair schemes used on damaged beams.

Table 4.1. Description of test specimens.

Specimen Type	No. of specimens	f_c' (ksi)	E_{pl} (ksi)	CFRP applied to web	CFRP applied to bot. flange	Remarks
U	2	5.4	29	No	No	Control beam
D50	1	5.4	29	No	No	Control beam
US1E29	2	5.4, 4.5	29	No	Yes	Scheme1
US1E22	1	4.5	22	No	Yes	Scheme1
US2E29	1	4.5	29	Yes	Yes	Scheme2
D50R1E29	1	5.4	29	Yes	No	Repair1
D50R2E29	1	4.5	29	Yes	Yes	Repair2
D75R1E29	1	4.5	29	Yes	No	Repair1

4.2 Material properties

4.2.1 Concrete

The composite beams were cast using normal weight concrete. A C-4 concrete mix was specified, which is designed for Iowa highway bridges according to the Iowa DOT requirements. The average concrete compressive strength, according to this mix, should be approximately 4,000 psi at 28 days. Several test cylinders were made during the casting operation. These cylinders were cured in a similar fashion as the beam concrete slab and later tested in a uni-axial compression testing machine at 7 days, 14 days, 21 days, and 28 days. Table 4.2 shows cylinder test results at 28 days, for the first five beams, with an average strength of 5,400 psi, while Table 4.3 shows the results of the remaining beams which had an average compressive strength of 4,500 psi. The corresponding average concrete compressive strength of the beams tested is shown in the third column of Table 4.1.

Table 4.2. Compressive strength of concrete used in the beams casted in the first pour.

Cylinder No.	Load (lbs)	Compressive stress (psi)
1	156,600	5,540
2	152,400	5,390
3	150,100	5,310
Average		5,410

Table 4.3. Compressive strength of concrete used in the beams casted in the second pour.

Cylinder No.	Load (lbs)	Compressive stress (psi)
1	122,410	4,330
2	127,780	4,520
3	131,455	4,650
Average		4,500

4.2.2 Steel Beams

Steel beams (W8 x 15) were used in this investigation; all beams were 11 ft. long. The material properties of the steel beams, provided by the supplier, were determined according to ASTM structural steel specification for ASTM A572 GR50. The yield and tensile strengths of the beams were 52.7 ksi and 72.0 ksi, respectively.

4.2.3 Stud Shear Connectors

The shear connectors used in this study (1/2 in. in diameter by 2 in. long headed steel studs) were commercially available from TRW-Nelson. Yield and tensile strengths of the shear studs, provided by the supplier, were 63.7 ksi and 78.3 ksi, respectively. Welding of the shear studs was done in the ISU Structures lab using a special welding gun from the same

supplier. Each stud was visually inspected to insure a proper weld, which was characterized by:

- Even fillet formation
- A shiny, bluish hue to the fillet surface
- A slight flow or blend of the fillet metal into the base material
- Good fillet height

Along with the visual inspection, a physical test was undertaken as well to insure proper welding. The physical test used in this study was the bend test. It is basically bending the shear stud using a steel pipe or a hammer. If the welding was done correctly, then the stud will bend up to 90 degrees as shown in Fig. 4.3 without failing in the weld. This test was performed initially on a similar base material before the welding of the shear connectors to the beams took place. Once the visual and physical tests were proven to be satisfactory, the welding process was carried out on the beams.

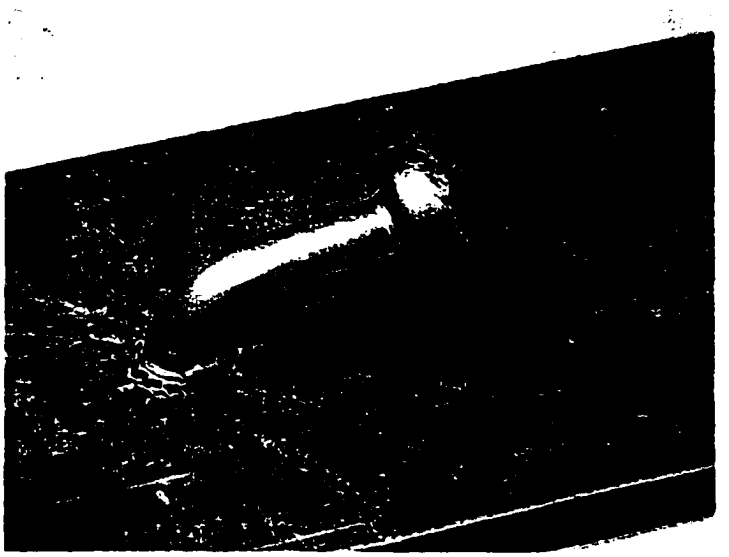

Figure 4.3. Photograph of shear stud after bend test.

4.2.4 CFRP Laminate

The CFRP plates were supplied by Structural Composites, Inc. Two grades of uni-directional pultruded plates were used in this investigation. The difference between the two grades is the modulus of elasticity; one grade has a modulus of elasticity of 23,000 ksi while the other has a modulus of elasticity of 29,000 ksi. These plates are produced in two standard thicknesses, 1.2 mm (.047 in.) and 1.4 mm (.055 in.), and four different widths: 50,80 ,100, and 120 mm (1.97, 3.15, 3.94, and 4.72 in.). In this study, the CFRP plates used were 1.4 mm (.055 in.) thick, and either 50 mm (~ 2 in.), or 100 mm (~ 4 in.) wide. The physical properties are summarized as follows:

Composition	Pultruded carbon fiber laminate with epoxy resin matrix
Color	Black
V_f	70% fiber content (volume fraction)
T_{GM}	$212 - 260^0$ F (glass transition temperature)

The mechanical properties of the CFRP plates are shown in Table 4.4.

Table 4.4. Mechanical properties of the CFRP plates.

Property	S&P CFK Laminate 150/2000	S&P CFK Laminate 200/2000
Modulus of Elasticity (E_{pl})	>23,000 ksi	>29,000 ksi
Ultimate Tensile Strength (F_{plu})	360 ksi	> 360 ksi
Ultimate Elongation(ε_{plu})	1.6%	1.3%

4.2.5 Epoxy

The epoxy used in this study was obtained from the same supplier of the CFRP plates metioned earlier. It is a two component, 100% solids, high modulus, high strength, moisture insensitive epoxy system designed for bonding Carbon Fiber Laminates to most building materials. The epoxy was supplied as a two component system and mixed 2:1 ratio by volume of componnets A and B. Component A is a 100% solid white gel and B is a 100% solid black gel; the blended mix produced a soft gray color gel. The physical properties of the mixed gel were provided by the supplier and the values were measured at 77^0 F as shown in Table 4.5.

Table 4.5. Properties of epoxy.

Viscosity	Smooth Gel
Potlife (3 oz)	1 hour
Geltime (5 mil)	2-3 hours
Tensile Strength	10,000 psi
Flexural Strength	12,000 psi
Compressive Strength	14,000 psi
Elongation	2%
Water Absorbtion (24 hours)	0.1%

4.3 Fabrication

4.3.1 Sand blasting

This study focussed on applying advanced composite materials to the tension side of the steel beams. Hence, the first step was to prepare the beam surface that will receive the CFRP plates. According to the supplier of the CFRP, the steel should be free from paint, oil, scales, rust, dust or any other contaminants that might weaken the bond between the steel and the CFRP. It was decided to sand blast the beams' tension flanges and the lower part of the

webs; sand blasting was completed by a local fabricator. The beams were sand blasted before casting the concrete since it was much easier to move them around.

4.3.2 Welding of Shear studs

The design of the shear studs assumed a full shear connection between the concrete slab and the steel beam. Since the strengthening schemes would result in different shear force for each scheme, it was decided to design the shear studs to carry the entire resultant force assuming the entire concrete slab would be in compression. This was due to the fact that the shear connection was not a variable in this study. Therefore, the number of required shear studs was calculated to transfer the maximum expected shear force resulting in the concrete slab. The required number of shear studs was calculated to be 64 numbers and was used in all specimens. They were arranged in two rows along the top flange and spaced uniformly along the beam on 4 in. centers as shown in Fig. 4.4. The welding procedure outlined earlier was followed and the visual and physical inspections previously noted were performed on all specimens.

4.3.3 Form-work and casting of the slabs

The steel beams were supported on a 4 in. x 4 in. wooden beams at the ends. The forms consisted of a 2 in. x 4 in. wooden frame covered by 1/2 in. commercial plywood that was supported by 2 in. x 4 in. legs.

Following the setup of the formwork, the formwork surfaces that would be exposed to concrete were coated with a bond releasing oil. This facilitated the removal of

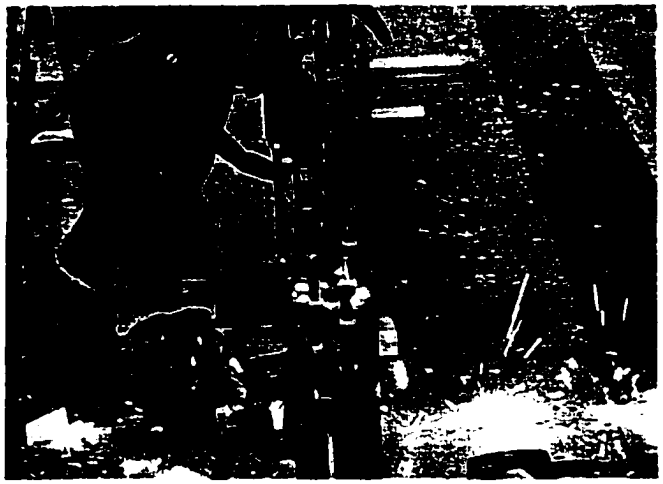

Figure 4.4. Photograph showing welding of shear studs.

the forms after initial curing was completed and the same forms then were reused for the next set of beams. The longitudinal steel reinforcing bars (#3 spaced on 8 in. centers) were placed on steel chairs and tied with steel ties, the transverse steel reinforcing bars (#3 spaced on 14 in. centers) then were placed on the top of the longitudinal bars and also tied. Figure 4.5 shows the final formwork of a typical beam before casting.

A local ready mix plant supplied the concrete for the specimens. The concrete was conveyed from the truck by wheelbarrows and shoveled to the forms. It was compacted using pneumatic vibrator to insure that no segregation of the fresh concrete took place. The surface of the concrete then was screeded and finished as illustrated in Fig. 4.6.
After pouring the concrete and finishing the concrete surface, the beams were covered with plastic sheets and left to cure. The forms were stripped after 7 days of curing when the compressive strength was approximately 3,800 psi. The second set of five beams was prepared using the same procedure.

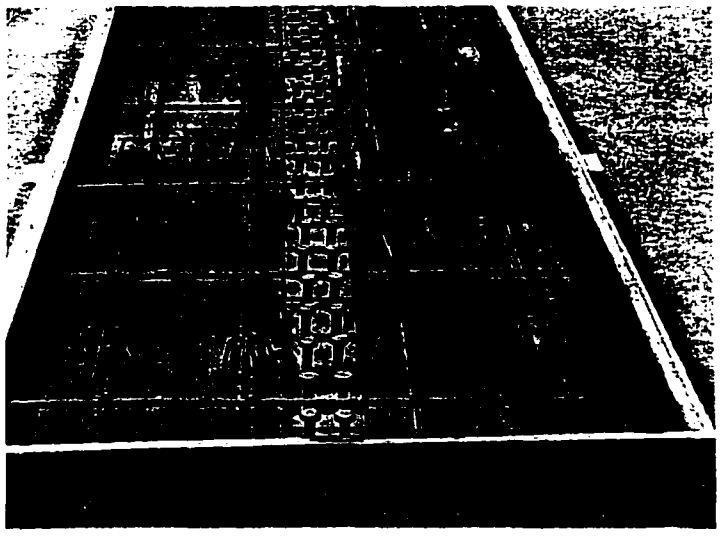

Figure 4.5. Photograph showing typical slab formwork and reinforcement.

4.3.4 Applying the CFRP laminates

The surface of each beam was prepared by sand blasting at the locations were the CFRP laminates to be applied. It should be mentioned that the epoxy supplier recommended that bonding of the CFRP laminates to the steel surface should be done as soon as possible after the sand blasting. However, the time between the sand blasting and the application of the CFRP was about six months, due to delays in obtaining the repair materials. Beam surfaces were only abraded with a steel brush wheel prior the application of the CFRP. Nevertheless, the bond between the CFRP and the steel surface was found to be excellent as will be shown in the next chapter.

The surfaces of the steel beam and the CFRP laminates were cleaned with acetone just prior to the application of the epoxy. This was done to insure that the surface was

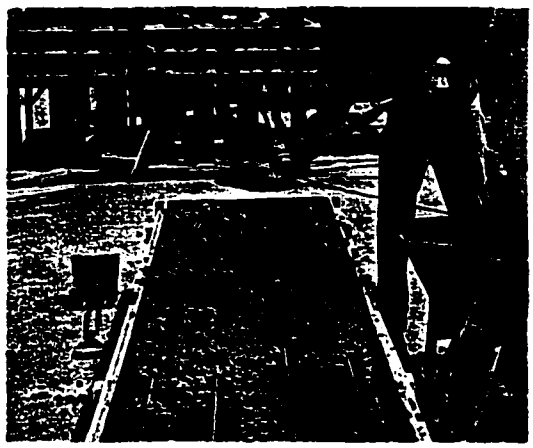

a. Placing concrete into forms

b. Vibrating the concrete

c. Screeding concrete

d. Finishing concrete

Figure 4.6. Casting of composite beams.

clean from any contaminants such as grease, dust, scale, etc. that might weaken the bond between the two materials.

Next, the two parts of the epoxy were mixed to the recommended consistency. The mix ratio was 1:2 by volume of part A to part B. First, part A was measured and placed in a plastic container, then part B was added to part A in the same container according the above ratio. Mixing was accomplished using a drill at low speed for about five minutes.

The thickness of epoxy recommended by the supplier was 1/4 in., based on field application to concrete surfaces. In this study, about half the recommended thickness (1/8 in.) was used, which was found to be sufficient as more experience was gained from the several tests conducted in this study. Once the epoxy was applied to both steel and CFRP plate, the plate was placed on the prepared area of steel and pressed against the steel by hand. A hard rubber roller was used to uniformly distribute the epoxy until the excess epoxy appeared on the sides of the CFRP plate; this excess was later removed. Wooden boards were used to apply further pressure and to hold the CFRP plate in place until the epoxy cured. The wooden boards were secured in place with C-clamps. Plastic sheets were used to separate the wooden boards from the CFRP plate to avoid any bonding between them. The clamps were released after 14 to 24 hours; by that time the epoxy had cured. Installation of the CFRP plates is illustrated in Figs. 4.7 and 4.8.

4.4 Test set up

All ten beams were tested as with four point bending static loading. As previously noted, each beam was 11 ft long with a 10 ft clear span (i.e. 6 in. of overhang at each support). Loading was applied using a 120 kip capacity hydraulic cylinder at each load

a. Cutting of CFRP plate

b. Mixing the two parts of epoxy

c. Applying the epoxy to the CFRP plate

d. Applying the epoxy to the steel beam

Figure 4.7. Steps in attaching the CFRP plate to the steel beam.

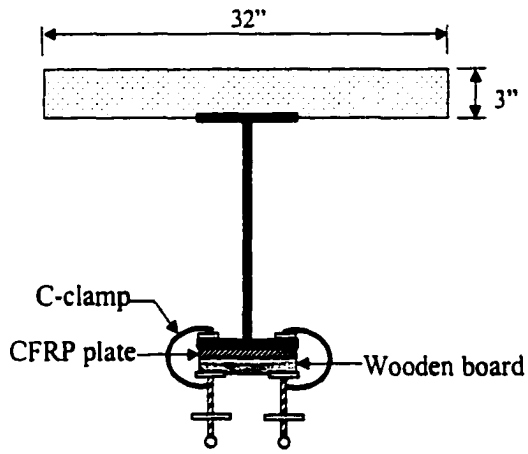

a. Schematic details of clamping the CFRP plate

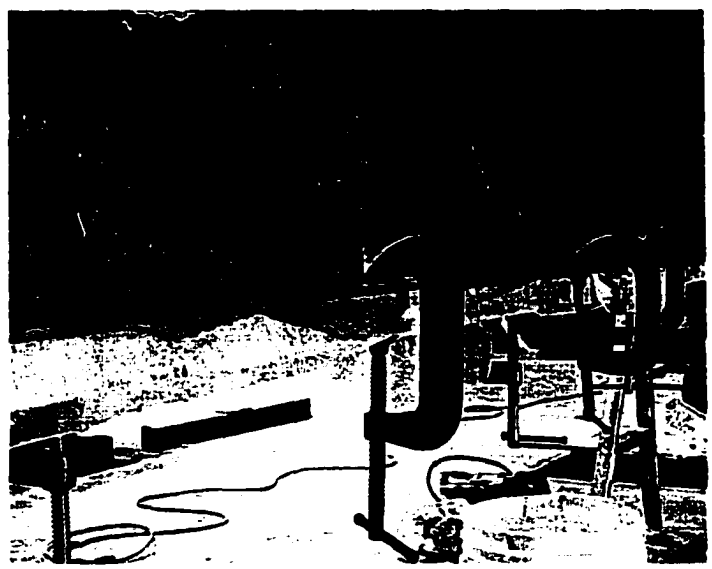

b. Photograph of clamping the CFRP plate

Figure 4.8. Applying uniform pressure to epoxy joint using wooden boards and C-clamps.

point, and these load points were 48 in. from the ends of the beam and 36 in. apart. A typical load set up is shown in Figs. 4.9 and 4.10. The first beam was tested using a steel tube to distribute the load as a line load in the transverse direction of the slab. However, due to slight differences in the elevation of the concrete slab in the transverse direction, the line loading created longitudinal cracks along the beam. Following this problem, it was decided to apply the load as point loads to avoid such problems.

The load was applied using a manually operated hydraulic pump. Each hydraulic cylinder was resting on a 50 kip capacity load cell that was placed on a 6 in. x 6 in. x 1 in. thick steel plate. A 6 in. x 6 in. x 1/2 in. thick neoprene pad was placed between the steel plate and the top of concrete slab. The hydraulic cylinder reacted against a steel tube that transferred the load to the tie down floor through the tension rods shown in Fig. 4.9b.

Typically all beams were initially loaded and unloaded to loads between 5,000 – 8,000 lbs before the actual test took place. This was done to "seat" the strain gages and to insure that all instrumentation devices were operating properly. Another reason was to observe any adverse effect the cyclic loading might induce on the bond between the CFRP plates and the steel.

All tests were load controlled, and data were recorded at a load increment of 500 lbs. This load was selected based on the analytical results of the previous chapter. It was necessary to use a small load increment such as this in order to capture the behavior in the nonlinear stage.

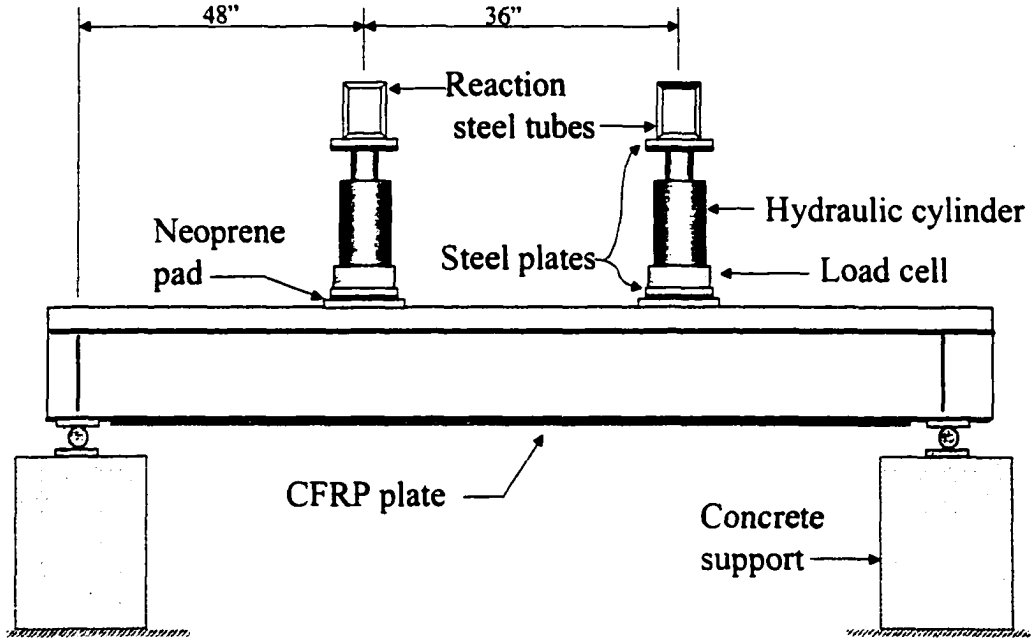

a. Side view

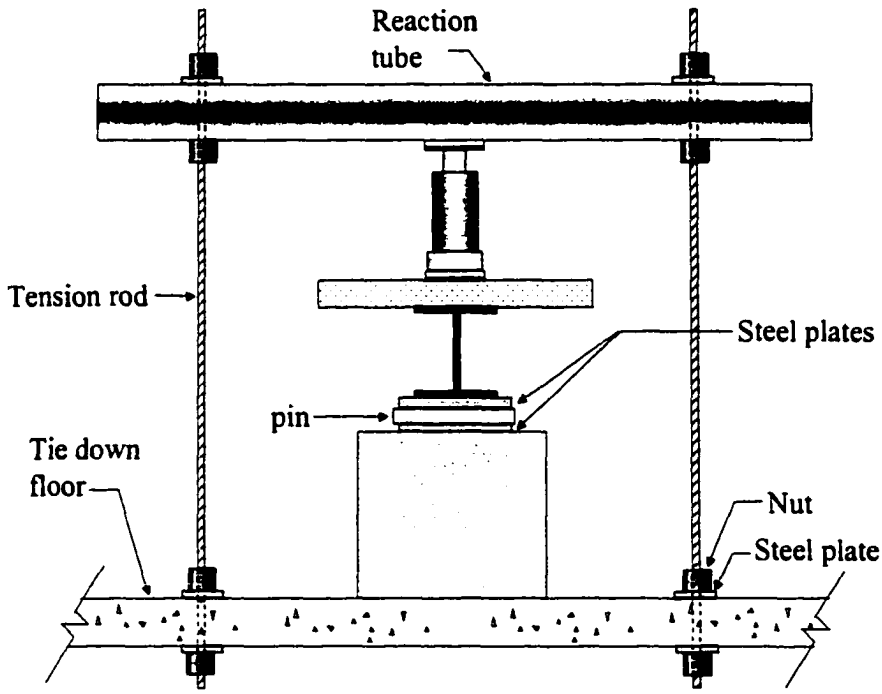

b. End view

Figure 4.9. Typical load setup used in beam tests.

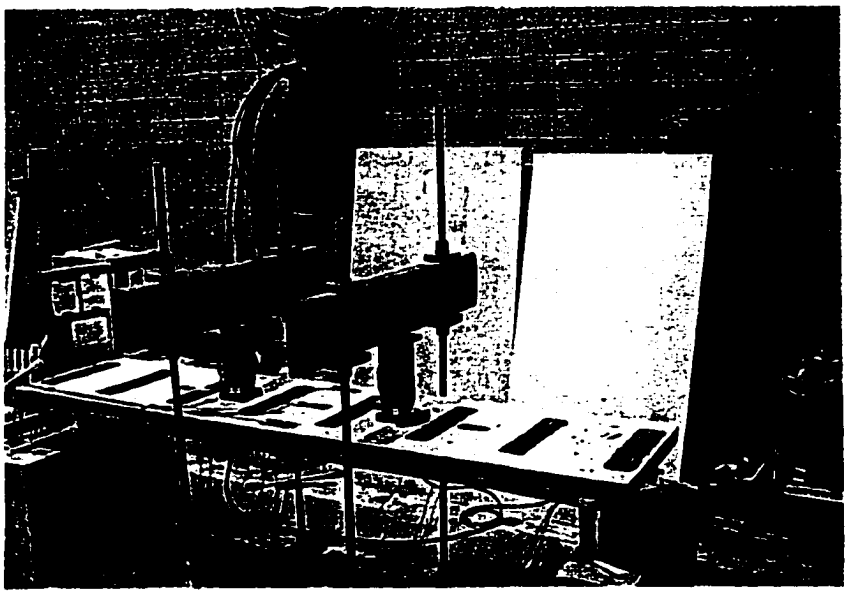

Figure 4.10. Photograph of a typical test setup.

4.5 Instrumentation

In order to observe the behavior of beams under investigation, extensive instrumentation was utilized on the beams. Strains, loads, deflections, and slip were measured at the desired locations as outlined in the following sections.

Data were collected using different measuring devices. Strains in the concrete slab as well as the steel beam were measured using electrical-resistance strain gages. A three-lead-wire system was used for all strain measurements. Strains in the steel were measured using CEA-06-250UW-120 from Measurements Group, Inc., Raleigh, NC. This type of gages has a gage length of 1/4 in. and a 120 ohms electrical resistance. The concrete gages were of the type F-2400 supplied by Precision Measurement Co., Ann Arbor, Michigan. These gages have lengths of 2.4 in. and a 120 ohms electrical resistance. Procedures recommended by the manufacturers were followed in the application of the strain gages.

Vertical deflections of the beams were measured using Celesco string potentiometers (Celescos). The slip between the steel beam and the concrete slab was measured using Direct Current Differential Transducers (DCDT's).

Data from strain gages, Celescos, DCDT's and the load cells were recorded automatically using a HP-3497 data acquisition system (DAS). The system was comprised of the data acquisition control unit (DACU), a personal computer, a monitor, and a printer. The DACU has several scanners capable of scanning 100 strain gages and 20 transducers (DCDT's). A 1/4-bridge circuit was used for the strain measurements. The instrumentation of the specimens is briefly discussed in the following sections.

4.5.1 Specimens U and D50

Specimen U and D50 are the control beams that are used for comparison with the strengthened and repaired beams. Two specimens of U type were tested and one specimen of D50. The three beams have similar instrumentation plans and similar load set ups. Each beam is instrumented with 5 concrete gages on the top of the concrete slab. Three gages at mid span and one at the 1/4 (quarter) and 3/4 (three-quarter) points, respectively as shown in Fig. 4.11. The steel gages were also applied at mid-span and the quarter points. Two steel gages were installed at the bottom surface of the top flange, two at the middle of the web (at the mid-span), and two on the top surface of the of bottom flange as shown in Fig. 4.11b.

Vertical deflections of the beams were measured at the mid-span and the quarter points using nine Celescos as illustrated in Fig. 4.12. The deflection of the bottom of the concrete slab was measured on both sides of the steel beam to insure symmetric loading and

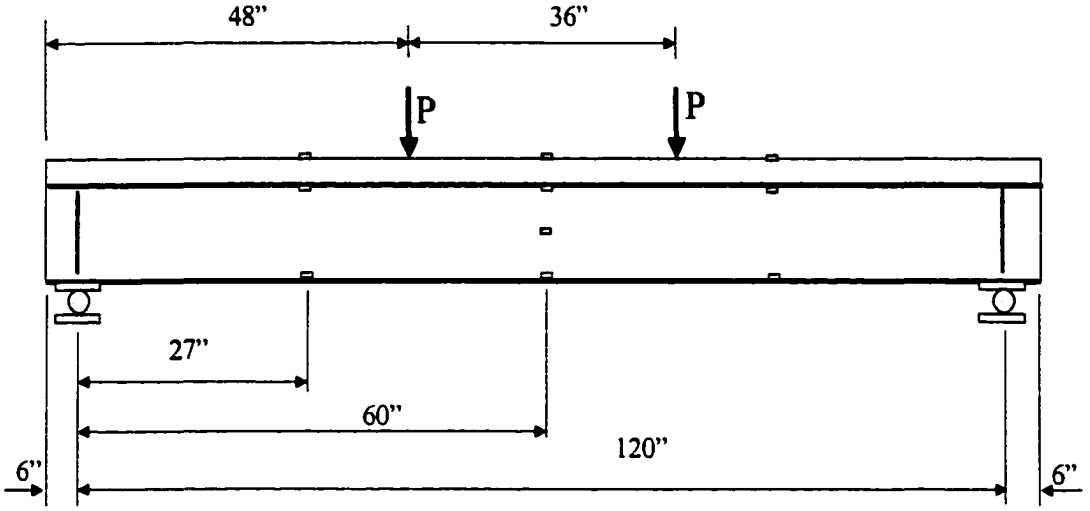

a. Side view

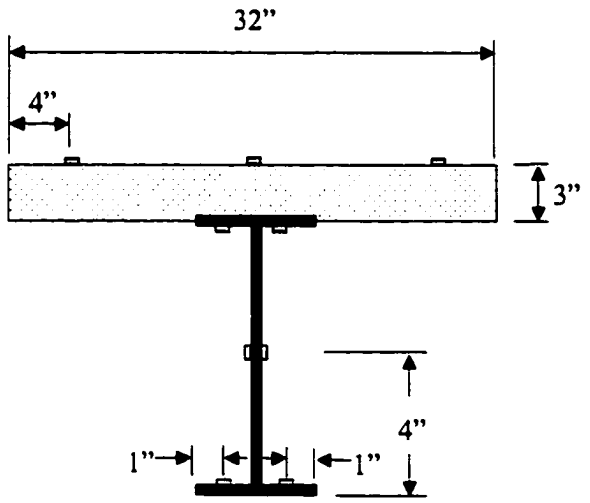

= Strain gage

b. Strain gages at midspan section

Figure. 4.11. Locations of strain gages on specimens U and D50.

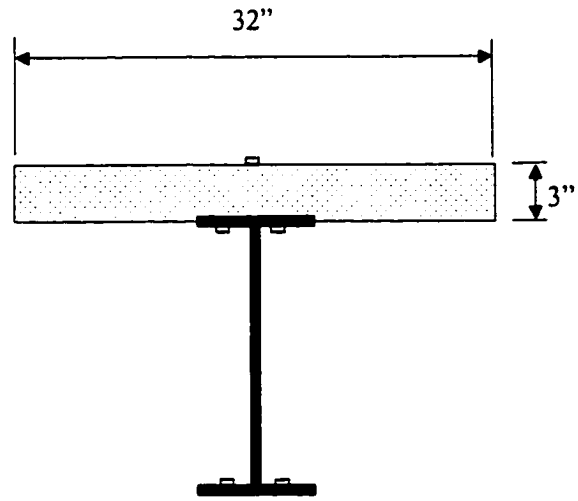

c. Strain gages at quarter and three-quarter sections

Figure. 4.11 Continued.

to observe any transverse rotation that might occur during loading. Reported deflections of the beam at any section are the average of the concrete slab and the steel beam deflections. Slip between the concrete slab and the steel beam was measured using DCDT's attached to the steel beam end as shown in Fig. 4.12. It should be mentioned that slip was not measured in these three specimens; however, it was measured in subsequent specimens.

4.5.2 Specimens US1E29 and US1E22

Specimen US1E29 and US1E22 are the undamaged beams strengthened using Strengthening Scheme1. In this scheme, the CFRP plate is applied only to the bottom flange of the steel beam. The only difference between the two specimens is the modulus of

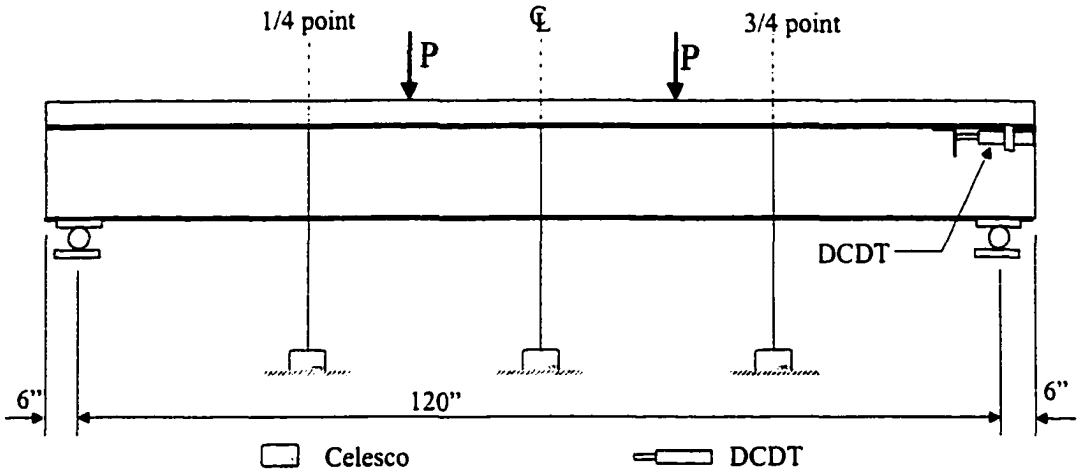

a. Side view

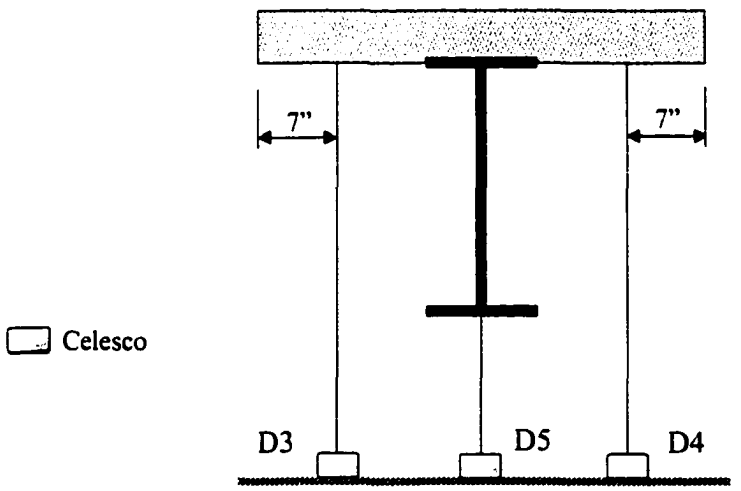

b. end view

Figure 4.12. Locations of Celescos and DCDT's on a typical beam specimen.

elasticity (stiffness) of the CFRP plate. Beam US1E29 was strengthened with a CFRP plate that has a modulus of elasticity of 29,000 ksi, while the modulus of elasticity of the CFRP plate used to strengthen Beam US1E22 was 22,000 ksi. The distribution of steel strain gages and concrete strain gages are similar to that used on the control specimens mentioned in the previous section. However, the strain gages applied to the CFRP plate were closely spaced to observe the longitudinal strain as well as the shear stress distribution along the beam. More gages were applied at the end of the CFRP plate to record the shear stress concentration anticipated at the plate ends as shown in Fig. 4.13.

Vertical deflections of these specimens were measured using the same Celescos distribution as shown previously in Fig. 4.12. Similarly, slip between the concrete slab and steel beam was measured using two DCDTs mounted at the two ends of the beam. The DCDTs were attached to the steel beam web. One leg of a steel angle was glued to the concrete slab bottom and the other leg of the angle was touching the DCDT's spring. Slip was measured as the relative movement of the steel angle and the spring of the DCDT.

4.5.3 Specimens US2E29 and D50R2E29

The major difference between these specimens and the specimens discussed in the previous section is the areas of the steel beam where the CFRP applied. US2E29 type beam is strengthened according to Strengthening Scheme 2. In this scheme, a 4 in. wide CFRP plate is applied to the bottom flange and a 2 in. wide CFRP plate is applied to the bottom part of the steel web. Locations of the strain gages along the bottom CFRP plate are similar to that shown in Fig. 4.13b, and locations of the gages along the side CFRP plate are shown

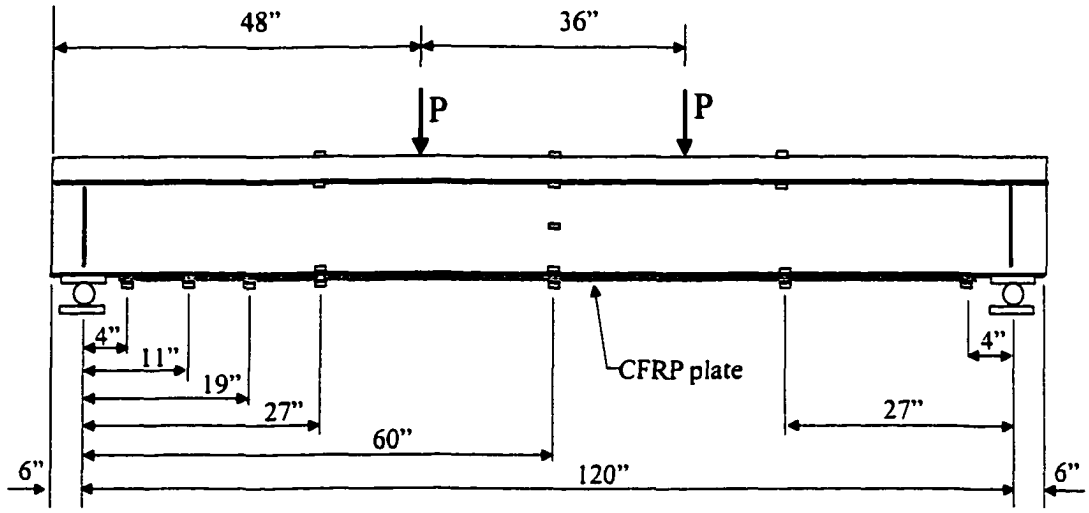

a. Side view

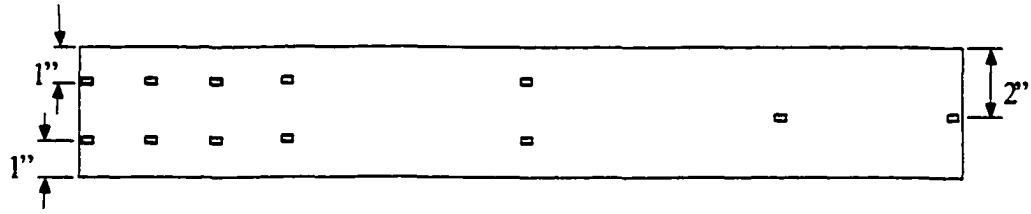

Bottom view of strain gages on the CFRP plate

Figure 4.13. Locations of strain gages in specimens US1E29 and US1E22.

in Fig. 4.14. These gages were installed symmetrically on both side plates as shown in the midspan section (see Fig. 4.14b).

D50R2E29 was repaired similar to US2E29; the only difference is the width of the CFRP plate applied to the damaged bottom flange of D50R2E29 beam. In this case, the width of the CFRP plate was 2 in. just to fit the width of the remaining width of the bottom flange. Locations of strain gages along the bottom flange are similar to that shown in Fig. 4.13b, except that there is only one row of strain gages along the center of the plate.

Again, vertical deflections of the beams and the slip between the concrete slab and the steel beam were measured according to the instrumentation plan shown in Fig. 4.12.

4.5.4 Specimens D50R1E29 and D75R1E29

These specimens were repaired using only 4-in. wide CFRP plates applied to the two sides of the web. The distribution of the strain gages is shown in Fig. 4.15. More gages were installed on the CFRP at the midspan section to observe the distribution of stresses across the width of the plate as illustrated in Fig. 4.15b.

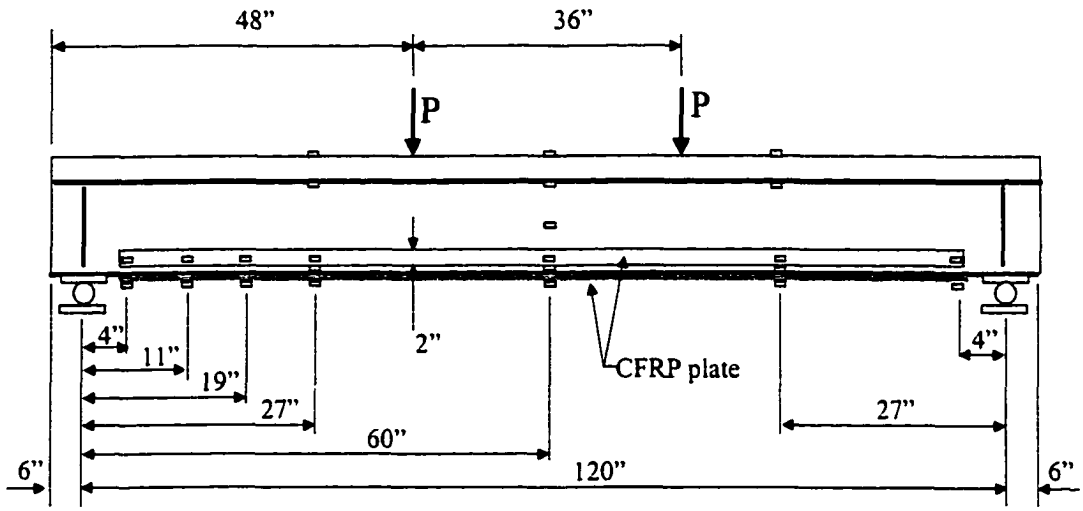

a. Side view

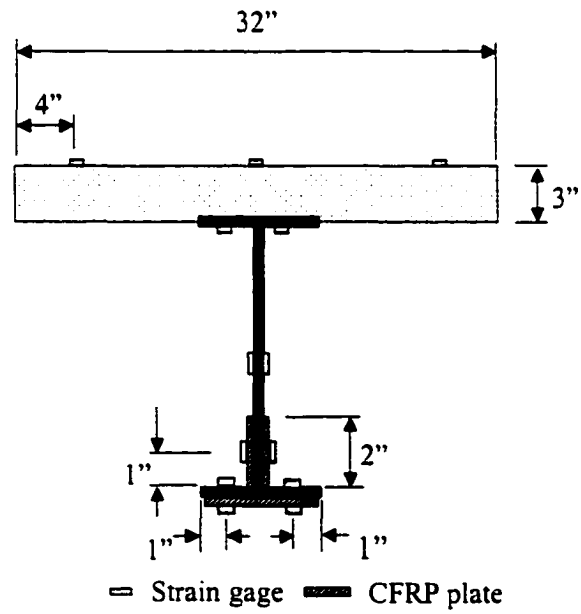

b. Section view at midspan

Figure 4.14. Locations of strain gages on specimens US2E29 and D50R2E29.

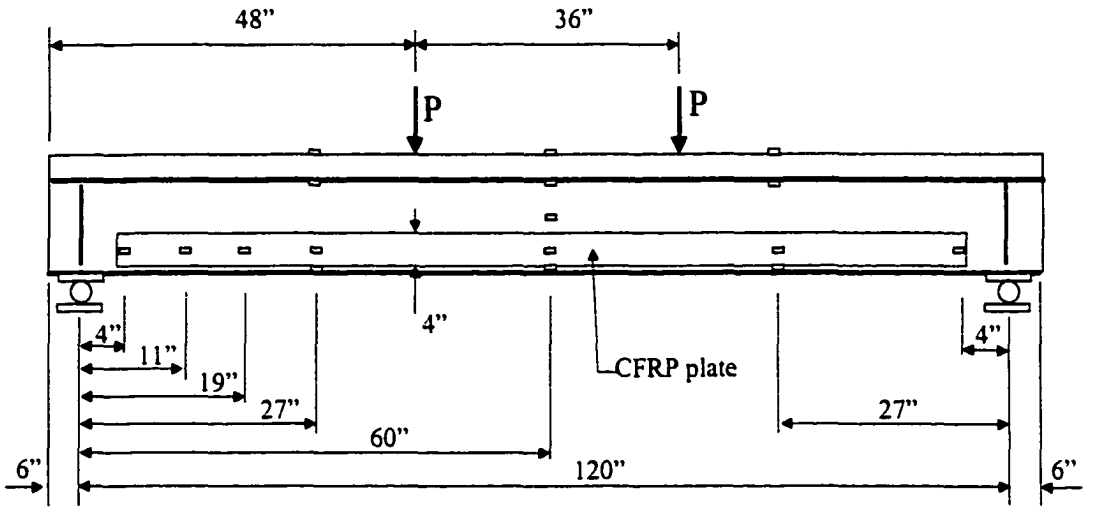

a. Side view

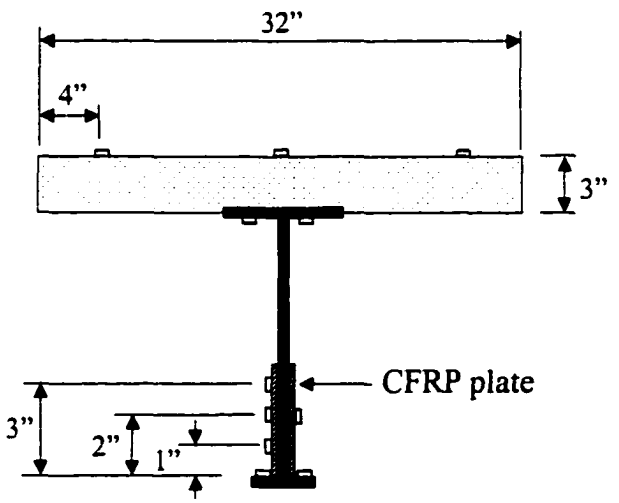

= Strain gage

b. Section view at midspan

Figure 4.15. Locations of strain gages on specimens D50R1E29 and D75R1E2

5. UNDAMAGED BEAMS TEST RESULTS

5.1 General

The test results of the various specimens of undamaged beams investigated in this study will be discussed in this chapter. At the same time, the analytical results developed in Chapter 3 will be compared to the experimental results wherever applicable. This will include beams designated as U, US1E29, US1E22, and US2E29, the description of these specimens was presented in Chapter 4. The results of each specimen will be discussed separately except in the case of identical specimens. Two control beams (i.e. Beam U) were tested. Two specimens of Beam US1E29 were also tested for reasons previously noted.

The test results that will be presented in this chapter include: strains in concrete, steel, and CFRP; deflection of the beams, and slip between concrete slab and steel beam. It should be noted that all loads reported in this chapter are the applied loads at each hydraulic cylinder (i.e. point load) as illustrated previously in Figs. 4.9 and 4.10. Longitudinal strains and shear stress distribution along the CFRP plate in the strengthened specimens will also be presented.

5.2 Beam U

Two specimens of this type were tested. The difference was mainly in the load distribution across the concrete slab (i.e. the transverse direction). The first beam (Beam U_1) was loaded with a line load using a steel tube across the slab as shown in Fig 5.1. Loading in the second beam (Beam U_2) was applied as a point load as shown in Fig. 5.2.

Using the line load resulted in the formation of longitudinal cracks at a magnitude of load that was much lower than the anticipated ultimate load as shown in Fig. 5.3. This was

Figure 5.1. Line Loading on Beam U_1.

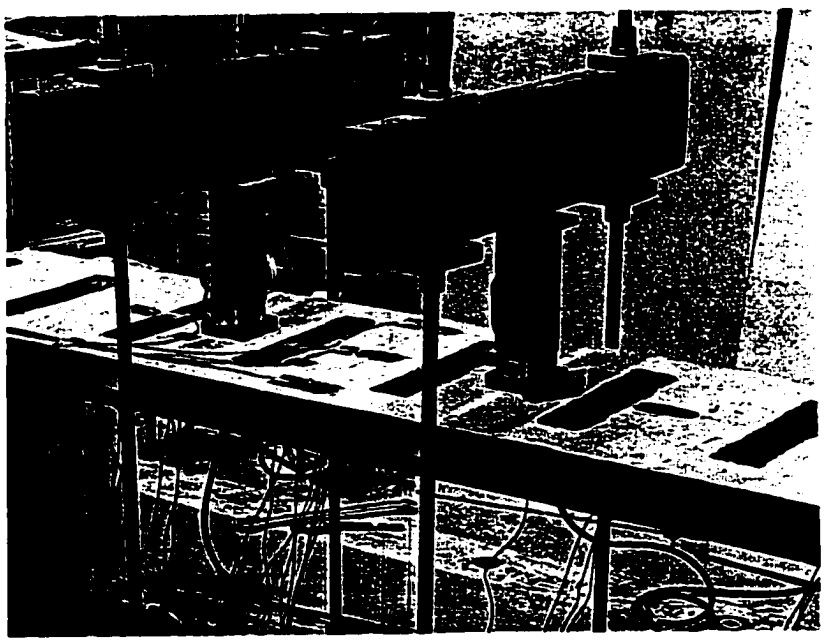

Figure 5.2. Points loading on Beam U_2.

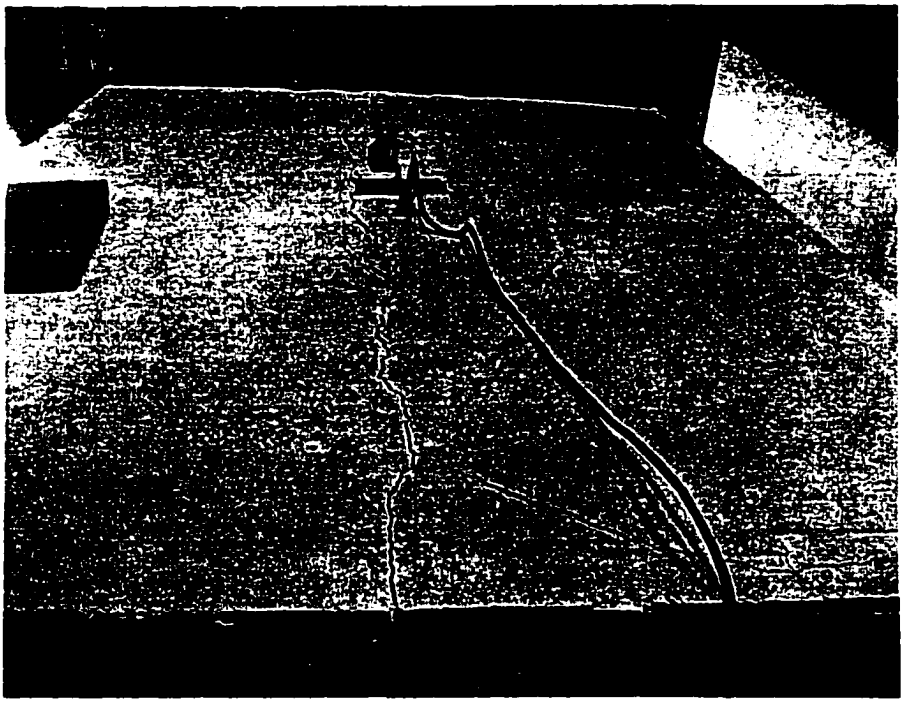

Figure 5.3. Longitudinal cracks caused by line loading on Beam U_1.

due to the transverse bending about the centerline of the steel beam. To overcome this problem, a second specimen was tested with loads applied directly above the steel beam using 6 in. x 6 in. steel plates. Using "point loads " did solve the premature longitudinal crack problem. However, longitudinal cracks were also observed in the second specimen, but this time the cracks were due to the tensile stresses caused by the shear studs. These cracks were mainly in area between the two hydraulic cylinders (i.e. the region of the maximum constant moment). In the second specimen, the cracks did not appear however, until close to the ultimate load. Nevertheless, the ultimate load of both specimens was almost identical as noted in the following paragraphs.

5.2.1 Beam U_1

The load deflection curve of Beam U_1 at midspan is shown in Fig. 5.4. As observed from this figure, the beam behaved linearly until the load reached 21,000 lbs. At this load, the bottom flange of the steel beam started to yield; the yield strain of the steel beam was calculated to be 1,800 microstrain. At the starting of yielding, the beam had already deflected 0.35 in. Longitudinal cracks (see Fig. 5.3) developed before the yield load was reached. Despite this problem, the testing was continued until the beam failed. An ultimate load of 30,500 lbs was reached which caused a deflection of 1.5 in. The load then dropped slightly to about 29,000 lbs while the deflection increased to 2 in. In this figure, the analytical (predicted) response is also shown. As noted, excellent agreement exists between the predicted and the experimental test results. The deviation of the two curves takes place in the inelastic region (i.e. between the elastic and ultimate). This is attributed to the residual stresses in the steel beam that normally reduces the predicted yield stress. Residual stresses can not be included in the analytical model, which results in the minor differences between the two curves.

Figure 5.5 shows the deflection at the midspan as measured by the three Celescos mounted to the concrete slab and the steel beam. It is noted that symmetry was maintained in the transverse direction. Midspan deflection of Beam U_1 (see Fig. 5.4) and subsequent beams was the average of the values obtained from the three Celescos.

Symmetry of the deflections was also maintained in the longitudinal direction, which is shown in Fig. 5.6. The deflection is symmetric about the centerline of the beam at all loading stages. Note that the deflection was measured only at the quarter points and at the midspan and a curve was fitted between the points.

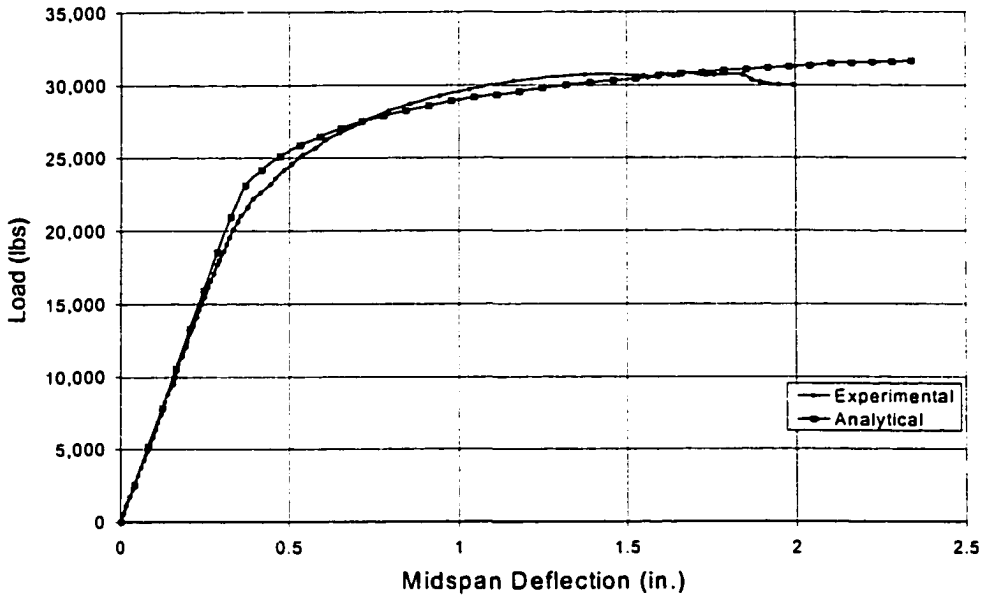

Figure 5.4. Midspan deflections of Beam U_1.

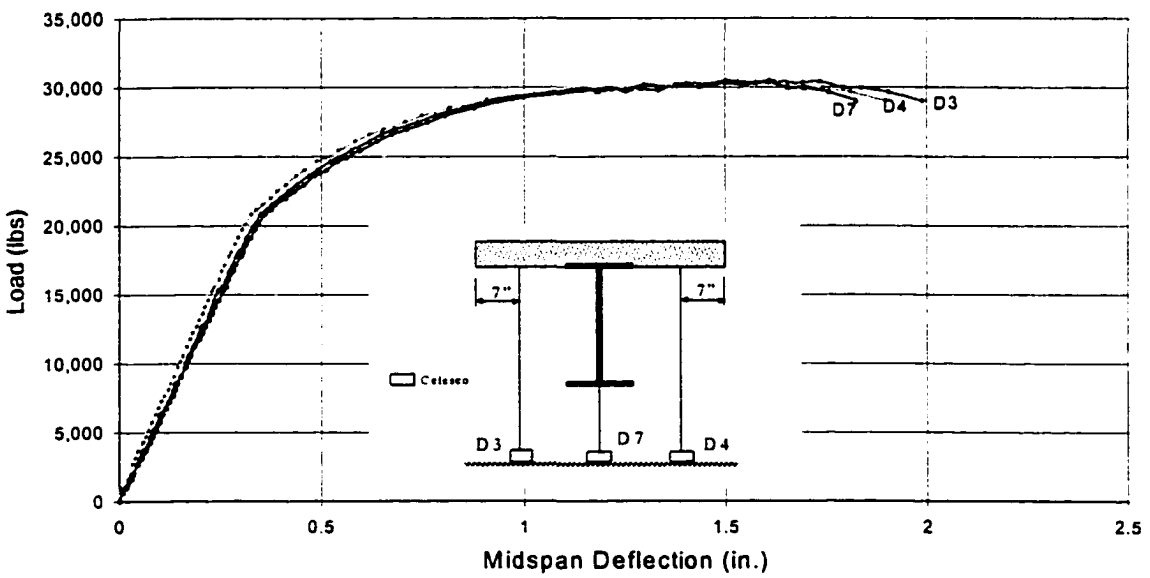

Figure 5.5. Midspan deflections of Beam U_1 measured by Celescos D3, D4, and D7.

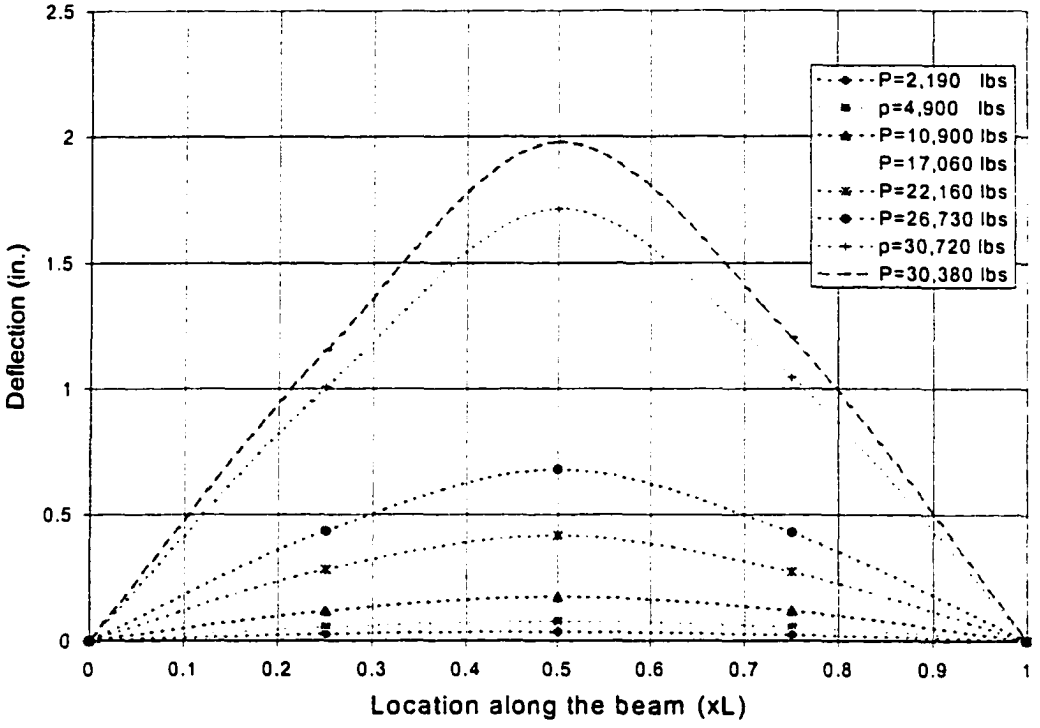

Figure 5.6. Deflections along Beam U_1 at different load levels.

At a load of 29,000 lbs, the top surface of the concrete slab failed at approximately 2,300 microstrain as can be seen in Fig. 5.7; at this point the test was terminated. Large ductility was observed prior to failure of the beam as indicated by the large deflections. It should be noted that numerous flexural cracks in the concrete slab were observed within the maximum constant moment (i.e. the region between the loading points). These cracks increased in width as the load was increased and shifted upwards from the bottom of the concrete slab as expected; the cracks stopped at about 2 in. from the top surface of the concrete slab. This was very close to the theoretical neutral axis, which was found to be 2.06 in.

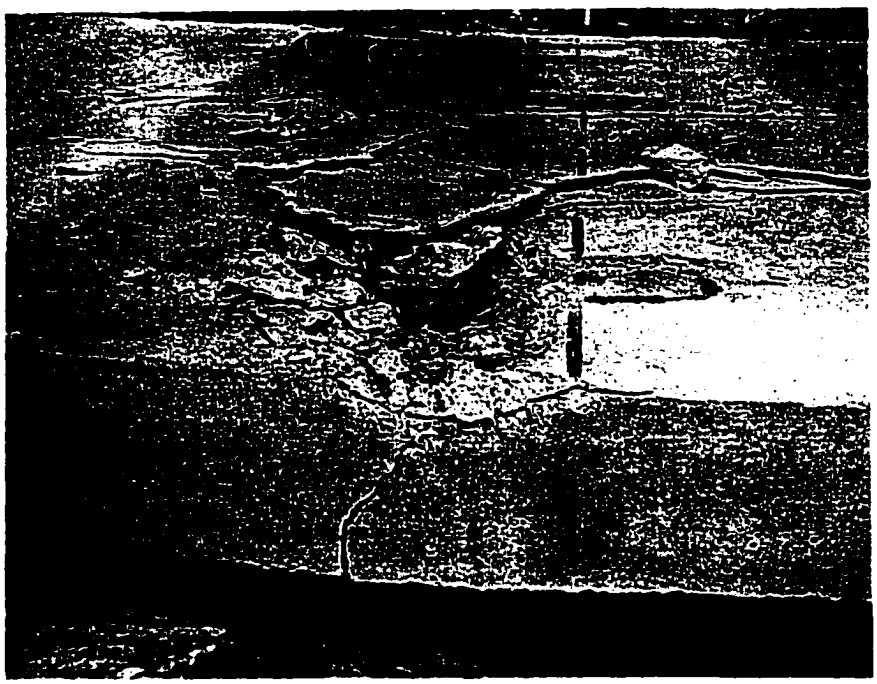

Figure 5.7. Crushing of concrete slab in Beam U_1.

Strain profiles across the depth of the composite beam for different magnitudes of applied loads are illustrated in Fig. 5.8b and Fig. 5.9. As noted previously, the loads are per load point; various loads were selected to show the change in strain from elastic behavior until close to ultimate. The theoretical position of the neutral axis was calculated for all load increments (see Fig. 5.8a) and was found to be approximately 2.9 in. in the elastic range (i.e. for loads < 23,000 lbs). This agrees very well with the experimental data shown in Fig. 5.8b. As can be noticed in this figure, at loads within the elastic range, the strain distribution remained linear as expected. However, at higher loads, the neutral axis started to shift upwards as higher nonlinear stresses in concrete started to develop and a larger moment arm

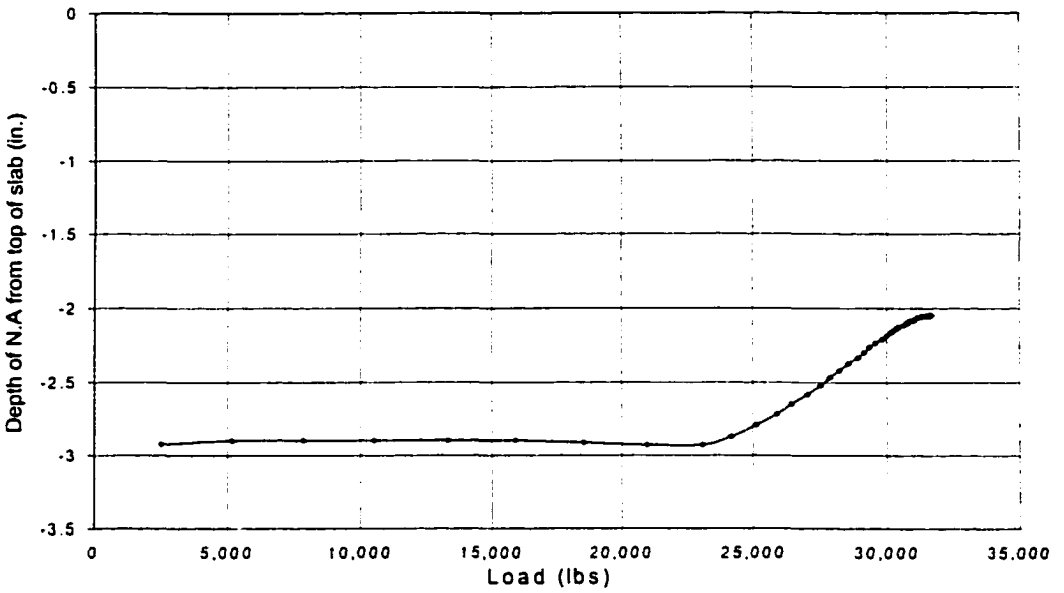

a. Theoretical position of neutral axis in Beam U_1

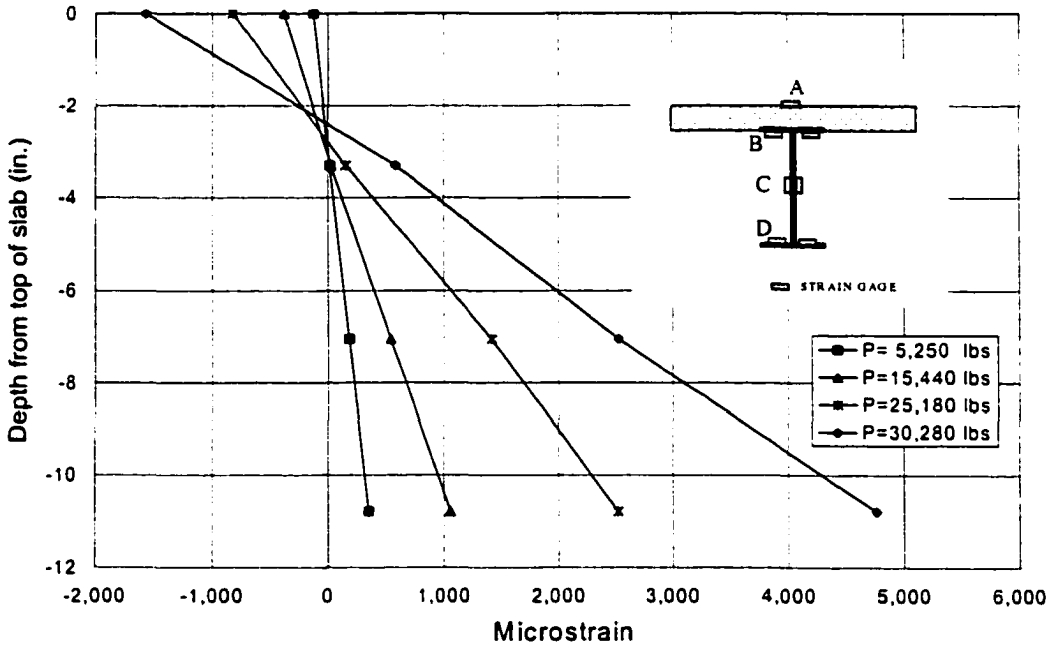

b. Strain profile at midspan of Beam U_1

Figure 5.8. Theoretical position of neutral axis and strain profile at midspan of Beam U_1.

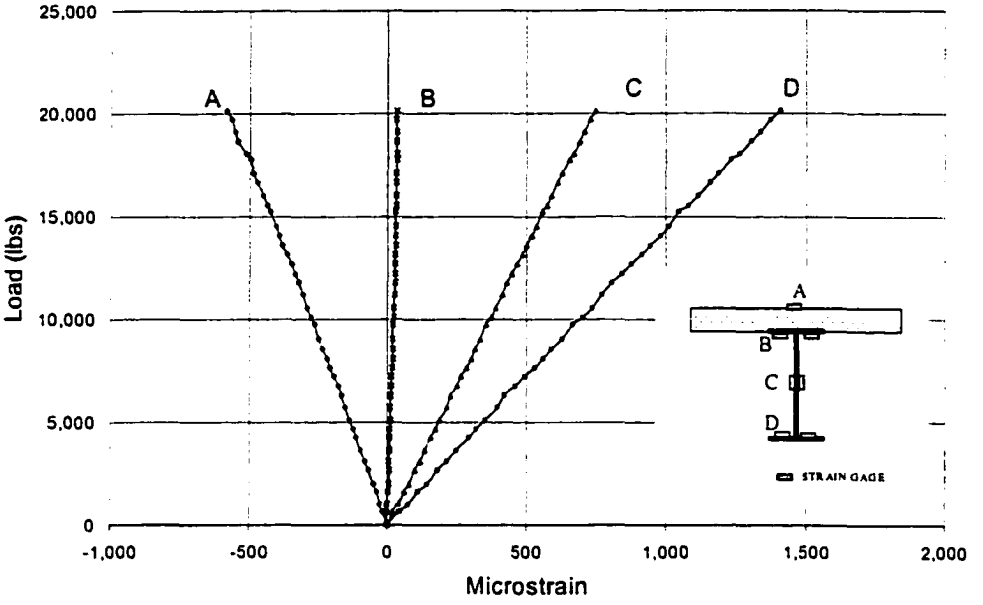

Figure 5.9. Strains at midspan of Beam U_1.

was needed to provide the required resisting moment.

The upward shift of the neutral axis is obvious in the figure as the load increased beyond 23,000 lbs. At this load, the bottom flange started to yield. This can be seen from the nonlinear curve of the strain distribution at loads higher than 23,000 lbs. To satisfy the equilibrium of internal forces, the shift of the neutral axis after the yielding of the steel occurred since the force component in the steel beam (tension) will remain constant, and the force in the concrete slab (compression) also has to remain constant. Hence, the increase in the moment capacity is only possible by increasing the moment arm between the two forces.

The strain in the top surface of the concrete slab for the entire load range is shown in Fig. 5.10. Very good correlation is observed between the experimental data and the analytical prediction. Again, the experimental and analytical curves slightly differ close to

the yield load (~ 23,000 lbs) and this is attributed to the residual stresses in the steel beam and the approximate nature of the mathematical model of the material behavior. The analytical curve was based on an ultimate concrete crushing strain of 3,000 microstrain; the observed crushing strain was slightly lower than this as illustrated in Fig. 5.10.

The strains in the bottom of the top flange of the steel beam as well as at mid height of the web are shown in Fig. 5.11 and Fig. 5.12, respectively. Again there is a reasonable correlation between the experimental and analytical curves. Deviation between the analytical and experimental curves is attributed to the reasons noted earlier.

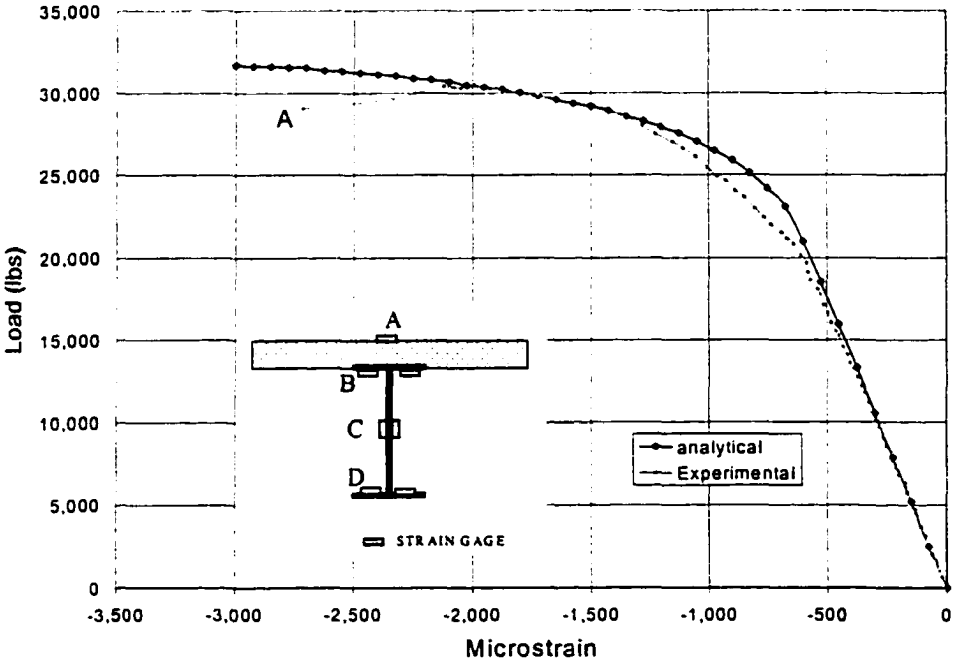

Figure 5.10. Strain in concrete top surface at midspan of Beam U_1.

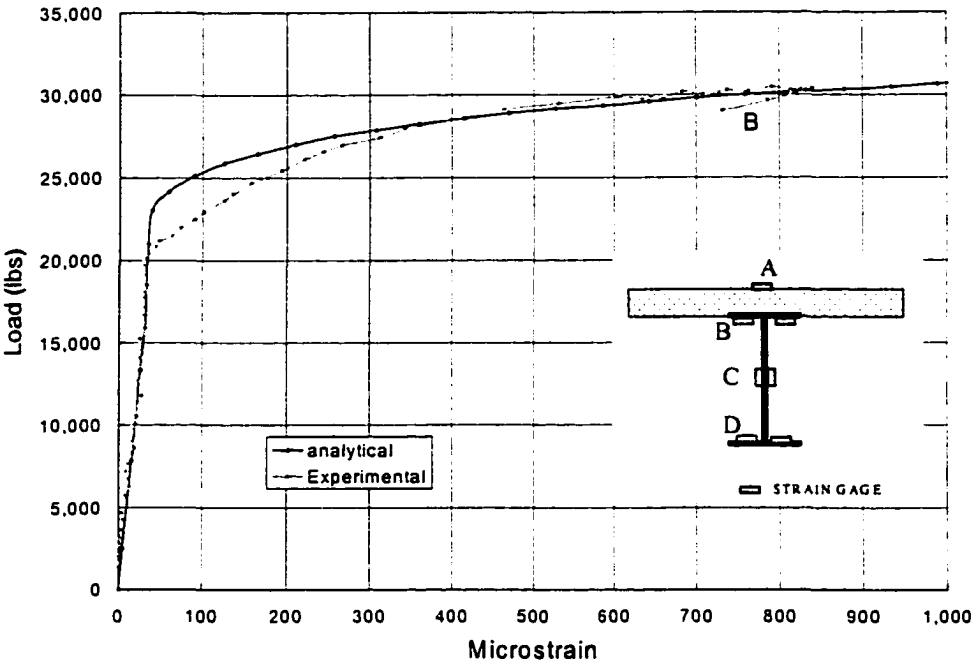

Figure 5.11. Strain in the bottom of top flange of the steel beam at midspan of Beam U_1.

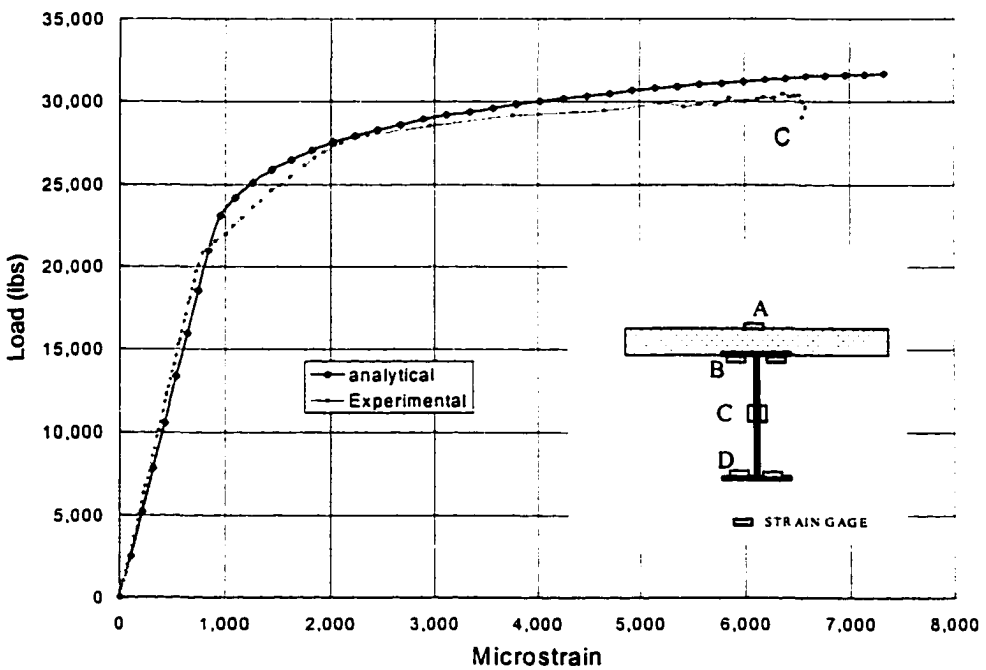

Figure 5.12. Midspan strains at mid height of the web of Beam U_1.

5.2.2 Beam U_2

As previously noted, the second beam specimen (Beam U_2) was tested under point loads. This specimen was tested to insure that the longitudinal cracks caused by the line load used on Beam U_2 did not dramatically affect the overall behavior of the beam. In addition, the second test was undertaken to determine if the experimental results were reproducible.

The test results of this specimen were very similar to that of Beam U_1. Midspan deflections for both beams are shown in Fig. 5.13. As can be seen in this figure, the response of both specimens was almost identical. This in fact shows that both loading systems will produce essentially the same results.

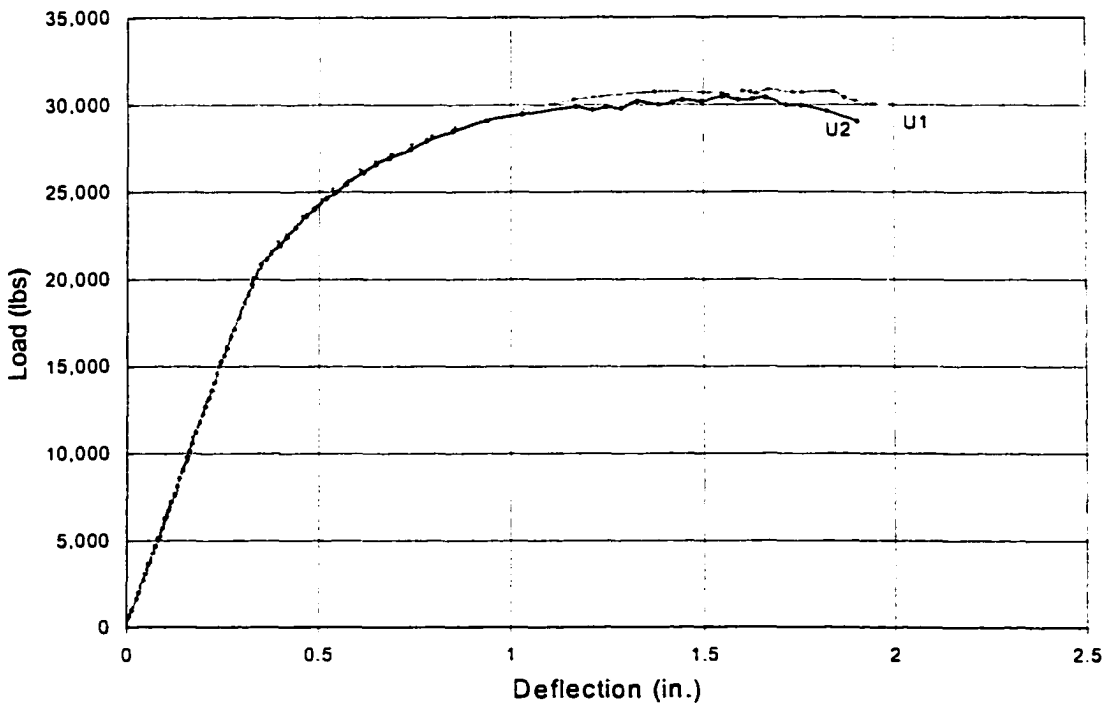

Figure 5.13. Midspan deflections in Beam U_1 and Beam U_2.

However, due to the fact that the line loading produced longitudinal cracks at an early stage of loading, there will be some confusion when more longitudinal cracks develop at higher loads due to tensile stresses caused by the shear studs as will be shown later. Because of this, the rest of the specimens were tested using point loads.

Since the strain distribution and other results of this specimen are similar to those of Beam U_1, they are not repeated here. It should be noted that in the next sections of this chapter and the following chapter, wherever Beam U is mentioned it refers to Beam U_2 unless otherwise stated.

5.3 Beam US1E29

This specimen was strengthened by applying the 4 in. wide CFRP plate to the bottom flange (Strengthening Scheme 1) as shown previously in Fig. 4.1. The purpose of this test was to determine the effect of the strengthening on the behavior of the beam. Two specimens of this type were tested. Discussion of Beam $US1E29_1$ results will be presented first, then Beam $US1E29_2$ results will be discussed in the following section.

5.3.1 Beam $US1E29_1$

This beam was the first specimen that was strengthened with the CFRP. The beam was tested one week after the application of the CFRP; one week is recommended by the CFRP and epoxy supplier for curing.

Midspan deflections are shown in Fig. 5.14a., which shows that the response is linear until the load reached 22,500 lbs; the response then becomes nonlinear as expected.

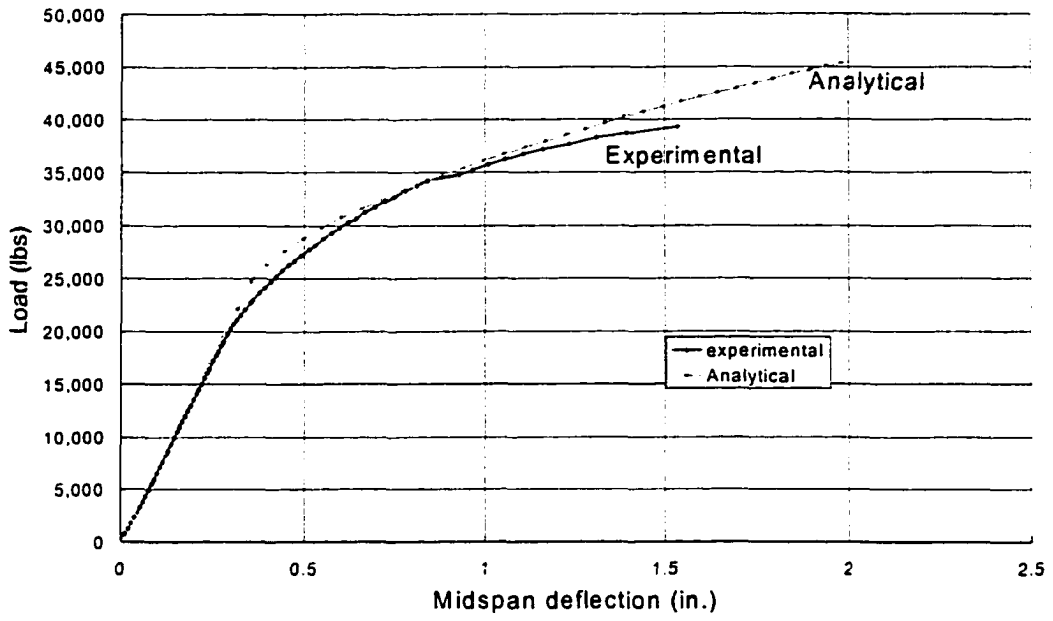

a. Analytical and experimental deflections at midspan

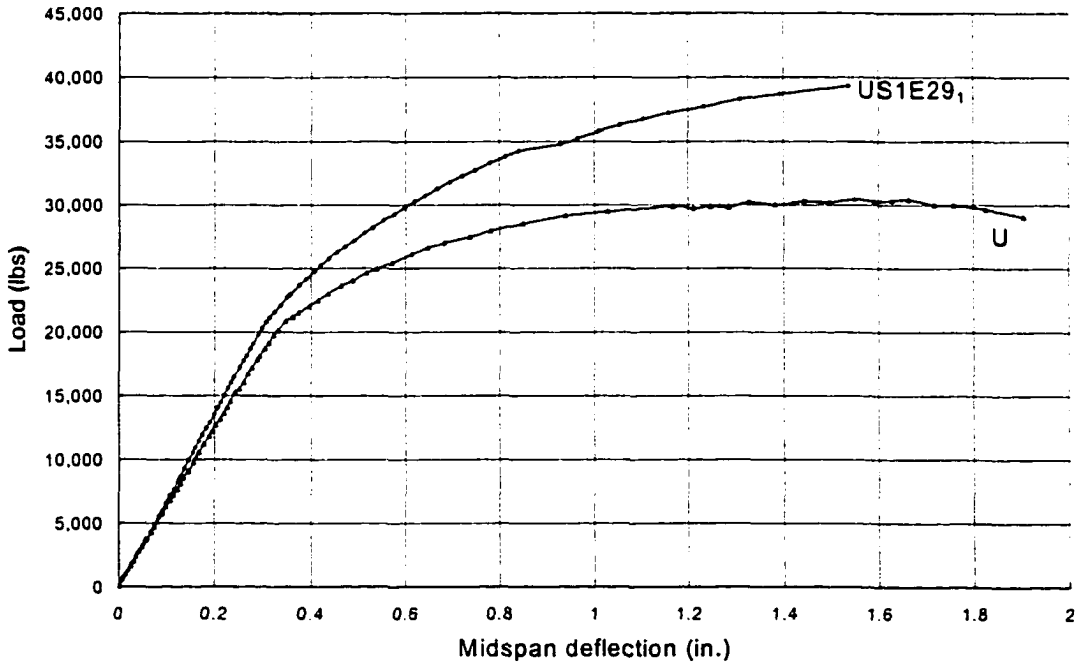

b. Comparison of midspan deflections of Beam US1E29$_2$ and Beam U

Figure 5.14. Midspan deflections of Beam US1E29$_1$.

However, the slope of the deflection curve will not "flatten out" as the case in a beam without CFRP reinforcement (i.e. control beam) as observed from Figure 5.14b.

The beam will continue to carry additional load beyond the yield point until failure. However, most of the elastic stiffness of the steel beam is lost once it starts to yield. Beyond the yield point, the stiffness is normally defined by the tangential modulus of elasticity (E_T), which is essentially zero as is normally the case when assuming elastic-perfectly plastic relation. On the other hand, the CFRP plate has a linear elastic constitutive relation. Since the CFRP has a constant stiffness (modulus of elasticity) until failure, the CFRP plate will immediately pick up load after the bottom flange starts to yield. This can be seen from the midspan strain profile shown in Fig. 5.15. Once the bottom flange starts to yield, the beam will tend to deflect and rotate excessively at the midspan as the plastic hinge starts to form in this region. However, the presence of the CFRP plate will tend to prevent the plastic flow in the bottom flange by applying a confining stress to prevent this. This can also be seen when comparing the deflection of the two beams at a load of 30,000 lbs. (see Fig. 5.14b), which is basically the failure load of Beam U_2. The deflection of the control beam (Beam U_2) at failure is very close to 2.0 in., while the deflection of Beam $US1E29_1$ at this magnitude of load is only 0.6 in.

Behavior similar to that of the Beam U specimens was observed in the elastic (linear) range. Longitudinal cracks developed between the loading points at an applied load of 34,000 lbs. At this magnitude of load, cracking sounds were heard, which was due to the slip between the concrete slab and the steel beam as indicated by the flat portion of the experimental curve at a load of about 34,000 lbs (see Fig. 5.14a). As previously noted, no

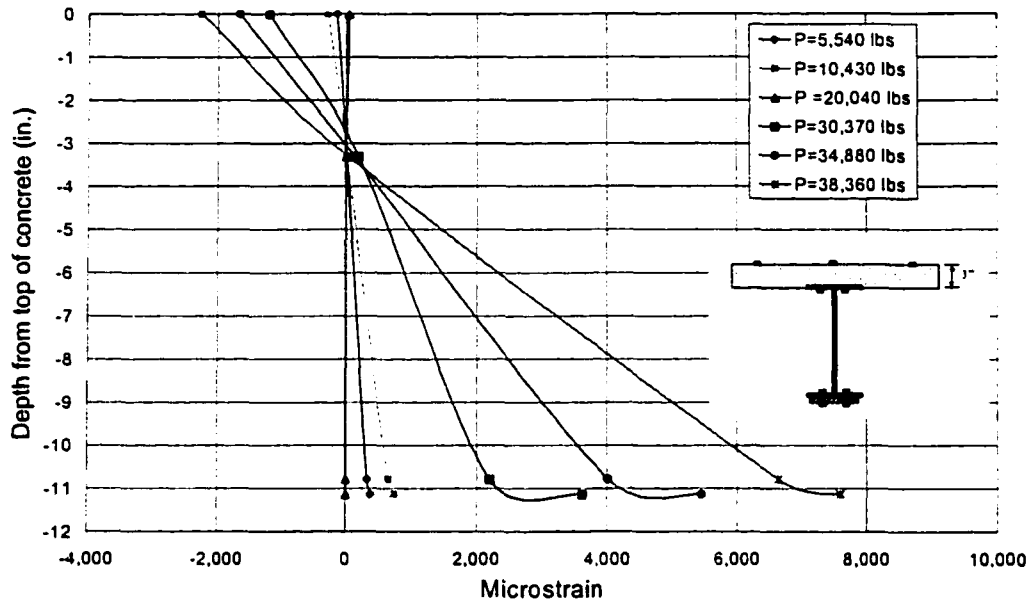

Figure 5.15. Strain profile at midspan of Beam US1E29$_1$.

measurement of slip was taken in this specimen. However, the strains in the top flange of the steel beam show a reversal of sign (i.e. stress changes from tension to compression) at this load as an indication of slip and redistribution of strain as illustrated in Fig. 5.16. Upon completion of the test, the shear connectors were exposed to see any signs of separation between the concrete and the shear studs. A gap was found between the shear stud and the concrete in the longitudinal direction as shown in Fig. 5.17, which further confirmed that slip had occurred at this load. The failure of this beam was due to the premature rupture of the CFRP plate, which was violent and sudden. At the end of the test, it was found that the CFRP failed approximately beneath the applied load as shown in Fig. 5.18. The last recorded strain in the CFRP was approximately 8,000 microstrain, which was considerably less than

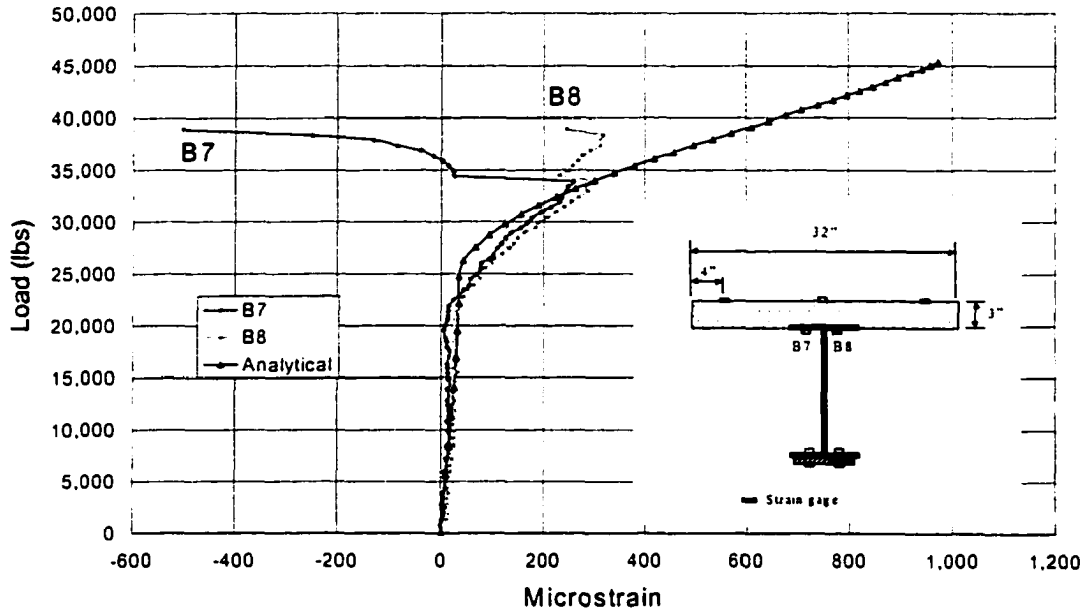

Figure 5.16. Reversal of strains in top flange due to slip in Beam US1E29$_1$.

Figure 5.17. Photograph of gap between shear connector and concrete in Beam US1E29$_1$.

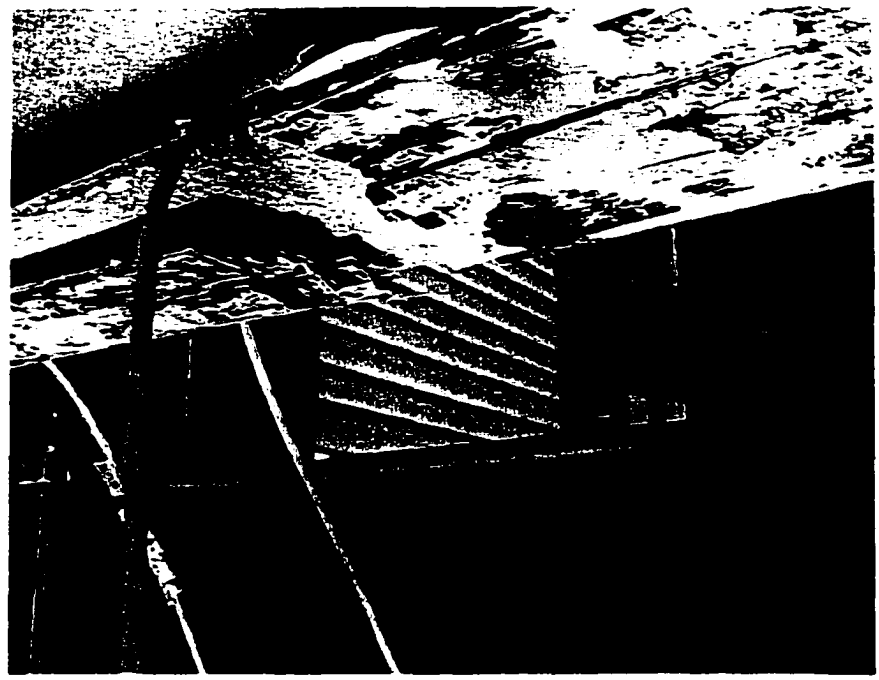

Figure 5.18. Photograph of ruptured CFRP plate in Beam US1E29$_1$.

the theoretical ultimate strain of 13,000 microstrain provided by the manufacturer. The strain profile shown earlier in Fig. 5.15 suggests that no delamination occurred prior to the failure of the CFRP plate. If delamination of the CFRP had taken place, a sudden reduction in the CFRP strain would have been recorded.

5.3.1.1 Longitudinal strains and shear stresses

The longitudinal strains along the CFRP plate are shown in Fig. 5.19a. These strains were measured at locations according to instrumentation plan shown in the previous chapter (see Fig. 4.13). It should be pointed out that measured strains are shown by the points on the graph. The lines that connect the points are only included for clarification and comparison of

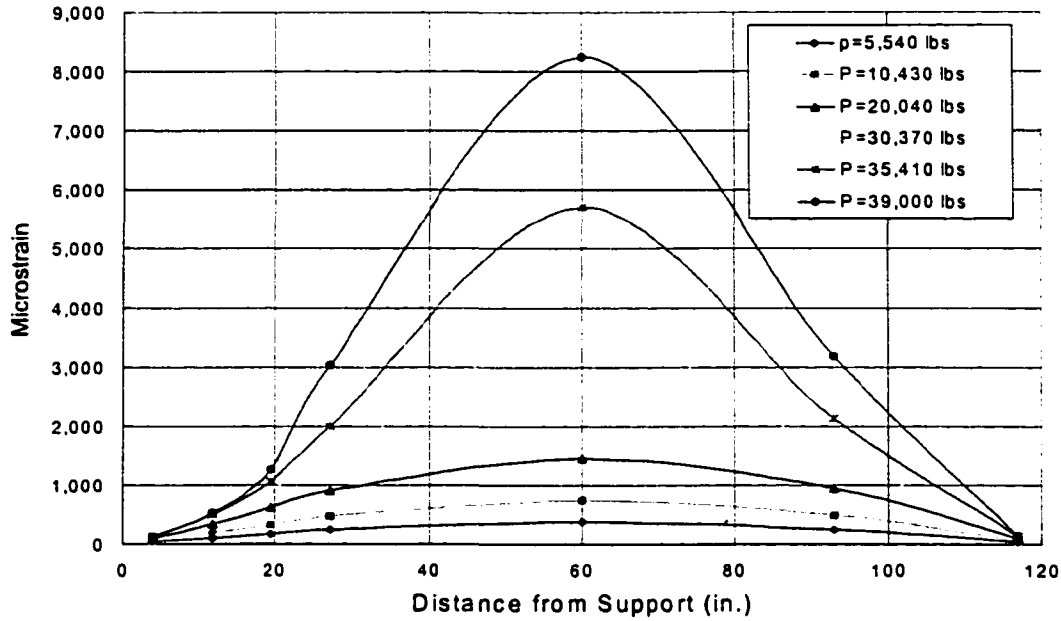

a. Longitudinal strains

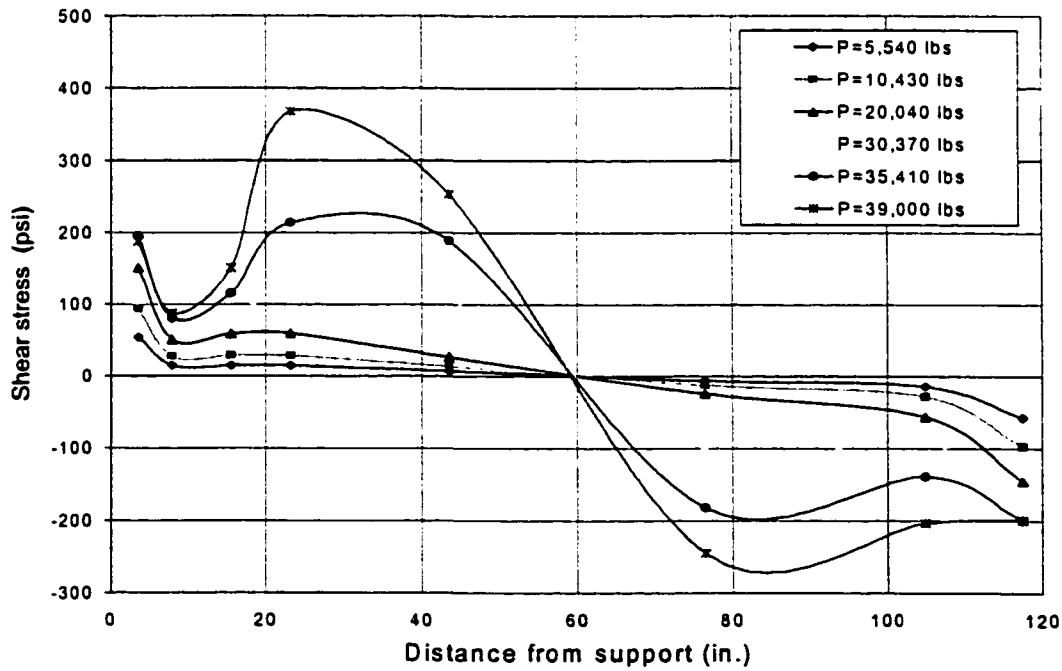

b. Shear stresses

Figure 5.19. Longitudinal strains and shear stresses in the CFRP plate in Beam US1E29$_1$.

strains at different magnitudes of applied loads. From this figure, it is observed that within the elastic range of loading (i.e. for loads < 25,000 lbs), the distribution of the strain along the CFRP is smooth and gradual. However, at higher loads, the distribution becomes like natural distribution curves with the highest strains within the middle two-thirds of the beam length. This is because as the steel yields in the maximum moment region and the yielding extends towards the ends of the beam, the CFRP plate will take more stress to compensate for the yielding steel.

Figure 5.19b shows the shear stresses (see Section 3.6) corresponding to the measured longitudinal strains. From this graph, one can see that at loads within the elastic limit, the shear stresses distribution follows the classical elastic theory of adhesive bonded joints. The joint (or plate end) will experience very high stress concentration. That is, the shear stress is highest at the edge of the CFRP plate and decreases away from the joint. However, as the steel starts to yield at the maximum moment region, the shear stress distribution deviates from the elastic theory predictions. This is due to the fact that as the steel yields at the maximum moment region, the CFRP plate will pick up the high stresses in this region. As the plastic stresses propagate away from the center of the beam, the CFRP plate will resist more longitudinal stresses. These stresses are transferred by very high shear stresses. This is observed from the shear stresses plots, where the highest shear stresses are not at the joint (edge of the CFRP plate). As can be seen from Fig.5.19b, the shear stresses are much higher at the quarter points than at the ends. Reviewing the location of the rupture of the CFRP plate, it was found to be very close to this location.

5.3.2 Beam US1E29$_2$

The second beam (Beam US1E29$_2$) was tested for additional data and confirmation of the repeatability of the experiment. Figure 5.20a shows the load-deflection relation at midspan. Again, this beam behavior was similar to that of Beam US1E29$_1$. The beam did not reach its ultimate predicted load due to slip between the concrete slab and the steel beam as shown in Fig. 5.21.

As in Beam US1E29$_1$, the longitudinal cracks started to form between the loading points at a load of 38,000 lbs. The same cracks then extended in the shear span (between the loading point and the support). Diagonal (shear) cracks were also observed in the shear span. It is noted that at this load, the slip between the concrete slab and the steel beam became large (as observed in Fig. 5.21) and the beam did not carry any significant additional load. A maximum deflection of 2.4 in. was reached at midspan before the CFRP plate ruptured similar to Beam US1E29$_1$. The response of this beam is compared to that of the control beam (Beam U) in Fig. 5.20b, which shows large ductility prior to failure.

For composite action to take place between the concrete slab and the steel beam, the shear connectors have to transfer the shear force between these elements. Slip occurs partly due to deformation of the concrete around the shear connector and partly to deformation of the shear connector. However, at small loads, the shear force is transferred mainly by the bond (chemical and mechanical) between the concrete and the steel; the shear connectors at this stage provide a clamping force that keeps both surfaces in contact for friction to take place. As seen from Fig. 5.21, for small loads within the elastic range (load < 25,000 lbs),

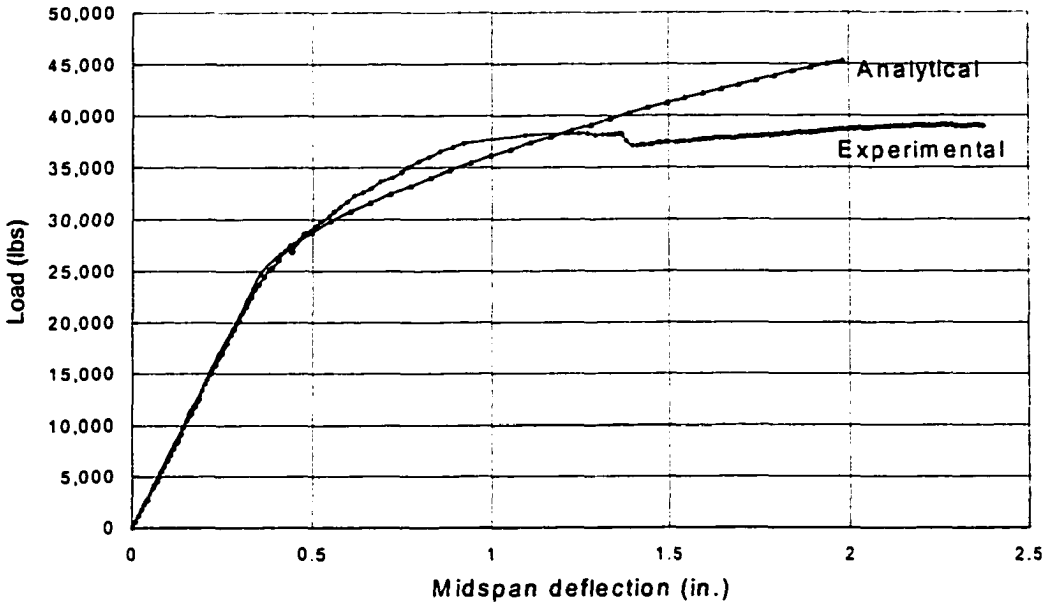

d. Analytical and experimental deflections at midspan.

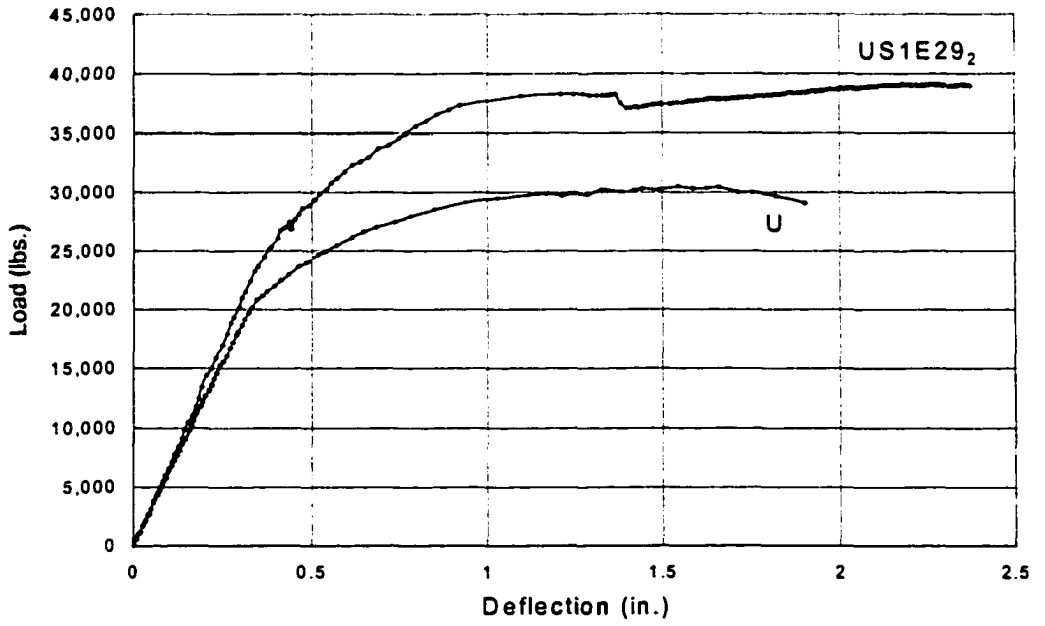

b. Comparison of midspan deflections of Beam US1E29$_2$ and Beam U

Figure 5.20. Midspan deflections of Beam US1E29$_2$.

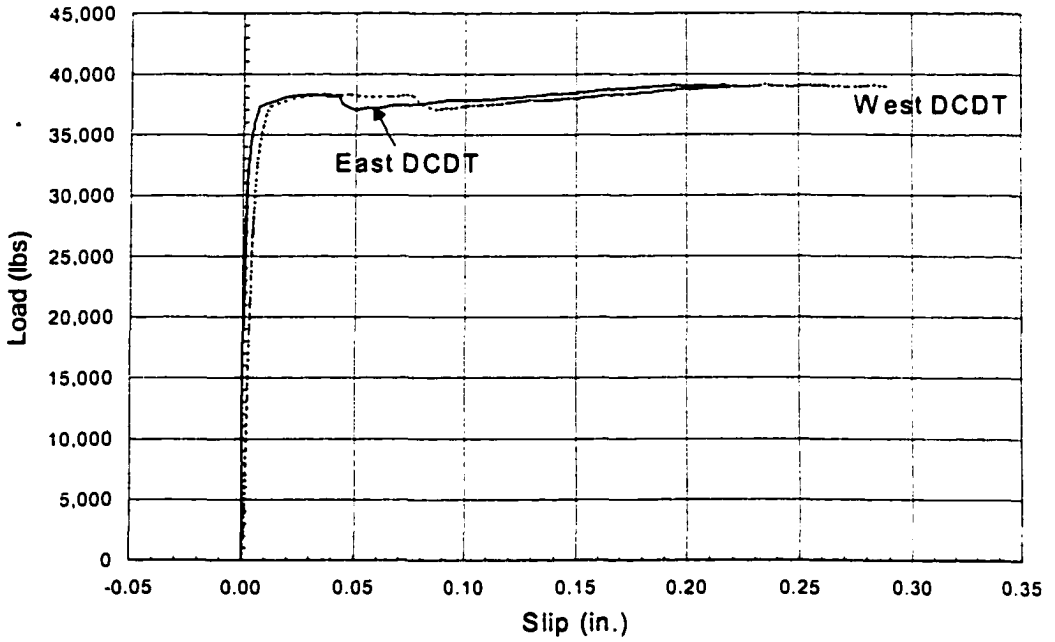

Figure 5.21. Slip between concrete slab and steel beam in Beam US1E29$_2$.

almost no slip occurred. However, at loads close to the ultimate, slip will occur depending on the amount of interaction between the concrete slab and the steel beam. The degree of interaction will affect the strain distribution across the depth of the composite section as illustrated in Fig. 5.22. This figure shows three cases of interaction between the concrete slab and the steel beam: the no interaction case, where no shear connection is provided; the complete (full) interaction case, where sufficient amount of shear connectors is provided to guarantee no slip will occur; and the partial interaction case, which is intermediate between the two limiting cases.

Slip in Beam US1E29 and the other strengthened beams is attributed to the formation

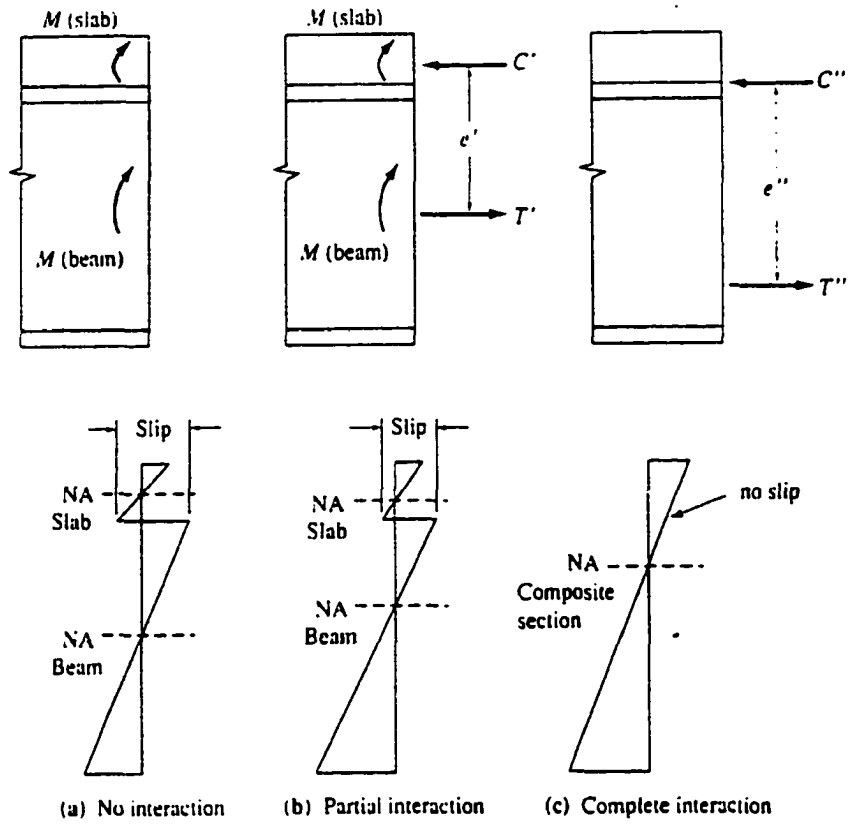

Figure 5.22. Strain variation in composite beams.

of longitudinal cracks. By reviewing the crack pattern in the concrete slab shown in Fig. 5.23, it is observed that the longitudinal cracks divided the slab section into three segments; one segment is between the shear studs and the other two are outside this zone. At high loads, slip of the outer concrete slab segments occurred since the bond was not sufficient to resist the interface shear force due to the limited contact surface area. The shear force is believed to be transferred partly by shear interlock along the beam at the interface of the concrete and the shear connectors and partly by the transverse reinforcement. In this case, it is obvious that the longitudinal cracks caused the initiation of slip rather than plastic

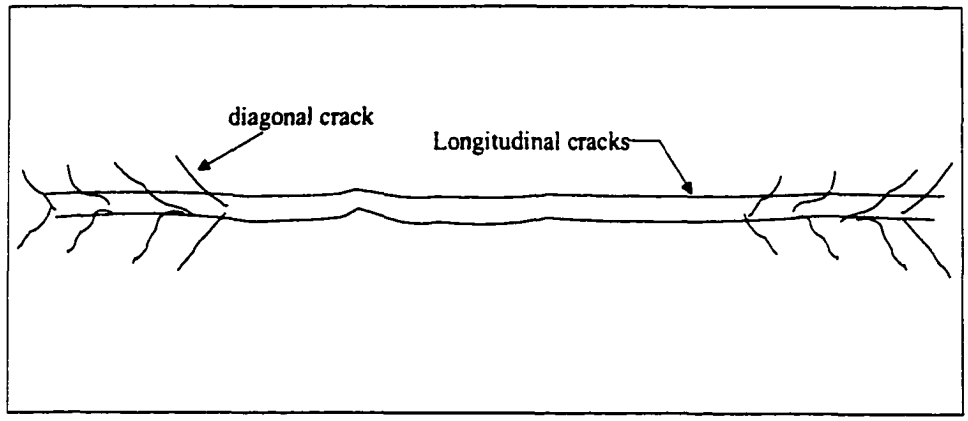

a. Plan view of crack pattern in concrete slab

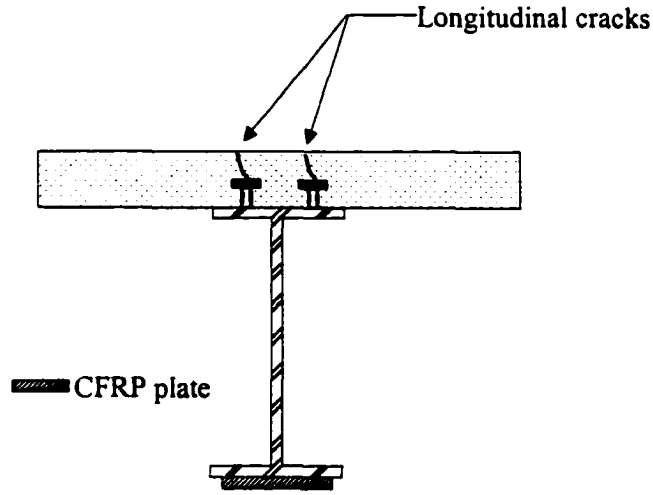

b. End View

Figure 5. 23. Typical longitudinal crack pattern in concrete slab of composite beams.

deformation of the shear connectors. After the test, the concrete slab was demolished and the shear connectors were visually inspected for any deformations. No sign of deformation was found on any of the shear connectors. Again, the slip caused strain redistribution across the depth of the beam section as shown in Fig. 5.24. In this figure, the strain profile corresponding to a load of 38,800 lbs (when slip occurred) is shown by a continuous line and a dashed line. The continues line cannot be true since the neutral axis will fall in the web of the steel beam, while the analytical neutral axis position was found to be approximately 2.5 in. The dashed line in the same figure is an assumed strain profile of what might be the true strain at that particular load based on the discussion in the previous paragraph and Fig. 5.22.

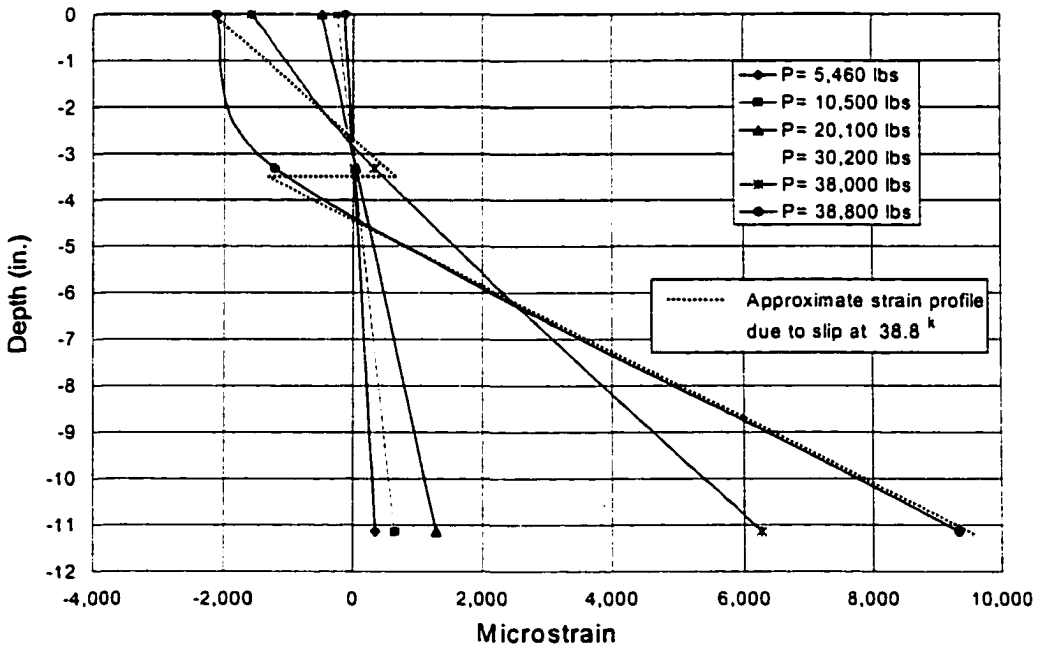

Figure 5.24. Midspan strain profile of Beam US1E29$_2$.

Figure 5.25 shows the change in top flange strains from tension to compression as a result of slip. Variation of strain as a function of slip is illustrated in Fig. 5.26. This figure shows that strain in the concrete did not change significantly after a slip of 0.02 in., while the strain in the steel beam continued to increase as an indication that the additional load was mainly carried by the steel beam.

The longitudinal strains and shear stresses for this specimen are shown Fig. 5.27. A behavior similar to that of Beam US1E29$_1$ is observed as expected; however, the magnitudes of longitudinal strains are higher at failure. The maximum longitudinal strain was close to 10,000 microstrain compared to 8,000 microstrain in Beam US1E29$_1$. Again no deterioration of bond between the CFRP plate and the steel beam was observed during testing. Although, the beam did not reach its ultimate load, the large deflections and high stresses in the CFRP plate prior to failure proved that bond between the CFRP and the steel beam was excellent.

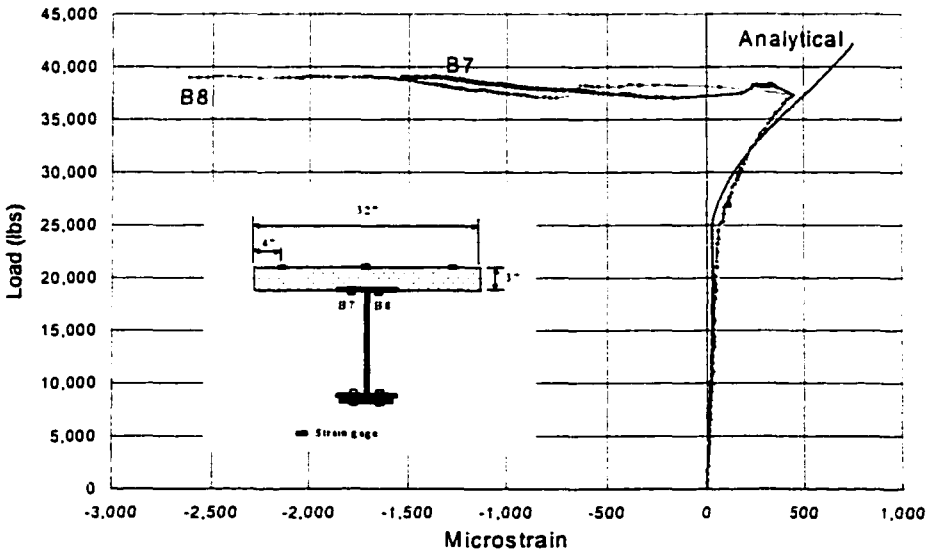

Figure 5.25. Reversal in top flange strains due to slip in BeamUS1E29$_2$.

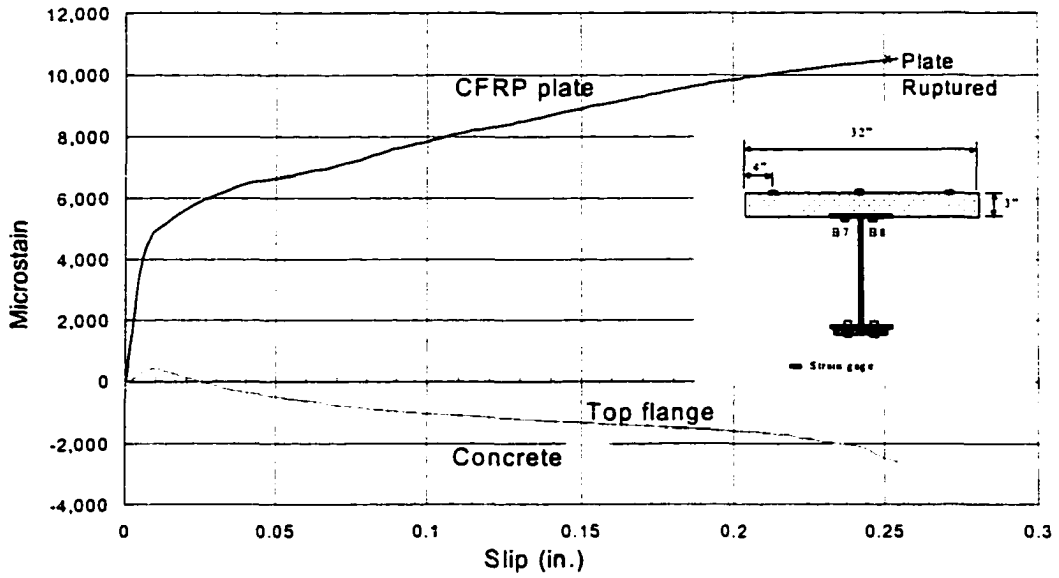

Figure 5.26. Strain variation at midspan as a function of slip in Beam US1E29$_2$.

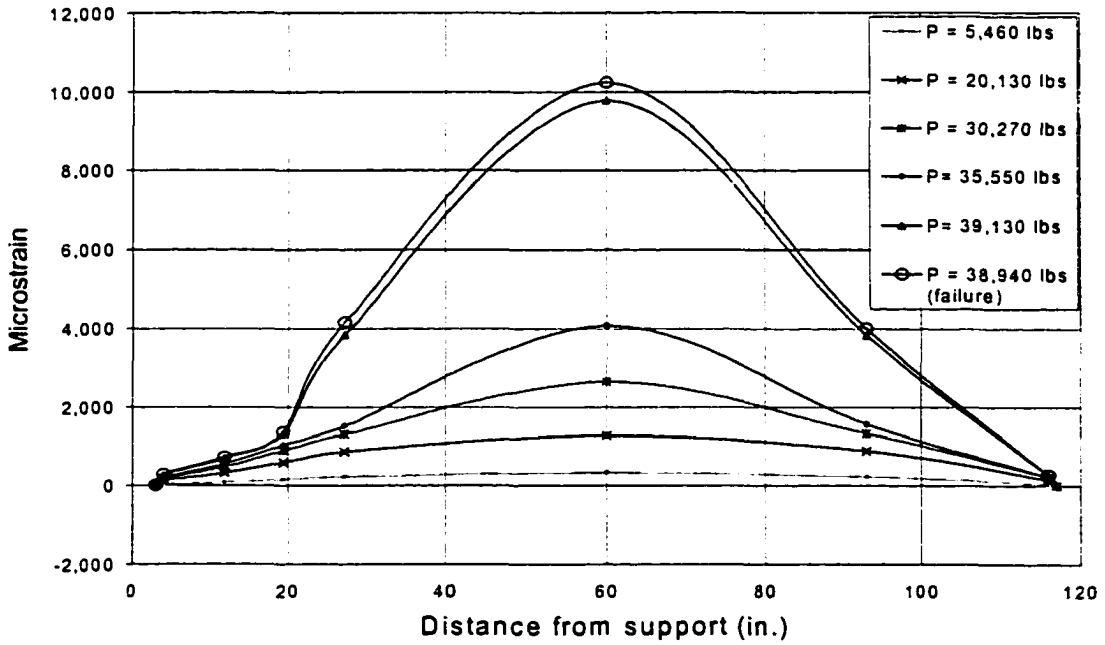

a. Longitudinal strains

Figure 5.27. Longitudinal strains and shear stresses in the CFRP plate in Beam US1E29$_2$.

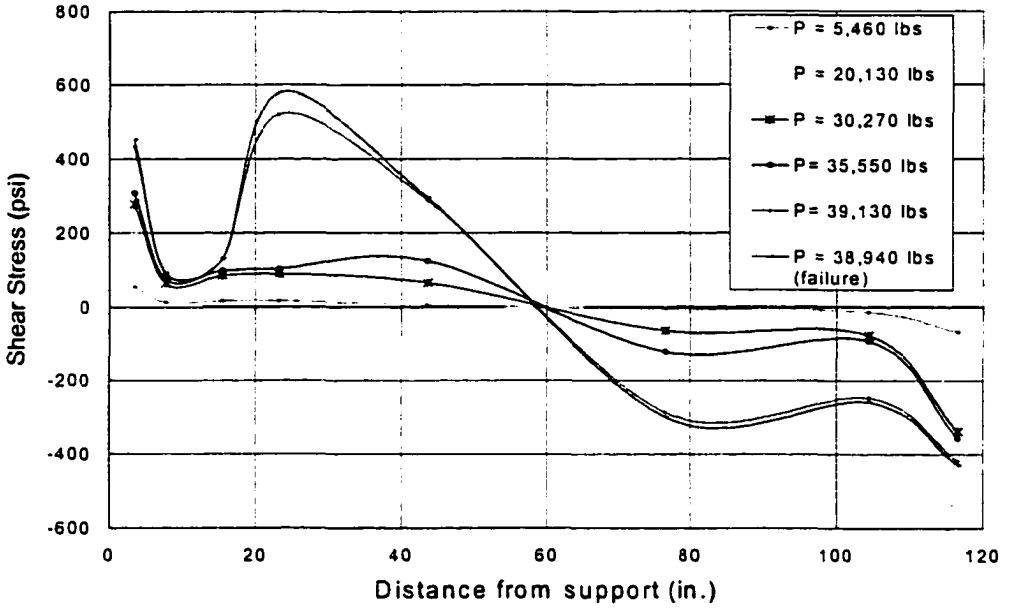

b. Shear stresses

Figure 5.27. Continued.

5.4 Beam US1E22

This specimen is similar to the previous one (i.e. Beam US1E29) except the CFRP plate has a modulus of elasticity of 22,000 ksi instead of 29,000 ksi. Similar behavior was observed as in the previous strengthened beams. Deflections of Beam US1E22 at midspan are shown in Fig. 5.28a. and compared to the control beam (Beam U) in Fig.5.28b; the response was linear until the applied load reached 25000 lbs. Slip between the concrete slab and the steel beam initiated the failure of the beam, which occurred at an applied load of 37,000 lbs as shown in Fig. 5.29. Again, the slip was preceded by the formation of longitudinal cracks caused by the localized tensile stresses in the transverse direction at the

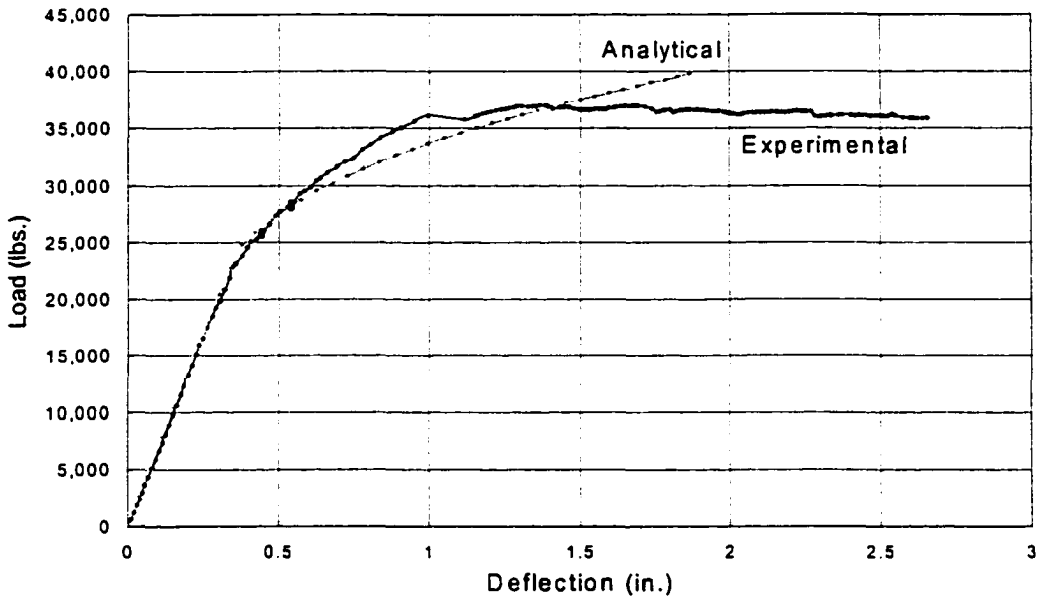

a. Analytical and experimental midspan deflections of BeamUS1E22

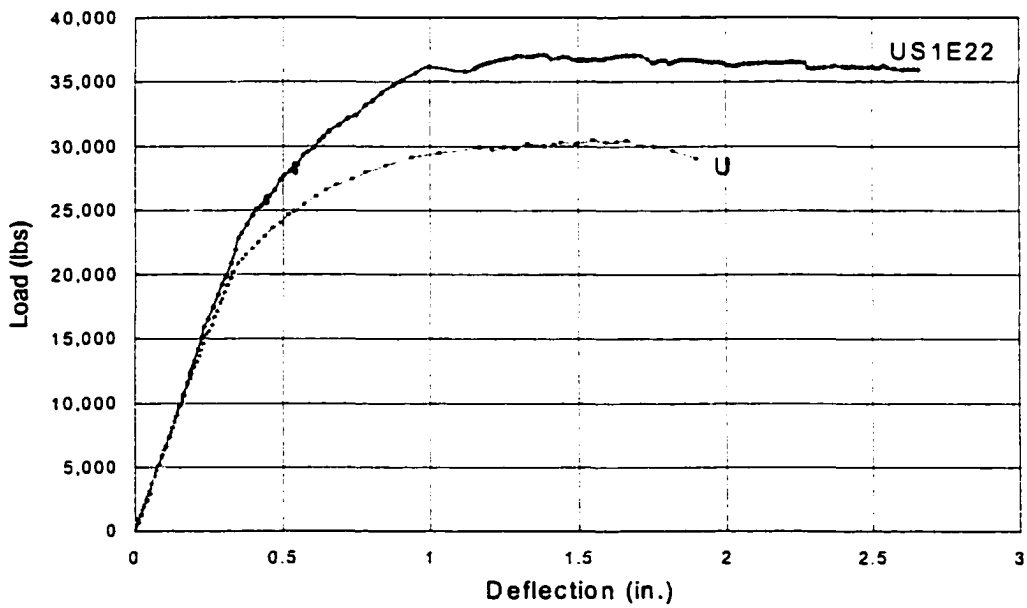

b. Comparison of midspan deflections with control beam (Beam U).

Figure 5.28. Midspan deflections of Beam US1E22.

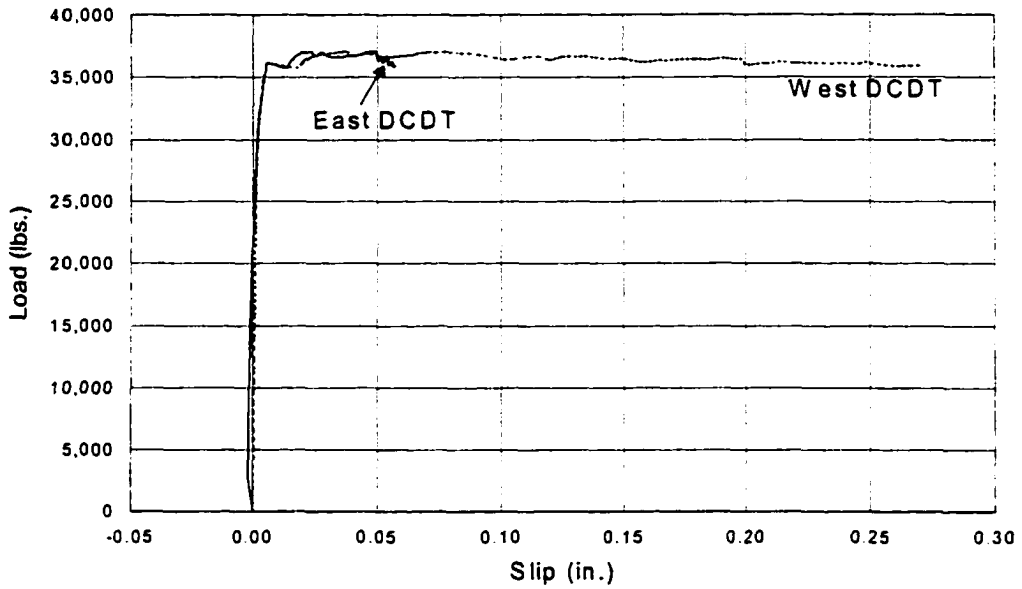

Figure 5.29. Slip between concrete slab and steel beam in Beam US1E22.

shear stud/ concrete interface in the region of the maximum moment. As may be seen in Fig. 5.29, the slip near the west support was larger than that near the east support. More cracks were observed on the west side of the beam before failure, even though, the loading was perfectly symmetric through out the test as illustrated by Fig. 5.30 (i.e. quarter point deflections and three-quarter point deflections essentially the same).

As may be seen in Fig. 5.28a, excellent correlation between the analytical and experimental results was found in the elastic range. This is due to the fact that full composite interaction between the concrete slab and the steel beam was maintained as evident from the strain profile at midspan shown in Fig. 5.31. From this figure, it is observed that the experimental strain profile varied linearly for loads less than 37,000 lbs, and the position of the neutral axis agrees very well with the analytical prediction (which was 3.1 in. for loads

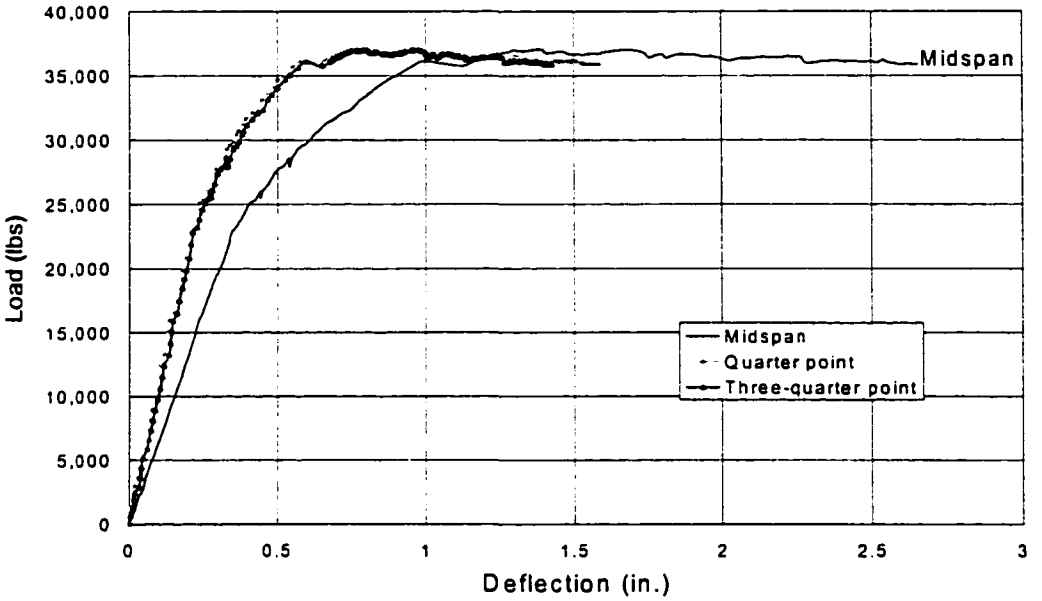

Figure 5.30. Deflections of Beam US1E22 at midspan and the quarter points.

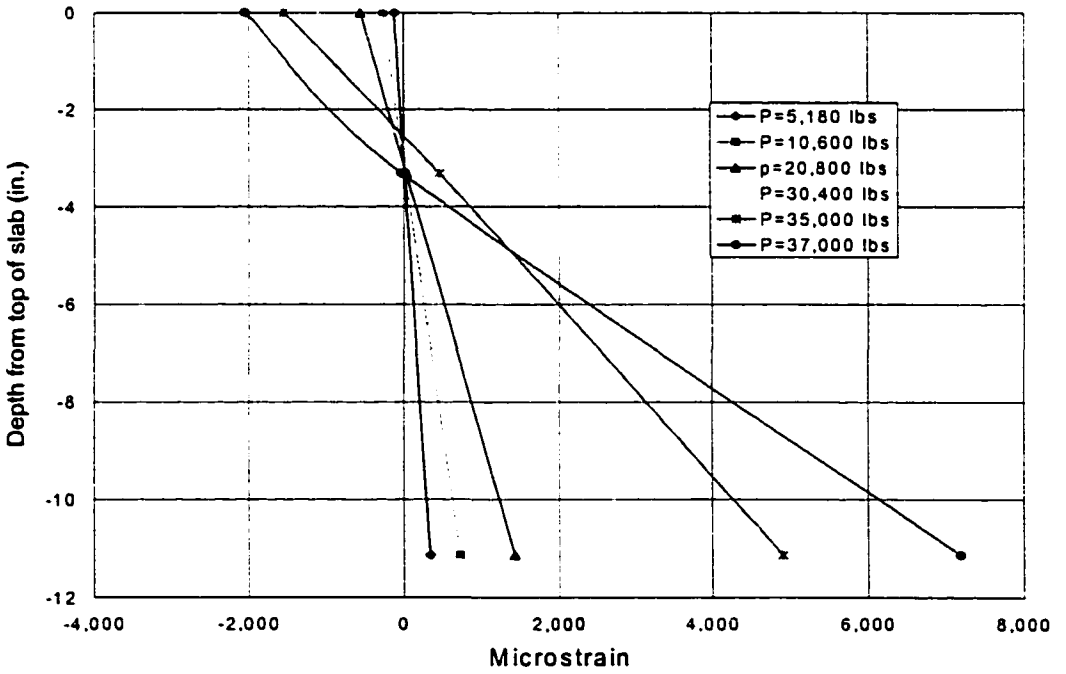

Figure 5.31. Strain profile at midspan of Beam US1E22.

< 30,000 lbs and 2.6 for higher loads) for all loads below 37,000 lbs.

Despite the fact that the ultimate predicted load was not obtained due to slip, high ductility was observed before failure. Large deflections were observed prior to failure, which gave sufficient warning before the CFRP eventually ruptured at an applied load of 37,000 lbs. Comparing the response of this beam to the control beam (Beam U) (see Fig. 5.28b), an increase of about 23 percent in the ultimate strength was achieved.

The longitudinal strains and shear stresses along the CFRP plate are shown in Fig. 5.32. This figure shows the maximum longitudinal strains in the CFRP plate of approximately 11,500 microstrain before it ruptured, which occurred very close to the location of the applied load where the stresses are highest. Again, no sign of delamination was observed in this beam.

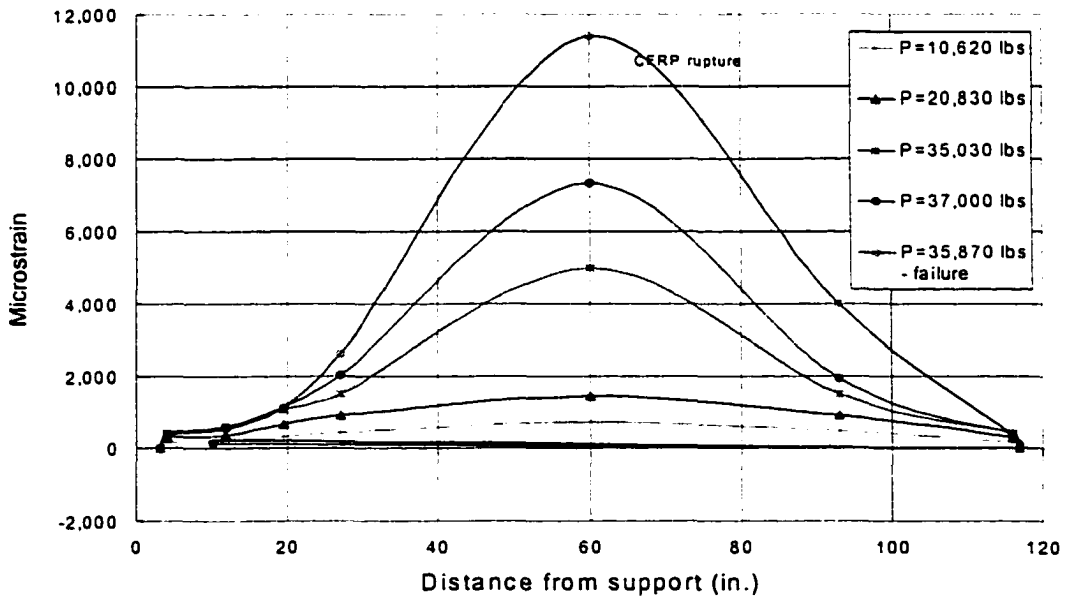

a. Longitudinal strains

Figure 5.32. Longitudinal strains and shear stresses in the CFRP plate in Beam US1E22.

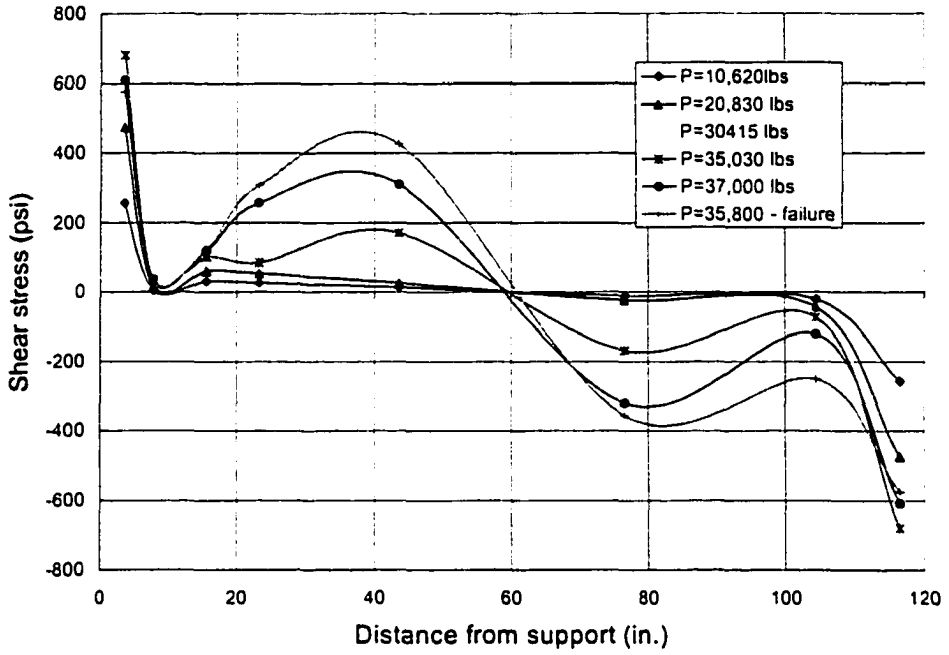

b. Shear stresses

Figure 5.32. Continued.

5.5 Beam US2E29

This beam was strengthened with 4 in. wide CFRP plate applied to the bottom flange of the steel beam and a 2 in. wide CFRP plate to the bottom of the web as previously shown in Fig. 4.1b. As noted from the previous discussions, the failure of Beam US1E29 and Beam US1E22 was mainly due to the slip between the concrete slab and the steel beam. The fact these specimens were scale models, imposed the use of thin concrete slabs; therefore, it was not possible to put double layers of reinforcement in the transverse direction. Based on the test results discussed earlier, it is apparent that the transverse reinforcement was not

sufficient to resist the tensile stresses in the transverse direction caused by the shear connectors. Of course, in a real life situation, there will be sufficient reinforcement in the transverse direction thus preventing such a problem. To overcome this problem in the test specimens, it was decided to use external reinforcement to supplement the transverse reinforcement in the concrete slab. One way, was to bond 4 in. wide uni-directional CFRP plates to the top of the concrete slab. These plates were of the same type used to strengthen Beam US1E22. The plates were cut in 20 in. lengths and placed on 14 in. centers in the longitudinal direction, similar to the distribution of the transverse steel reinforcement, as shown in Fig. 5.33. It should be mentioned; however, that the addition of the CFRP plates to the top of the concrete slab will not have any effect on the strength of the beam since the fiber orientation of the plates is in the transverse direction.

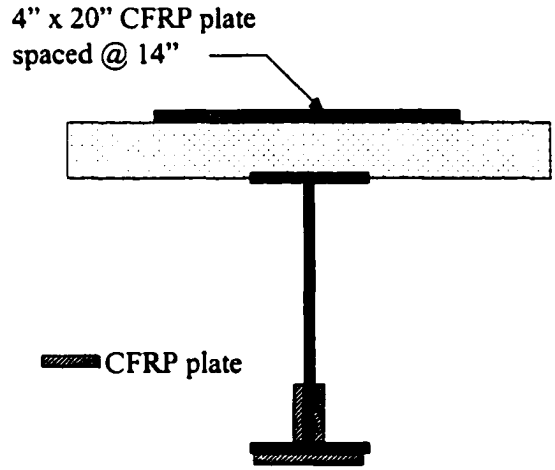

a. Section view

Figure 5.33. CFRP plates applied in the transverse direction of concrete slab in Beam US2E29.

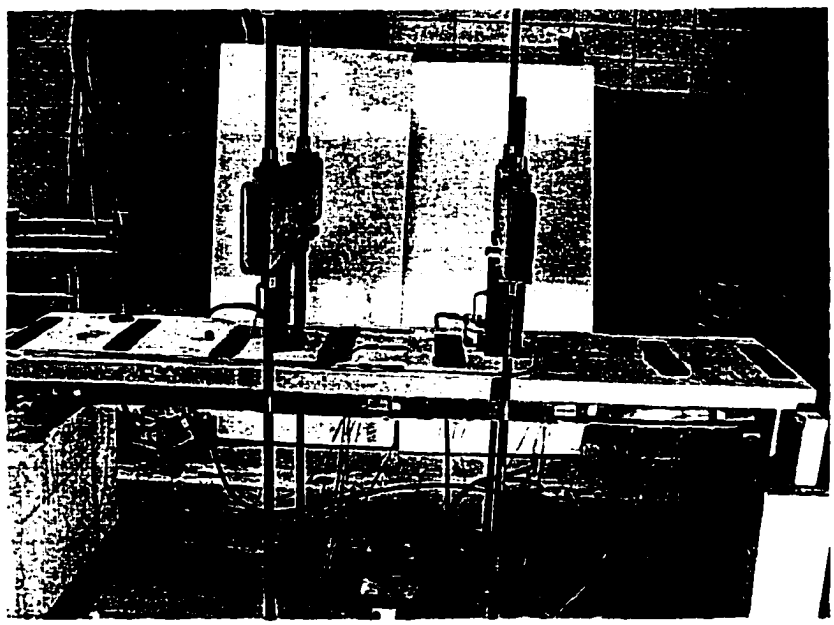

b. Photograph showing the transverse CFRP plates on concrete slab

Figure 5.33. Continued.

The beam was tested in a similar way as the previous beams; however, the behavior of this beam was quite different than the previous strengthened beams. Deflections of the beam at midspan are shown in Fig. 5.34a. and the response of this beam is compared to the control beam (Beam U) in Fig. 5.34b. In Fig.5.34a there is excellent correlation between the analytical and the experimental data until a load of 45,000 lbs is reached. The load then decreased due to slip between the concrete and the steel beam as may be observed in Fig. 5.35.

Due to the presence of the transverse CFRP plates, the longitudinal cracks did not develop before a load of 43,000 lbs. In the previous strengthened beams, the slip occurred at approximately 37,000 lbs. The confining force, applied by the transverse plates, delayed the

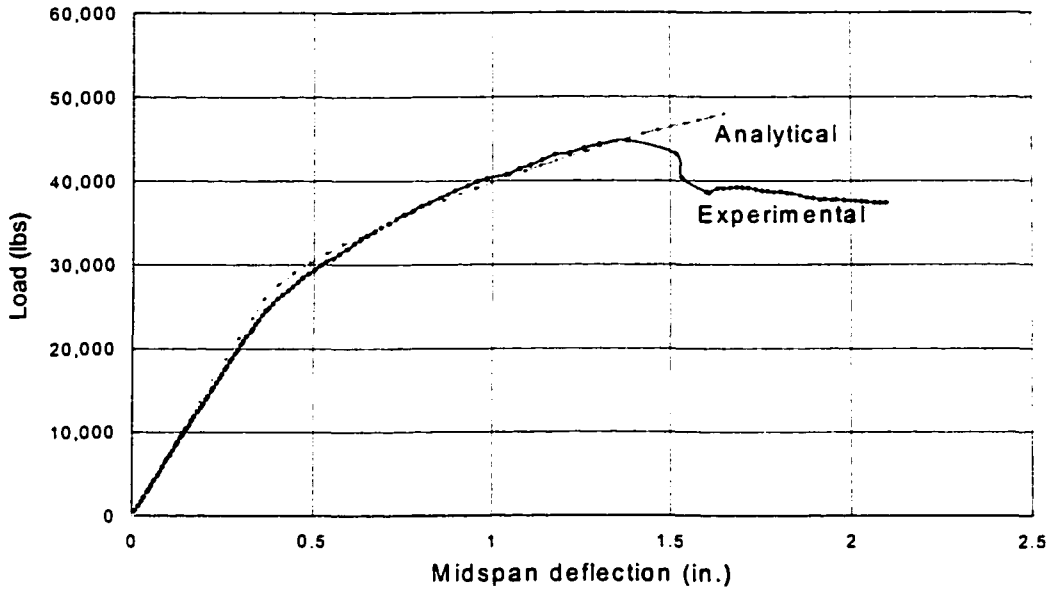

a. Analytical and experimental midspan deflections of Beam US2E29

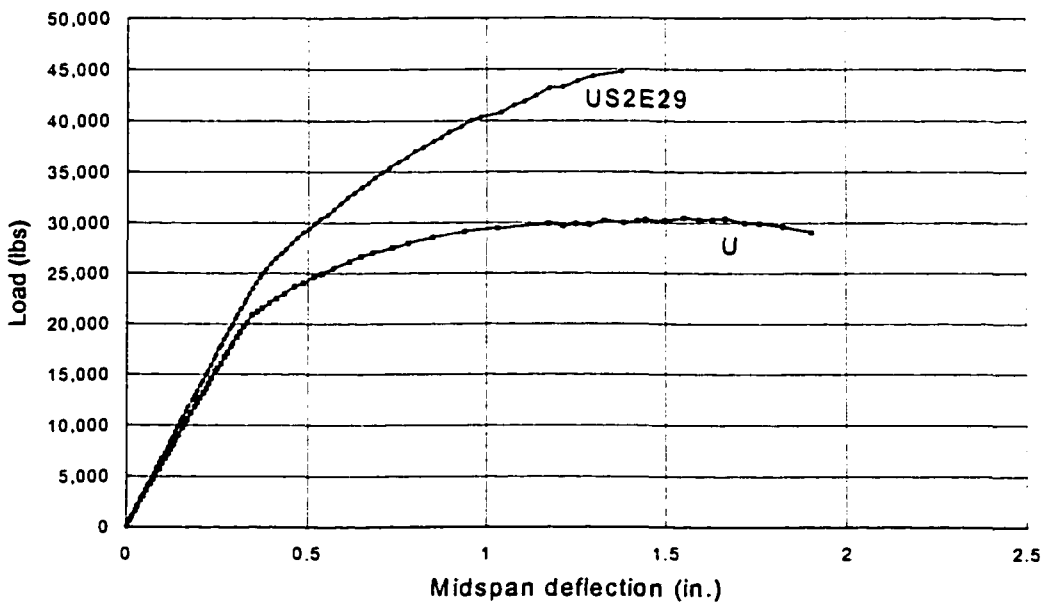

b. Comparison of mid-span deflection with control Beam U

Figure 5.34. Midspan deflections of Beam US2E29.

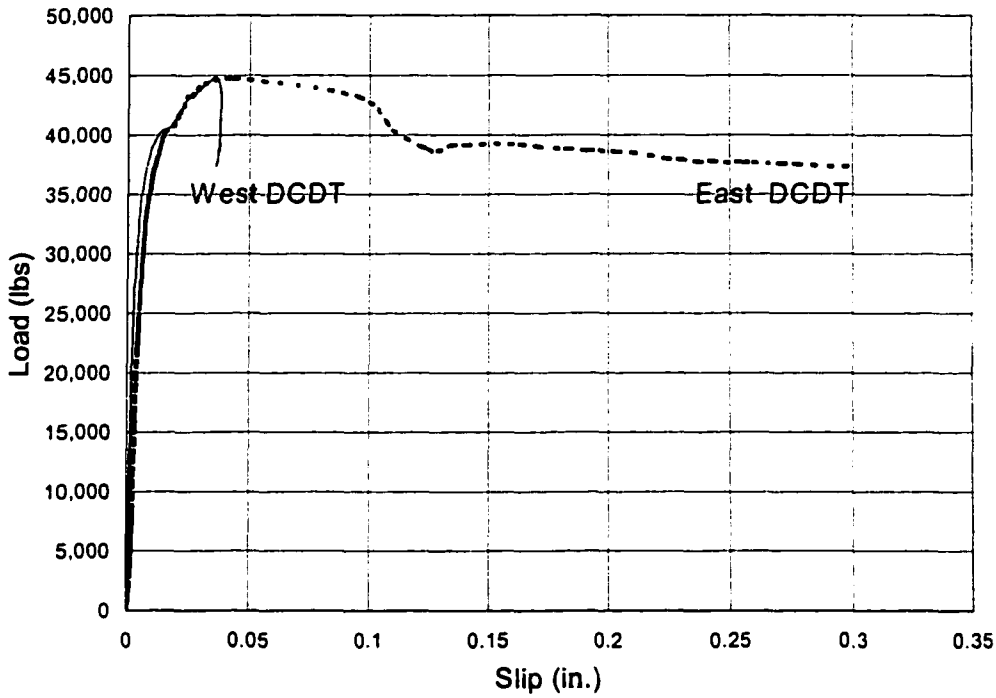

Figure 5.35. Slip between concrete slab and steel beam in Beam US2E29.

formation of longitudinal cracks. This in turn prevented any relative slip of concrete slab and the entire section behaved as a full composite section until the applied load reached 45,000 lbs. At this load, one of the transverse CFRP plates in the maximum moment region delaminated from the concrete, and the slab cracked severely in the longitudinal direction due to the loss of the confining force. Strains measured along the delaminated CFRP plate are presented in Fig. 5.36; the high strains experienced by the plate indicate its role in resisting the tensile stresses in the transverse direction. The beam eventually failed by crushing of concrete as shown in Fig. 5.37.

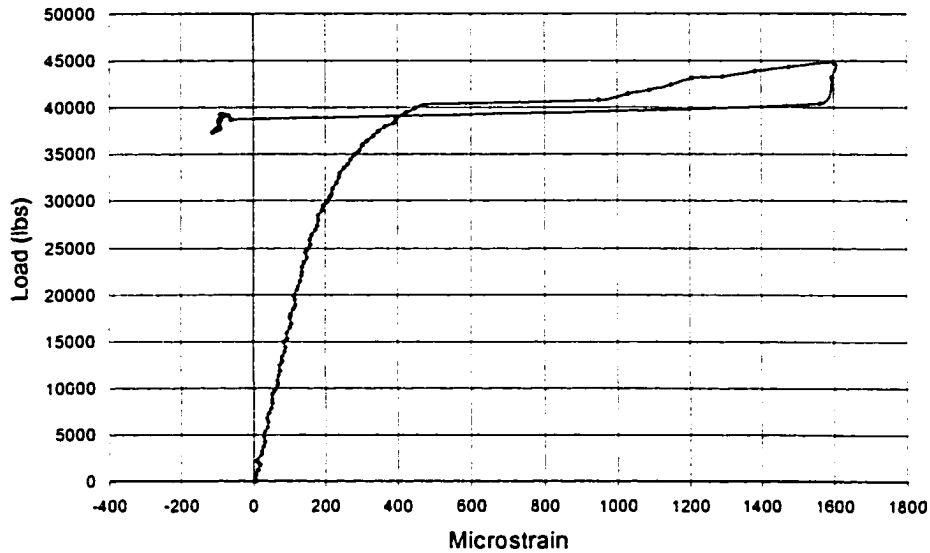

Figure 5.36. Strains in the transverse CFRP plate that failed in Beam US2E29.

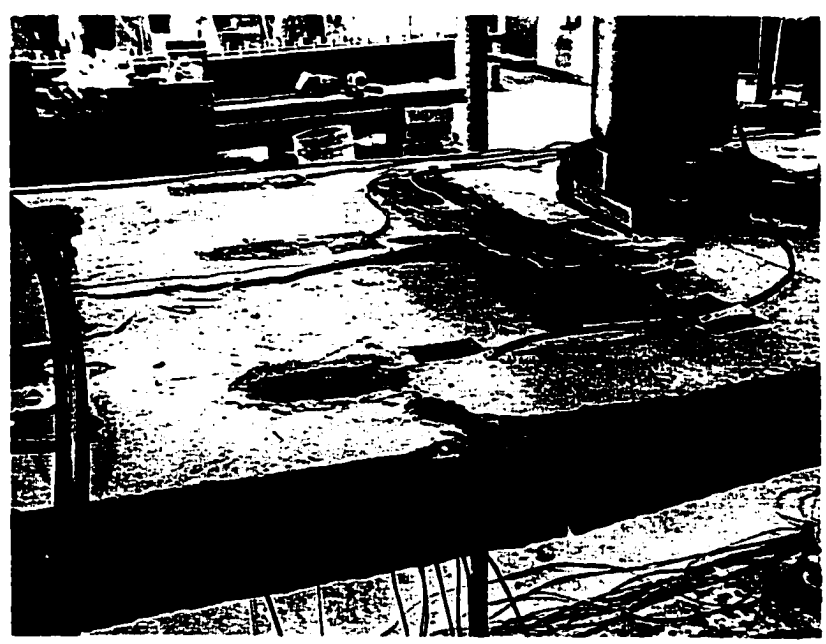

Figure 5.37. Photographs showing delamination of CFRP plate and crushing of concrete slab in Beam US2E29.

The transverse CFRP strengthened the slab and reflected the true behavior of the composite beam when full interaction between the concrete slab and the steel beam was maintained. To illustrate this, the predicted strains in the concrete slab and the bottom CFRP plates are compared to the measured strains in Fig.5.38. As may be seen in this figure, the correlation between the predicted and the experimental strains was excellent until failure.

Longitudinal and shear stresses in the bottom CFRP plate are shown in Fig. 5.39. A similar behavior was observed as in the previous beams; however, the longitudinal and shear stresses were smaller than those observed in the previous beams (i.e. Beam US1E29 and Beam US1E22). For example, the maximum longitudinal strain and maximum shear stress

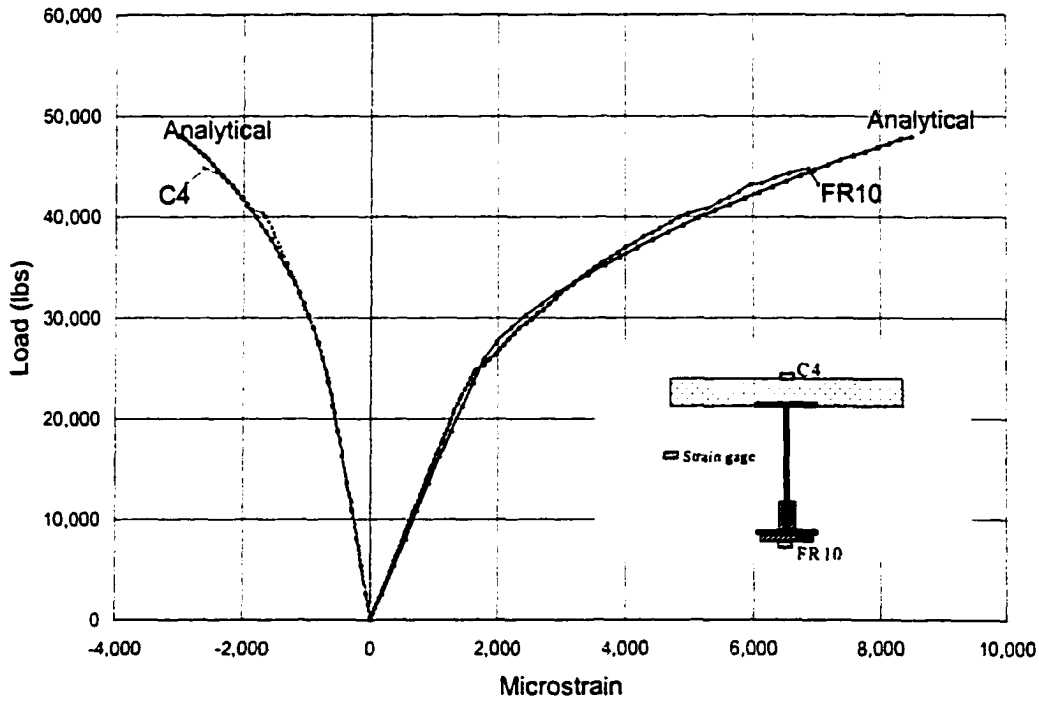

Figure 5.38. Strains at midspan of Beam US2E29.

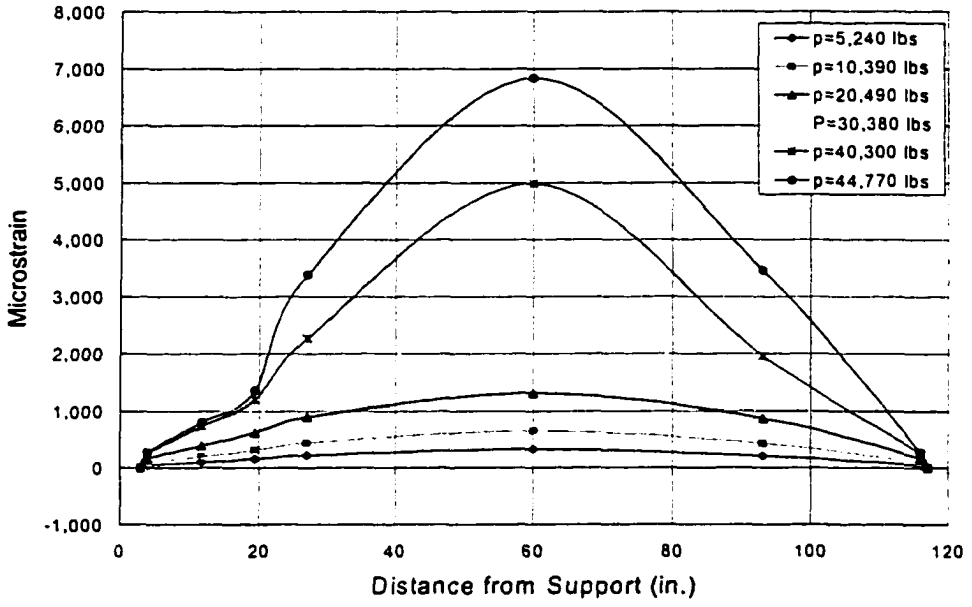

a. Longitudinal strains in the bottom CFRP

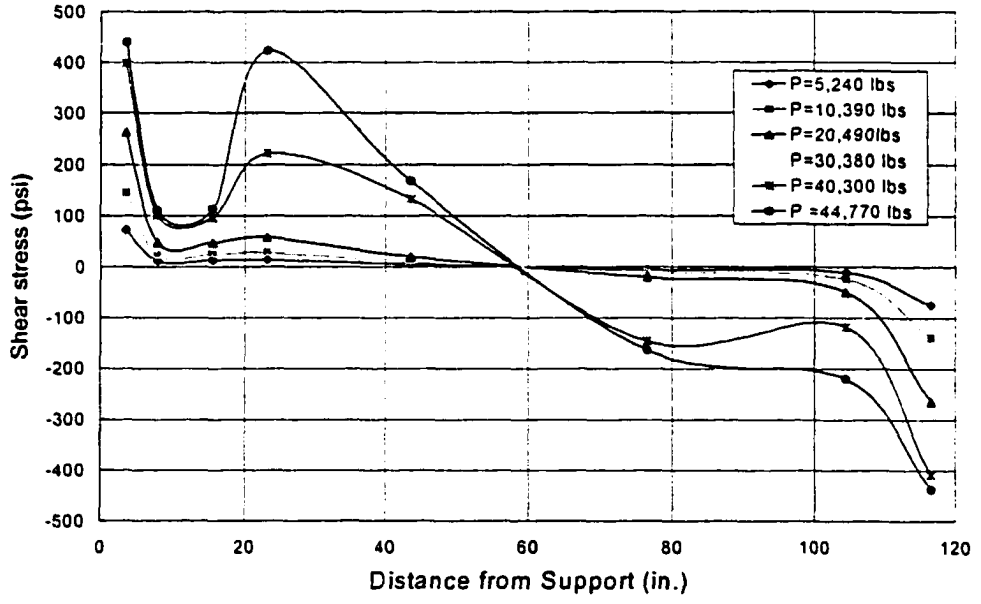

b. Shear stresses in the bottom CFRP

Figure. 5.39. Longitudinal strains and shear stresses in the CFRP plates in Beam US2E29.

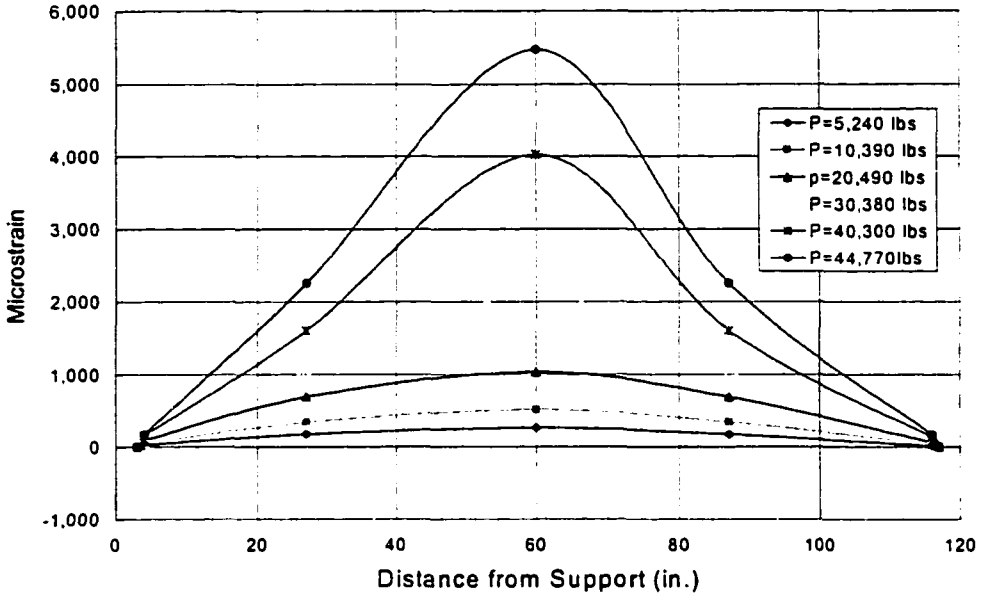

c. Longitudinal strains in the side CFRP

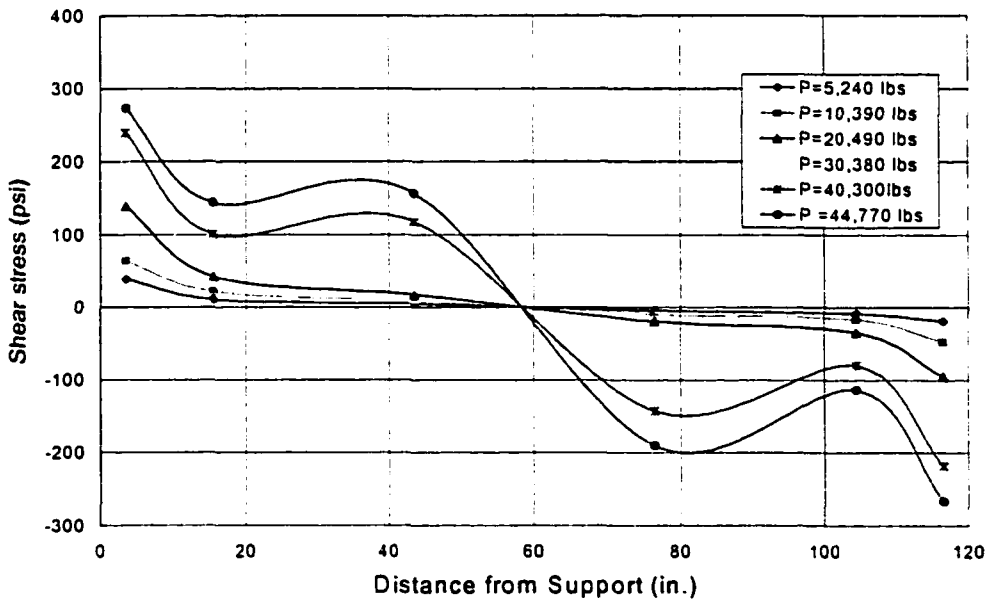

d. Shear stresses in the side CFRP

Figure. 5.39. Continued.

in Beam US2E29 were 7,000 microstrain and 450 psi, respectively, while in Beam US1E29 the magnitudes were 10,000 microstrain and 600 psi, respectively. The CFRP plates applied to the steel web reduced the strains in the bottom CFRP plate as illustrated in Fig. 5.39c and 5.39d. Adding CFRP plate to the web may not be very efficient in increasing the ultimate flexural strength, but it is very efficient in reducing the shear stresses in the bottom CFRP plate. This is very crucial to the success of this strengthening technique since the flexural strength gained by adding the CFRP is highly dependent on the shear strength at the interface of the steel beam and the CFRP plate.

5.6 Strengthening effect

Based on the test results presented in the previous sections, it is obvious that the addition of the CFRP plates did not affect the response significantly in the elastic range. This is something that was expected since the elastic response is a function of the elastic section properties: E (modulus of elasticity), and I (moment of inertia). The CFRP plate is very thin compared to the original composite section; therefore, the moment of inertia is almost unchanged by the addition of the CFRP plate. However, a small increase in the stiffness was achieved as observed in the load deflection plots. The applied load causing yielding of the steel beam was slightly increased by the addition of the CFRP plate; strengthened beams yielded at an applied load of 25,000 lbs. compared to 20,000 lbs. in the control beam (i.e. Beam U). At a load of 25,000 lbs, midspan deflection in the strengthened beams was approximately 0.4 in. compared to 0.55 in. in the control beam.

On the other hand, a significant increase in the stiffness in the inelastic range was observed in the strengthened beams. Failure of the control beam, Beam U, occurred at an

applied load of 30,900 lbs when the midspan deflection was approximately 2.0 in. At the same load, the strengthened beams only deflected 0.55 to 0.6 in.

Predicted and measured ultimate loads for all specimens are summarized in Table 5.1. The predicted increase in the ultimate load ranged between 26 to 52 percent. However, the measured increase in the ultimate load, ranged between 21 to 45 percent due to the premature slip failures. It should be noted that the percentage increase in the measured loads was calculated with respect to the average of measured loads in Beams U_1 and U_2.

Table 5.1 Summary of undamaged beams test results.

Beam	Predicted ultimate load (lbs)	Measured ultimate load (lbs)	Predicted gain in strength (%)	Measured gain in strength (%)	Mode of failure
U_1	31,500	31,000			Crushing of concrete
U_2	31,500	30,900			Crushing of concrete
US1E29$_1$	45,000	38,900	43	26	Slip/CFRP plate rupture
US1E29$_2$	45,000	38,500	43	24	Slip/CFRP plate rupture
US1E22	39,900	37,500	26	21	Slip/CFRP plate rupture
US2E29	48,000	45,000	52	45	Slip/ crushing of concrete

6. DAMAGED BEAMS TEST RESULTS

6.1 General

Discussion of the test results as well as the analytical results of the damaged beams will be presented in this chapter; this will include specimens designated as D50, D50R1E29, D50R2E29, and D75R1E29; the description of these specimens was presented in Chapter 4. The purpose of testing these specimens was to investigate the effect of damage, caused by simulated corrosion (i.e. removal of a portion of bottom flange), on the stiffness and strength of the beams. Damaged beams were repaired and tested to investigate the possibility of restoring the beams to their original strength.

One control specimen (Beam D50) was tested in the case of the 50 percent damaged beams, and the remaining two specimens (Beams D50R1E29 and D50R2E29) were damaged and repaired using the repairing schemes outlined in Chapter 4. However, there was no control specimen in the case of Beam D75. This was based on the results of Beams U and D50; the experimental results and the analytical results of these two specimens were found to have excellent correlation. Thus, it was possible to save on materials and utilize available specimens to investigate other repair schemes.

The analytical midspan deflections of Beam U (which was discussed in Chapter 5), Beam D50, and Beam D75 are compared in Fig. 6.1. As may be seen in this figure, both stiffness and strength were significantly reduced due to the damage induced to the bottom flange of Beams D50 and D75. Again, all loads reported here are point loads (i.e. loads at each hydraulic cylinder).

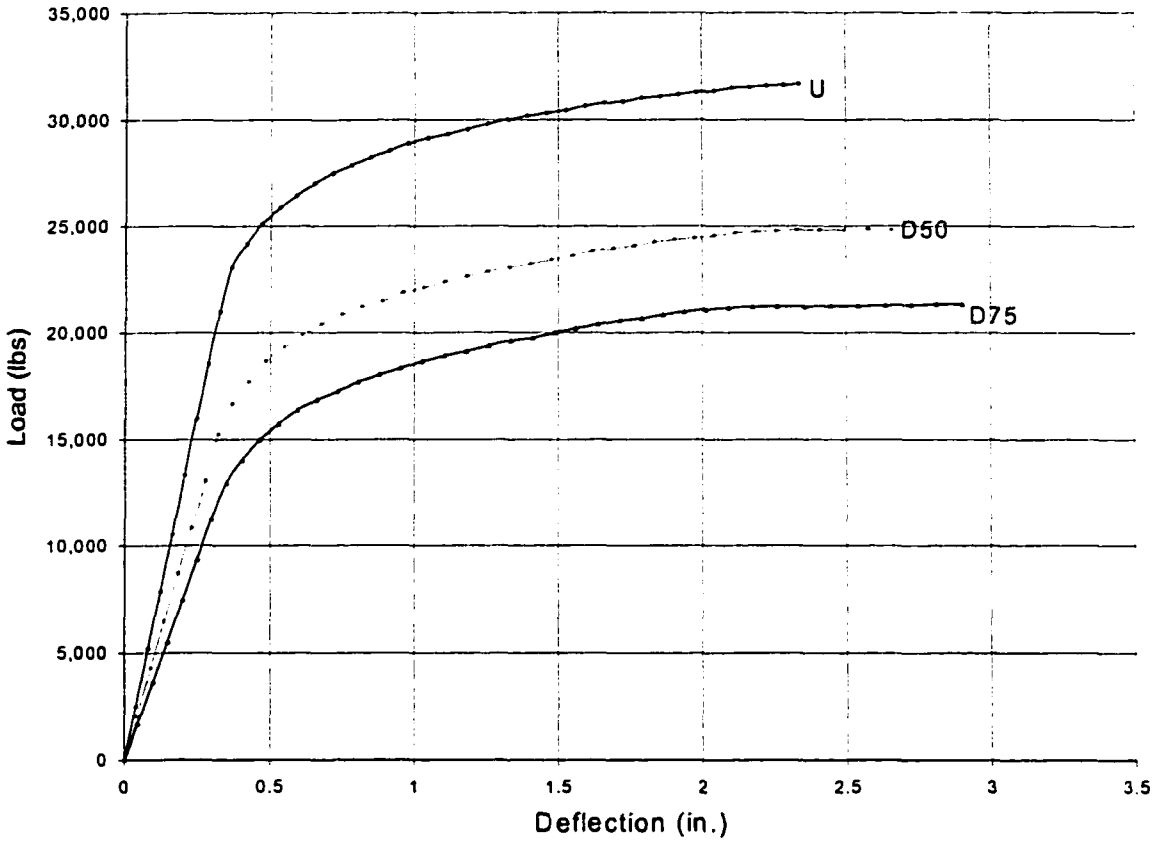

Figure 6.1. Analytical midspan deflections of Beam U, Beam D50, and Beam D75.

6.2 Beam D50

The damage to this beam was induced by the removal of 50 percent of the bottom flange area. Load setup and instrumentation of this beam were presented in Chapter 4 (see Sections 4.4 and 4.5).

Midspan deflections of Beam D50 are shown in Fig. 6.2a and deflections along the beam are shown in Fig. 6.2b. The beam behaved as expected as illustrated by the excellent correlation between the measured and the analytical data shown in Fig. 6.2a. As may be seen

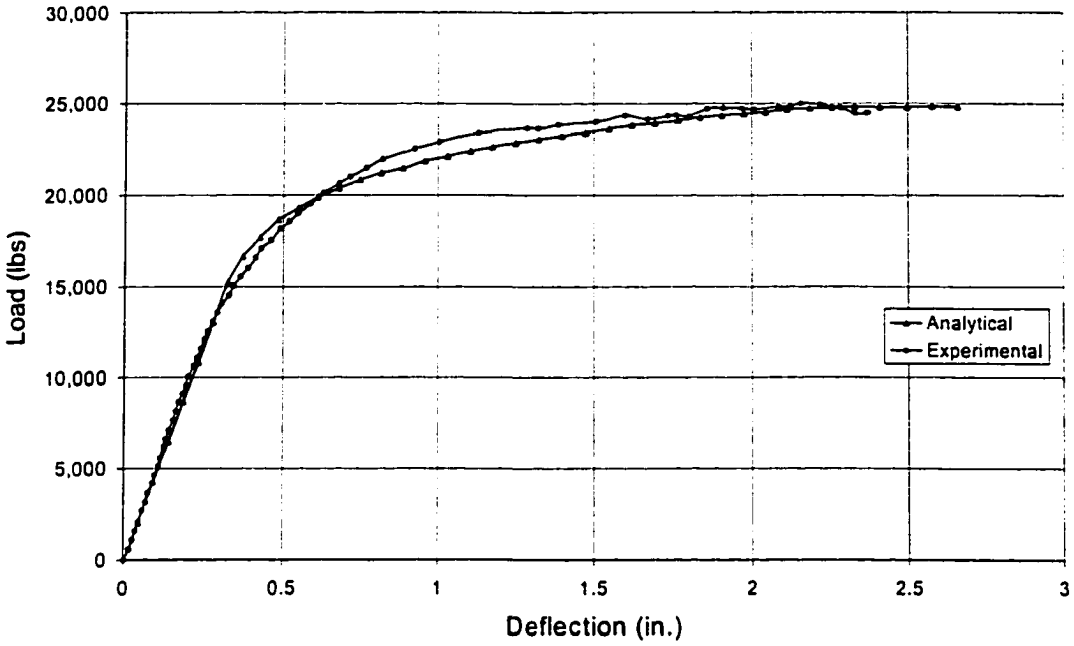

a. Midspan deflections

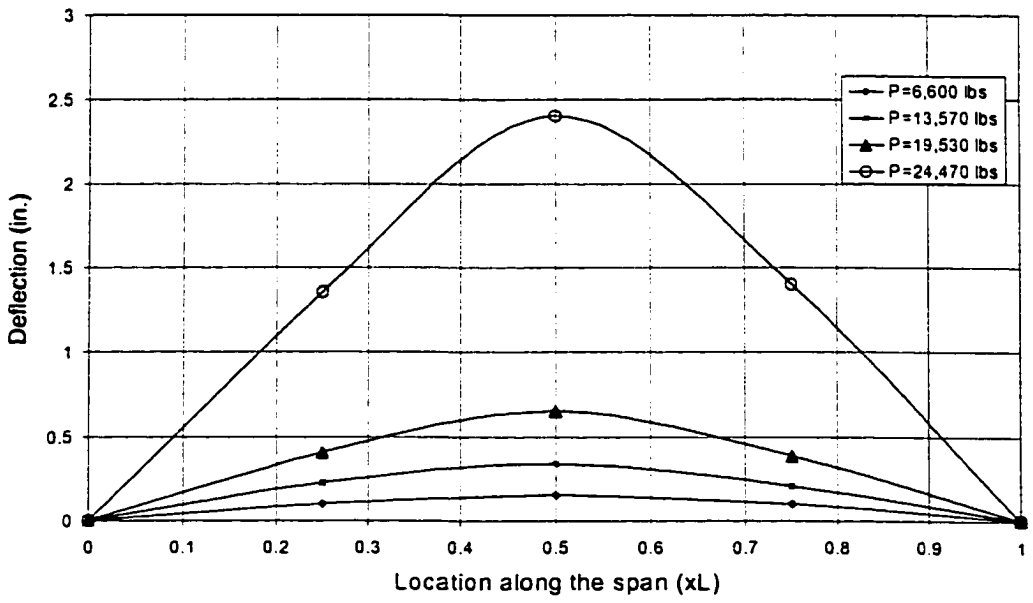

b. Deflections along the beam

Figure 6.2. Deflections of Beam D50.

in this figure, large ductility was observed prior to failure as indicated by large deflections at midspan. It is interesting to note that a more ductile behavior was observed in Beam D50 in comparison with Beam U. At the failure load, Beam D50 deflected approximately 2.4 in., while Beam U deflected approximately 2.0 in.; this is because Beam D50 had less bottom flange area (i.e. more under reinforced). Failure of this beam was due to crushing of the top surface concrete, similar to that of Beams U_1 and U_2 discussed in Section 5.2. Figure 6.2b shows the change in deflections along the beam due to various applied loads. As may be seen in this figure, deflections became large everywhere along the beam at ultimate load (i.e. at load of 24,470 lbs) due to the yielding of the steel beam. It is also noted that symmetry of applied loads was maintained throughout the test as indicated by the identical response at the quarter points of the beam.

The strain profile at midspan is shown in Figure 6.3a; the theoretical position of the neutral axis is shown in Fig. 6.3b. It is noted that the strain at various applied load magnitudes varied linearly as an indication of full composite interaction between the concrete slab and the steel beam. A very good agreement was found between the theoretical and the experimental location of the neutral axis (N.A). For instance, at an applied load of 19,500 lbs, the theoretical N.A and the experimental N.A were 2.38 in. and 2.43 in., respectively, which further confirmed the validity of the full interaction assumption.

6.3 Beam D50R1E29

This beam was damaged similar to Beam D50; the repairing scheme consisted of attaching the 4 in. wide CFRP plates to both sides of the web. Again, the goal was to restore the strength of this beam to the undamaged beam (Beam U) strength.

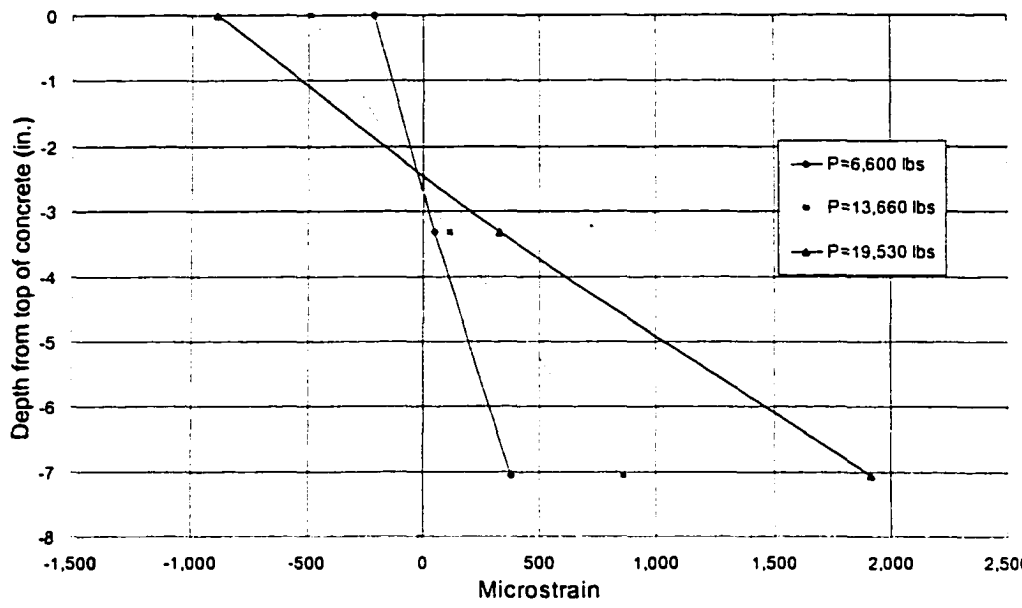

a. Strain profile at midspan of Beam D50

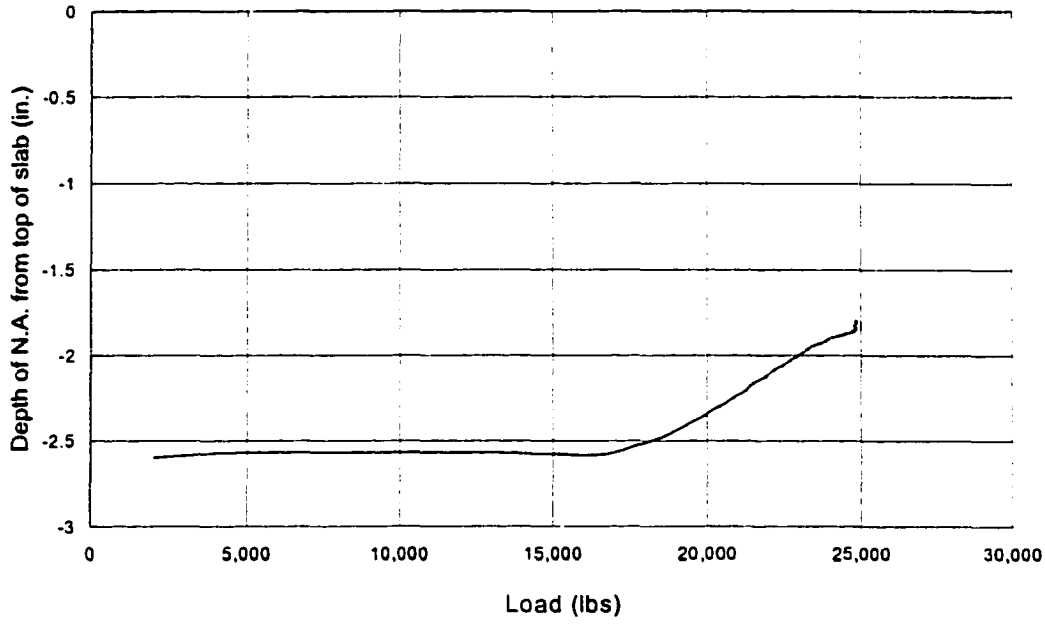

b. Theoretical position of neutral axis in Beam D50

Figure 6.3. Strain profile and theoretical position of neutral axis at midspan of Beam D50.

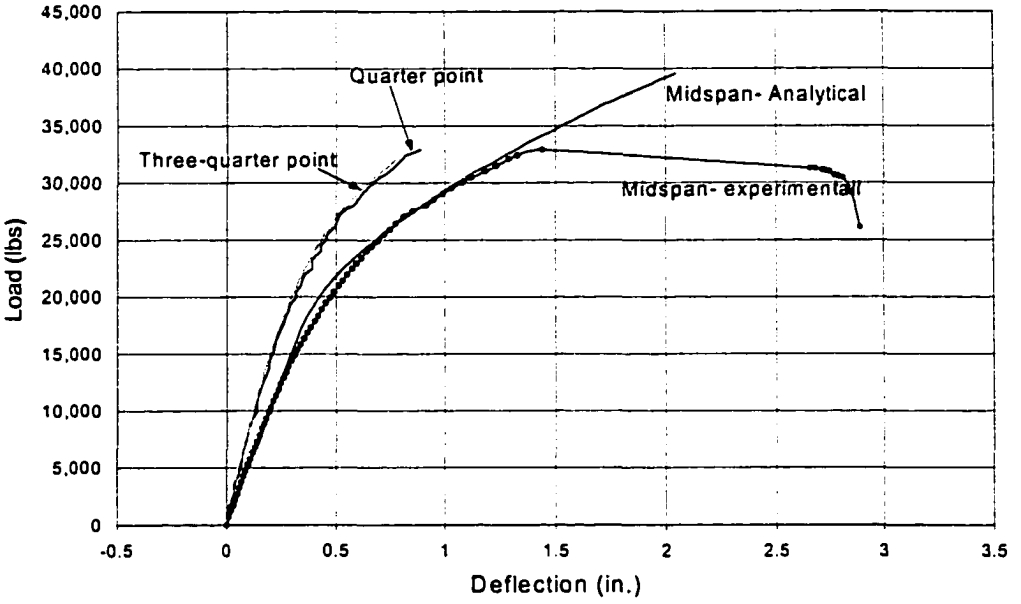

Figure 6.4. Midspan and quarter points deflections of Beam D50R1E29.

Shown in Fig. 6.4, is a plot of the deflections of the beam measured at the midspan and the quarter points; the analytical deflection at the midspan is also included. As seen in this figure, a very close agreement between the analytical and the measured midspan deflections existed until the applied load reached 33,000lbs. Like in the specimens discussed in the previous chapter (see Section 5.3.), longitudinal cracks developed just prior to this load which initiated the slip failure of the beam. Although slip between the concrete and the steel beam was not measured in this beam, it was reflected by the strain profile shown in Fig. 6.5, where it is obvious as a result of slip the concrete strains were reduced, while the strains in the CFRP plate were increased.

Despite the fact that the beam did not attain its ultimate predicted load, reasonable results were achieved. This can be seen from the comparison of the responses of

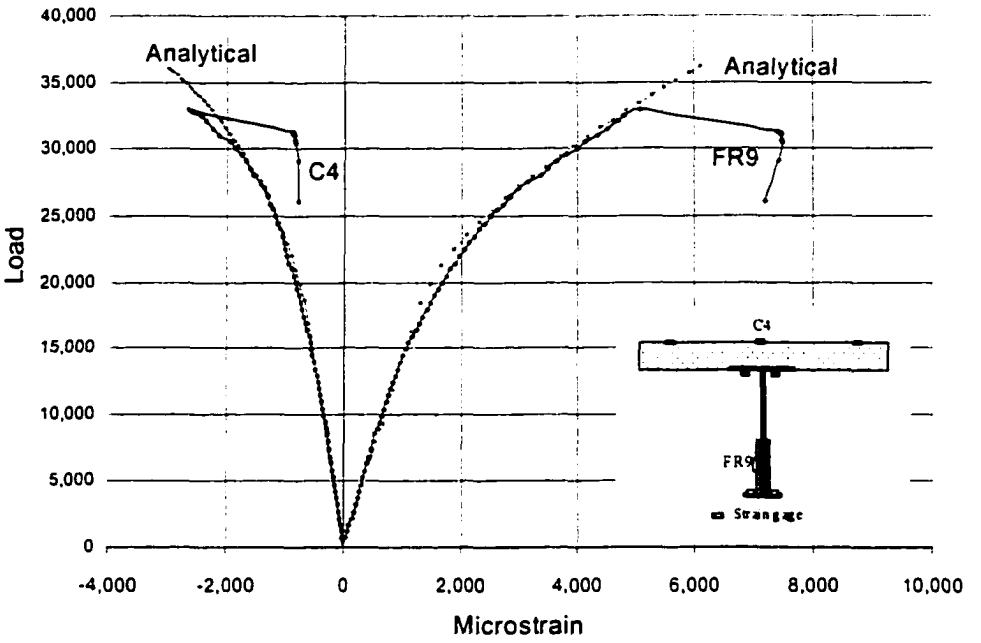

Figure 6.5. Strains at the midspan of Beam D50R1E29.

Beams D50, D50R1E29, and U illustrated in Fig. 6.6, where it is obvious that both stiffness and strength were increased in the repaired beam (Beam D50R1E29). Taking the applied load causing yielding in Beam D50, which was 15,000 lbs, as the reference point, the deflections of the three beams were compared at this load as a measure of stiffness in the elastic range. The measured deflections of Beam D50, Beam D50R1E29, and Beam U at an applied load of 15,000 lbs were 0.396 in., 0.315 in., and 0.240 in., respectively. Approximately, 50 percent of the lost stiffness in Beam D50 was restored in Beam D50R1E29, as illustrated in Table 6.1.

Table 6.1. Effect of repair on the elastic stiffness.

Beam	Midspan deflection (in.)	Stiffness reduction (%)
D50	0.396	65
D50R1E29	0.315	31
U	0.24	0

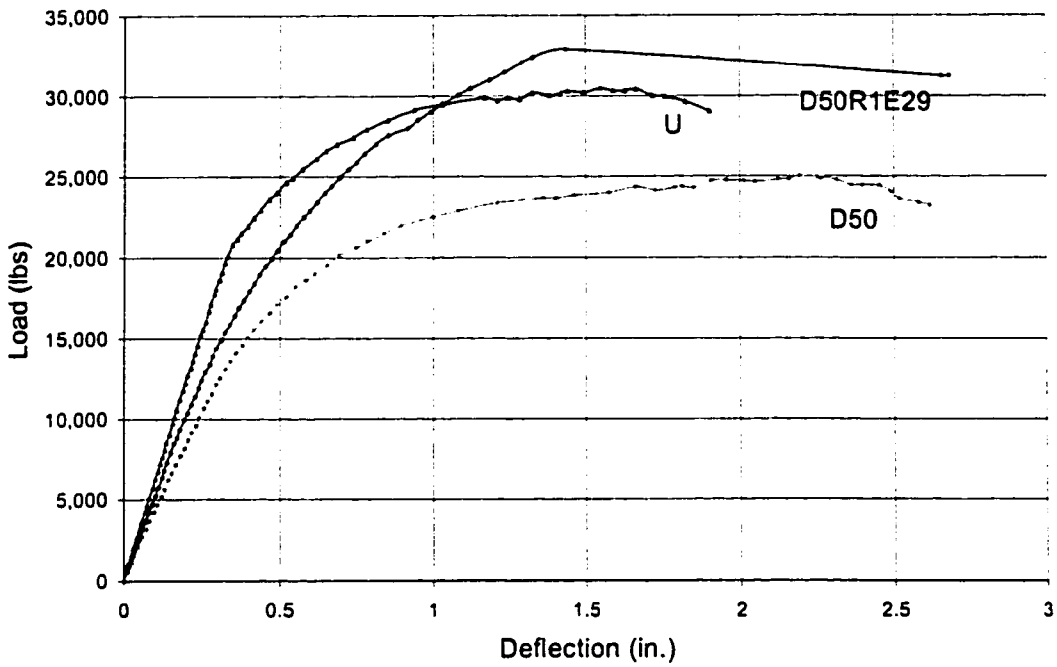

Figure 6.6. Comparison of midspan deflections in Beam U, Beam D50, and Beam D50R1E29.

In the inelastic range, significant stiffness was gained as observed in Fig. 6.6. In addition, the ultimate strength of the original beam (Beam U) was fully restored; in fact the ultimate load of Beam D50R1E29 reached 33,000 lbs, exceeding the failure load (31,000lbs) of Beam U. This clearly shows that the repair technique was very effective.

Longitudinal strains and shear stresses along the center of the CFRP plate are shown in Fig. 6.7. The behavior was similar to that of the beams previously presented (refer to Chapter 4 for discussion). No sign of delamination was observed prior to failure; the CFRP plate remained attached to the steel until the test was terminated due to slip failure.

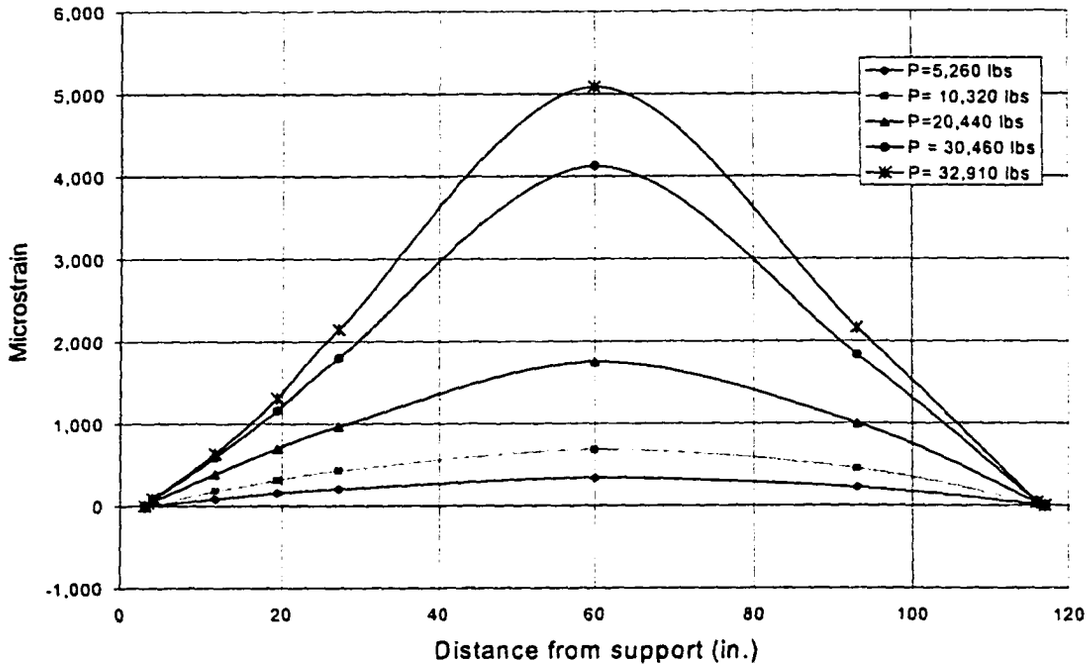

a. Longitudinal strains

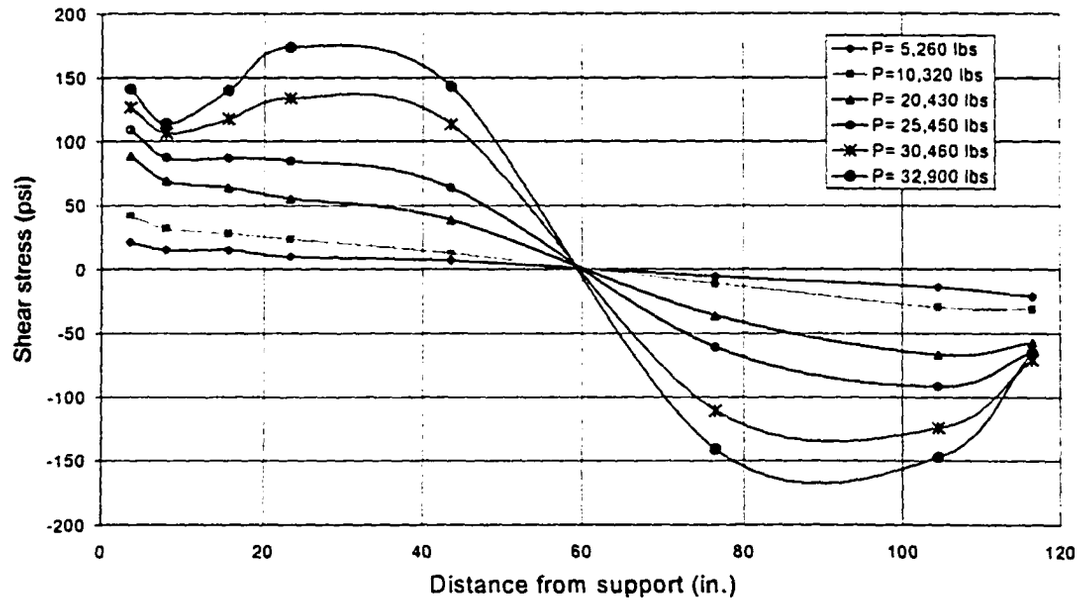

b. Shear stresses

Figure 6.7. Longitudinal strains and shear stresses in the CFRP plate in Beam D50R1E29.

6.4 Beam D50R2E29

This beam was repaired using 2 in. wide CFRP plates applied to both sides of the web and the bottom flange (see Fig. 4.2b). The total area of CFRP plates used in this beam was 75 percent of the area of CFRP used in the previous beam (Beam D50R1E29); however, analytically, both schemes should result in an equivalent strengthening effect. As previously noted, it is more efficient to attach the CFRP plates to the bottom flange due to larger moment arm; however, in certain field situations it may not be possible to attach the CFRP directly to the bottom flange (e.g. due to corrosion or riveted joints). In this case, the web may be used alone to strengthen the beam as illustrated in the previous beam (Beam D50R1E29), or a combination of the bottom flange and the web as is the case in this beam.

Failure of the previous beam (Beam D50R1E29) was caused by the slip between the concrete slab and the steel beam. For reasons previously noted (see Section 5.5), transverse CFRP plates were attached to the top of the concrete slab of Beam D50R2E29; details of the type of CFRP plates and distribution along the slab were also presented in Section 5.5 (see Fig. 5.33).

Midspan deflections as well as the deflections at the quarter points are presented in Fig. 6.8. Unlike Beam D50R1E29, the concrete slab of Beam D50R2E29 was restrained in the transverse direction; thus, minimizing development of longitudinal cracks. This is evident from the excellent agreement between the analytical and experimental midspan deflections shown in this figure; the measured and predicted strains at the midspan also show excellent correlation as illustrated in Fig. 6.9.

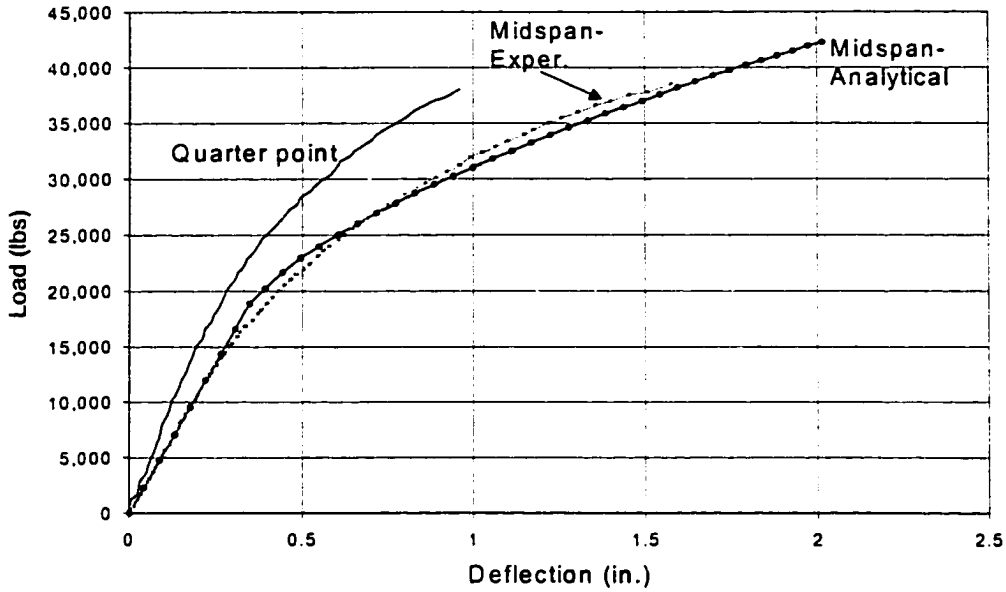

Figure 6.8. Midspan and quarter points deflections of Beam D50R2E29.

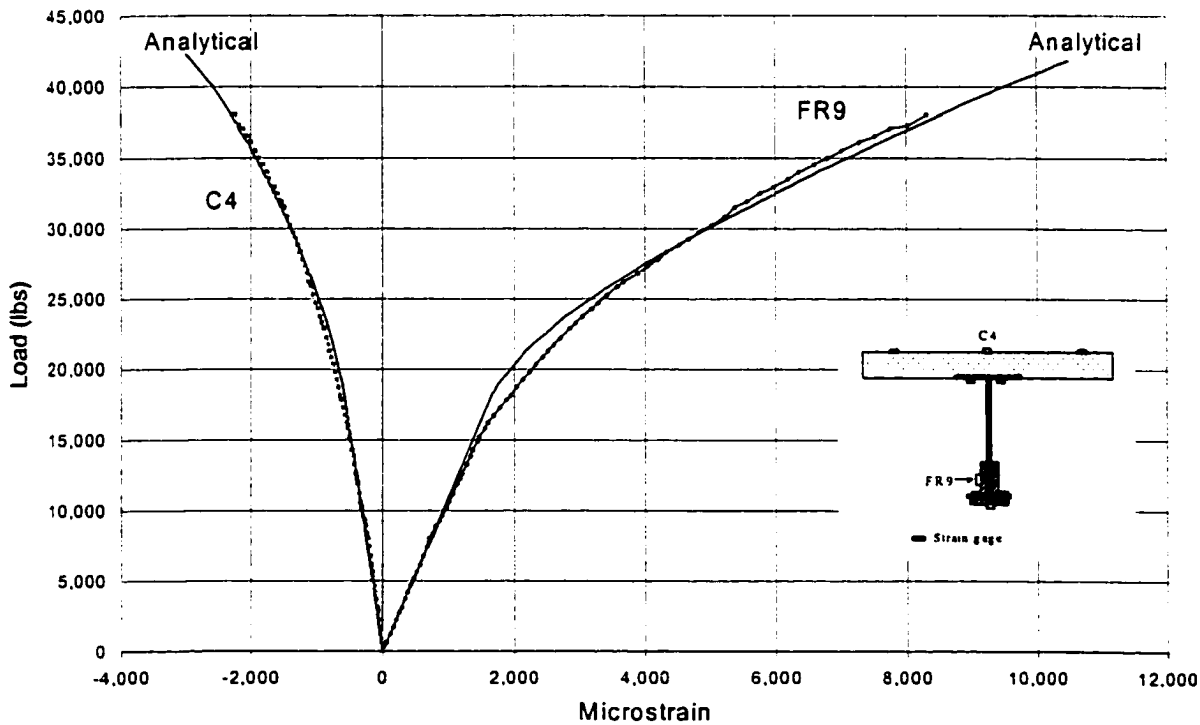

Figure 6.9. Strains at midspan of Beam D50R2E29.

Measured slip between the concrete slab and the steel beam is presented in Fig. 6.10. The first few cracks at the top surface of the concrete slab (between the loading points) developed at a load of 33,000 lbs; these cracks were very fine (hair cracks) and hardly visible. As may be observed in Fig. 6.10, the slip corresponding to this load was approximately 0.016 in.. At an applied load of 37,000 lbs, one of the transverse CFRP plates delaminated from the concrete slab in the maximum moment region. This was followed by crushing of the concrete slab at a load of 38,000 lbs; the measured strain in the concrete at this load was 2,400 microstrain, while the theoretical ultimate concrete crushing strain was assumed to be 3,000 microstrain. Since the predicted ultimate load was based on 3,000 microstrain, it was slightly higher than the measured load (see Fig. 6.8).

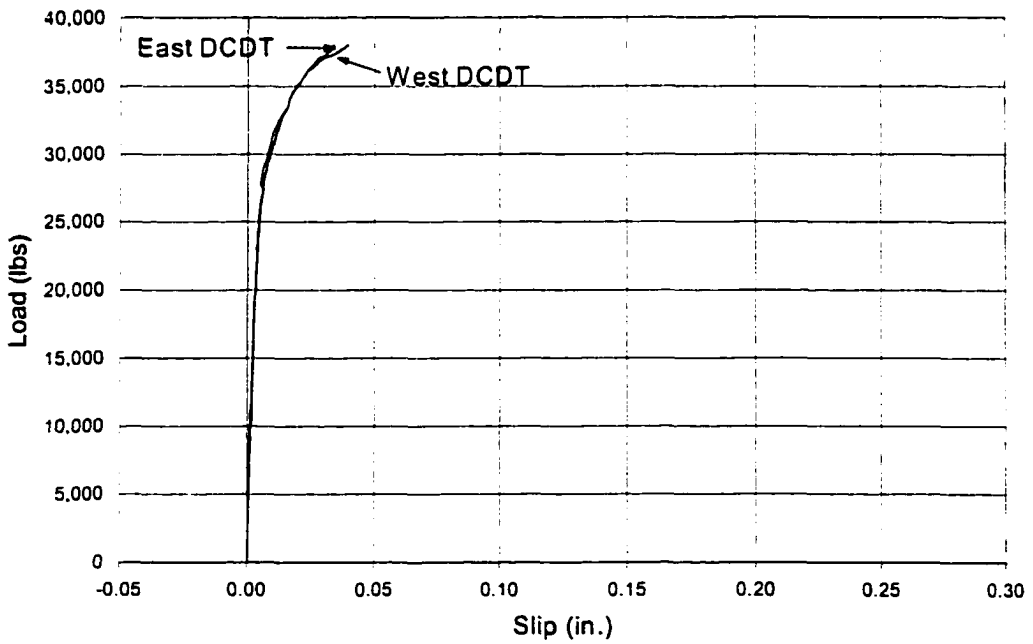

Figure 6.10. Slip between concrete slab and steel beam in Beam D50R2E29.

Figure 6.11 compares the responses of Beam U, Beam D50, and Beam D50R2E29. As may be seen in this figure, approximately 50 percent of the elastic stiffness was restored with similar results to those previously listed in Table 6.1. However, the gain in ultimate strength was much higher than in the previous beam (Beam D50R1E29). The ultimate applied load in Beam D50R2E29 was 38,000 lbs, which was 52 percent higher than that of Beam D50 and 23 percent higher than that of Beam U. Again, this clearly shows that the repair method not only restored the original strength, but also exceeded the required strength by 23 percent. In addition, the stiffness was significantly increased in the inelastic range.

The longitudinal strains and shear stresses in the bottom CFRP plate as well as the side CFRP plates are shown in Fig. 6.12. Behavior similar to that of Beam US2E29 was observed (see Section 5.5 for discussion). As observed in Figs. 6.12b and 6.12d, the peek

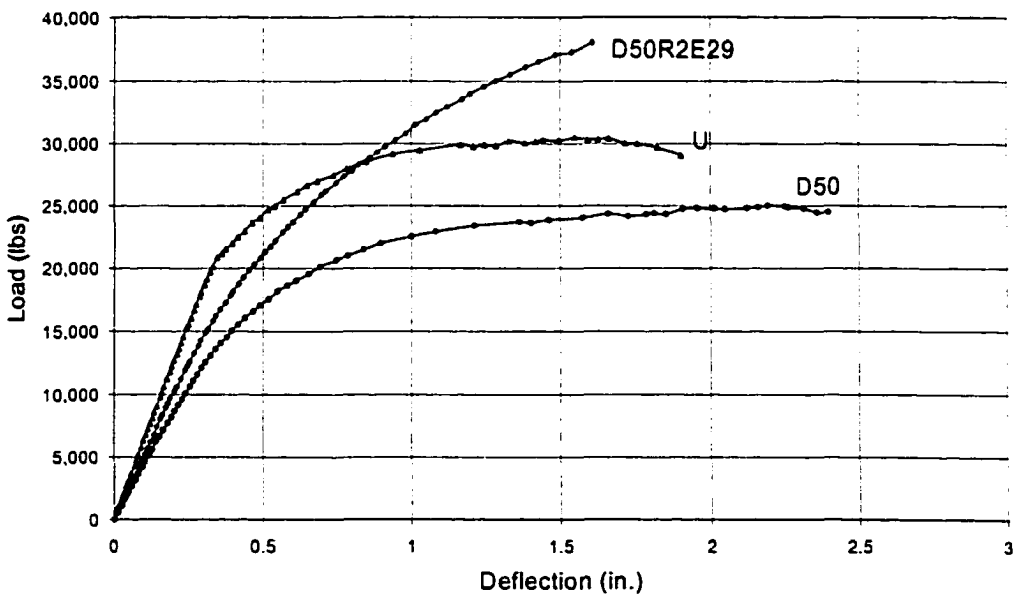

Figure 6.11. Comparison of midspan deflections in Beam U, BeamD50, and Beam D50R2E29.

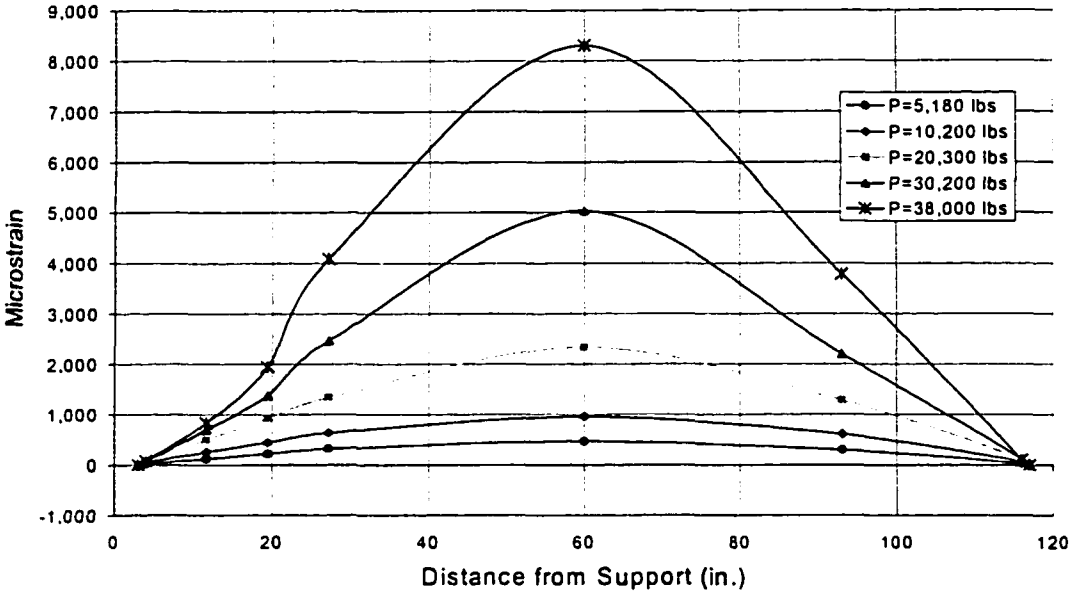

a. Longitudinal strain in the bottom CFRP plate

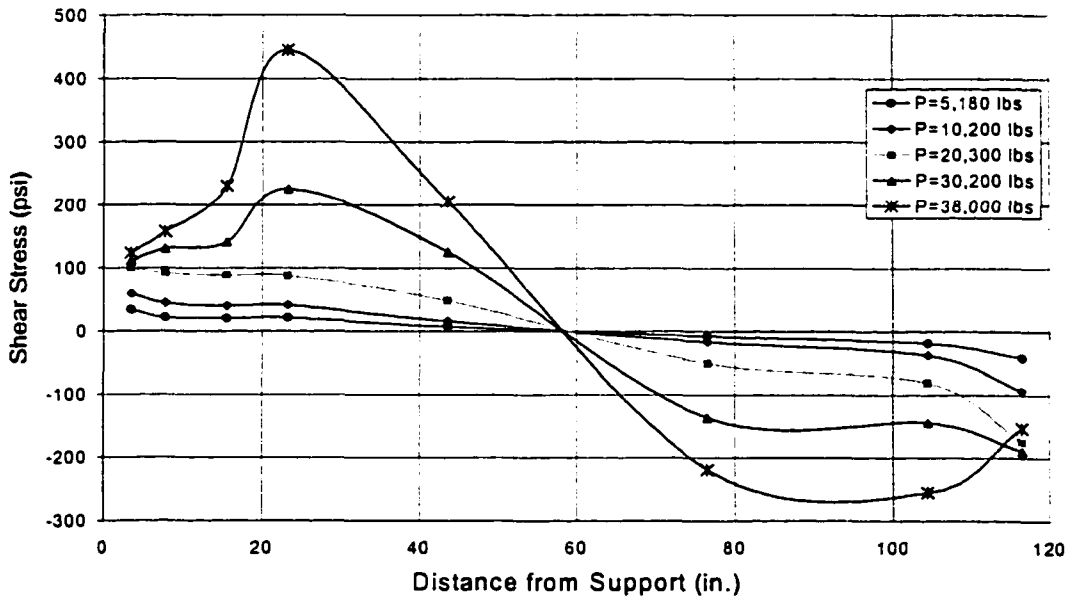

b. Shear stresses in the bottom CFRP plate

Figure 6.12. Longitudinal strains and shear stresses in the CFRP plate in Beam D50R2E29.

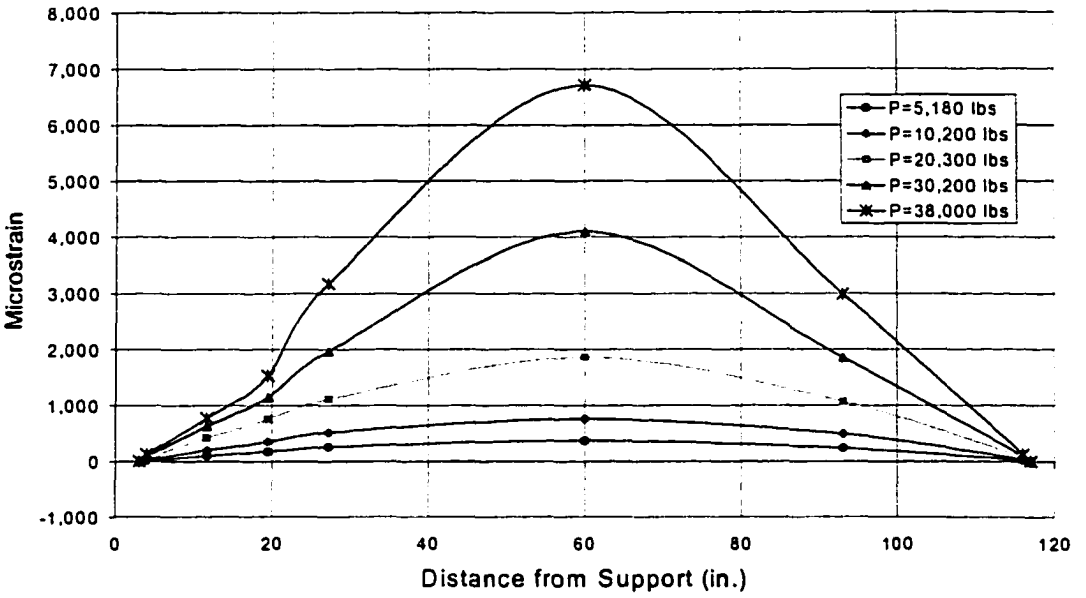

c. Longitudinal strains in the side CFRP plate

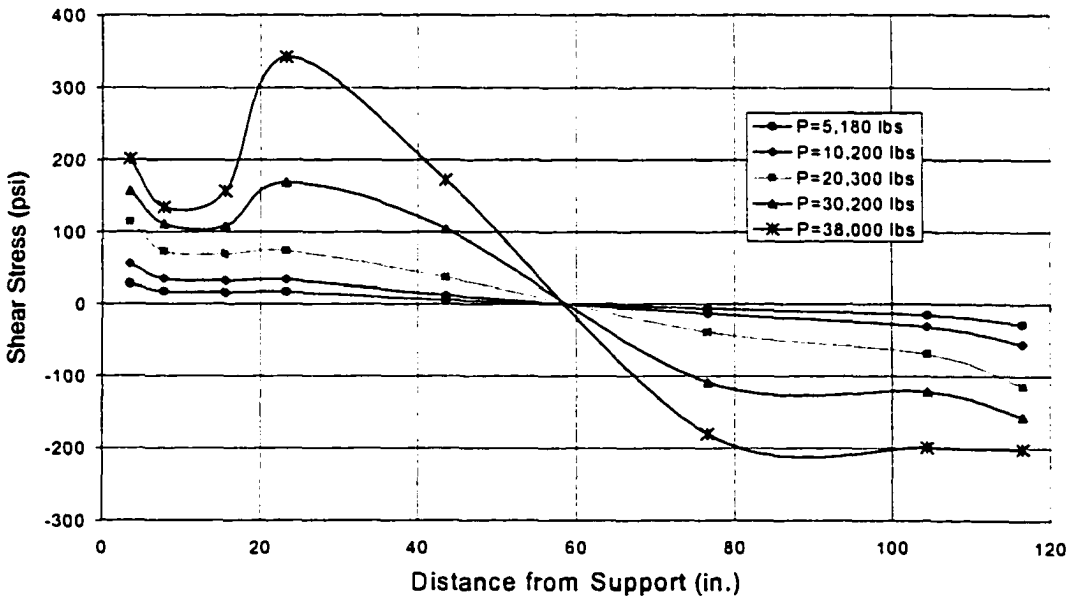

d. Shear stresses in the side CFRP plate

Figure 6.12. Continued.

shear stress occurred away from the plate ends at the ultimate load, 38,000 lbs, due to the yielding of the steel beam as noted previously (see Section 5.3.1.1).

6.5 Beam D75R1E29

More damage was induced to this beam than the previous two beams (i.e. Beams D50R1E29 and D50R2E29). In this beam, 75 percent of the bottom flange was removed which represents a severe case of damage. As illustrated previously in Fig. 6.1, more than 32 percent of the beam strength was lost due to this damage. The beam was repaired in a similar way to that of Beam D50R1E29, the CFRP plates were attached to the sides of the steel beam web (see Fig. 4.15) since most of the bottom flange was removed. Transverse CFRP plates were also attached to the top of the concrete slab (see Fig. 5.33) for reasons previously discussed in Section 5.5.

Midspan and quarter points deflections are presented in Fig. 6.13. The strains at the midspan are shown in Fig. 6.14. The behavior was similar to that of Beam D50R1E29; the main cause of failure was the slip between the concrete slab and the steel beam. Slip measured at the two ends of the beam is shown in Fig. 6.15. As may be seen in this figure, the slip became large once the applied load reached a magnitude of 33,000 lbs. This was mainly due to the delamination of one of the transverse CFRP plates in the maximum moment region, similar to that previously observed in Beam D50R2E29.

Even though the measured ultimate load was less than the predicted ultimate load, the repaired beam was capable of resisting loads that were higher than the ultimate load of the undamaged beam (Beam U) as illustrated in Fig. 6.16. As previously noted, the deflection

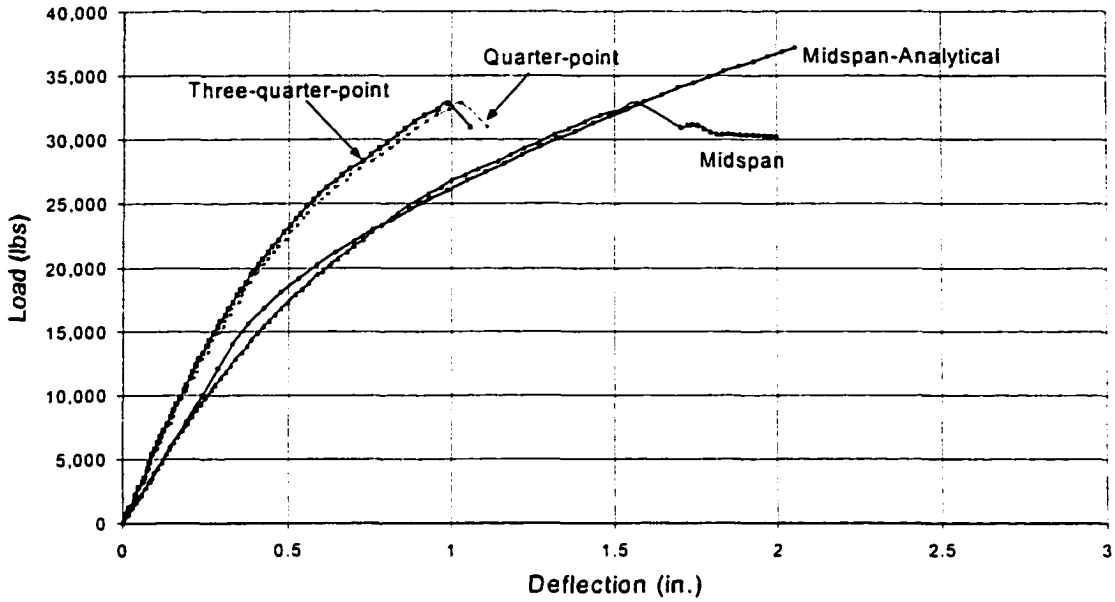

Figure 6.13. Midspan and quarter points deflections of Beam D75R1E29.

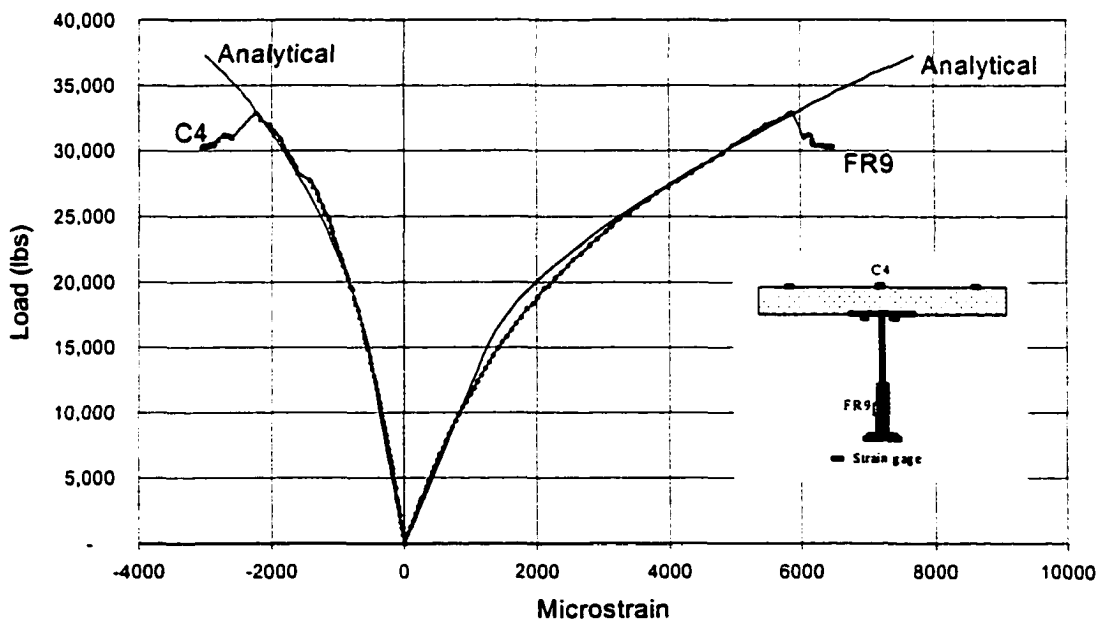

Figure 6.14. Strains at the midspan of Beam D75R1E29.

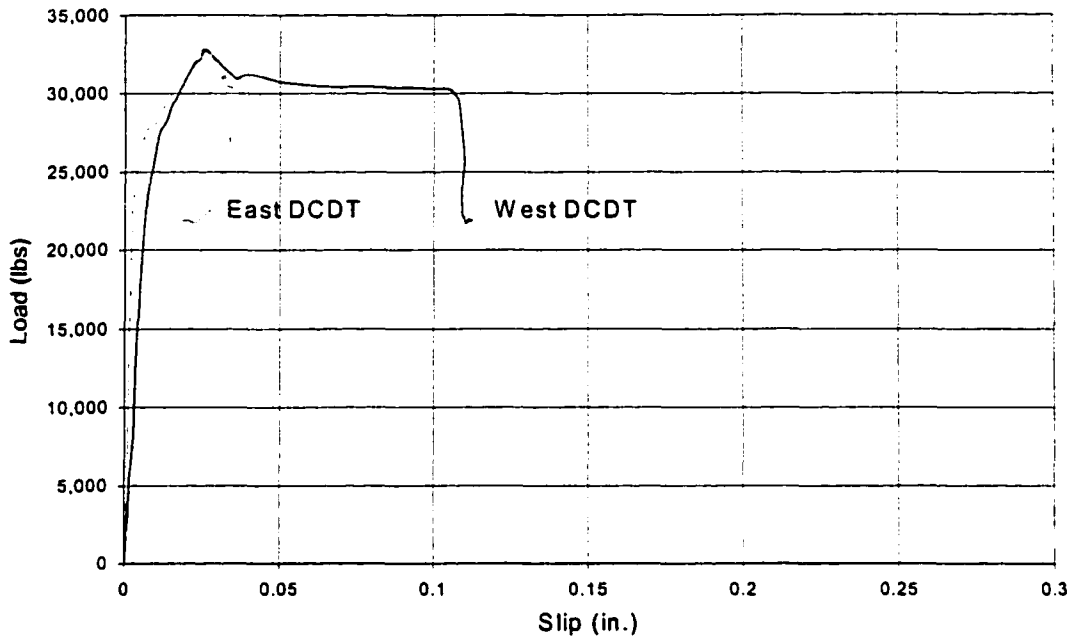

Figure 6.15. Slip between the concrete slab and the steel beam in Beam D75R1E29.

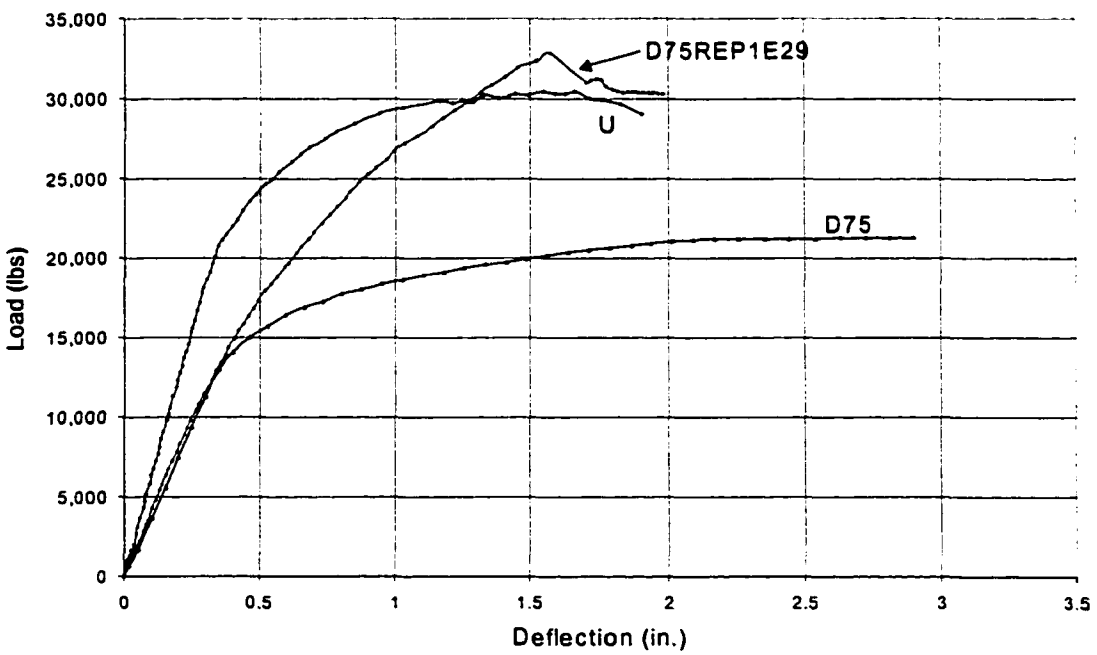

Figure 6.16. Comparison of experimental midspan deflections in Beam U, Beam D75, and Beam D75R1E29.

curve of Beam D75 was determined analytically. As observed in Fig. 6.16, no apparent increase in the stiffness was achieved in the elastic range. However, the observed experimental deflections of the previous beams, close to the yield load, were always larger than the analytical deflections and this beam should be no exception. The effect of repairing is obvious in the inelastic range on both the strength and the stiffness.

6.6 Summary of damaged beams test results

In summary, it can be stated that the repairing method was very effective. The stiffness and the strength in all repaired beams were significantly increased. Predicted and measured ultimate loads as well as the mode of failures of all specimens are summarized in Table 6.2. The predicted and measured gains in strength were calculated with respect to the undamaged beam (Beam U_2). Measured gains ranged between 6 and 24 percent. However, when the measured ultimate loads were compared to the damaged control beams (Beams D50 and D75), the range was much higher. For example, in the case of D50 specimens, the gain in strength was found to be 32 and 52 percent for Beams D50R1E29 and D50R2E29, respectively.

Table 6.2. Summary of damaged beams test results.

Beam	Predicted ultimate load (lbs)	Measured ultimate load (lbs)	Predicted gain in strength (%)	Measured gain in strength (%)	Mode of failure
U_2	31,500	31,000	0	0	Crushing of concrete
D50	24,800	25,000	-21	-19	Crushing of concrete
D50R1E29	39,500	32,900	25	6	Slip
D50R2E29	42,200	38,000	34	24	Crushing of concrete
D75	21,300	----	-32	----	----
D75R1E29	34,500	32,850	10	6	Slip/crushing of concrete

7. SUMMARY AND CONCLUSIONS

7.1 General summary

This study focused on the behavior of steel-concrete composite beams strengthened with CFRP plates. An extensive literature review was conducted to identify related work, but very little research was found in this area. There was only one study [23] that dealt exclusively with strengthening of steel composite beams with CFRP plates. However, nothing was reported on the shear stresses in the adhesive-CFRP plate interface, which is vital to this strengthening technique. Another issue, which was not dealt with in any of the previous studies, was the behavior of damaged/repaired composite sections. In addition, no special analytical tool for the purpose of implementing this strengthening technique in a simple form was available. The work presented in this dissertation was an attempt to address those issues and to add to the understanding of the behavior of composite steel beams strengthened/repaired with CFRP plates.

The first part of the study was concerned with developing an analytical procedure to predict the behavior of strengthened/repaired composite section and to predict deformations in the strengthened/repaired member. Nonlinear constitutive relations were assumed for both the concrete slab and the steel beam, and a linear relation was assumed for the CFRP. The numerical model developed was used to evaluate the response of the section and the member in the elastic, inelastic, and ultimate states. After the model was verified with the experimental results, a parametric study was conducted to investigate some of the important geometrical variables as well as the material variables. In addition, damage analyses of an analytical bridge system were completed using a grillage analysis to investigate the influence

of the damage in the girders on load distribution. Damage in the exterior girder as well as the interior girder was induced by incremental reduction of the bottom flange area to simulate corrosion. The bridge was loaded using several different loading cases to induce maximum stresses in the damaged girders.

In the experimental part of this study, a total of ten beams were tested under a four-point bending; six beams were in the undamaged state (two control beams and four strengthened), while the remaining four beams were damaged and repaired (one control beam and three repaired). The undamaged beams were strengthened using two different schemes: Scheme 1 consisted of attaching the CFRP plate to the bottom flange, while Scheme 2 consisted of attaching the CFRP plates to the tension flange as well as to the lower portion of the web of the steel beam. Damaged beams were also repaired utilizing Schemes 1 and 2. Different widths of the CFRP plates were used depending on the strengthening scheme. Two types of CFRP plates were used; the first one had a modulus of elasticity of 29,000 ksi and the second one had a modulus of elasticity of 22,000 ksi.

7.2 Conclusions

Based on the analytical and the experimental results, the following conclusions were made:

7.2.1 Analytical study

- Section and member behaviors were accurately predicted using the proposed nonlinear numerical analysis; strains were accurately predicted in the section in all ranges of loading.

- Analyses showed that the relationship between the percentage damage of the bottom flange and the reduction in the section ultimate moment was essentially linear with a ratio of 2.5:1 (i.e. for a 2.5% loss in bottom flange area, there is a 1% reduction in the ultimate moment).
- The limiting strain in the CFRP plate of 1%, determined by the parametric study, was found to be a reasonable limit for effective strengthening and ductility of the investigated sections.
- Combining a thin CFRP plate with high stiffness (i.e. high modulus of elasticity) is more effective than using thick plate with less stiffness in order to reduce peel stresses.
- The concrete compressive strength (within the range investigated, i.e. between 3 and 6 ksi) has negligible effect on the ultimate strength of composite beams; if the compressive strength is unknown, a 4 ksi compressive strength can be assumed when conducting section analyses without introducing significant error in the analysis results.
- Yield stress of the steel beam will affect the behavior of the section considerably; therefore, the actual yield stress of the steel beam needs to be known before conducting any strengthening/repair section analyses.
- Grillage analysis, for the particular bridge investigated, indicated that for small girder damage, no notable redistribution of load was found. However, for severe damage ($I = .6I_g$) in the girder, considerable load redistribution was noted. In the later case, the neighboring girders adjacent to the damaged girders need to be strengthened as well.

7.2.2 Experimental study

- Applying load on to the concrete slab by either a line load across the slab width or as a point load right above the steel beam did not affect the behavior or the strength of the composite beam.
- Undamaged beams tests revealed that the strengthening method is viable and effective. Strength gain up to 45% was possible despite the slip failure at the steel/concrete interface.
- A very high stiffening effect was observed in the strengthened specimens in the inelastic range. Strengthened specimens deflected approximately 30% of that of the control (unstrengthened) specimens at an applied load of 30,000 lbs.
- Attaching the CFRP plates to the web of the steel beam reduced the shear stresses in the adhesive layer of the bottom CFRP plate considerably due to the downward shift in the neutral axis.
- In the inelastic range (after steel yielding), shear stresses in the adhesive layer were more critical (higher) in the yielded zone than in the CFRP plate ends.
- No sign of delamination or bond failure at the bond line was noted in all the beams tested. All failures were due to either crushing of concrete or rupture of the CFRP plate. Bond between steel and CFRP was not a problem for the system investigated.
- Failure of the undamaged/strengthened and damaged/repaired specimens was ductile; however, the ductility was slightly less than the undamaged and damaged (control) specimens.

- The beam that was strengthened with CFRP plate with a modulus of elasticity of 22,000 ksi showed a more ductile behavior than the beam strengthened with a CFRP plate with a modulus of elasticity of 29,000 ksi.
- Damaged and repaired specimens recovered 50% of the elastic stiffness and much higher stiffness was gained in the inelastic range. Deflections of repaired specimens were approximately 30% of that of the control (damaged) specimen at the failure load of the control specimen. The ultimate strength was fully restored in all repaired beams; the ultimate load of the repaired beams exceeded the original strength.

7.3 Recommendations

This study covered some of the aspects related to bonding CFRP plates to steel beams. There are still some issues that need to be further studied and resolved. Some of the areas needing additional work are:

- The need to devise a methodology of selecting the best and durable adhesive for steel applications which will take into account both short and long term performance.
- Testing of beams with thicker CFRP plates to increase stiffness and strength in the elastic range.
- Testing of strengthened beams with multiple CFRP plates with profiled or bolted ends to minimize peel stresses.

- Investigate a feasible way to prestress the CFRP plates to utilize the high strength and stiffness of the CFRP and use the plates more effectively to resist live load stresses.
- Develop tests to determine the anchorage or development length required for CFRP plates bonded to steel. Variables include the thickness of the adhesive, thickness and width of the CFRP plate, surface preparation, and the lap length.
- Durability studies of the best system of epoxy and CFRP. The effect of moisture, temperature, and sustained and fatigue loads need to be studied both in laboratory and in the field (i.e. natural weathering) in a very systematic way.

APPENDIX A

DERIVATION OF N.A. QUADRATIC EQUATION COEFFICIENTS

The derivation of the coeffecients of the quadratic equation resulting from the remaining strain cases (i.e. case2, case3, and case 4) are presented in this appendix.

Case 2 $0 < \varepsilon_s < \varepsilon_y$ and $\varepsilon_o < \varepsilon_c < \varepsilon_u$

From equilibrium of forces:

$$\sum F_i = 0$$

$$F_i = \sigma_i \times A_i$$

$$\sum F_i = \sum f_{pli} \times A_{pli} + \sum f_{is} \times A_{is} + \sum f_{ic} \times A_{ic} = 0 \qquad \text{(A.1)}$$

Where subscripts c, and s refer to concrete and steel, respectively.

Replacing steel and CFRP stresses by its Hooke's law equivalent (see Eq. 3.2), the equilibrium equation becomes

$$\sum \varepsilon_{pli} E_{pli} A_{pli} + \sum \varepsilon_{is} E_{is} A_{is} + \sum f_{ic} A_{ic} = 0 \qquad \text{(A.2)}$$

The strain at any element is given by Eq. 3.1, which is repeated here.

$$\varepsilon_i = \varepsilon_c \times (c - d_i)/c \qquad \text{(A.3)}$$

Substitute the above relation for strain in the steel and CFRP elements; and the stress in concrete by the relation given by Eq. 3.5.

$$\sum \varepsilon_c \left(\frac{c - d_{pli}}{c} \right) E_{pli} A_{pli} + \sum \varepsilon_c \left(\frac{c - d_{is}}{c} \right) E_{is} A_{is}$$
$$+ \sum f_c^{'} \left[1 - \frac{0.15}{\varepsilon_u - \varepsilon_o} * (\varepsilon_{ci} - \varepsilon_o) \right] \times A_{ic} = 0 \qquad \text{(A.4)}$$

Substitute the value of ε_{ci} in terms of ε_c in the above equation.

$$\sum \varepsilon_c \left(\frac{c - d_{pli}}{c} \right) E_{pli} A_{pli} + \sum \varepsilon_c \left(\frac{c - d_{is}}{c} \right) E_{is} A_{is}$$
$$+ \sum f_c^{'} \left[1 - \frac{0.15}{\varepsilon_u - \varepsilon_o} * \left(\varepsilon_c (\frac{c - d_{ic}}{c}) - \varepsilon_o \right) \right] \times A_{ic} = 0 \qquad \text{(A.5)}$$

Multiply the above equation by c^2, expand and rearrange terms will result in the following expression:

$$A_2 \, c^2 + B_2 \, c + D_2 = 0 \qquad \text{(A.6)}$$

where

$$A_2 = \left[\left(\varepsilon_c E_{is} A_{is} \right) + \left(\varepsilon_c E_{pli} A_{pli} \right) + A_{ic} f_c^{'} \{ 1 - 0.15 * (\frac{\varepsilon_c - \varepsilon_o}{\varepsilon_u - \varepsilon_o}) \} \right] \qquad \text{(A.7a)}$$

$$B_2 = -\left[\left(\varepsilon_c E_{is} A_{is} d_{is} \right) + \left(\varepsilon_c E_{pli} A_{pli} d_{pli} \right) - A_{ic} f_c^{'} d_{ic} \{ 0.15 * (\frac{\varepsilon_c}{\varepsilon_u - \varepsilon_o}) \} \right] \qquad \text{(A.7b)}$$

$$D_2 = 0 \qquad \text{(A.7c)}$$

Case 3 $\varepsilon_s \geq \varepsilon_y$ and $0 < \varepsilon_c < \varepsilon_o$

This case is similar to Case 1, except the stress in the steel is taken as the yield stress (i.e. $f_s = f_y$). Again, the equilibrium equation is repeated next and the same procedure is followed to arrive at the final expression of Case 3

$$\sum F_i = \sum f_{pli} \times A_{pli} + \sum f_{is} \times A_{is} + \sum f_{ic} \times A_{ic} = 0 \tag{A.1}$$

$$\sum \varepsilon_{pli} E_{pli} A_{pli} + \sum f_y A_{is} + \sum f_{ic} A_{ic} = 0 \tag{A.8}$$

Substituting the stress in concrete by the relation given by Eq. 3.4, the above equation becomes as follows:

$$\sum \varepsilon_{pli} E_{pli} A_{pli} + \sum f_y A_{is} + \sum f_c^{"} \left[2\frac{\varepsilon_{ci}}{\varepsilon_o} - \left(\frac{\varepsilon_{ci}}{\varepsilon_o} \right)^2 \right] \times A_{ic} = 0 \tag{A.9}$$

Writing ε_i in terms of ε_c as given by Eq. 3.1 and performing some algebraic manipulation, the final expression of Case 3 becomes

$$A_3 \, c^2 + B_3 \, c + D_3 = 0 \tag{A.10}$$

where

$$A_3 = \left[\left(f_y A_{is} \right) + \left(\varepsilon_c E_{pli} A_{pli} \right) + A_{ic} f_c^{"} \left\{ 2\left(\frac{\varepsilon_c}{\varepsilon_o} \right) - \left(\frac{\varepsilon_c}{\varepsilon_o} \right)^2 \right\} \right] \tag{A.11a}$$

$$B_3 = -\left[\left(\varepsilon_c E_{pli} A_{pli} d_{pli}\right) + 2A_{ic} f_c^{'} d_{ic}\left\{\left(\frac{\varepsilon_c}{\varepsilon_o}\right) - \left(\frac{\varepsilon_c}{\varepsilon_o}\right)^2\right\}\right] \quad \text{(A.11b)}$$

$$D_3 = -A_{ic} f_c^{'}\left(\frac{\varepsilon_c}{\varepsilon_o}\right)^2 d_{ic}^2 \quad \text{(A.11c)}$$

Case 4 $\varepsilon_s \geq \varepsilon_y$ and $\varepsilon_o < \varepsilon_c < \varepsilon_u$

This case is similar to Case 2, except the stress in the steel is taken as the yield stress (i.e. $f_s = f_y$). Following the same procedure as in Case 2, the final expression is written as follows:

$$A_4\, c^2 + B_4\, c + D_4 = 0 \quad \text{(A.12)}$$

where

$$A_4 = \left[\left(f_y A_{is}\right) + \left(\varepsilon_c E_{pli} A_{pli}\right) + A_{ic} f_c^{'}\left\{1 - 0.15 * \left(\frac{\varepsilon_c - \varepsilon_o}{\varepsilon_u - \varepsilon_o}\right)\right\}\right] \quad \text{(A.13a)}$$

$$B_4 = -\left[\left(\varepsilon_c E_{pli} A_{pli} d_{pli}\right) - A_{ic} f_c^{'} d_{ic}\left\{0.15 * \left(\frac{\varepsilon_c}{\varepsilon_u - \varepsilon_o}\right)\right\}\right] \quad \text{(A.13b)}$$

$$D_4 = 0 \quad \text{(A.13c)}$$

APPENDIX B

COMPUTER PROGRAM FOR SECTION/MEMBER ANALYSIS

```
**********************************************************************
*    This program was developed by Abdullah Al-Saidy.
*    Last Updated.....2/20/2001
**********************************************************************
*      This program is intended for the calculations of moment and
* curvature of concrete-steel composite section with the option of
* including the effect of strengthening with carbon fiber reinforced
* polymers (CFRP) plates. The assumed material constitutive relations
* of the concrete and steel takes into account the nonlinear behavior of
* these materials. Hognestad's parabola is assumed for the concrete;
* elastic-perfectly plastic relation is assumed for the structural
* steel; and the CFRP plates are assumed to have linear relation until failure.
*
*       Midspan deflections, in the elastic and the inelastic ranges,
* are also calculated for symmetric concentrated loads. If a single
* point load applied at the midspan, the output load should be devided by two.
*
*      In the case when only section analysis is required (i.e. moment-
* curvature), the span length should be input as equal to  zero.
*
*      The ultimate crushing strain of concrete is assumed as 0.003.
*
*
*
*
**********************************************************************


      REAL span,a
      REAL C1,EC,ECU,TC,BC,Ttf,Wtf,DW,TW,TBF,WBF,APL(20),dpl(20)
      REAL fc,E,Fy,Fplu(20),Epl(20),ultstrain(20)
      REAL FPL(20),MPL(20),strain(20)
      REAL TOTALF(40),CC1(40),BM(40),PHI(40),TOPSTRAIN(40)
      REAL P1(40), displacement(40),two(40),three(40)
      CHARACTER  OUTPUT*12,ANS*12
      INTEGER N,counter
      E = 29000
      ECU = .003

      PRINT*, 'PLEASE ENTER THE OUTPUT FILE NAME'
      READ(*,'(A)')OUTPUT
      OPEN(50,FILE=OUTPUT)
      WRITE(50,*)' ******* INPUT DATA *********'
      WRITE(50,*)' ---------------------------'

*  ************************************************
*     INPUT FOR CONCRETE SLAB
*  ************************************************
      PRINT*,'ENTER THE THICKNESS AND WIDTH OF THE SLAB IN INCHES '
      READ(*,*)TC,BC
      PRINT*,'YOU HAVE ENTERED :'
```

```
      WRITE(*,10)TC,BC
      WRITE(50,10)TC,BC
10    FORMAT(//,'TC = ',F10.4,4X,'BC = ',F10.4,/)

      PRINT*, 'ENTER THE SPAN LENGTH AND SHEAR SPAN,a, in inches'
      READ(*,*)span,a

      WRITE(50,101)span,a
101   FORMAT(/,'SPAN = ', F10.4, 4X, ' a = ', F10.4,/)

      PRINT*,'ENTER THE CONCRETE COMPRESSIVE STRENGTH IN ksi'
      READ(*,*)fc
      PRINT*,'ENTER CONCRETE ULTIMATE STRAIN ECU'
      READ(*,*)ECU
      WRITE(50,11)fc,ECU
11    FORMAT('fc = ',F10.4,4X,'Ecu = ',F10.4,/)

*     ***********************************************
*      INPUT FOR STEEL BEAM  TOP FLANGE
*     ***********************************************
      PRINT*,'ENTER THE YIELD STRESS IN ksi'
      READ(*,*)Fy
      WRITE(50,12)E,Fy
12    FORMAT('E  = ',F10.4,4X, 'Fy  = ',F10.4,/)
      PRINT*,'ENTER  THICKNESS AND WIDTH OF THE TOP FLANGE'
      READ(*,*)Ttf,Wtf
      WRITE(50,13)Ttf,Wtf
13    FORMAT('Ttf = ',F10.4,4x,'btf = ',F10.4,/)

*     ***********************************************
*      INPUT FOR STEEL BEAM WEB
*     ***********************************************
      PRINT*,'ENTER THE THICKNESS AND DEPTH OF THE WEB IN INCHES'
      READ(*,*)TW,DW
      WRITE(50,14)TW,DW
14    FORMAT('tw = ',F10.4,4X,'dw  = ',F10.4,/)
      PRINT*,'ENTER THE YIELD STRESS in ksi'
      READ(*,*)Fyw
      WRITE(50,*)Fyw

*     ************************************************
*       INPUT FOR THE STEEL BEAM BOTTOM FLANGE
*     ************************************************
      PRINT*,'ENTER THE THICKNESS AND WIDTH OF BOTTOM FLANGE IN INCHES'
      READ(*,*)TBF,WBF
      TBF = Ttf
      WBF = Wtf
      WRITE(50,15)TBF,WBF
15    FORMAT('Tbf = ',F10.4,4X,'Wbf = ',F10.4,/)
      PRINT*,'ENTER THE YIELD STRESS IN ksi'
      READ(*,*)Fybf
```

```
      WRITE(50,*)Fybf

*     ************************************************
*       INPUT FOR THE FRP PLATE
*     ************************************************
      PRINT*,'ENTER THE NUMBER OF FRP LAYERS YOU WOULD LIKE TO USE'
      READ(*,*)NL
       IF (NL .GE. 1)THEN
        WRITE(50,*)'******** INPUT DATA FOR FRP MATERIAL *********'
        WRITE(50,*)
        WRITE(50,*) 'THE NUMBER OF FRP LAYERS  =',NL
        WRITE(50,*)'  '
        WRITE(50,*)' APL          Epl         Fplu        dpl '
        WRITE(50,*)'(in^2)       (ksi)       (ksi)       (in)'
        WRITE(50,*)'-------------------------------------------------'
       END IF

      IF (NL .GE. 1 ) THEN
       DO 17  I =1,NL
        PRINT*,'LAYER # ',I
        PRINT*,'ENTER THE AREA IN INCHES'
        READ(*,*)APL(I)
        PRINT*,'ENTER THE ULTIMATE STRESS AND MODULUS OF ELASTICITY'
        READ(*,*)Fplu(I),Epl(I)
        PRINT*,'ENTER THE DEPTH TO THE CENTER OF THE PLATE'
        PRINT*,   'FROM TOP OF CONCRETE'
        READ(*,*)dpl(I)
        WRITE(*,16)APL(I),Fplu(I),Epl(I),dpl(I)
        WRITE(50,16)APL(I),Fplu(I),Epl(I),dpl(I)
16     FORMAT(F6.4,9X,F8.2,9X,F8.2,8X,F6.3)
         ultstrain(I)= Fplu(I)/Epl(I)
17     CONTINUE
      END IF

      WRITE(50,*)'-------------------------------------------------'
      WRITE(50,*)'  '
      WRITE(50,*) ' ******* END OF INPUT *******'
      WRITE(50,*) '        '

*     ************************************************
*         STRAIN INCREMENTS
*     ************************************************
       H = TC + Ttf+DW+TBF
       CI = .4*H
       EC = 0
       DO 19 J=1,40

        TOTALF(J)     =0.0
        CC1(J)        =0.0
        BM(J)         =0.0
        PHI(J)        =0.0
```

```
      P1(J)        =0.0
      displacement(J) =0.0
      TOPSTRAIN(J)   =0.0
      two(j)       =0.0
      three(j)     =0.0
19    CONTINUE

      DELTA = ECU/40
      L = ECU/DELTA

      DO 100 J=1,L
        EC = EC + DELTA
20    CONTINUE

      CALL CONCRETE(C1,EC,fc,BC,TC.CC,TMFC,ECO,FC1)
        CON = CC
        MC  = TMFC
      print*,'con & MC& C1',CON,MC,C1
      PRINT*,'ECO & FC',ECO,FC

      CALL TOPFLANGE(C1,EC,Ttf,Wtf,TC,E,Fy,FTtf,TMTF)
        FTOP = FTtf
        MTF  = TMTF

      CALL WEB(C1,EC,DW,TW,TC,Ttf,Fy,E,TFW,TMW)
        FWEB = TFW
        MWEB = TMW

      CALL BOTFLANGE(C1,EC,TBF,WBF,TC,Ttf,DW,Fy,E,TFBF,TMBF)
        FBOT = TFBF
        MBOT = TMBF

*     ******************************************************
*          FORCES AND MOMENTS IN THE FRP PLATE
*     ******************************************************

        TFPL = 0.0
        TMPL = 0.0
      IF (NL .GE. 1)THEN
       DO 25  I = 1,NL
        strain(I) = (C1 - dpl(I))*EC/C1

       IF (ABS(strain(I)) .GT. ABS(ultstrain(I))) THEN
       WRITE(*,*)'RUPTURE FAILURE OF FRP PLATE'
       WRITE(50,*)'RUPTURE FAILURE OF FRP PLATE'
       GO TO 10000
       END IF

        FPL(I) = APL(I)*strain(I)*Epl(I)
        MPL(I) = -FPL(I)*dpl(I)
```

```
      TFPL = TFPL + FPL(I)
      TMPL = TMPL + MPL(I)
25    CONTINUE
     END IF

*    ****************************************************
*     CALCULATION OF THE RESULTANT FORCE
*    ****************************************************
      NETFORCE = CON+FTOP+FWEB+FBOT+TFPL
     IF(ABS(NETFORCE).LT. 1.0) THEN
      GO TO 40
     END IF

     IF(NETFORCE .LT. 0.0)THEN
      C1 = C1 + .001
     ELSE
      C1 = C1 - .001
     END IF

     if (C1 .LT. (TC/10))then
     PRINT*,'C1 IS TOO SMALL'
     write(50,*) 'C1 IS TOO SMALL'
     go to 10000
     elseif (C1 .GT.H)then
     PRINT*,'C1 IS TOO LARGE'
     WRITE(50,*) 'C1 IS TOO LARGE'
     go to 10000
     end if

      GO TO 20
40     CC1(J)  = C1
      TOPSTRAIN(J)=EC
      TOTALF(J)= ABS(NETFORCE)
      BM(J)   = MC+MTF+MWEB+MBOT+TMPL
      PHI(J)  = EC/C1

      IF (span .EQ. 0.0) THEN
       GO TO 100
      END IF

      P1(J)   = BM(J)/a
100   CONTINUE
10000 CONTINUE

     WRITE(50,*) '_____________________________________________'
     WRITE(50,*) ' FORCES IN THE SECTION AT ULTIMATE STRENGTH'
     WRITE(50,*) '_____________________________________________'
     WRITE(50,98)CON,FTOP,FWEB
98    FORMAT(//,'CON =',F8.2,3X,'FTOP=',F8.2,3X,'FWEB=',F8.2)
     WRITE(50,99)FBOT,TFPL,NETFORCE
99    FORMAT('FBOT=',F8.2,3X,'TFPL= ',F8.2,3X,'NETFORCE=',F8.2,//)
```

```
      WRITE(50,*) '    ******  OUTPUT RESULTS ***********'
      WRITE(50,*) '_____________________________________'
      WRITE(50,*) 'TOTAL FORCE     DEPTH TO N.A     STRAIN'
      WRITE(50,*) '-------------------------------------'
      DO 120 J=1,L
       WRITE(*,110)TOTALF(J),CC1(J),TOPSTRAIN(J)
       WRITE(50,110)TOTALF(J),CC1(J), TOPSTRAIN(J)
110     FORMAT(2x,F8.4,7X,F10.4,8X,F8.6)
120    CONTINUE

       WRITE(50,*) '_____________________________________________'
       WRITE(50,*) ' MOMENT (in_k)       CURVATURE (radians/in)'
       WRITE(50,*) '---------------------------------------------'
      DO 140 J=1,L
       WRITE(*,130)  BM(J),PHI(J)
       WRITE(50,130) BM(J),PHI(J)
130     FORMAT(4X,F10.3,10X,F10.6)
140    CONTINUE

        IF (span .EQ. 0.0) THEN
          GO TO 20000
        END IF

C ************************************************************
C           DEFLECTION CALCULATION                 *
C ************************************************************
      WRITE(50,*)
      WRITE(50,*)' ****** MIDSPAN DEFLECTION **********'
      WRITE(50,*)
      WRITE(50,*)'_____________________________________'
      WRITE(50,*)'   LOAD      DISPLACEMENT'
      WRITE(50,*)'  (kips)       (in.) '
      WRITE(50,*)'_____________________________________'
      WRITE(50,*)

      DO 2000  J =1,L
        P     = P1(J)
        PHIA   = PHI(J)
        count  = J
       CALL deflection(count,L,P,PHIA,BM,PHI,span,a,DELTA)

       displacement(J) = DELTA

2000    CONTINUE
        DO 2001 I =1,L
            WRITE(50,*) P1(I),displacement(I)
2001      CONTINUE

20000     STOP
        END
```

```
**************************************************************************
*
*      SUBROUTINE CONRETE  FOR THE CALCULATION OF THE TOTAL FORCE AND
*THE MOMENT DUE TO THE FORCES IN EACH SEGMENT OF THE CONCRETE DECK
*
**************************************************************************

    SUBROUTINE CONCRETE ( C1,EC,fc,BC,TC,CC,TMFC,ECO,FC1)
     REAL C1,EC,fc,BC,TC,CC,TMFC
     INTEGER N

*      MODCON = (1800000 + 460*0.85*fc*1000)/1000
     MODCON = 57*SQRT(fc*1000)
     ECO   = 2*.85*fc/MODCON
     ECU = .0038

     TMFC=0.0
     CC = 0.0
     N=10

     IF (C1 .GT. TC) THEN
      STRIP1= TC/N
     ELSE
      STRIP1 = C1/N
     END IF

      ASTRIP1 = STRIP1*BC

     DO 800  I= 1,N

      DP1= STRIP1 * (I-.5)
      strain = (C1-DP1)*EC/C1

      IF (STRAIN .LE. ECO )THEN
       FC1 = ASTRIP1* 0.85*fc* (2*strain/ECO - (strain/ECO)**2)
      ELSE
       FC1 = ASTRIP1 * 0.85*fc* (1-(.15*(strain - ECO )/(ECU-ECO)))
      END IF

       MFC  = -FC1 * DP1
       CC   = CC + FC1
       TMFC = TMFC + MFC

800     CONTINUE
      RETURN
      END
```

```
      ************************************************************************
      *      SUBROUTINE TOPFLANGE
      * THIS PART WILL DEVIDE THE TOP STEEL FLANGE IN N-SEGMENTS AND THE
      * CENTROID OF EACH SEGMENT WILL CALCULATED. THE FORCE IN EACH
SEGMENT
      * THEN WILL BE CALCULATED USING THE STRESS-STRAIN RELATION OF STEEL.
      * THE MOMENT DUE TO THE FORCE IN EACH SEGMENT IS THEN CALCULATED
      * AND THE SUM OF THE TOTAL FORCE AND MOMENT IS RETUNED TO THE MAIN
      * PROGRAM.
      *
      ************************************************************************

          SUBROUTINE TOPFLANGE (C1,EC,Ttf,Wtf,TC,E,Fy,FTtf,TMTF)
          REAL C1,EC,Ttf,Wtf,TC,E,Fy,FTtf,TMTF
          INTEGER N

          strainy = Fy/E
          TMTF = 0.0
          FTtf = 0.0

          N=5
          STRIP2  = Ttf/N
          ASTRIP2 = STRIP2*Wtf

          DO 850  I=1,N

           DP2 = TC + STRIP2 *(I-.5)
           strain = (C1-DP2)*EC/C1

          IF (ABS(strain) .LT. strainy) THEN
           Ftf = ASTRIP2 * E *strain
          ELSE
           Ftf = ASTRIP2 * Fy*strain/ABS(strain)
          END IF

           MTF  = -Ftf * DP2
           FTtf = FTtf + Ftf
          TMTF  = TMTF + MTF

      850   CONTINUE
          RETURN
          END
```

```
************************************************************************
*               SUBROUTINE WEB
* THE SAME PROCEDURE WILL BE FOLLOWED AS IN THE PREVIOUSE SUBROUTINE.
* THIS WILL CALCULATE THE CONTRIBUTION OF THE FORCES IN THE WEB TO THE
* TOTAL FORCE AND MOMENT.
*
************************************************************************

    SUBROUTINE WEB (C1,EC,DW,TW,TC,Ttf,Fy,E,TFW,TMW)
     REAL C1,EC,DW,TW,TC,Ttf,Fy,E,TFW,TMW
     INTEGER N

      strainy = Fy/E
      TMW = 0.0
      TFW  = 0.0


      N=10
      STRIP3  = DW/N
      ASTRIP3  = STRIP3 * TW

    DO 900  I =1,N

      DP3 = TC + Ttf + STRIP3*(I- 0.5)
      strain = (C1-DP3)*EC/C1

      IF (ABS(strain) .LT. strainy) THEN
        FW = ASTRIP3 * E *strain
      ELSE
        FW = ASTRIP3 * Fy*strain/ABS(strain)
      END IF

        MW  = -FW * DP3
        TFW = TFW + FW
        TMW = TMW + MW

900    CONTINUE
      RETURN
      END

************************************************************************
*         SUBROUTINE BOTFLANGE
*      CONTRIBUTION OF THE BOTTOM FLANG
************************************************************************

    SUBROUTINE BOTFLANGE(C1,EC,TBF,WBF,TC,Ttf,DW,Fy,E,TFBF,TMBF)
      REAL C1,EC,TBF,WBF,TC,Ttf,DW,Fy,E,TFBF,TMBF
      INTEGER N
      strainy= Fy/E
```

```
      TMBF = 0.0
      TFBF = 0.0

      N =5
      STRIP4  = TBF/N
      ASTRIP4 = STRIP4 * WBF

     DO 950  I=1,N

      DP4    = TC+Ttf+DW+ STRIP4*(I-.5)
      strain = (C1-DP4)*EC/C1

     IF (ABS(strain) .LT. strainy) THEN
      FBF = ASTRIP4*E*strain
     ELSE
      FBF = ASTRIP4*Fy*strain/ABS(strain)
     END IF

      MBF  = -FBF * DP4
      TFBF = TFBF + FBF
      TMBF = TMBF + MBF

950   CONTINUE
     RETURN
     END


C  ***************************************************************
C    SUBROUTINE deflection
C  ***************************************************************

     SUBROUTINE deflection(count,L,P,PHIA,BM,PHI,span,a,DELTA)

      REAL P,BM(40),PHI(40),span,a,DELTX,MX,X,PHX,FX(40)
      REAL DELTA
      INTEGER  N,C

       DO 2490  k =1,40
          FX(k) = 0.0
2490     CONTINUE
         N = 20
       DELTX = a/N
        x    =0.0

       DO 2510  I = 1,N

         X = X + DELTX
        MX = P * X

         DO 2500 J = 1,count
```

```
          IF (MX .EQ. BM(J)) THEN
            PHX = PHI(J)
          END IF

          IF( MX .LT. BM(J))THEN
            PHX = PHI(J)/a * X

          ELSEIF(MX .GT. BM(J) .AND. MX .LT. BM(J+1)) THEN
            DELTAM  = BM(J+1) - BM(J)
            MDIFFR  = MX - BM(J)
            FRACTN  = MDIFFR/DELTAM
            DELTAPHI= PHI(J+1) - PHI(J)
            PHIDIFFR= FRACTN * DELTAPHI

            PHX  = PHI(J)+ PHIDIFFR

          ENDIF

2500        CONTINUE
               FX(I) = PHX * X

2510      CONTINUE

C ***********************************************
C  NUMERICAL INTEGRATION USING SIMPSON'S RULE
C
C    EVEN = EVEN NUMBERS
C    ODD  = ODD  NUMBERS
C ***********************************************

       EVEN = 0.0

      DO 2501  I =2,N-2,2
       EVEN = EVEN + FX(I)
2501   CONTINUE

       ODD = 0.0

      DO 2502   I = 1,N-1,2
       ODD = ODD + FX(I)
2502   CONTINUE

        FN = FX(N)

      AREA  = DELTX/3 * (2*EVEN + 4*ODD + FN)
c      write(50,*)AREA
      DELTA = AREA + PHIA/2 *((span**2)/4 - a**2)

     RETURN
     END
```

REFERENCES

1. Klaiber, F.W., Dunker, K.F., Wipf, T.J., and Sanders, W.W. (1987) "Methods of Strengthening Existing Highway Bridges." *NCHRPReport No. 293*, TRB, National Research Council, Washington, D.C., 114 pp.

2. Mckenna, J.K. and Erki, M.A. (1994)."Strengthening of reinforced concrete flexural members using externally applied steel plates and fiber composite sheets- a survey." *Canadian Journal of Civil Engineering*, Vol. 21, pp. 16-24.

3. Dorton, R. A. and Reel, R. (1997). "Methods for Increasing Live Load Capacity of Existing Highway Bridges." *NCHRP Synthesis 249*, TRB, National Research Council, Washington, D.C., 66 pp.

4. Albrecht, P., Sahli, A., Crute, D, Albrecht,Ph. and Evans, B.(1984) "Application of adhesives to Steel Bridges." *Report FHWA/RD-84/037*. FHWA, U.S. Department of Transportation, pp 35-106 and pp.170.

5. Mays, G.C. and Huthchinson, A.R. (1992). *Adhesives in Civil Engineering*. Cambridge University Press, Cambridge, England.

6. Petronio, M. (1997). *Handbook of Adhesives, 2nd edn.* (Ed. Skiest, I), Van Nostrand Reinhold Co., New York, 1977, Chapter 6.

7. Jones, R., Swamy, R.N., Bloxham, J., and Bouderbalah, A. (1980). "Composite behavior of concrete beams with epoxy bonded external reinforcement." *The International journal of Cement Composites*, Vol. 2, No.2, pp. 91-107.

8. Albrecht, P. and Sahli, A. (1986). "Fatigue Strength of Bolted and Adhesively Bonded Structural Steel Joints." *Fatigue in Mechanically Fastened Composite and Metallic Joints, ASTM STP 927,* John M. Potter, Ed., American Society for Testing and Materials, Philadelphia, pp. 72-94.

9. Hart-Smith, L.J. (1985). "Designing to Minimize Peel Stresses in Adhesive-Bonded Joints." *Delamination and Debonding of Material. ASTM STP 876.* W.S. Johnson, Ed., American Society for Testing and Materials, Philadelphia, pp. 238-266.

10. Adams, R.D., Atkins, R.W., Harris, J.A., and Kinloch, A.J. (1986). " Stress Analysis and Failure Properties of Carbon-Fibre-Reinforced-Plastic/Steel Lap joints." *Journal of Adhesion*. Vol. 20, pp. 29-53.

11. Adams, R.D., Comyn, J., and Wake, W.C. (1997). *Structural Adhesives Joints in Engineering*. Chapman & Hall, London, p. 126.

12. Kinloch, A.J., Ed., (1983). *Durability of Structural Adhesives*. Applied Science, London.

13. Springer, G.S. (1979). "Environmental Effects on Epoxy Matrix Composites." *Composite Mterials: Testing and Design (Fifth Conference). ASTM STP 674.* S.W. Tsai, Ed., American Society for Testing and Materials, pp. 291-312.

14. Chajes, M.J., Mertz, D. R., Thomson, T. A., and Farschman, C. A. (1994). "Durability of Composite Materials Reinforcement." In *Infrastructure:New Materials and Methods of Repair, Proc., The Third Materials Engineering Conference.* Basham, K. D., Ed., San Diego, California, pp. 598-605.

15. Roy, A. Grontcharova-Benard, E., Gacougnolle, J-L, and Davies, P. (2000). "Hygrothermal Effects on Failure Mechanisms of Composites/Steel Bonded Joints." *Time Dependent and Nonlinear Effects in Polymer and Composites, ASTM STP 1357,* R. A. Schapery and C. T. Sun, Eds., American Society for Testing and Materials, West Coshhocken, PA, pp. 357-371.

16. Davis, P. and Roy, A. (2000). "Accelerated Marine Aging of Composites and Composite/Metal Joints." In *Recent Developments in Durability Analysis of Composite Systems.* Cardon et al., Eds, Balkema, Roterdam, pp. 253-258.

17. GangarRao, H. V. and Burdine, E. B. (1999). " Stiffening of Steel Stringer Bridges Using Carbon Fiber Reinforced Polymers." *Draft of Final Report.* West Virginia Department of Transportation, Charleston, West Virginia.

18. Bourban, P. E., McKnight, S. H., Shully, S.B, Kharabari, V. M., and Gillespie, J. W. (1994). "Durability of Steel/Composites Bonds for Rehabilitation of Structural Components." In *Infrastructure: New Materials and Methods of Repair, Proc., The Third Materials Engineering Conference.* Basham, K. D., Ed., San Diego, California, pp. 295-302.

19. Karbhari, V.M. and Shully, S.B. (1995). "Use of Composites for Rehabilitation of Steel Structures – Determination of Bond Durability." *Journal of Materials in Civil Engineering,* November, pp. 239-245.

20. Cusens, A. R. and Smith, D. W. (1980). "A study of epoxy resin adhesive joints in shear." *The Structural Engineer,* Vol. 58A, No.1, pp. 13-18.

21. May, G.C. and Tilly, G. P. (1982). " Long Endurance Fatigue Performance of Bonded Structural Joints." *International Journal of Adhesion and Adhesives,* April, pp. 109-113.

22. Macdonald, M.D. (1981). "Strength of Bonded Shear Joints Subjected to Movement During Cure." *International Journal of Cement Composites and Lightweight Concrete,* Vol. 3, No. 4, pp. 267-272.

23. Sen, R., Liby, L., Spillet, K., Mullins. G. (1995). "Strengthening Steel Composite Bridge Memebers Using CFRP Laminates." In *Non-Metallic (FRP) Reinforcement for Concrete*

structures, proceedings of the Second International RILEM Symposium, Taerwe, L., Ed., Ghent, Belgium, pp. 551- 558.

24. Mertz, D.R. and Gillespie, J.W. (1996). "Rehabilitation of Steel Bridge Girders through the Application of Advanced Composites Materials." *Final Report, NCHRP -93-ID011*, TRB, National Research Council, Washington, D.C., 30 pp.

25. Taylor, M., Luke, S., and Collins, S. (2000). " Composites Technology for Structural Upgrading." In *Railway Engineering-2000, Proc., 3rd International Conference,* London, U.K, 5-6 July.

26. Barnes, F.J., Hill, P.S., Peel, D. (2000). " The Use of Carbon Fibre to Strengthen Railway Structures – Case Studies." In *Railway Engineering-2000, Proc., 3rd International Conference,* London, U.K, 5-6 July.

27. Frieze, P.A., Barnes, F.J. (1996). "Composite Materials for Offshore Application-New Data and Practice." *Proceedings of the 28th Annual Offshore Technology Conference*, pp. 247-253.

28. Hognestad, E. (1951). "A study of Combined Bending and Axial Load in Reinforced Concrete Members." *Bulletin No. 399*, University of Illinois Engineering Experimental Station.

29. AISC (1994). *Manual of Steel Construction, Load & Resistance Factor Design.* 2nd ed. American Institute of Steel Construction, Chicago, IL.

30. Sen, R., Liby, L., Mullins, G., and Spillet, K. (1996). "Strengthening Steel Composites Beams with CFRP Laminates." In *Materials for the new millennium: proceedings of the Fourth Materials Engineering Conference.* Chong, K. P., Ed, Washington, D.C., November 10-14, pp. 1601-1607.

31. AASHTO (1996). *Standard Specifications for Highway bridges.* 16th Edition, American Association of State Highway and Transportation Officials, Washington, D.C.

32. AASHTO (1994). *LRFD Bridge Design Specification.* First Edition, American Association of State Highway and Transportation Officials, Washington, D.C.

33. Barker, R. M. and Pucket, J. A. (1997). *Design of Highway Bridges.* John Wiley & Sons, New York, NY, pp. 290-291.

34. Hambly, E. C. (1991). *Bridge Deck Behavior.* Chapman & Hall. London.

35. West, R. (1973). "The use of a grillage analogy for the analysis of slab and pseudo-slab bridge decks." *Research Report 21, Cement and Concrete Association,* London.

36. West, R. (1973). "Recommendations on the use of grillage analysis for slab and pseudo-slab bridge decks." *Publication 46.017, Cement and Concrete Association and Construction Industry Research and Information Association,* London.

37. Smith, K. N. and Mikelstein, I. (1988). "Load distribution in edge stiffened slab and slab-on-girder bridge decks." *Canadian Journal of Civil Engineering,* Vol. 15, pp. 977-983.

38. Jaeger, L.G. and Bakht, B. (1982). "The Grillage analogy in bridge analysis." *Canadian Journal of Civil Engineering*, Vol. 9, pp. 224-235.

39. Bakht, B. and Jaeger, L.G. (1988). "Dealing with varying moments of inertia of girders in bridge analysis." *Canadian Journal of Civil Engineering*, Vol. 15, pp. 232-239

40. Kostem, C. N. and Ragazzo, S. C. (1993). "Grillage Analogy for Multigirder Bridges." In *Computing in Civil and Building Engineering.* Cohn, L. F., Ed, Anaheim, California, June 7-9, pp.188-192.

41. Amer, A., Arockiasamy, M., and Shahawy, M. (1999). "Load Distribution of Existing Solid Slab Based on Field Tests." *Journal of Bridge Engineering,* pp. 189-193.

42. Zokaie, T. (2000). "AASHTO-LRFD Live Load Distribution Specifications." *Journal of Bridge Engineering,* pp. 131-138.

43. Chan, T. H. and Chan, J. H. (1999). "The use of eccentric beam elements in the analysis of slab-on-girder bridges." *Structural Engineering and Mechanics,* Vol. 8, No.1, pp. 85-102.

44. STAAD III/v. 22. (1998). *Research Engineers, Inc.* Yorba Linda, CA.